

Rational design of ionic compounds for electrocatalytic reduction of carbon dioxide

Thèse N° 7440

Présentée le 16 août 2019

à la Faculté des sciences de base

Laboratoire de chimie organométallique et médicinale

Programme doctoral en chimie et génie chimique

pour l'obtention du grade de Docteur ès Sciences

par

Dmitry VASILYEV

Acceptée sur proposition du jury

Prof. K. Sivula, président du jury

Prof. P. J. Dyson, directeur de thèse

Prof. P. Broekmann, rapporteur

Dr S. Katsyuba, rapporteur

Prof. R. Buonsanti, rapporteuse

2019

Acknowledgements

First of all, I would like to thank my advisor, Prof. Paul J. Dyson, for providing me an opportunity to join his team. Without his constant belief in me and continuous support of my ideas it would be impossible to experiment with new things, sometimes very adventurous from the first glance. So far, applying for a PhD position in Paul's group was one of the best choices I made.

It is surprising, how enjoyable the atmosphere in LCOM was, despite all the differences in our backgrounds, habits and interests. I would like to thank Sveta, Erfan, Martin, Felix, Antoine, Hristo and all the other members of our group for being friendly, creative, professional and able to work together in harmony.

My most fruitful projects were made in a collaboration with the Interfacial Electrochemistry Group from the University of Bern, led by Prof. Peter Broekmann. Therefore, I would like to thank Peter and his group, particularly Prof. Sasha Rudnev, for their expertise, positivity and eagerness to work together.

Furthermore, I am happy, that the amount of the efforts dedicated to the administrative and organizational part of my studies was reduced to the minimum, so I could concentrate on my direct duties. For that I would like to acknowledge secretariat of LCOM, particularly Jacqueline and her team (Tiffany and Tania) for solving all the general administrative issues; Benjamin, Annelise and Gladis from the ISIC chemical store for organizing the material support of my studies; Gil from the mechanical workshop for patiently spending time on manufacturing and tuning electrochemical sandwich cell on the basis of my drawings.

I believe I was very lucky to meet and become friends with a number of outstanding people. Particularly, Cornel and Serhii were always sharing the worries and joys with me, so that the worries were three times easier to bear and the joys three times brighter. The list will not be complete without my old friend Sasha Sedykh, who was always there to have a nice chat and travel a bit. Additionally, I would like to acknowledge Racquel, Kostya, Zhenya, Anton and Misha for all the crazy stuff we did

together, innumerable hikes, ski trips, travels and just enjoying the company of each other. Separately I have to mention Phillip and the Dolivo Juku school at Lausanne, who has accepted me in the wonderful family of Aikido Yoshinkan.

The last but the not least important people I want to thank are my family: my Mom and Dad, who were always around with the support when I needed so; my brother, who is always fun to hang out with and who, I hope, will soon complete his PhD path as well; and my grandfather, who was always a source of inspiration for me.

Lausanne, 31st May 2019.

Abstract

Electrochemical reduction of carbon dioxide is one of the plausible approaches towards renewable energy carriers. When coupled with electricity, which can be provided by sustainable technologies, it becomes a method of high importance with potential value for future energy challenges. However, the electrochemical version of the CO₂ reduction reaction (CO₂RR) proceeds through highly energetic intermediates, therefore efficient catalytic and co-catalytic systems are needed.

Recently, considerable attention was dedicated to application of ionic liquids (ILs) as promising promoters for the CO₂RR. While most efforts in this domain have been concentrated on spectroscopic and electrochemical investigation of existing IL-based systems and on the development of more active electrodes, there are only a limited number of studies discussing the structure/activity relationships of ILs in the CO₂RR. Our aim was to fill this gap and to find new classes of ILs that are able to promote CO₂RR. Another aim of our project was to delineate the basic trends in the structures of the active co-catalysts and provide descriptors for the promoting activity.

In this work three new classes of ILs are evaluated for the CO₂RR. Within each IL series the structures of the cationic core were varied, the dependencies of the stabilities and activities of the ILs on the structure are discussed. Additionally, a fundamentally new type of ionic systems based on deep eutectic solvents were applied to the CO₂RR and found to be highly active, cheap and non-toxic alternatives for the conventional ILs. Based on the obtained results, the charge and its accessibility are suggested to be the main descriptors for the activity of the catalysts in non-aqueous environments.

Keywords

carbon dioxide reduction; electrochemistry; ionic liquids; deep eutectic solvents; non-aqueous electrolytes

Résumé

Réduire électrochimiquement le dioxyde de carbone est l'une des approches possibles pour en faire un vecteur d'énergie renouvelable. Si cette démarche est couplée à une source d'énergie verte, elle devient une méthode intéressante pour répondre aux challenges énergétiques. Cependant, la réduction électrochimique du dioxyde de carbone (CO₂RR) s'accomplit via des intermédiaires très énergétiques. Il y a donc besoin qu'un système catalytique et co-catalytique efficace émerge.

Récemment, l'attention s'est tournée sur l'application des liquides ioniques (ILs) comme promoteur efficace de la CO₂RR. Comme la plupart des efforts dans le domaine se sont concentrés sur l'investigation spectroscopique et électrochimique de ces systèmes ainsi qu'au développement d'électrodes plus actives ou au design des cellules électrochimiques, il n'y a qu'une poignée de travaux mettant en relation la structure et l'activité des ILs. Notre but était donc de remplir ce manque en trouvant de nouveaux ILs capable de promouvoir la CO₂RR, de décrire les relations fondamentales entre leur structure et leur activité afin d'en dégager des descripteurs promouvant la réaction.

Dans ce travail trois nouvelles classes d'ILs ont été évaluées pour la CO₂RR. Chaque série possède une variation dans la structure du cation et la dépendance entre stabilité et activités seront discutées. De plus, un nouveau type de système ionique, les solvants eutectiques profonds ont été appliqués à la CO₂RR et apparaissent comme une alternative très active, peu chère et non toxique. Basé sur les résultats obtenus, la charge et l'accessibilité du cation apparaissent comme les descripteurs principaux de l'activité des catalyseurs en environnement non aqueux.

Mots-clés

réduction de dioxyde de carbone; électrochimie; liquides ioniques; solvants eutectiques profonds; non aqueux électrolytes

Contents

Acknowledgements	i
Abstract.....	iii
Keywords.....	iii
Résumé	iv
Mots-clés.....	iv
List of Figures.....	vii
List of Schemes	ix
List of Abbreviations.....	x
List of Tables.....	xvi
Chapter 1 Literature Review.....	13
1.1 Introduction	13
1.2 Redox Shuttles	15
1.3 Pyridinium Salts and Dihydropyridines.....	17
1.4 Ionic Liquids	20
1.5 Functionalized Ionic Liquids and Deep Eutectic Solvents	26
1.6 Summary	27
1.7 References	29
Chapter 2 Triazolium Ionic Liquids.....	43
2.1 Introduction	43
2.2 Results.....	45
2.3 Summary	52
2.4 Experimental.....	54
2.4.1 Electrochemical measurements.....	54
2.4.2 Synthesis and characterization of compounds.	55
2.5 Supporting Information.....	61
2.6 References	74
Chapter 3 Pyrazolium Ionic Liquids.....	75

3.1	Introduction	75
3.2	Results.....	76
3.3	Summary	82
3.4	Experimental.....	83
	3.4.1 Materials and methods.....	83
	3.4.2 Synthesis and characterization of the compounds.....	83
3.5	Supporting Information.....	89
	3.5.1 CV data.....	89
	3.5.2 NMR spectra	94
3.6	References	116
Chapter 4	Guanidinium Ionic Liquids	117
4.1	Introduction	117
4.2	Results.....	118
4.3	Summary	123
4.4	Experimental.....	124
	4.4.1 Materials and methods.....	124
	4.4.2 Synthesis and characterization of the compounds.....	124
4.1	Supporting Information.....	127
4.2	References	135
Chapter 5	Deep Eutectic Solvents	137
5.1	Introduction	137
5.2	Results.....	138
5.3	Summary	144
5.4	Experimental.....	145
	5.4.1 Materials and methods.....	145
	5.4.2 Viscosities of electrolytes and the current densities for the electrolysis	146
	5.4.3 Cyclic voltammetry data	147
5.1	References	153
Chapter 6	Conclusions	157
	Curriculum Vitae.....	159

List of Figures

Figure 1.1. Promotion of CO ₂ RR.....	14
Figure 1.2. Initial proposed mechanism for the reduction of CO ₂ in the presence of tetraalkylammonium salts and facilitation of the process in the presence of crown ethers.	15
Figure 1.3. Pyridine-based catalysts suggested for the CO ₂ RR.	17
Figure 1.4. Comparison of cyclic voltammetry data for various ionic co-catalytic systems without and with IR-correction. Adapted from ref. 91.....	24
Figure 1.5. Effect of field stabilization on the CO ₂ RR. Left: Ag(111) and Pt(111) without field stabilization. Right: Ag(111) with field stabilization. Adapted from ref. 111.	25
Figure 1.6. Ionic promoters probed for the CO ₂ RR. A: The most active co-catalysts cations. B: Other organic salt cations. C: Anions used in the study.	25
Figure 2.1. A: Substituted Im IL, used for the research. B: Hypothesized binding modes of CO ₂ and Im ILs on the Ag electrode. C: “Normal” and abnormal carbenes.....	43
Figure 2.2. Cations of the Tz ILs employed in the current project.	46
Figure 2.3. CV data on the stability of the Tz ILs.	48
Figure 2.4. Left: CV curves for [DMTz]TFSI recorded at different scan rates. Right: Relation of the peak current densities to the square root of the scan rate. Experimental conditions: 0.02 M IL in 0.1 M TBAP in MeCN, glassy carbon polished working electrode.....	49
Figure 2.5. CV curves for the Tz ILs under N ₂ and CO ₂ atmospheres. Experimental conditions: 0.02 M IL in 0.1 M TBAP in MeCN, Ag polished polycrystalline working electrode.	51
Figure 2.6. Left: Results of potential controlled electrolysis for [MBTz]TFSI - electrolysis traces and FE _{CO} . Right: CVs of [MBTz]TFSI displayed with the electrolysis potentials.....	52
Figure 3.1. Pz cations used in this study.....	76
Figure 3.2. CVs for the Pz ILs under Ar, illustrating the differences in stability of diversely substituted Pz cations (Ag polished disk electrode, 0.1 M NBu ₄ PF ₆ in dry acetonitrile, 0.02 M IL additive).....	77
Figure 3.3. Example of the change in the CV after addition of CO ₂ using Pz12 as the co-catalyst (red – argon atmosphere, black – carbon dioxide atmosphere). The performance of the silver electrode towards CO ₂ reduction with and without Pz IL additives are compared in the inset. CVs for the other Pz ILs under CO ₂ are provided in the SI (Figures S3.1 – S3.5).	78
Figure 3.4. Dependency of the Faradaic efficiency in the formation of the detected products on voltage employing Pz1235B. Conditions: cathode – Ag foil; anode – Pt foil; catholyte –	

0.1 M NBu ₄ PF ₆ in MeCN, 0.02 M IL, saturated with CO ₂ ; anolyte – 0.5 M H ₂ SO ₄ (aq); separator – Nafion 117.....	79
Figure 3.5. Decrease of the electrochemical reduction onset potential for the conversion of CO ₂ to CO using co-catalyst Pz1235 in the presence of water.	81
Figure 3.6. Possible intermediate structures between the Pz cations and the CO ₂ ^{•-} radical anion leading to a lowering of the overpotential in the reduction of CO ₂ to CO.....	82
Figure 4.1. Cations of the synthesized Gua ILs.	118
Figure 4.2. Cyclic voltammograms for the Gua ILs under N ₂ , illustrating stability of diversely substituted Gua cations (Ag polished disk electrode, NBu ₄ PF ₆ (0.1 M) in acetonitrile, IL additive (0.02 M), system flushed with N ₂).	120
Figure 4.3. Comparison of CV data, recorded in the presence and in the absence of the co-catalysts on the example of [MBGua]PF ₆ (Ag polished disk electrode, NBu ₄ PF ₆ (0.1 M) in acetonitrile, IL additive (0.02 M), system flushed with CO ₂).	120
Figure 4.4. Performance of [MB5Gua]Tf ₂ N for the CO ₂ RR. Potentiostatic electrolysis followed by online GC measurements, Ag working electrode, IL additive (0.02 M) and NBu ₄ PF ₆ (0.1 M) in acetonitrile. Inset: Faradaic efficiencies for CO.	121
Figure 4.5 Suggested bonding modes for Gua ILs and CO ₂ -based intermediates, two projections. Left: interaction of CO ₂ intermediate with unhindered Gua ILs. Right: blocking of the stabilizing interaction by introduction of cyclic substituents.	122
Figure 4.6. Comparison of the activities of diversely substituted Gua ILs. Left: CV data for the representative Gua ILs (Ag electrode, IL additive (0.02 M) and NBu ₄ PF ₆ (0.1 M) in acetonitrile). Right: structures of the corresponding Gua ILs.....	122
Figure 5.1 Left: Ionic liquids (green) and OH-functionalized compounds (magenta) that promote the CO ₂ RR. Right: choline DES.	138
Figure 5.2. Cyclic voltammograms (CVs) of the urea and EG-based DESs employed for the ERC: Ag working electrode, CO ₂ atmosphere, undivided cell.	139
Figure 5.3. Cyclic voltammograms of [Ch]Cl/EG (1/2) DES solutions in a) water; b) MeCN; c) 3EOH; d) PC under N ₂ (green) and under CO ₂ (magenta). Insets: FEs obtained during potentiostatic electrolysis in presence of CO ₂ . All curves were recorded using Ag electrodes. Estimated error for the determination of the FE is ±5%.	143
Figure 5.4. Mixtures of MeCN with a) [EMImOH]Cl (1M, left); b) [EMImOH]Cl + EG (1M and 2M respectively, right).	144

List of Schemes

Scheme 1.1. Mechanism of the CO ₂ RR catalysis by one-electron redox shuttles (Q).	16
Scheme 1.2. Various mechanisms proposed for the promoting activity of pyridinium ions for the CO ₂ RR.....	18
Scheme 1.3. Reduction of CO ₂ by organic hydrides derived from benzimidazolium salts.	20
Scheme 1.4. Mechanistic pathway for the IL-mediated CO ₂ RR proposed by Wang et al. ⁷⁷	21
Scheme 2.1. Synthesis of 1,3,4-substituted Tz ILs.....	45
Scheme 2.2. A: Retrosynthetic analysis for 1,3-substituted triazoles. B: Approach including click reaction. C: Approach including alkylation of 1,2,3-triazole.	46
Scheme 4.1. Synthesis of Gua ILs.....	118

List of Abbreviations

CV	Cyclic voltammetry
3EOH	2-(2-ethoxyethoxy)ethanol
BMI _m	1-butyl-3-methylimidazolium
Bn	Benzyl
Bu	Butyl
Ch	Choline
CO ₂ RR	CO ₂ reduction reaction
DBTz	1,3-dibutyl-1,2,3-triazolium
DES	Deep eutectic solvents
DMSO	Dimethylsulfoxide
DMTz	1,3-dimethyl-1,2,3-triazolium
DPyrMBGua	N-(di(pyrrolidin-1-yl)methylene)-N-methylbutan-1-aminium
DPyrPipGua	N-butyl-1,3-dimethylimidazolidin-2-iminium
EG	Ethylene glycol
EMI _m OH	2-hydroxyethyl-1-methylimidazolium
EtOAc	Ethyl acetate
Fc	Ferrocene
FE	Faradaic efficiency
Gua	Guanidinium
HER	Hydrogen evolution reaction
IL	Ionic liquid
Im	Imidazolium
MB5Gua	N-butyl-1,3-dimethylimidazolidin-2-iminium
MBnBuTz	1-benzyl-3-methyl-4-butyl-1,2,3-triazolium
MBnPhTz	1-benzyl-3-methyl-4-phenyl-1,2,3-triazolium
MBPhTz	1-butyl-3-methyl-4-phenyl-1,2,3-triazolium
MBTz	1-butyl-3-methyl-1,2,3-triazolium
Me	Methyl
MeCN	Acetonitrile
NADH	Nicotinamide adenine dinucleotide
NCH	N-heterocyclic carbene
NMR	Nuclear magnetic resonance
PC	Propylene carbonate
PCET	Proton-coupled electron transfer
PCHT	Proton-coupled hydride transfer
PEG	Polyethylene glycol
Ph	Phenyl
PMBGua	N-(bis(dimethylamino)methylene)-N-methylbutan-1-aminium

Pyrd	Pyrrolidinium
Pz	Pyrazolium
Pz12	1,2-dimethylpyrazolium
Pz123	1,2,3-trimethylpyrazolium
Pz1234	1,2,3,4-tetramethylpyrazolium
Pz12345	1,2,3,4,5-pentamethylpyrazolium
Pz1235	1,2,3,5-tetramethylpyrazolium
Pz1235B	1-butyl-2,3,5-trimethylpyrazolium
Pz124	1,2,4-trimethylpyrazolium
RVC	Reticulated vitreous carbon
TBAF	Tetrabutylammonium fluoride
Tf	Trifluoromethylsulfonyl
TFSI	Bis(trifluoromethylsulfonyl)imide
TMS	Trimethylsilyl
Tz	Triazolium

List of Tables

Table 3.1. Faradaic efficiencies for different products as a function of the reduction potential for CO ₂ electrolysis employing Pz1235B	80
Table 3.2. Faradaic efficiencies for different products as a function of the reduction potential for CO ₂ electrolysis employing [BMIm][BF ₄].	80
Table 5.1. Reduction onset potentials for the CO ₂ RR and product distribution at optimal potentials for chronoamperometric experiments employing DESs or DES-like systems (neat or as an additive in various solvents). ^[a]	142

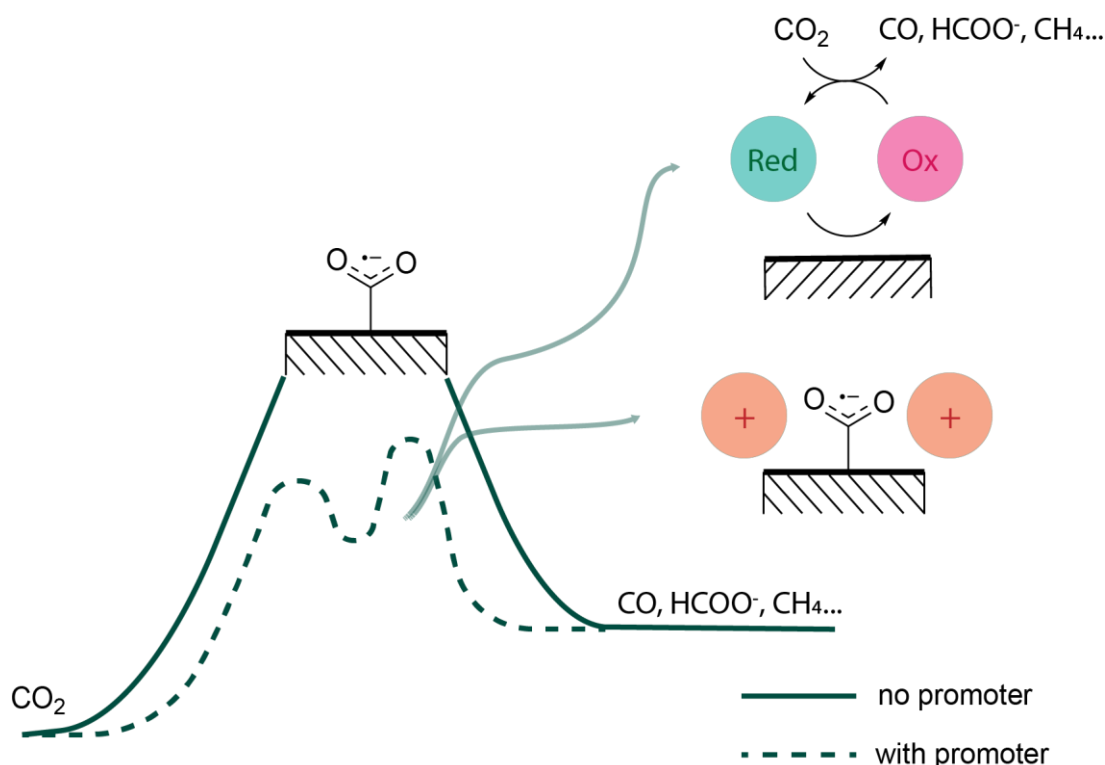
Chapter 1 Literature Review

1.1 Introduction

Transformations of carbon dioxide into useful products is an important topic due to the abundance of anthropogenic CO₂ accumulating in the atmosphere (in 2018 alone more than 37 Gt of CO₂ was emitted from human activity).¹ Indeed, growing interest in CO₂ utilization can be illustrated by the appearance of companies aiming to use CO₂ for the production of a number of materials including carbon nanotubes and fibers, plastics, carbonates, chemical building blocks, methane and methanol.² Therefore, the development of methods that efficiently valorize CO₂, such as the electrochemical carbon dioxide reduction reaction (CO₂RR), when coupled with a renewable source of energy, could contribute significantly to reducing fossil fuels and the associated production of CO₂.³

In 2013 an important review was published entitled, 'Organic molecules as mediators and catalysts for photocatalytic and electrocatalytic CO₂ reduction'.⁴ In the ensuing years, the field has progressed tremendously, albeit with some contentious issues. For several appealing systems numerous debates on the origin of their activity and even on the validity of their assignment as catalysts have been witnessed. Recently, a number of publications have attempted to refine the range of actual catalysts and discussed the major methodological issues. Therefore, it is timely to review the topic of organic catalysts for CO₂RR from the point of view of these fresh perspectives and to consider the main challenges that are faced. It should be noted that the expression "organic promoters for the CO₂RR" can be attributed to a very broad range of systems, and in this review we consider only CO₂RR to fuels, accomplished on metal or inert carbon electrodes and catalyzed or promoted by metal-free, non-enzymatic compounds, used as additives to the electrolyte or as the electrolyte itself. Complementary to this work are a number of useful reviews covering general trends for the CO₂RR,^{5–8} cell design,⁹ application of metal complex catalysis,^{7,10} metal-free electrodes,¹¹ enzymatic catalysis¹² and photoelectrochemistry.^{13–15}

The high reduction overpotential, i.e. the difference between the thermodynamic onset potential and the observed one, is one of the key factors hampering the CO₂RR. The need to apply extra voltage for the transformation not only makes the reduction less energetically attractive, but also results in lower current densities (which define the amount of the product being produced) and lower selectivity for the target process due to increased rates of side reactions. The origins of high overpotentials are believed to be derived from the high energies of the intermediates generated during the catalytic process (Figure 1.1).¹⁶ Side reactions, especially the hydrogen evolution reaction, HER, lower the Faradaic and energy efficiencies of the transformation.¹⁷ Adjustment of the composition of the electrolyte represents a powerful and simple way to influence the outcome of the reduction, as in most configurations of the cell an electrolyte is present and, depending upon its composition, it can drastically influence the overpotential, current densities and even the selectivity of the process, as will be demonstrated below. Electrolyte additives with defined structures and, consequently, tailored properties, are accessible via organic chemistry and provide a powerful approach to enhance the catalytic properties of the entire system.

Figure 1.1. Promotion of CO₂RR.

1.2 Redox Shuttles

Due to their high stabilities and solubilities in organic solvents, tetraalkylammonium salts are presently the component of choice in supporting electrolytes when the electrochemical reduction of CO_2 is conducted in organic solvents. These salts were shown to promote the CO_2RR by Bockris et al,¹⁸ and the initial report was followed by studies exploring the possible routes of the reduction, with a one-electron reduction of the NR_4^+ cation proposed to be the key step in the reaction (Figure 1.2).^{19,20} Combining crown ethers with tetraalkylammonium salts further enhances the CO_2RR ,²⁰ believed to be due to the formation of a crown- $^+\text{NR}_4$ complex when size of the crown allows the cation to fit into the cavity (Figure 1.2). However, the catalytic role of persubstituted ammonium cations was later disputed as evidence for the formation of $^+\text{NR}_4$ was elusive.²¹ Moreover, cyclic voltammograms do not reveal reduction waves for solutions containing tetraalkylammonium salts in the absence of CO_2 and varying the alkyl group does not significantly alter the onset potential for the CO_2RR , which supports an outer sphere reduction mechanism.

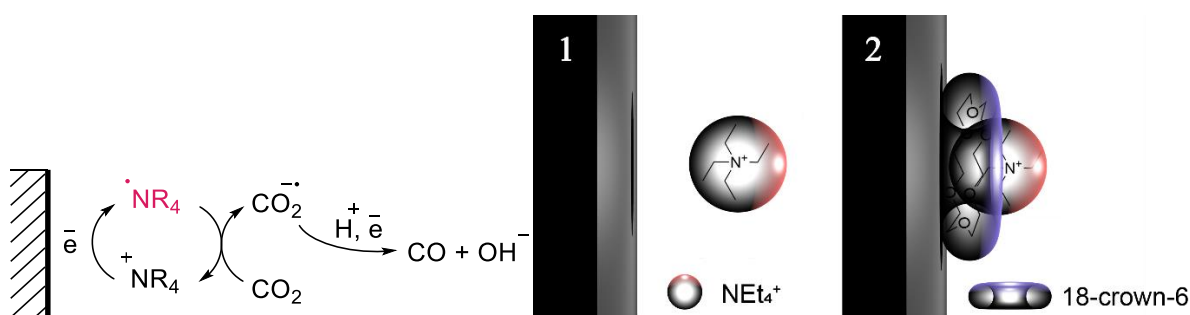
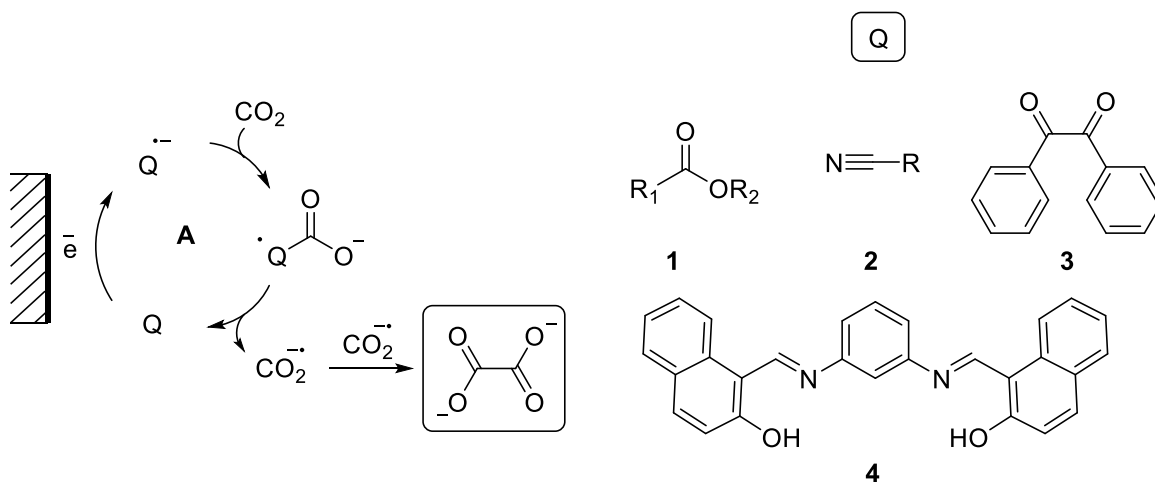


Figure 1.2. Initial proposed mechanism for the reduction of CO_2 in the presence of tetraalkylammonium salts and facilitation of the process in the presence of crown ethers.

A straightforward strategy to change the mechanism of the CO_2RR is to employ redox shuttles, these are compounds that can serve as electron transfer agents between the surface of the electrode and the substrate (namely CO_2 in the CO_2RR). Several catalysts based on this principle have been suggested and the first confirmed redox shuttle catalysts for the CO_2RR were based on aromatic esters and nitriles (Scheme 1.1, shuttles **1** and **2**). When employed in media with a low availability of protons, the distribution of the reduction products switches from a mixture of CO and oxalate to only oxalate.^{22–24} Initially, the reaction was believed to occur through an outer sphere single electron transfer from the reduced form of the catalyst to CO_2 . Later, however, evidence for an inner-sphere mechanism was obtained, which implies the formation of a bond between the C-atom in CO_2 and

the O- or N-atom of the catalyst, with subsequent formation of CO_2 radical anions which then dimerize.^{23,24} Another somewhat more sophisticated mechanism which cannot be ruled out is based on a two-centered process, taking place through the formation of a derivative of 2-((hydroxycarbonyl)oxy)acetic acid with its subsequent decomposition to oxalate.²⁵



Scheme 1.1. Mechanism of the CO_2RR catalysis by one-electron redox shuttles (Q).

The range of suitable electron transfer agents is not limited to aromatic nitriles and esters. For instance, 1,2-diphenylethane-1,2-dione (Scheme 1.1, **3**), acts as a redox shuttle in the CO_2RR ,²⁶ reducing the overpotential for CO_2 by ca. 900 mV. Oxalate was identified as the only product of the reduction of CO_2 with a current efficiency of 70%. The catalytic role of **3** was confirmed and in the presence of pyridine, with isonicotinic acid (71%) and oxalic acid (12%) obtained, confirming the radical mechanism.²⁷ The di-Schiff base *N,N'*-bis(2-hydroxy-1-naphthaldehyde)-*m*-phenylenediimine (Scheme 1.1, **4**) also serves as an electron transfer catalyst affording oxalate with a current efficiency of 57%.²⁸ Compound **4** also catalyzes the synthesis of isonicotinic acid from a mixture of pyridine and CO_2 .²⁹

Although electron shuttles are attractive catalysts due to their high propensity for oxalate formation, the high reduction potentials usually associated with them and, therefore, overpotentials for the CO_2RR , make them less attractive.⁴ Another problem can be coupling of the shuttle with CO_2 instead of transferring the electron, as is the case for benzophenone.^{30,31}

1.3 Pyridinium Salts and Dihydropyridines

However, the range of the catalysts for the CO₂RR is not limited to redox shuttles and a landmark report described pyridinium salts as catalysts for the CO₂RR (Figure 1.3).³² Combined with a hydrogenated Pd electrode and 0.01 M additives of pyridinium salts, the formation of MeOH was observed with Faradaic efficiencies of up to 30%. In subsequent studies it was shown that along with Pd electrodes, Pt electrodes ($FE_{CH_3OH} = 22\%$, $I = 50 \mu A/cm^2$),³³ and illuminated p-type semiconductors ($FE_{CH_3OH} = 96\%$, $E = -0.25 - -0.20$ V vs. SCE for GaAs; $FE_{CH_3OH} = 2.7\%$, $E = -1.1$ V vs SCE, for pyrite) can be used.^{34–36} It was found that substituents which increase the basicity of pyridine N-atom improve catalytic performance and sterically bulky substituents on the *para*-position to the N-atom lower the activity.³⁷

Inspired by pyridinium catalysts, a range of N-heterocyclic compounds were probed as catalysts for the CO₂RR (Figure 1.3). Pyridoxine (vitamin B₆, **6**) was reported to catalyze CO₂RR with a FE_{CH_3OH} around 5%.³⁸ Pyridazine also exhibits a lower FE_{CO} compared to pyridinium catalysts (3.6 vs 14% respectively).³⁹ Initially, mercaptopteridine **8** was reported to transform CO₂ and formic acid to methanol on a glassy carbon electrode.⁴⁰ However, a subsequent study indicated that **8** does not function as an electrocatalyst for the CO₂RR,⁴¹ and this conclusion was later supported by calculations.⁴²

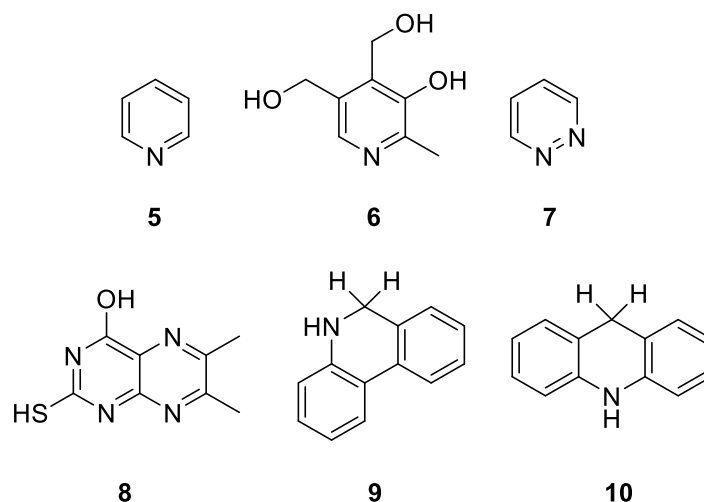
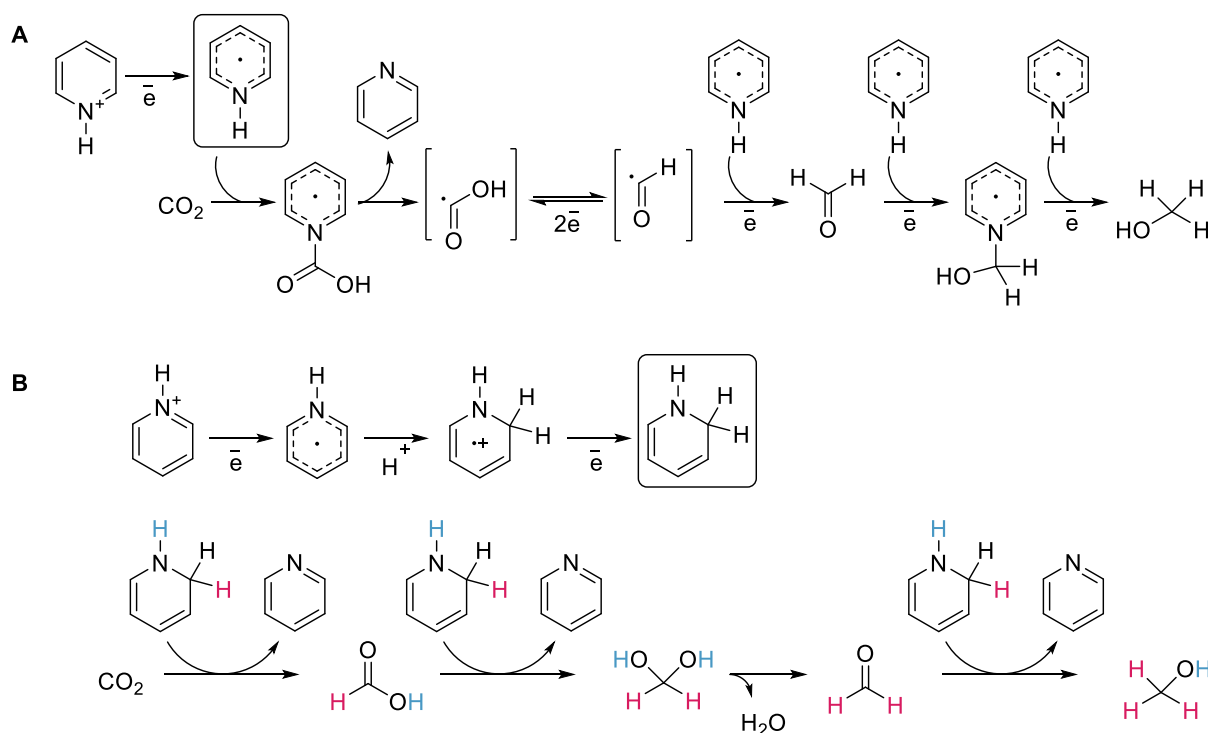


Figure 1.3. Pyridine-based catalysts suggested for the CO₂RR.

The activity of the pyridinium catalyst was originally attributed to the formation of a pyridinium radical, serving as a hydrogenating source.³² Later the pyridinium radical was considered to be a

one-electron charge-transfer mediator, that forms a reduced neutral pyridine-CO₂ complex (Py-COOH⁰, Scheme 1.2, **A**).^{33,43,44} The corresponding carbamate was investigated in order to clarify the properties of the possible intermediate.^{45,46} Yet, the electrochemical potential for the formation of the reduced intermediate was found to be more negative than the actual reduction potential.^{47,48} Taking this into consideration, the mechanism of the co-catalytic activity of pyridinium salts was rather considered to be due to facilitating proton-coupled electron transfer (PCET) or proton-coupled hydride transfer (PCHT) from the surface of the actual catalyst, i.e. the cathode.⁴⁷



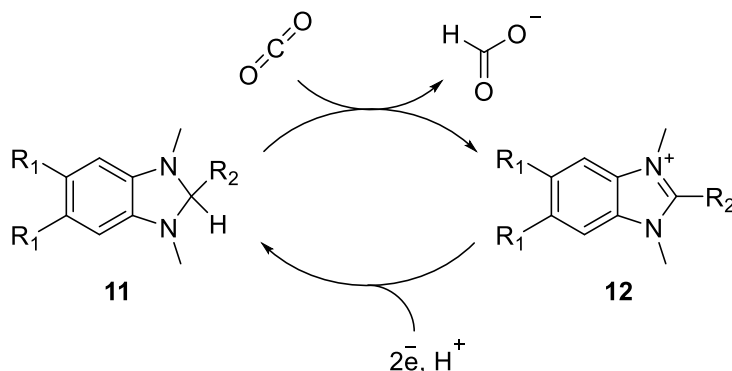
Scheme 1.2. Various mechanisms proposed for the promoting activity of pyridinium ions for the CO₂RR.

A further study on the reduction mechanism proposed the formation of dihydropyridine intermediates in the CO₂RR. Notably, 1,2-dihydropyridine was suggested to be the key intermediate for both electrochemical^{49–51} and photoelectrochemical⁵² reductions (Scheme 1.2, **B**). Inspired by this hypothesis and the similarity between pyridines/dihydropyridines and nature's redox NADP⁺/NADPH pair, organic hydrides derived from pyridines were also considered as potential CO₂RR catalysis.^{53,54} Dihydropyridines have a hydricity between that of Hantzsch ester and NaBH₄ and might be able to reduce CO₂ directly. Although 1,2- and 1,4-dihydropyridines were isolated, they were not found to react with CO₂.⁵⁵ The isolated dihydropyridines, however, reduced CO₂ to formic acid and methanol when potential was applied.

The nature of the activity of the pyridinium catalysts continued to be debatable, with some reports questioning the co-catalytic role of pyridinium ions in the CO₂RR. For instance, on platinum⁵⁶ or gold⁵⁷ electrodes, the pyridinium ion was shown to act as a facilitating HER acid, i.e. like conjugated acids of aniline and benzylamine,⁵⁸ as no products for the CO₂RR were detected. Further research focused the electrochemistry of pyridinium on glassy carbon (RVC), Pt, Ag, Au and Cu electrodes in aqueous electrolytes.^{59,60} It was shown that the observed changes in the CV curves during electrolysis in the presence of CO₂ are not due to the CO₂RR, but result from alternative pathways for the HER. Moreover, in the presence of pyridinium ions, deposits on the electrode were observed to form in both the presence and in the absence of CO₂, which might influence the electrolysis as well and hamper the interpretation of the results.⁶⁰ Protonated pyridine was also ruled out as a possible catalyst for the CO₂RR on a Pt electrode, with pyridinium ions being smoothly reduced to piperidine in both presence and absence of CO₂, without any sign of the CO₂RR.⁶¹ The only CO₂ reduction product that was hypothesized to be formed on a Pt electrode was CO, which is an efficient poison of the catalytic surface inhibiting the reduction reaction.⁶² Using a similar system *in situ* IR spectroscopy allowed formate to be detected in <3% yield, which is slightly facilitated in the presence of pyridinium salts.⁶³

The range of experimental conditions employed for the CO₂RR hamper comparisons and it cannot be excluded that pyridinium-based compounds catalyze the CO₂RR under certain conditions. Moreover, methodological drawbacks include the misuse of electrochemical methods, lack of internal standards for the determination of products, and impurities in the electrolytes. Cyclic voltammetry experiments must be followed by electrolysis at different potentials in order to reveal the actual reduction products. The application of internal standards for product determination is especially relevant when small concentrations of products are formed, as impurities and signals from catalyst decomposition products may prevent quantification of the CO₂RR products.⁶⁴

Despite the uncertainty of the catalytic role of pyridinium ions in the CO₂RR, inorganic hydrides such as boranes⁶⁵ and borohydrides⁶⁶ can reduce CO₂ to formate (the latter even in absence of a catalyst). Organic benzimidazole-based hydrides have also been successfully employed in the CO₂RR (Scheme 1.3).⁶⁷ Formate was the main reduction product, and the organic hydride could be regenerated electrochemically from the resulting benzimidazolium salt.



Scheme 1.3. Reduction of CO₂ by organic hydrides derived from benzimidazolium salts.

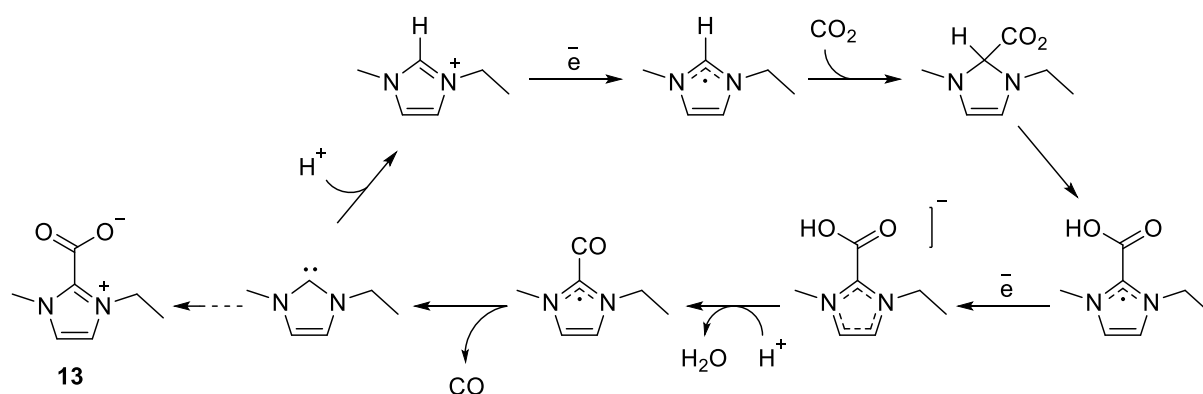
An attempt to define general descriptors for N-heterocycles that are active in the CO₂RR was made, which is based on calculated molecular Pourbaix diagrams and correlating the CO₂RR activity of the N-heterocycle with the position of the triple point, where the conditions are optimal for both electron and/or proton transfer.⁶⁸ Pourbaix diagrams might be useful when two-electron reductions involving organic mediators are considered, e.g. for the prediction of the properties of organic hydrides. However, this approach considers only solution-phase thermodynamics and does not take into account the role of the cathode, which can be key for the transformation.

1.4 Ionic Liquids

Ionic liquids (ILs) have received considerable attention in electrochemical applications^{69,70} due to their large potential windows,⁷¹ good ionic conductivities,⁷² low volatilities⁷³ and their ability to dissolve high concentrations of CO₂.⁷⁴ In this pioneering study Im ILs were shown to lower the reduction overpotential from > 700 mV to 170 mV when combined with a silver cathode.¹⁷ Moreover, the parasitic HER was suppressed, which resulted in a FE_{CO} close to 100%. It is important to underline that the electrode is not innocent in this process as no reaction is detected when a glassy carbon electrode is employed.⁷⁵ IL additives can also switch the selectivity of the CO₂RR. For example, on a lead electrode oxalate is the main reduction product whereas in the presence of an IL the dominant product is carbon monoxide.⁷⁶

Numerous studies have been devoted to the elucidation of the mechanism for the promotion of CO₂RR by ILs. In the original paper, the promoting effect was attributed to the formation of an IL-CO₂ adduct, although the structure of the adduct was not described.¹⁷ In a computational study the most plausible pathway was found to consist of the initial one electron generation of a radical from the Im cation and formation of an adduct with CO₂, followed by electron transfer and subsequent

decomposition of the adduct to water and CO, with the regeneration of the original Im cation (Scheme 1.4).⁷⁷ Formation of the IL-CO₂ adduct correlates with the known chemistry of Im salts, which easily form N-heterocyclic carbenes (NHCs) via deprotonation of the acidic 2-proton under basic conditions^{78,79} (note that the cathode can serve as a powerful base)⁸⁰ or by electrochemical reduction.^{81,82} The resulting NHC reacts rapidly with available electrophiles,⁷⁹ e.g. CO₂.^{83,84} In synthetic chemistry this phenomena was employed, for example, to activate CO₂ and chemically reduce it with silanes to produce methanol.⁸⁵



Scheme 1.4. Mechanistic pathway for the IL-mediated CO₂RR proposed by Wang et al.⁷⁷

The calculated mechanism was supported by experimental data concerning the CO₂RR overpotential in the presence of water employing Im salts as co-catalysts.⁸⁶ Their behavior differed from other investigated ionic co-catalysts, and was attributed to the suppression of side reactions due to the regeneration of the imidazolium (Im) structure during the reduction from the reaction of the NHC with water. Furthermore, CO₂-Im adducts (e.g. **13**, Scheme 1.4) were identified in low concentrations in the post-electrolysis mixtures.^{76,86,87} Carboxylates adducts are stable under ambient conditions and can be synthesized and isolated.⁸⁸ An attempt to introduce this adduct into the electrolysis cycle was not successful, i.e. the adduct was not further reduced to the CO₂ reduction products and the starting IL,⁸⁷ which indicates the formation of the carboxylate is a parasitic reaction. Moreover, 2-substituted Im co-catalysts, lacking an acidic proton at the C2 and cannot form carboxylates, are more active for the CO₂RR than non-substituted Im ILs and are also more stable.^{87,87,86,89} If radical formation followed by the coupling with CO₂ at the 2-position is the key step for the reduction, then 2-substituted Im rings should not act as co-catalysts as they cannot form carbenes at the C2. Im salts can form non-classical (abnormal) carbenes at the C₄ and C₅ positions and, replacing the protons at the C₄ and C₅ positions of the Im ring with methyl groups dramatically reduces activity, suggesting

that the protons in these position play a key role (e.g. providing two H-bonds, participating in the formation of a stabilize CO₂-IL complex).⁸⁹ However, the possibility that the reduction reaction with substituted and non-substituted Im ILs operate via different mechanisms cannot be excluded.

The influence of the length of the N-alkyl chain on the CO₂RR is unclear. According to one study, as the alkyl chain increases from ethyl to octyl the FE and onset potential both increase.⁹⁰ The increase in the reduction onset potential was attributed to the reduced contribution of side reactions, particularly dimerization of Im cations (due to steric effects) and the HER (due to the increasing hydrophobicity of the cations with the length of the alkyl chains). However, in another report the opposite trend was observed with a positive influence of longer alkyl chains on the CO₂RR.⁸⁶ In the most recent study the length of the alkyl chain was found to be negligible for the CO₂RR.⁹¹ In addition, in a series of tetraalkylammonium salts the smallest cations displayed more positive onset potentials.⁸⁶

Further improvements in the onset potential can be achieved with Im ILs by adding water to the system.⁸⁶ This phenomenon was thoroughly investigated and confirmed by several research groups,^{92–96} and it has been suggested that water acts as a proton source for the reduction process and promotes mass transport.⁹³ In addition, commonly used ILs based on tetrafluoroborate anions are unstable and hydrolysis of the BF₄⁻ anion can occur, which lowers the pH of the solution and increase the availability of protons.⁹⁴

The influence of the anion on the CO₂RR is complicated as it appears to depend on the structure of the cathode material employed. For Cu and Ag polycrystalline electrodes, the nature of the anion (PF₆⁻, BF₄⁻, Br⁻, ClO₄⁻, SO₄²⁻ and HCO₃⁻) has negligible effect on the formation of the carbon-based products.^{86,97,98} However, the anion might have a considerable influence on the CO₂RR when it interacts strongly with the surface of the electrode or changes the pH of the solution. For instance, enhancement of the CO₂RR by adsorbed halides was demonstrated for Ag nanocoral electrodes (Cl⁻)⁹⁹ and for plasma-activated Cu electrodes (Cl⁻<Br⁻<I⁻).¹⁰⁰ The nature of the anion alters the performance of the electrochemical system when employing pure ILs as electrolytes (NTf₂⁻>BF₄⁻>tris(perfluoroalkyl)trifluorophosphate in terms of activity for the [BMIm]-based ILs),⁷⁵ as physical properties of the IL strongly influence the solubility of CO₂ and mass transport.⁹³

The anion has a considerable impact on the reduction process if it directly forms intermediates with CO₂, such as when ILs with base-derived anions are used.^{101,102} Here, the activity of the IL is dependent on the formation of transition state intermediates between CO₂ and the base-derived anion, e.g. 1,2,4-triazolide, which can react with CO₂ stoichiometrically and reversibly,¹⁰³ and leads to the formation of formate at low overpotentials. Another example of an IL with anion-derived activity was demonstrated with Im salts with the BF₃Cl⁻ anion.¹⁰⁴ In the presence of CO₂ a new peak appears on the CV scan, which disappears when the electrolyte is purged with N₂. This work is intriguing as it represents a new CO₂ activation process involving Lewis pairs, which was inspired by the lability of B-halide bonds.¹⁰⁵ Unfortunately, the products for this reduction were not determined, although conventional ILs were inactive under the conditions (possibly due to the use of a Pt electrode which does not favor CO production).^{106,107}

The inconsistencies regarding the role of the IL ions on the CO₂RR are partly due to the problems associated with correcting for uncompensated Ohmic resistance (IR drop). For more conductive aqueous electrolytes this problem can be relevant in some reactions;¹⁰⁸ for organic electrolytes, which usually possess higher resistances, not including a IR drop correction significantly distorts the results. To illustrate this problem, corrected and not corrected CV curves were compared for different compositions of Im-based ILs. In the uncorrected curves significant differences are observed between the different ILs, whereas following correction, the differences were found to be negligible (Figure 1.4).⁹¹

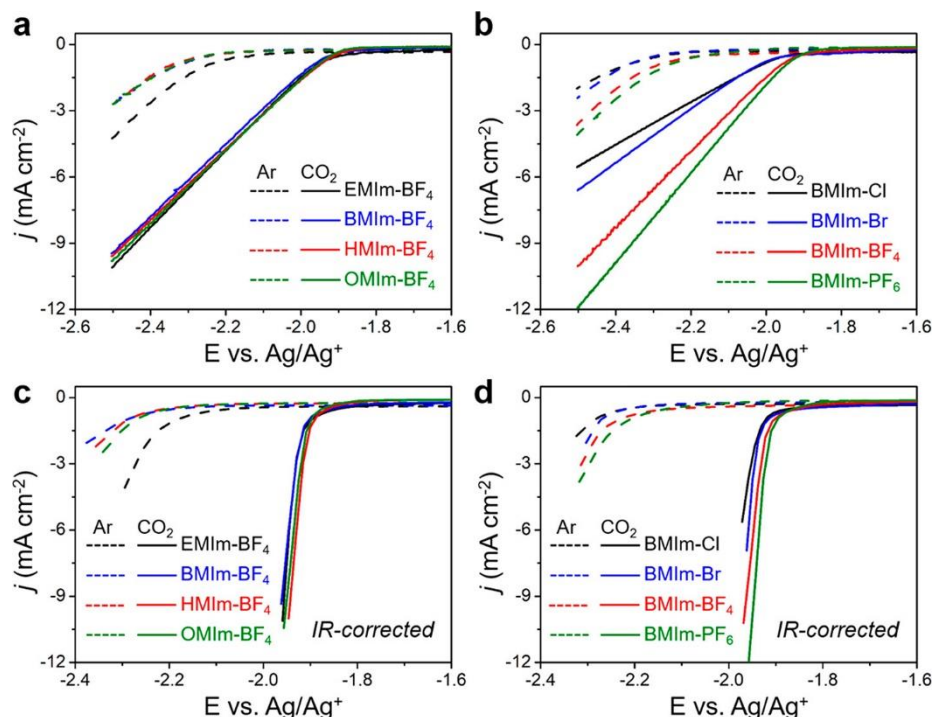


Figure 1.4. Comparison of cyclic voltammetry data for various ionic co-catalytic systems without and with IR-correction. Adapted from ref. 91.

The mechanism by which Im ILs enhance the CO₂RR was probed by *in operando* sum frequency generation spectroscopy.¹⁰⁹ When a potential is applied, the IL participates in the formation of an electric double layer, which is further supported by calculations¹¹⁰ and other electrochemical experiments.¹⁰⁷ Under certain potentials, irrespective of the presence of CO₂ in solution, a structural transition in the IL occurs. Notably, this potential accurately corresponds to the voltage where the CO₂RR also occurs. The origin of the catalytic effect is believed to be derived from the increased abundance and high degree of alignment of the IL cations leading to a sharp growth of the local electrical field in the proximity of the electrode.¹⁰⁹ Stabilization of the key reduction intermediates by the local cation-induced electric field is supported by DFT calculations (Figure 1.5).¹¹¹ The positive effect of water additives may then be explained by reducing the negative potential for the IL transition.¹¹²

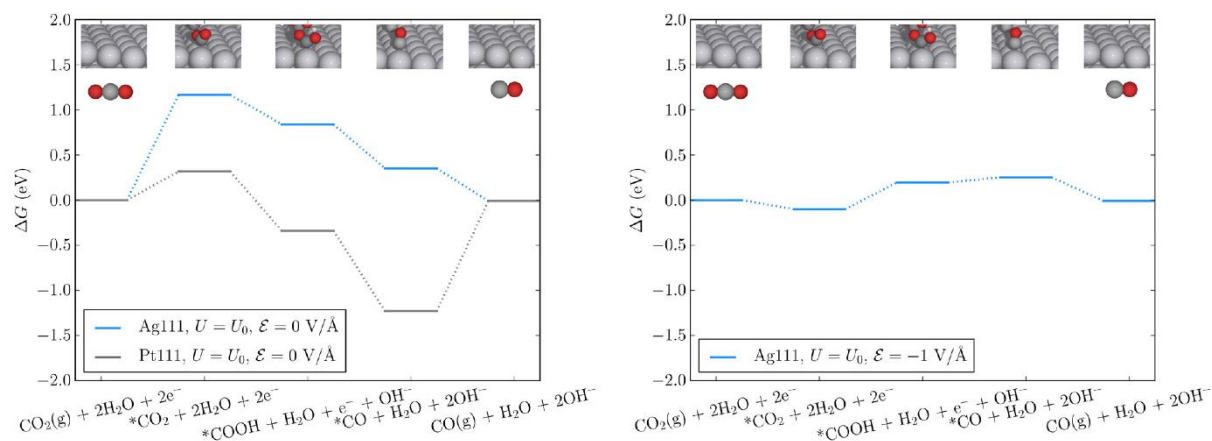


Figure 1.5. Effect of field stabilization on the CO₂RR. Left: Ag(111) and Pt(111) without field stabilization. Right: Ag(111) with field stabilization. Adapted from ref. 111.

The scope of active ILs able to co-catalyze the CO₂RR is not limited to Im ILs (Figure 1.6). Pyrazolium-based ILs are stable co-catalysts that result in quantitative Faradaic efficiencies for CO at high current densities.¹¹³ Fully substituted pyrazolium cations display good performance in the CO₂RR, which opposes pyrazolium CO₂ adduct formation and supports modification of the electric double layer as the most possible origin of the co-catalytic activity. An study probing different cations in the CO₂RR revealed Im and pyrrolidinium ILs as the most active compounds from the range tested (Figure 1.6).⁸⁶

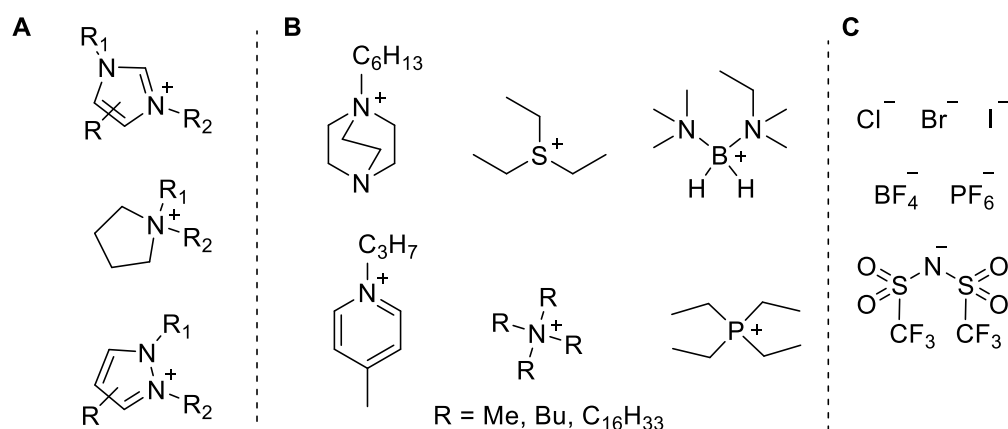


Figure 1.6. Ionic promoters probed for the CO₂RR. A: The most active co-catalysts cations. B: Other organic salt cations. C: Anions used in the study.

N-alkylpyridinium ILs do not act as co-catalysts for the CO₂RR when used with the most widespread electrode materials.^{32,60} However, some N-arylpyridinium salts do behave as co-catalysts with Cu electrodes.¹¹⁴ It was found that the arylpyridinium salts serve as precatalysts and form deposits on

the electrode during the reduction, which increases the selectivity for C₂ products, yielding C₂H₄ (FE_{C₂H₄} = 41%) and C₂H₅OH (FE_{C₂H₅OH} ≤ 27%). N-butyl pyridine and protonated pyridine did not show such activity, which is consistent with the previous reports (see above).

In general, ILs are characterized by their low volatility,⁷³ which significantly simplifies their utilization, but can hamper recycling. To overcome this issue an approach for the CO₂RR was devised that employed the distillable IL dimethylammonium dimethylcarbamate as the medium for the reduction.¹¹⁵ This IL, derived from dimethylamine and CO₂, breaks down at 60°C into volatile components that can be easily removed.¹¹⁶ Optimum results were obtained using dimethylammonium dimethylcarbamate with In as the electrode material, yielding CO (FE = 44.5%) and formate (FE = 39.7%) as the predominant products of the reduction.

1.5 Functionalized Ionic Liquids and Deep Eutectic Solvents

Functionalized ILs were also explored in the CO₂RR with, for example, hydroxy-tagged ILs showing higher co-catalytic activity compared to simple (alkyl) ILs.¹¹⁷ Introduction of the OH-group lowers the reduction onset potential by 70 mV compared to structurally related unfunctionalized analogues. This observation is in accordance with other studies based on homogeneous metal catalysis, which show that hydroxyl groups in proximity to metal catalyst facilitate the reduction of CO₂.¹¹⁸ Therefore, the presence of hydroxyl groups in the proximity of the electrode surface presumably enhances the CO₂RR. To ensure close proximity of the hydroxy-group with the electrode, the cation should be modified with the group since the cations associate with the electrode, and in this context choline derivatives represent a naturally occurring class of cations endowed with a OH-group. Moreover, choline chloride is the basic component of deep eutectic solvents (DESS), which resemble ILs in many ways, i.e. similar conductivities, low volatilities, high solubility of CO₂, etc.^{119–121} The impact of choline chloride on several electrochemical reactions including the CO₂RR was reported.¹²² Choline chloride was used in aqueous bicarbonate solutions, which provided the pH necessary for the reduction and served as a source of CO₂. However, the reduction process was investigated by CV only, without information on electrolysis and the product distribution. Subsequently, choline chloride and choline chloride/urea (1/2) based electrolytes mixed with KCl (to improve conductivity) were shown to slightly improve the FE_{CO} compared to pure KCl electrolyte.⁹⁸ However, the j_{CO} value remained the same for both choline/KCl and pure KCl electrolytes at the same potentials. The influence of choline additives on the reduction onset potential was not investigated (CV data was not

presented), and addition of urea (the second component of the DES) did not result in any improvement compared to pure choline chloride. However, the effect of the choline derivatives might not be pronounced in aqueous solutions where the impact of the OH group is diminished. Choline chloride tends to be poorly soluble in acetonitrile, frequently used for electrochemistry, which hampers its application.¹²³ The solubility of choline chloride can be increased in organic solvents by employing the DES principle, i.e. harnessing strong interactions between the chloride and ethylene glycol (as hydrogen bond donor).¹²³ The resulting systems showed high selectivities for CO (FE_{CO} up to 100%) and lowered onset potentials.

While organic promoters of the CO_2RR are largely limited to the classes described above, there are, however, several systems which have not been mentioned thus far, but are of relevance. For instance, attempts to reduce CO_2 in monoethanolamine were made,¹²⁴ since monoethanolamine is an industrial solvent used to capture CO_2 .¹²⁵ Reduction was highly dependent on the employed electrode (smooth metal electrodes based on silver - $FE_{CO} = 33.4\%$, $FE_{HCOO^-} = 2.0\%$ at -0.8 V and indium - $FE_{CO} = 17.0\%$, $FE_{HCOO^-} = 45.4\%$ at -0.8 V were evaluated. The activity was significantly improved when porous metal electrodes were used or surfactants (e.g. CTAB) added. In an investigation of silver-base complexes in the CO_2RR , it was found that the base alone, i.e. 3,5-diamino-1,2,4-triazole (DAT), decreased the reduction overpotential and increased the current density and Faradaic efficiency for CO formation when used with Ag/C electrodes.¹²⁶ The co-catalytic effect of DAT was attributed to weakening of the CO-bond at the silver electrode and to the suppression of HER.¹²⁷

1.6 Summary

Active organic systems for the CO_2RR can be divided into three main groups, i.e. redox shuttles forming radicals, organic hydrides and ionic compounds. Electron shuttles appear to be the catalysts of choice for the synthesis of oxalate and in general require high overpotentials, which can be adjusted by tuning of the shuttle structure. The application of organic hydrides results in the formation of formate, and the applicability of the catalyst is defined by the hydricity of the hydride and ease of its regeneration on the electrode. Ionic systems tune the activity of the actual reduction catalyst, i.e. the electrode, and can be used for a synthesis of various products (CO, formate and methane are the most widespread outcomes). The activity of this system depends on the properties of the double layer formed in the reduction process, and the activity of the catalyst can be improved by introduction of the functional groups (e.g. OH).

As the origin of the catalytic and co-catalytic activities of organic systems become unraveled, rational design of the promoters becomes possible and can be achieved using the same principles applied to the rational design of traditional organic catalysis. Indeed, transferring concepts from organic chemistry to electrochemistry could be fruitful.

Importantly, the evaluation of different organic promoters should take into account that the formation of reactive intermediates can result in various side reactions, which hamper analysis of the system. The data from cyclic voltammetry experiments and electrolysis should be corrected for the uncompensated resistance and followed by careful analysis of the reduction products with the application of internal standards in order to avoid errors. To provide unambiguous conclusions on the applicability of organic promoters for industrial CO₂RR, their performance must also be assessed at high current densities ($> 200 \text{ mA/cm}^2$).¹²⁸ Based on the versatility of organic promoters and the ease of tuning the microenvironment of the electrode using them, significant improvements in activity can be envisaged, which may lead to industrial applications.

1.7 References

- (1) Figueres, C.; Le Quéré, C.; Mahindra, A.; Bäte, O.; Whiteman, G.; Peters, G.; Guan, D. Emissions Are Still Rising: Ramp up the Cuts. *Nature* **2018**, *564*, 27–30.
- (2) Peter, S. C. Reduction of CO₂ to Chemicals and Fuels: A Solution to Global Warming and Energy Crisis. *ACS Energy Lett.* **2018**, *3*, 1557–1561.
- (3) Whipple, D. T.; Kenis, P. J. a. Prospects of CO₂ Utilization via Direct Heterogeneous Electrochemical Reduction. *J. Phys. Chem. Lett.* **2010**, *1* (24), 3451–3458.
- (4) Oh, Y.; Hu, X. Organic Molecules as Mediators and Catalysts for Photocatalytic and Electrocatalytic CO₂ Reduction. *Chem. Soc. Rev.* **2013**, *42* (6), 2253–2261.
- (5) Costentin, C.; Robert, M.; Savéant, J.-M. Catalysis of the Electrochemical Reduction of Carbon Dioxide. *Chem. Soc. Rev.* **2013**, *42*, 2423–2436.
- (6) Qiao, J.; Liu, Y.; Hong, F.; Zhang, J. A Review of Catalysts for the Electroreduction of Carbon Dioxide to Produce Low-Carbon Fuels. *Chem. Soc. Rev.* **2014**, *43*, 631.
- (7) Francke, R.; Schille, B.; Roemelt, M. Homogeneously Catalyzed Electroreduction of Carbon Dioxide - Methods, Mechanisms, and Catalysts. *Chem. Rev.* **2018**, *118*, 4631–4701.
- (8) Durst, J.; Rudnev, A.; Dutta, A.; Fu, Y.; Herranz, J.; Kaliginedi, V.; Kuzume, A.; Permyakova, A. A.; Paratcha, Y.; Broekmann, P.; et al. Electrochemical CO₂ Reduction – A Critical View on Fundamentals, Materials and Applications. *Chimia* **2015**, *69*, 769–776.
- (9) Weekes, D. M.; Salvatore, D. A.; Reyes, A.; Huang, A.; Berlinguette, C. P.; Blusson, S. Electrolytic CO₂ Reduction in a Flow Cell. *Acc. Chem. Res* **2018**, *51*, 910–918.
- (10) Finn, C.; Schnittger, S.; Yellowlees, L. J.; Love, J. B. Molecular Approaches to the Electrochemical Reduction of Carbon Dioxide. *Chem. Commun.* **2012**, *48* (10), 1392–1399.
- (11) Mao, X.; Hatton, T. A. Recent Advances in Electrocatalytic Reduction of Carbon Dioxide Using Metal-Free Catalysts. *Ind. Eng. Chem. Res* **2015**, *54*, 4033–4042.
- (12) Chiranjeevi, P.; Bulut, M.; Breugelmans, T.; Patil, S. A.; Pant, D. Current Trends in Enzymatic Electrosynthesis for CO₂ Reduction. *Curr. Opin. Green Sustain. Chem.* **2019**, *16*, 65–70.

-
- (13) Kalyanasundaram, K.; Graetzel, M. Artificial Photosynthesis : Biomimetic Approaches to Solar Energy Conversion and Storage. *Curr. Opin. Biotechnol.* **2010**, *21* (3), 298–310.
- (14) Kumar, B.; Llorente, M.; Froehlich, J.; Dang, T.; Sathrum, A.; Kubiak, C. P. Photochemical and Photoelectrochemical Reduction of CO₂. *Annu. Rev. Phys. Chem.* **2012**, *63*, 541–569.
- (15) Kalamaras, E.; Maroto-Valer, M. M.; Shao, M.; Xuan, J.; Wang, H. Solar Carbon Fuel via Photoelectrochemistry. *Catal. Today* **2018**, *317*, 56–75.
- (16) Benson, E. E.; Kubiak, C. P.; Sathrum, A. J.; Smieja, J. M. Electrocatalytic and Homogeneous Approaches to Conversion of CO₂ to Liquid Fuels. *Chem. Soc. Rev* **2009**, *38* (1), 89–99.
- (17) Rosen, B. A.; Salehi-Khojin, A.; Thorson, M. R.; Zhu, W.; Whipple, D. T.; Kenis, P. J. A.; Masel, R. I. Ionic Liquid – Mediated Selective Conversion of CO₂ to CO at Low Overpotentials. *Science* **2011**, *334*, 643–644.
- (18) Taniguchi, I.; Aurian-Blajeni, B.; Bockris, J. O. Photo-Aided Reduction of Carbon Dioxide to Carbon Monoxide. *J. Electroanal. Chem. Interfacial Electrochem.* **1983**, *157* (1), 179–182.
- (19) Taniguchi, I.; Aurian-Blajeni, B.; Bockris, J. O. The Mediation of the Photoelectrochemical Reduction of Carbon Dioxide by Ammonium Ions. *J. Electroanal. Chem. Interfacial Electrochem.* **1984**, *161* (2), 385–388.
- (20) Bockris, J. O.; Wass, J. C. The Photoelectrocatalytic Reduction of Carbon Dioxide. *J. Electrochem. Soc.* **1989**, *136* (9), 2521.
- (21) Berto, T. C.; Zhang, L.; Hamers, R. J.; Berry, J. F. Electrolyte Dependence of CO₂ Electroreduction: Tetraalkylammonium Ions Are Not Electrocatalysts. *ACS Catal.* **2015**, *5*, 703–707.
- (22) Filardo, G.; Gambino, S.; Silvestri, G.; Gennaro, A.; Vianello, E. Electrocarboxylation of Styrene through Homogeneous Redox Catalysis. *J. Electroanal. Chem. Interfacial Electrochem.* **1984**, *177* (1–2), 303–309.
- (23) Gennaro, A.; Isse, A. A.; Severin, M.-G.; Vianello, E.; Bhugun, I.; Savéant, J.-M. Mechanism of the Electrochemical Reduction of Carbon Dioxide at Inert Electrodes in Media of Low Proton Availability. *J. Chem. Soc., Faraday Trans.* **1996**, *92* (20), 3963–3968.

- (24) Gennaro, A.; Isse, A. A.; Savéant, J.-M.; Severin, M.-G.; Vianello, E. Homogeneous Electron Transfer Catalysis of the Electrochemical Reduction of Carbon Dioxide. Do Aromatic Anion Radicals React in an Outer-Sphere Manner? *J. Am. Chem. Soc.* **1996**, *118*, 7190–7196.
- (25) Savéant, J. Molecular Catalysis of Electrochemical Reactions . Mechanistic Aspects. **2008**, 2348–2378.
- (26) Koshechko, V. G.; Lopushanskaya, V. A. Electrochemical Conversion of Carbon Dioxide Catalyzed by Benzil. *Theor. Exp. Chem.* **2006**, *42* (1), 33–36.
- (27) Ghobadi, K.; Zare, H. R.; Khoshro, H.; Jafari, A. A. Excellent Electrocatalytic Activity of Benzil for Direct Reduction of CO₂ as Well as Indirect Reduction of Pyridine: A Kinetic View of the Electrocarboxylation Process. *J. Energy Chem.* **2017**, *26* (3), 569–573.
- (28) Ghobadi, K.; Zare, H. R.; Gorji, A.; Benvidi, A. Electrochemical Activation of CO₂ by a Di-Schiff Base of N, N'-Bis(2-Hydroxy-1-Naphthaldehyde)-m-Phenylenediimine. *Polyhedron* **2018**, *155*, 13–19.
- (29) Ghobadi, K.; Zare, H. R.; Khoshro, H.; Gorji, A. Communication—Electrosynthesis of Isonicotinic Acid via Indirect Electrochemical Reduction of Pyridine in the Presence of CO₂. *J. Electrochem. Soc.* **2016**, *163* (3), H240–H242.
- (30) Wawzonek, S.; Gundersen, A. Polarographic Studies in Acetonitrile and Dimethylformamide V. Behavior of Aromatic Ketones and Aldehydes. *J. Electrochem. Soc.* **1960**, *107*, 537–540.
- (31) Zhao, S.-F.; Horne, M.; Bond, A. M.; Zhang, J. Electrocarboxylation of Acetophenone in Ionic Liquids: The Influence of Proton Availability on Product Distribution. *Green Chem.* **2014**, *16* (4), 2242–2251.
- (32) Seshadri, G.; Lin, C.; Bocarsly, A. B. A New Homogeneous Electrocatalyst for the Reduction of Carbon Dioxide to Methanol at Low Overpotential. *J. Electroanal. Chem.* **1994**, *372* (1–2), 145–150.
- (33) Barton Cole, E.; Lakkaraju, P. S.; Rampulla, D. M.; Morris, A. J.; Abelev, E.; Bocarsly, A. B.; Cole, E. B.; Lakkaraju, P. S.; Rampulla, D. M.; Morris, A. J.; et al. Using a One-Electron Shuttle for the Multielectron Reduction of CO₂ to Methanol: Kinetic, Mechanistic, and Structural Insights. *J.*

Am. Chem. Soc. **2010**, *132* (33), 11539–11551.

- (34) Barton, E. E.; Rampulla, D. M.; Bocarsly, A. B. Selective Solar-Driven Reduction of CO₂ to Methanol Using a Catalyzed p-GaP Based Photoelectrochemical Cell. *J. AM. CHEM. SOC* **2008**, *130*, 6342–6344.
- (35) Bocarsly, A. B.; Gibson, Q. D.; Morris, A. J.; L'esperance, R. P.; Detweiler, Z. M.; Lakkaraju, P. S.; Zeitler, E. L.; Shaw, T. W. Comparative Study of Imidazole and Pyridine Catalyzed Reduction of Carbon Dioxide at Illuminated Iron Pyrite Electrodes. *ACS Catal.* **2012**, *2*, 1684–1692.
- (36) Xu, S.; Li, L.; Carter, E. A. Why and How Carbon Dioxide Conversion to Methanol Happens on Functionalized Semiconductor Photoelectrodes. *J. Am. Chem. Soc.* **2018**, *140*, 16749–16757.
- (37) Barton Cole, E. E.; Baruch, M. F.; L'Esperance, R. P.; Kelly, M. T.; Lakkaraju, P. S.; Zeitler, E. L.; Bocarsly, A. B. Substituent Effects in the Pyridinium Catalyzed Reduction of CO₂ to Methanol: Further Mechanistic Insights. *Top. Catal.* **2015**, *58* (1), 15–22.
- (38) Lee, J. H. Q.; Lauw, S. J. L.; Webster, R. D. The Electrochemical Reduction of Carbon Dioxide (CO₂) to Methanol in the Presence of Pyridoxine (Vitamin B6). *Electrochem. commun.* **2016**, *64*, 69–73.
- (39) Portenkirchner, E.; Enengl, C.; Enengl, S.; Hinterberger, G.; Schlager, S.; Apaydin, D.; Neugebauer, H.; Knör, G.; Sariciftci, N. S. A Comparison of Pyridazine and Pyridine as Electrocatalysts for the Reduction of Carbon Dioxide to Methanol. *ChemElectroChem* **2014**, *1* (9), 1543–1548.
- (40) Xiang, D.; Magana, D.; Dyer, R. B. CO₂ Reduction Catalyzed by Mercaptopteridine on Glassy Carbon. *J. Am. Chem. Soc.* **2014**, *136*, 14007–14010.
- (41) Saveant, J.-M.; Tard, C. C. Attempts To Catalyze the Electrochemical CO₂-to-Methanol Conversion by Biomimetic 2e⁻ + 2H⁺ Transferring Molecules. *J. Am. Chem. Soc.* **2015**, *138*, 1017–1021.
- (42) Lim, C.-H.; Holder, A. M.; Hynes, J. T.; Musgrave, C. B. Dihydropteridine/Pteridine as a 2H⁺/2e⁻ Redox Mediator for the Reduction of CO₂ to Methanol: A Computational Study. *J. Phys. Chem. B* **2017**, *121*, 4158–4167.

- (43) Morris, A. J.; McGibbon, R. T.; Bocarsly, A. B. Electrocatalytic Carbon Dioxide Activation: The Rate-Determining Step of Pyridinium-Catalyzed CO₂ Reduction. *ChemSusChem* **2011**, 4 (2), 191–196.
- (44) Lim, C.-H.; Holder, A. M.; Musgrave, C. B. Mechanism of Homogeneous Reduction of CO₂ by Pyridine: Proton Relay in Aqueous Solvent and Aromatic Stabilization. *J. Am. Chem. Soc.* **2012**, 135, 142–154.
- (45) Kamrath, M. Z.; Relph, R. A.; Johnson, M. A. Vibrational Predissociation Spectrum of the Carbamate Radical Anion, C₅H₅N-CO₂⁻, Generated by Reaction of Pyridine with (CO₂)_m⁻. *J. Am. Chem. Soc.* **2010**, 132, 15508–15511.
- (46) Tossell, J. A. Calculation of the Properties of Molecules in the Pyridine Catalyst System for the Photochemical Conversion of CO₂ to Methanol. *Comput. Theor. Chem.* **2011**, 977 (1–3), 123–127.
- (47) Ertem, M. Z.; Konezny, S. J.; Moyses Araujo, C.; Batista, V. S. Functional Role of Pyridinium during Aqueous Electrochemical Reduction of CO₂ on Pt(111). *J. Phys. Chem. Lett.* **2013**, 4, 745–748.
- (48) Keith, J. A.; Carter, E. A. Theoretical Insights into Pyridinium-Based Photoelectrocatalytic Reduction of CO₂. *J. Am. Chem. Soc.* **2012**, 134, 17.
- (49) Lim, C.-H.; Holder, A. M.; Hynes, J. T.; Musgrave, C. B. Reduction of CO₂ to Methanol Catalyzed by a Biomimetic Organo-Hydride Produced from Pyridine. *J. Am. Chem. Soc.* **2014**, 136, 16081–16095.
- (50) Keith, J.; Carter, E. Theoretical Insights into Electrochemical CO₂ Reduction Mechanisms Catalyzed by Surface Bound Nitrogen Heterocycles. *J. Phys. Chem. Lett.* **2013**, 4, 4058 – 4063.
- (51) Keith, J. A.; Carter, E. A. Electrochemical Reactivities of Pyridinium in Solution: Consequences for CO₂ Reduction Mechanisms. *Chem. Sci.* **2013**, 4 (4), 1490.
- (52) Lessio, M.; Carter, E. A. What Is the Role of Pyridinium in Pyridine-Catalyzed CO₂ Reduction on p-GaP Photocathodes? *J. Am. Chem. Soc.* **2015**, 137, 13251.
- (53) Alherz, A.; Lim, C.-H.; Kuo, Y.-C.; Lehman, P.; Cha, J.; Hynes, J. T.; Musgrave, C. B. Renewable

Hydride Donors for the Catalytic Reduction of CO₂ : A Thermodynamic and Kinetic Study. **2018**.

- (54) Lim, C.-H.; Holder, A. M.; Hynes, J. T.; Musgrave, C. B. Catalytic Reduction of CO₂ by Renewable Organohydrides. *J. Phys. Chem. Lett* **2015**, *6*, 42.
- (55) Giesbrecht, P. K.; Herbert, D. E. Electrochemical Reduction of Carbon Dioxide to Methanol in the Presence of Benzannulated Dihydropyridine Additives. *ACS Energy Lett.* **2017**, *2*, 549–555.
- (56) Costentin, C.; Canales, J. C.; Haddou, B.; Saveánt, J.-M. Electrochemistry of Acids on Platinum. Application to the Reduction of Carbon Dioxide in the Presence of Pyridinium Ion in Water. *J. Am. Chem. Soc* **2013**, *11*, 31.
- (57) Lucio, A. J.; Shaw, S. K. Pyridine and Pyridinium Electrochemistry on Polycrystalline Gold Electrodes and Implications for CO₂ Reduction. *J. Phys. Chem. C* **2015**, *119*, 25.
- (58) Crețu, R.; Kellenberger, A.; Vasilcsin, N. Enhancement of Hydrogen Evolution Reaction on Platinum Cathode by Proton Carriers. *Int. J. Hydrogen Energy* **2013**, *38* (27), 11685–11694.
- (59) Peroff, A. G.; Weitz, E.; Van Duyne, R. P. Mechanistic Studies of Pyridinium Electrochemistry: Alternative Chemical Pathways in the Presence of CO₂. *Phys. Chem. Chem. Phys.* **2016**, *18* (3), 1578–1586.
- (60) Lebègue, E.; Agullo, J.; Bélanger, D. Electrochemical Behavior of Pyridinium and *N*-Methyl Pyridinium Cations in Aqueous Electrolytes for CO₂ Reduction. *ChemSusChem* **2018**, *11* (1), 219–228.
- (61) Olu, P.-Y.; Li, Q.; Krischer, K. The True Fate of Pyridinium in the Reportedly Pyridinium-Catalyzed Carbon Dioxide Electroreduction on Platinum. *Angew. Chemie* **2018**, *130* (45), 14985–14988.
- (62) Costentin, C.; Saveánt, J.-M.; Cédric Tard, C. Catalysis of CO₂ Electrochemical Reduction by Protonated Pyridine and Similar Molecules. Useful Lessons from a Methodological Misadventure. *ACS Energy Lett.* **2018**, *3*, 695–703.
- (63) Dunwell, M.; Yan, Y.; Xu, B. In Situ Infrared Spectroscopic Investigations of Pyridine-Mediated CO₂ Reduction on Pt Electrocatalysts. *ACS Catal.* **2017**, *7*, 5410–5419.

- (64) Feaster, J. T.; Jongerius, A. L.; Liu, X.; Urushihara, M.; Nitopi, S. A.; Hahn, C.; Chan, K.; Nørskov, J. K.; Jaramillo, T. F. Understanding the Influence of [EMIM]Cl on the Suppression of the Hydrogen Evolution Reaction on Transition Metal Electrodes.
- (65) Von Wolff, N.; Lefè, G.; Berthet, J.-C.; Thuéry, P. T.; Cantat, T. Implications of CO₂ Activation by Frustrated Lewis Pairs in the Catalytic Hydroboration of CO₂ : A View Using N/Si⁺ Frustrated Lewis Pairs. *ACS Catal.* **2016**, *6*, 4526–4535.
- (66) Knopf, I.; Cummins, C. C. Revisiting CO₂ Reduction with NaBH₄ under Aprotic Conditions: Synthesis and Characterization of Sodium Triformatoborohydride. *Organometallics* **2015**, *34*, 1601–1603.
- (67) Lim, C.-H.; Ilic, S.; Alherz, A.; Worrell, B. T.; Bacon, S. S.; Hynes, J. T.; Glusac, K. D.; Musgrave, C. B. Benzimidazoles as Metal-Free and Recyclable Hydrides for CO₂ Reduction to Formate. *J. Am. Chem. Soc.* **2019**, *141*, 272–280.
- (68) Marjolin, A.; Keith, J. a. Thermodynamic Descriptors for Molecules That Catalyze Efficient CO₂ Electroreductions. *ACS Catal.* **2015**, *5* (2), 1123–1130.
- (69) Faggion, D.; Gonçalves, W. D. G.; Dupont, J. CO₂ Electroreduction in Ionic Liquids. *Front. Chem.* **2019**, *7*, 102.
- (70) Watanabe, M.; Thomas, M. L.; Zhang, S.; Ueno, K.; Yasuda, T.; Dokko, K. Application of Ionic Liquids to Energy Storage and Conversion Materials and Devices. *Chem. Rev.* **2017**, *117*, 7190–7239.
- (71) Hayyan, M.; Mjalli, F. S.; Hashim, M. A.; AlNashef, I. M.; Mei, T. X. Investigating the Electrochemical Windows of Ionic Liquids. *J. Ind. Eng. Chem.* **2013**, *19* (1), 106–112.
- (72) Hapiot, P.; Lagrost, C. Electrochemical Reactivity in Room-Temperature Ionic Liquids. *Chem. Rev.* **2008**, *108*, 2238–2264.
- (73) Earle, M. J.; Esperança, J. M. S. S.; Gilea, M. A.; Lopes, J. N. C.; Rebelo, L. P. N.; Magee, J. W.; Seddon, K. R.; Widegren, J. A. The Distillation and Volatility of Ionic Liquids. *Nature* **2006**, *439* (831–834).
- (74) Lei, Z.; Dai, C.; Chen, B. Gas Solubility in Ionic Liquids. *Chem. Rev.* **2013**, *114* (2), 1289–1326.

- (75) Tanner, E. E. L.; Batchelor-Mcauley, C.; Compton, R. G. Carbon Dioxide Reduction in Room-Temperature Ionic Liquids: The Effect of the Choice of Electrode Material, Cation, and Anion. *J. Phys. Chem. C* **2016**, *120*, 26442–26447.
- (76) Sun, L.; Ramesha, G. K.; Kamat, P. V.; Brennecke, J. F. Switching the Reaction Course of Electrochemical CO₂ Reduction with Ionic Liquids. *Langmuir* **2014**, *30*, 6302–6308.
- (77) Wang, Y.; Hatakeyama, M.; Ogata, K.; Wakabayashi, M.; Jin, F.; Nakamura, S. Activation of CO₂ by Ionic Liquid EMIM–BF₄ in the Electrochemical System: A Theoretical Study. *Phys. Chem. Chem. Phys.* **2015**, *17*, 23521–23531.
- (78) Arduengo, A. J. I.; Harlow, R. L.; Kline, M. A Stable Crystalline Carbene. *J. Am. Chem. Soc.* **1991**, *113*, 361–363.
- (79) Herrmann, W. A.; Köcher, C. N-Heterocyclic Carbenes. *Angew. Chemie Int. Ed. English* **1997**, *36* (20), 2162–2187.
- (80) Köster, F.; Dinjus, E.; Duñach, E. Electrochemical Selective Incorporation of CO₂ into Terminal Alkynes and Diynes. *European J. Org. Chem.* **2001**, *2001* (13), 2507–2511.
- (81) Gorodetsky, B.; Ramnial, T.; Branda, N. R.; Clyburne, J. A. C. Electrochemical Reduction of an Imidazolium Cation: A Convenient Preparation of Imidazol-2-Ylidenes and Their Observation in an Ionic Liquid. *Chem. Commun.* **2004**, *0* (17), 1972.
- (82) Feroci, M.; Chiarotto, I.; Forte, G.; Vecchio Cipriotti, S.; Inesi, A. Stability and CO₂ Capture Ability of Electrogenenerated N -Heterocyclic Carbene in Parent 1-Butyl-3-Methylimidazolium Ionic Liquid (BMIm-X): The Role of X⁻. *ChemElectroChem* **2014**, *1* (8), 1407–1414.
- (83) Duong, H. A.; Tekavec, T. N.; Arif, A. M.; Louie, J. Reversible Carboxylation of N-Heterocyclic Carbenes. *Chem. Commun.* **2004**, *0* (1), 112.
- (84) Guillaume, de R.; H. Devillers, C.; Kunz, D.; Cattey, H.; Digard, E.; Andrieu, J. Electrosynthesis of Imidazolium Carboxylates. *Org. Lett.* **2013**, *15* (17), 4410–4413.
- (85) Riduan, S. N.; Zhang, Y.; Ying, J. Y. Conversion of Carbon Dioxide into Methanol with Silanes over N-Heterocyclic Carbene Catalysts. *Angew. Chemie Int. Ed.* **2009**, *48* (18), 3322–3325.

- (86) Zhao, S.-F.; Horne, M.; Bond, A. M.; Zhang, J. Is the Imidazolium Cation a Unique Promoter for Electrocatalytic Reduction of Carbon Dioxide? *J. Phys. Chem. C* **2016**, *120*, 23989–24001.
- (87) Watkins, J. D.; Bocarsly, A. B. Direct Reduction of Carbon Dioxide to Formate in High-Gas-Capacity Ionic Liquids at Post-Transition-Metal Electrodes. *ChemSusChem* **2014**, *7* (1), 284–290.
- (88) Holbrey, J. D.; Reichert, W. M.; Tkatchenko, I.; Bouajila, E.; Walter, O.; Tommasi, I.; Rogers, R. D. 1,3-Dimethylimidazolium-2-Carboxylate: The Unexpected Synthesis of an Ionic Liquid Precursor and Carbene-CO₂ Adduct. *Chem. Commun.* **2003**, *347* (1), 28–29.
- (89) Lau, G. P. S.; Schreier, M.; Vasilyev, D.; Scopelliti, R.; Grätzel, M.; Dyson, P. J. New Insights into the Role of Imidazolium-Based Promoters for the Electroreduction of CO₂ on a Silver Electrode. *J. Am. Chem. Soc.* **2016**, *138*, 7820–7823.
- (90) Wang, Q.; Chen, A. C.; Zhong, A. J.; Zhang, C. B. Effect of Alkyl Chain Length of Imidazolium Cation on the Electroreduction of CO₂ to CO on Ag Electrode in Acetonitrile. *Aust. J. Chem.* **2016**, *70*, 293–300.
- (91) Lim, H.-K.; Kwon, Y.; Kim, H. S.; Jeon, J.; Kim, Y.-H.; Lim, J.-A.; Kim, B.-S.; Choi, J.; Kim, H. Insight into the Microenvironments of the Metal–Ionic Liquid Interface during Electrochemical CO₂ Reduction. *ACS Catal.* **2018**, *8*, 2420–2427.
- (92) Rudnev, A. V.; Zhumaev, U. E.; Kuzume, A.; Vesztergom, S.; Furrer, J.; Broekmann, P.; Wandlowski, T. The Promoting Effect of Water on the Electroreduction of CO₂ in Acetonitrile. *Electrochim. Acta* **2016**, *189*, 38–44.
- (93) Rudnev, A. V.; Fu, Y.-C.; Gjuroski, I.; Stricker, F.; Furrer, J.; Kovács, N.; Vesztergom, S.; Broekmann, P. Transport Matters: Boosting CO₂ Electroreduction in Mixtures of [BMIm][BF₄]/Water by Enhanced Diffusion. *ChemPhysChem* **2017**, *18* (22), 3153–3162.
- (94) Rosen, B. A.; Zhu, W.; Kaul, G.; Salehi-Khojin, A.; Masel, R. I. Water Enhancement of CO₂ Conversion on Silver in 1-Ethyl-3-Methylimidazolium Tetrafluoroborate. *J. Electrochem. Soc.* **2012**, *160* (2), H138–H141.
- (95) Hailu, A.; Shaw, S. K. Efficient Electrocatalytic Reduction of Carbon Dioxide in 1-Ethyl-3-

- Methylimidazolium Trifluoromethanesulfonate and Water Mixtures. *Energy Fuels* **2018**, *32*, 12695–12702.
- (96) Figueiredo, M. C.; Ledezma-Yanez, I.; Koper, M. T. M. In Situ Spectroscopic Study of CO₂ Electroreduction at Copper Electrodes in Acetonitrile. *ACS Catal.* **2016**, *6*, 2382–2392.
- (97) Resasco, J.; Lum, Y.; Clark, E.; Zeledon, J. Z.; Bell, A. T. Effects of Anion Identity and Concentration on Electrochemical Reduction of CO₂. *ChemElectroChem* **2018**, *5* (7), 1064–1072.
- (98) Verma, S.; Lu, X.; Ma, S.; Masel, R. I.; Kenis, P. J. A. The Effect of Electrolyte Composition on the Electroreduction of CO₂ to CO on Ag Based Gas Diffusion Electrodes. *Phys. Chem. Chem. Phys.* **2016**, *18*, 7075–7084.
- (99) Hsieh, Y.-C.; Senanayake, S. D.; Zhang, Y.; Xu, W.; Polyansky, D. E. Effect of Chloride Anions on the Synthesis and Enhanced Catalytic Activity of Silver Nanocoral Electrodes for CO₂ Electroreduction. *ACS Catal.* **2015**, *5* (9), 5349–5356.
- (100) Gao, D.; Scholten, F.; Roldan Cuenya, B. Improved CO₂ Electroreduction Performance on Plasma-Activated Cu Catalysts via Electrolyte Design: Halide Effect. *ACS Catal.* **2017**, *7*, 5112–5120.
- (101) Hollingsworth, N.; Taylor, S. F. R.; Galante, M. T.; Jacquemin, J.; Longo, C.; Holt, K. B.; De Leeuw, N. H.; Hardacre, C. Reduction of Carbon Dioxide to Formate at Low Overpotential Using a Superbase Ionic Liquid. *Angew. Chemie - Int. Ed.* **2015**, *54*, 14164–14168.
- (102) Hollingsworth, N.; Taylor, S. F. R.; Galante, M. T.; Jacquemin, J.; Longo, C.; Holt, K. B.; de Leeuw, N. H.; Hardacre, C.; Karl, T. R.; Trenberth, K. E.; et al. CO₂ Capture and Electrochemical Conversion Using Superbasic [P66614][124Triz]. *Faraday Discuss.* **2015**, *183* (0), 389–400.
- (103) Gurkan, B.; Goodrich, B. F.; Mindrup, E. M.; Ficke, L. E.; Massel, M.; Seo, S.; Senftle, T. P.; Wu, H.; Glaser, M. F.; Shah, J. K.; et al. Molecular Design of High Capacity, Low Viscosity, Chemically Tunable Ionic Liquids for CO₂ Capture. *J. Phys. Chem. Lett.* **2010**, *1* (24), 3494–3499.
- (104) Snuffin, L. L.; Whaley, L. W.; Yu, L. Catalytic Electrochemical Reduction of CO₂ in Ionic Liquid

EMIMBF₃Cl. *J. Electrochem. Soc.* **2011**, *158* (9), F155–F158.

- (105) Hartman, J. S.; Schrobilgen. Contribution from the Mixed Tetrahaloborate Ions. Detection and Study by Nuclear Magnetic Resonance. *Inorg. Chem.* **1972**, *11*(5), 940–951.
- (106) Tomita, Y.; Teruya, S.; Koga, O.; Hori, Y. Electrochemical Reduction of Carbon Dioxide at a Platinum Electrode in Acetonitrile-Water Mixtures. *J. Electrochem. Soc.* **2000**, *147*, 4164–4167.
- (107) Rosen, B. A.; Haan, J. L.; Mukherjee, P.; Braunschweig, B.; Zhu, W.; Salehi-Khojin, A.; Dlott, D. D.; Masel, R. I. In Situ Spectroscopic Examination of a Low Overpotential Pathway for Carbon Dioxide Conversion to Carbon Monoxide. *J. Phys. Chem. C* **2012**, *116*, 15307–15312.
- (108) van der Vliet, D.; Strmcnik, D. S.; Wang, C.; Stamenkovic, V. R.; Markovic, N. M.; Koper, M. T. M. On the Importance of Correcting for the Uncompensated Ohmic Resistance in Model Experiments of the Oxygen Reduction Reaction. *J. Electroanal. Chem.* **2010**, *647* (1), 29–34.
- (109) García Rey, N.; Dlott, D. D. Structural Transition in an Ionic Liquid Controls CO₂ Electrochemical Reduction. *J. Phys. Chem. C* **2015**, *119*, 20892–20899.
- (110) Urushihara, M.; Chan, K.; Shi, C.; Nørskov, J. K. Theoretical Study of EMIM⁺ Adsorption on Silver Electrode Surfaces. *J. Phys. Chem. C* **2015**, *119*, 20023–20029.
- (111) Chen, L. D.; Urushihara, M.; Chan, K.; Nørskov, J. K. Electric Field Effects in Electrochemical CO₂ Reduction. *ACS Catal.* **2016**, *6*, 7133–7139.
- (112) García Rey, N.; Dlott, D. D. Effects of Water on Low-Overpotential CO₂ Reduction in Ionic Liquid Studied by Sum-Frequency Generation Spectroscopy. *Phys. Chem. Chem. Phys. Phys. Chem. Chem. Phys.* **2017**, *19* (19), 10491–10501.
- (113) Vasilyev, D.; Shirzadi, E.; Rudnev, A. V.; Broekmann, P.; Dyson, P. J. Pyrazolium Ionic Liquid Co-Catalysts for the Electroreduction of CO₂. *ACS Appl. Energy Mater.* **2018**, *1*, 5124–5128.
- (114) Han, Z.; Kortlever, R.; Chen, H.-Y.; Peters, J. C.; Agapie, T. CO₂ Reduction Selective for C₂ Products on Polycrystalline Copper with N-Substituted Pyridinium Additives. *ACS Cent. Sci.* **2017**, *3*, 853–859.

- (115) Chen, L.; Guo, S.-X.; Li, F.; Bentley, C.; Horne, M.; Bond, A. M.; Zhang, J. Electrochemical Reduction of CO₂ at Metal Electrodes in a Distillable Ionic Liquid. *ChemSusChem* **2016**, *9*, 1271–1278.
- (116) Kreher, U.; Rosamilia, A.; Raston, C.; Scott, J.; Strauss, C.; Kreher, U. P.; Rosamilia, A. E.; Raston, C. L.; Scott, J. L.; Strauss, C. R. Self-Associated, “Distillable” Ionic Media. *Molecules* **2004**, *9* (6), 387–393.
- (117) Zhang, L.; Wu, N.; Zhang, J.; Hu, Y.; Wang, Z.; Zhuang, L.; Jin, X. Imidazolium Ions with an Alcohol Substituent for Enhanced Electrocatalytic Reduction of CO₂. *ChemSusChem* **2017**, *10* (24), 4824–4828.
- (118) Costentin, C.; Drouet, S.; Robert, M.; Savéant, J.-M. A Local Proton Source Enhances CO₂ Electroreduction to CO by a Molecular Fe Catalyst. *Science* **2012**, *338*, 90–94.
- (119) Zhang, Q.; De Oliveira Vigier, K.; Sebastien, R. F.; Jerome, F. Deep Eutectic Solvents : Syntheses, Properties and Applications. *Chem Soc Rev* **2012**, *41*, 7108–7146.
- (120) Smith, E. L.; Abbott, A. P.; Ryder, K. S. Deep Eutectic Solvents (DESs) and Their Applications. *Chem. Rev.* **2014**, *114* (21), 11060–11082.
- (121) Garcia, G.; Aparicio, S.; Ullah, R.; Atilhan, M. Deep Eutectic Solvents: Physicochemical Properties and Gas Separation Applications. *Energy Fuels* **2015**, *29*, 2616–2644.
- (122) Zhu, W.; Rosen, B. A.; Salehi-Khojin, A.; Masel, R. I. Monolayers of Choline Chloride Can Enhance Desired Electrochemical Reactions and Inhibit Undesirable Ones. *Electrochim. Acta* **2013**, *96*, 18–22.
- (123) Vasilyev, D. V.; Rudnev, A. V.; Broekmann, P.; Dyson, P. J. A General and Facile Paradigm for the Electrochemical Reduction of Carbon Dioxide Inspired by Deep Eutectic Solvents. *ChemSusChem* **2019**.
- (124) Chen, L.; Li, F.; Zhang, Y.; Bentley, C. L.; Horne, M.; Bond, A. M.; Zhang, J. Electrochemical Reduction of Carbon Dioxide in a Monoethanolamine Capture Medium. *ChemSusChem* **2017**, *10* (20), 4109–4118.
- (125) Rochelle, G. T. Amine Scrubbing for CO₂ Capture. *Science* **2009**, *325*, 1652–1654.

- (126) Tornow, C. E.; Thorson, M. R.; Ma, S.; Gewirth, A. A.; Kenis, P. J. A. Nitrogen-Based Catalysts for the Electrochemical Reduction of CO₂ to CO. *J. Am. Chem. Soc.* **2012**, 10–13.
- (127) Schmitt, K. G.; Gewirth, A. A. In Situ Surface-Enhanced Raman Spectroscopy of the Electrochemical Reduction of Carbon Dioxide on Silver with 3,5-Diamino-1,2,4-Triazole. *J. Phys. Chem. C* **2014**, 118, 17567–17576.
- (128) Burdyny, T.; Smith, W. A. CO₂ Reduction on Gas-Diffusion Electrodes and Why Catalytic Performance Must Be Assessed at Commercially-Relevant Conditions. *Energy Environ. Sci.* **2019**.

Chapter 2 Triazolium Ionic Liquids

2.1 Introduction

The origin of the promotion of the CO₂RR by imidazolium ILs (Im ILs) is still under discussion (see Chapter 1, 1.4). This ambiguity leads to a lack of clear recommendations towards the optimal structure of the Im co-catalyst, i.e. which functions should be present in which positions of the Im ring. To address that issue, we have explored the applicability of a range of the Im ILs with diverse substitution patterns (Figure 2.1 **A**) for the CO₂RR.¹

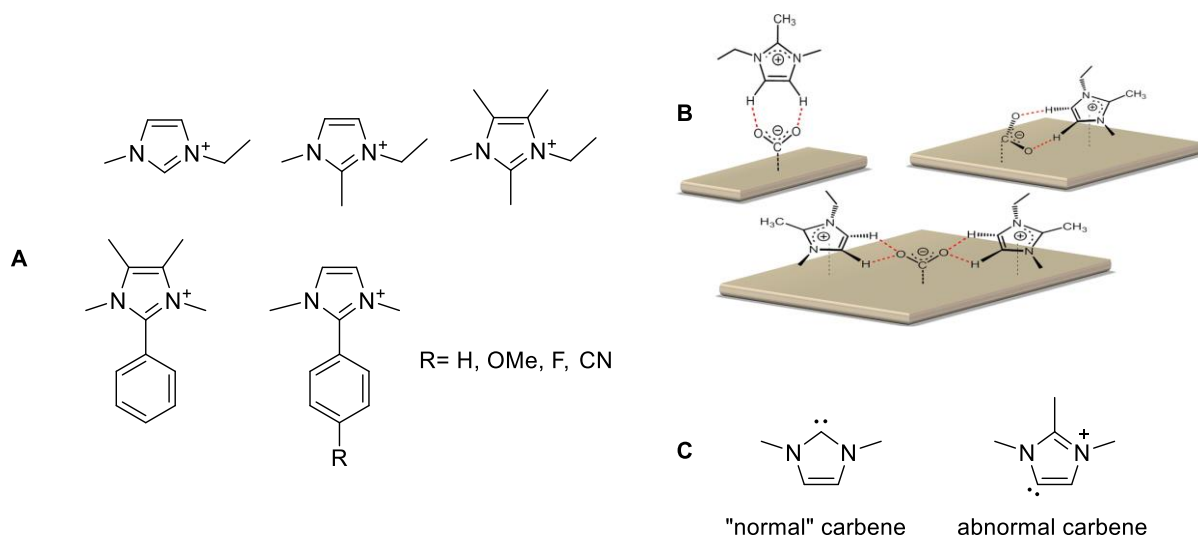


Figure 2.1. **A:** Substituted Im IL, used for the research. **B:** Hypothesized binding modes of CO₂ and Im ILs on the Ag electrode. **C:** "Normal" and abnormal carbenes.

It was clearly demonstrated that substitution in the C2 position of the Im core by alkyl or aromatic moieties improves the co-catalytic properties of the IL, whereas substituents at the C4 and C5 significantly decrease the performance of the system. We were able to relate the low activity of 4,5-substituted Im ILs to the possible binding modes of CO₂ with the IL cation on the surface of the silver electrode, where CO₂-based intermediates are stabilized by hydrogen bonding (Figure 2.1 **B**). Meanwhile, improved activity of 2-substituted Im ILs can be explained by suppression of alternative reduction pathways and side reactions. For instance, NHC formation is suppressed, which is considered as a parasite reaction as formation of the adduct of NHC and CO₂ is very stable and therefore

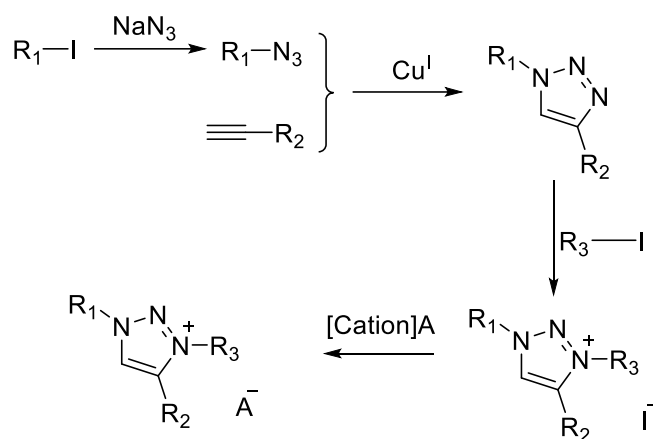
inhibits the CO₂RR. Carbenes can be formed from 2-substituted Im ILs as well (so-called abnormal carbenes, Figure 2.1 C), but their formation is less favorable compared to classic NHCs. The difference in stabilities and ease of formation for “normal” and abnormal NHCs can be illustrated by the fact that for coordination compounds abnormal binding accounts for only around 2% of the overall amount of characterized NHC-complexes.²

Thus, introduction of a substituent in the C2 position of the Im ring is beneficial for the catalysis, which contrasts with the assumptions that the CO₂-Im adduct plays an important role in the reduction. However, corresponding 2-substituted Im ILs are less available compared to the classic ionic liquids with 1-butyl-3-methylimidazolium ([BMIm]) cation, which hampers their application and makes them unattractive for the further development. To address this issue, we investigated a new class of ionic liquids, based on the 1,2,3-triazolium cation, since a wide and diverse range of substituents can be introduced into their structure with considerable ease.

In terms of structure, 1,2,3-triazolium ILs (further – Tz ILs) are similar to Im ILs and differ in the second position of the aromatic ring, where the carbon atom is replaced by nitrogen. This modification results in the absence of an acidic proton at the second position and, therefore, prevents the possibility of NHC formation. Moreover, the N2 atom possesses a lone pair and therefore can serve as weak nucleophile, which suggests additional binding modes for CO₂. Another advantage of the Tz derivatives is their availability by Huisgen cycloaddition (namely copper-catalyzed click reaction), which is a powerful and mild approach affording a range of substituted triazoles.³ Moreover, Tz ILs were reported to possess higher stability towards alkaline conditions compared to Im salts and decomposition potentials, suitable for the CO₂RR.⁴ To the best of our knowledge Tz ILs have not been applied as co-catalysts for the CO₂RR.

2.2 Results

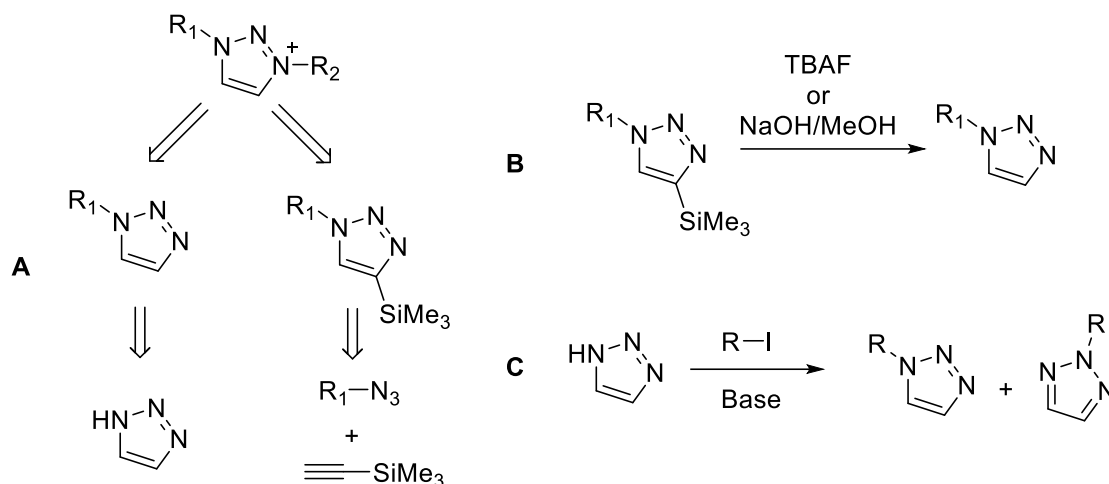
The approach for the synthesis of substituted Tz ILs is presented in Scheme 2.1. The starting organic azides are readily synthesized from corresponding iodides. While benzylazide is a stable high-boiling compound, butylazide is a flexible volatile liquid (bp = 71°C at 225 mm Hg),⁵ which tends to spontaneously explode under stress when pure.^{6,7} Therefore, for the next step butylazide was used directly as an ether extract without prior purification. The Tz core is synthesized by the Cu(I)-catalyzed 1,3-dipolar cycloaddition of terminal alkynes and azides. The reaction proceeds smoothly under ambient conditions, providing the corresponding triazoles in excellent yield. In the next step the triazoles are alkylated with iodomethane and the iodide anion exchanged for Tf₂N⁻ (TFSI) or BF₄⁻.



Scheme 2.1. Synthesis of 1,3,4-substituted Tz ILs.

Direct synthesis of 4,5-non-substituted Tz ILs using the click reaction is more challenging as acetylene (a gas) is required. To circumvent this issue two approaches have been suggested (Scheme 2.2 **A**). First, trimethylsilyl (TMS) acetylene can be employed as the alkyne component. After the cycloaddition reaction the TMS group is easily removed using either tetrabutylammonium fluoride (TBAF) or a methanolic solution of NaOH, yielding N-substituted triazoles (Scheme 2.2 **B**). The disadvantage of this approach is necessity to purify the products chromatographically, as it is demanding to separate the siloxane by-products by other means. Alternatively, 1H-1,2,3-triazole is commercially available and can be easily N-alkylated in the presence of bases. However, in this case 2-alkyltriazoles are formed as by-products along with the target 1-alkyltriazoles (Scheme 2.2 **C**). As a simple solution for the issue, we use the crude mixture in the subsequent alkylation step (towards 1,3-substituted Tz) without further purification. The 2-alkyltriazole is not alkylated under ambient conditions and was easily separated from the product by extraction with diethyl ether. Although

both approaches described above are valid, we mainly used the last one, starting from 1H-1,2,3-triazole.



Scheme 2.2. **A**: Retrosynthetic analysis for 1,3-substituted triazoles. **B**: Approach including click reaction. **C**: Approach including alkylation of 1,2,3-triazole.

The Tz ILs selected and synthesized for the investigation are presented in Figure 2.2. Butyl, benzyl and phenyl groups were chosen as substituents for the Tz ILs: butyl as an inert alkyl group, allowing comparison with classic [BMIm] ILs, and aromatic groups as they can potentially orient the Tz ring due to π -stacking of the cations and possible interaction of the aromatic ring with the electrode. The 1,3,4-substituted Tz ILs are easier to prepare than the unsubstituted Tz ILs, which makes them particularly attractive systems to probe for the CO_2RR . The TFSI anion was selected due to the large potential windows of TFSI ILs, their generally lower melting points, viscosities and good solubilities in organic solvents.

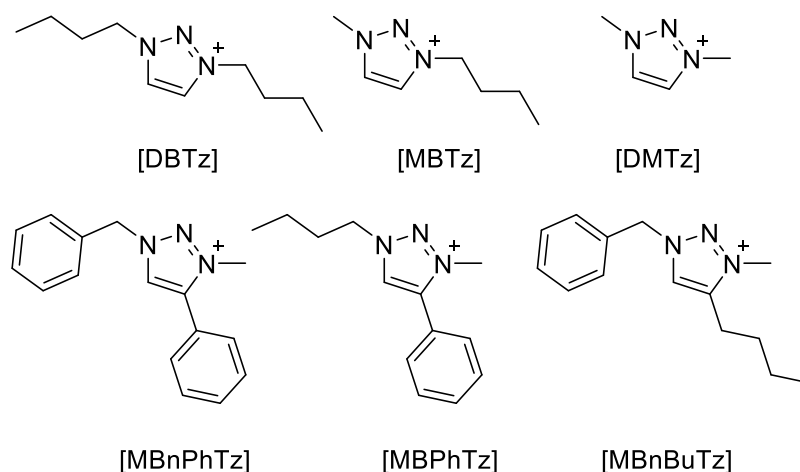


Figure 2.2. Cations of the Tz ILs employed in the current project.

To probe the ability of the Tz ILs to act as co-catalysts in the CO₂RR the corresponding compound (0.02 M) was dissolved in a 0.1 M solution of tetrabutylammonium hexafluorophosphate (TBAP) in acetonitrile. Polished polycrystalline silver and glassy carbon electrodes were used as the cathodes. The choice of the electrodes is based on the fact that ILs do not normally have catalytic activities on their own, but improve the performance of the actual catalyst, i.e. the electrodes. Silver is a well-established catalyst for the CO₂RR, having large FE_{CO} at reasonable potentials.⁸ Meanwhile, glassy carbon electrodes do not exhibit catalytic properties and are used as an inert electrode, which allows the stability of the system to be probed in the presence of CO₂.

First, the electrochemical behavior of the systems in the presence and absence of CO₂ was evaluated by cyclic voltammetry (CV) experiments. Experiments under N₂ atmosphere were performed to determine the potential windows of the Tz ILs (Figure 2.3). Tz ILs without aromatic substituents showed better stability. Benzyl substituents have the most destabilizing effect, which is probably due to the low stability of the benzyl group under strongly reducing conditions, e.g. benzylamines can be easily cleaved under the conditions of the Birch reduction, forming toluene and free amines.⁹ The introduction of the phenyl group in the Tz ring also results in the destabilization of the co-catalyst, which may be a consequence of the formation of a larger electron-deficient conjugated system. For the 1,3-alkyl substituted Tz, dibutyl Tz is more stable than dimethyl Tz, presumably due to the larger sterics and stronger electron donating effect of the butyl group compared to the methyl one.

Under N₂, CVs obtained using a Ag working electrode correspond to those obtained with a glassy carbon electrode (Figure 2.3, solid green vs dashed blue lines), suggesting that specific interactions between the electrodes and the Tz cation are not essential and allowing the CVs for the Ag and C electrodes, recorded under CO₂, to be compared.

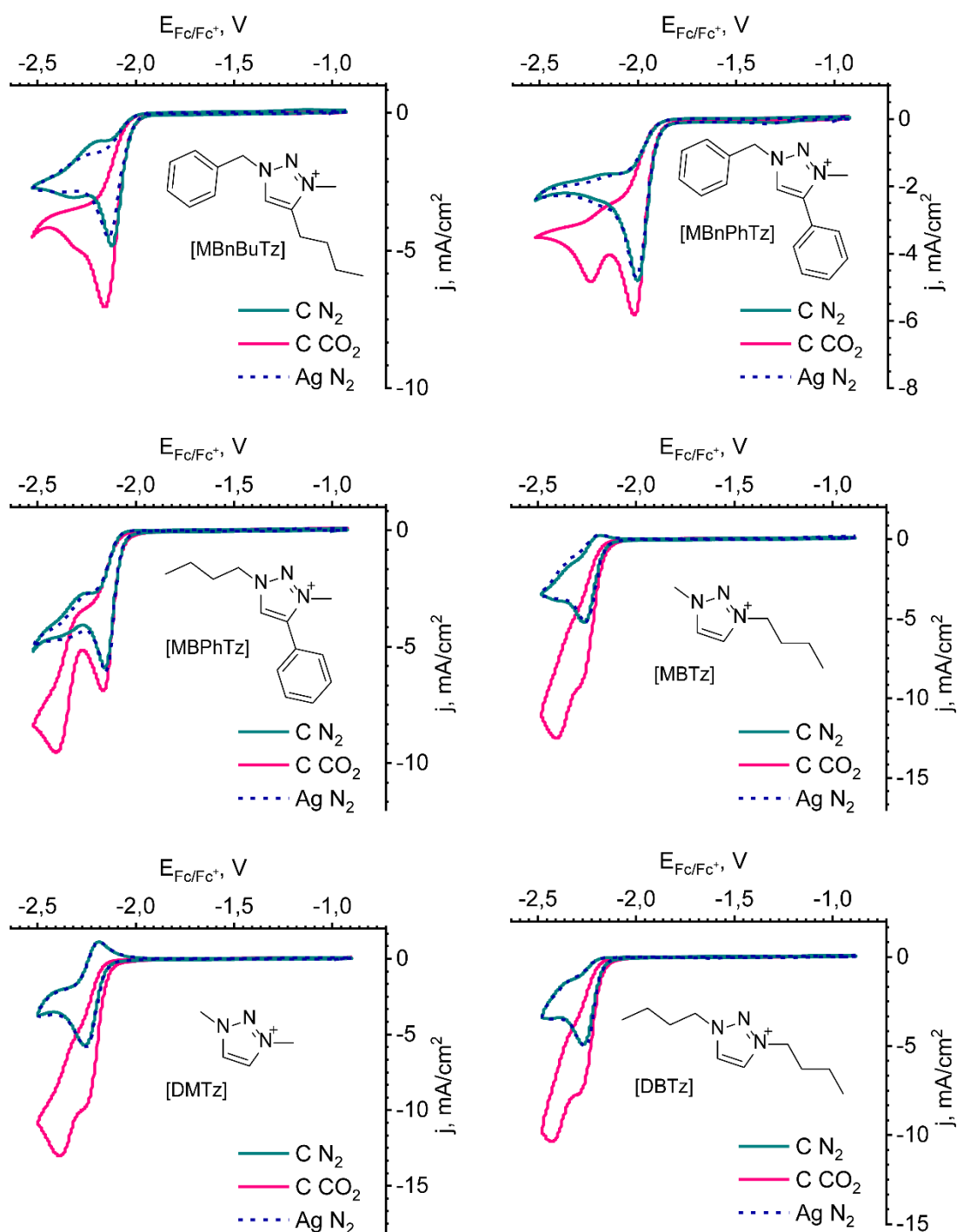


Figure 2.3. CV data on the stability of the Tz ILs.

The shapes of the decomposition curves are different for the 1,3,4- and 1,3-substituted Tz cations. For the 1,3,4-Tz ILs no peaks appear on the backward oxidation scan, which implies fully irreversible reduction of the species. The reduction curves for the 1,3-alkyl ILs have an extremum for the oxidative part of the curve along with the one appearing during the reduction, which might imply a certain

degree of reversibility for the degradation process. The CVs are not symmetric, with minima (extremum attributed to the reduction wave) higher in amplitude than the maxima (extremum attributed to the oxidation wave). Such shape can be a sign of a partial decomposition of the formed reduction product. For the deeper understanding of the reduction of the Tz cations, CV curves at different scan rates were recorded (Figure 2.4 left).

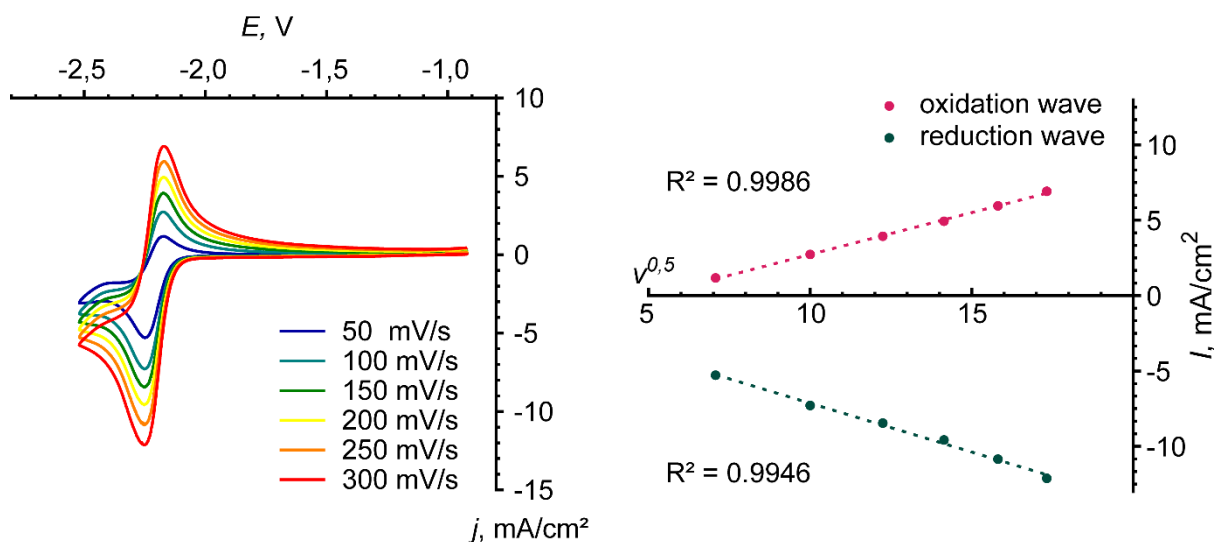


Figure 2.4. Left: CV curves for [DMTz]TFSI recorded at different scan rates. Right: Relation of the peak current densities to the square root of the scan rate. Experimental conditions: 0.02 M IL in 0.1 M TBAP in MeCN, glassy carbon polished working electrode.

The CV curve becomes more symmetrical at higher scan rates, further supporting decomposition of the reduced species as the reason for the asymmetry of the CV. The peak-to-peak separation for all curves is ca. 77 mV, which is larger than that of a fully reversible process (57 mV).¹⁰ In general, the difference may result from quasi-reversibility of the reduction or from non-ideality of the system (large resistances between the working and the reference electrodes, which are normal when employing organic electrolytes). In order to clarify which of these reasons is in operation, the CV experiment was performed for ferrocene (Fc). The reduction of Fc is a one-electron and fully reversible process, which allows it to be used as a standard for the electrochemical measurements. In our case peak-to-peak separation for the Fc couple was 76 mV, indicating the reduction of Tz to be a reversible one-electron process. The relation of the current density to the square root of the scan rate is linear for both the reduction and oxidation waves, which shows fast electron transfer and, therefore, diffusion control of the reduction reaction (Figure 2.4 right).

Following the measurements under a N_2 atmosphere, the reaction mixtures were flushed with CO_2 and the CV experiments were performed again. In the accordance with the data on the 1m ILs, 1,3,4-substituted Tz ILs showed no significant co-catalytic activity, which is concluded from a lack of difference of the onset potentials and only minor differences in the current densities in the presence and absence of CO_2 (Figure 2.5). However, in the case of 1,3-alkylated Tz ILs, [DMTz]Tf₂N, [BMTz]Tf₂N and [DBTz]Tf₂N, when CO_2 is present in the system the onset potentials of the reduction waves shift in a positive direction and are followed by the disappearance of the oxidation peaks. These changes indicate a new Faradaic process in the system due to the presence of CO_2 . The CV curves have a peak, nearly corresponding to the reduction peak of the co-catalyst under N_2 . This observation may imply that the reduction wave consists of two simultaneous processes, i.e. reduction of CO_2 and decomposition of the co-catalysts, with the latter limiting the reduction. As no catalytic current is observed when the glassy carbon electrode is used instead of the Ag electrode, and hence the role of the Ag electrode appears to be essential for catalysis and it seems unlikely that the Tz IL serves as a redox shuttle as shown in Scheme 1.1 in the section 1.2.

However, even when the glassy carbon electrode is employed, the shape of the CV curve is different in the presence and absence of CO_2 . When carbon dioxide is in the mixture, the reduction current increases, the oxidation peaks disappear and the process loses all signs of reversibility. A possible explanation for these changes is that CO_2 reacts rapidly with the reduced form of triazolium cation. However, a shift in the onset potential does not occur.

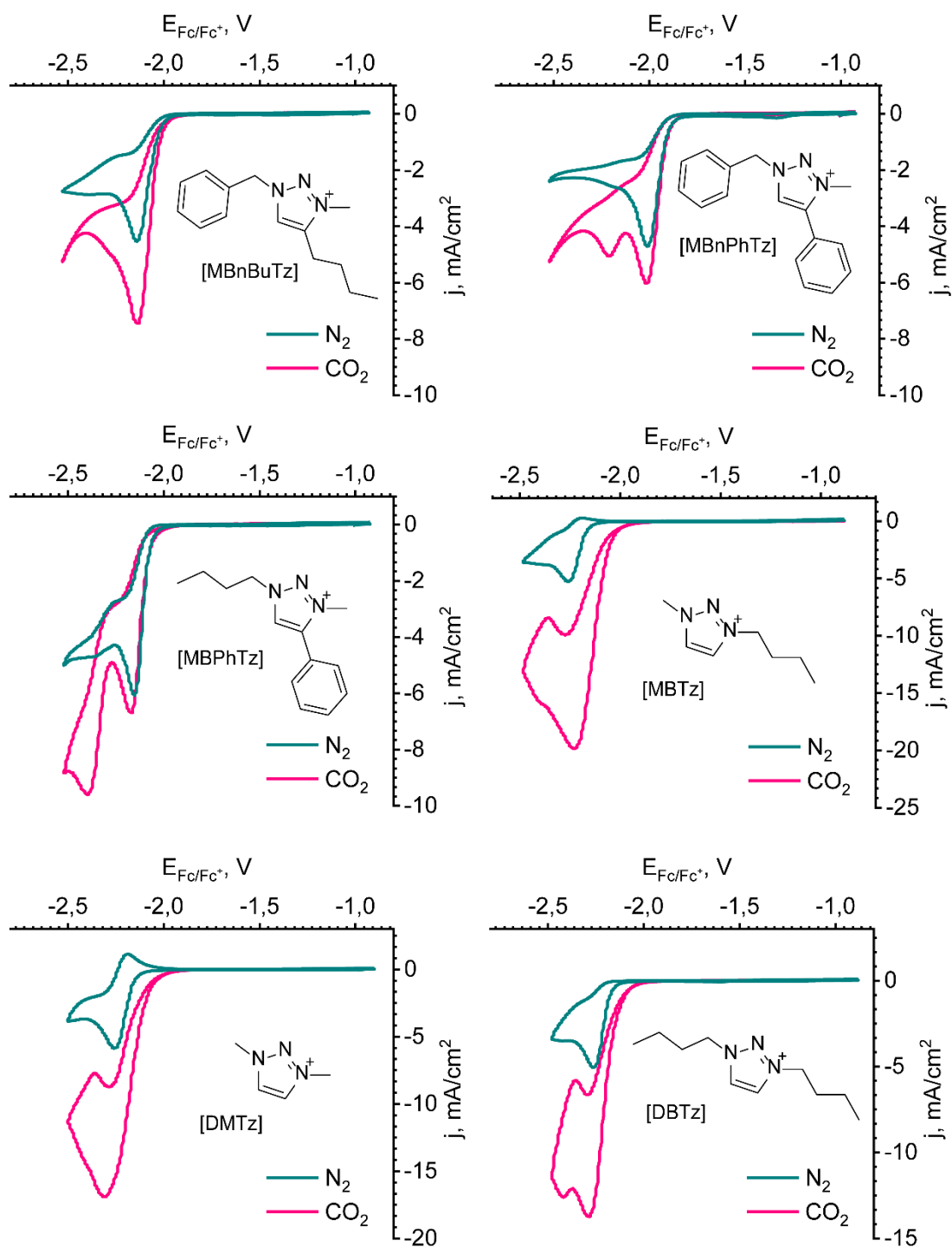


Figure 2.5. CV curves for the Tz ILs under N_2 and CO_2 atmospheres. Experimental conditions: 0.02 M IL in 0.1 M TBAP in MeCN, Ag polished polycrystalline working electrode.

Since CV experiments are unable to assess performance of the co-catalytic systems as the nature of the products and their contribution to the overall reduction process remains unknown, potentiostatic electrolysis combined with online GC analysis was performed. For this purpose, the [MBTz]-based IL was selected as the model compound, having the largest difference between decomposition and CO₂RR potentials. Electrolysis was performed at three different potentials (Figure 2.6).

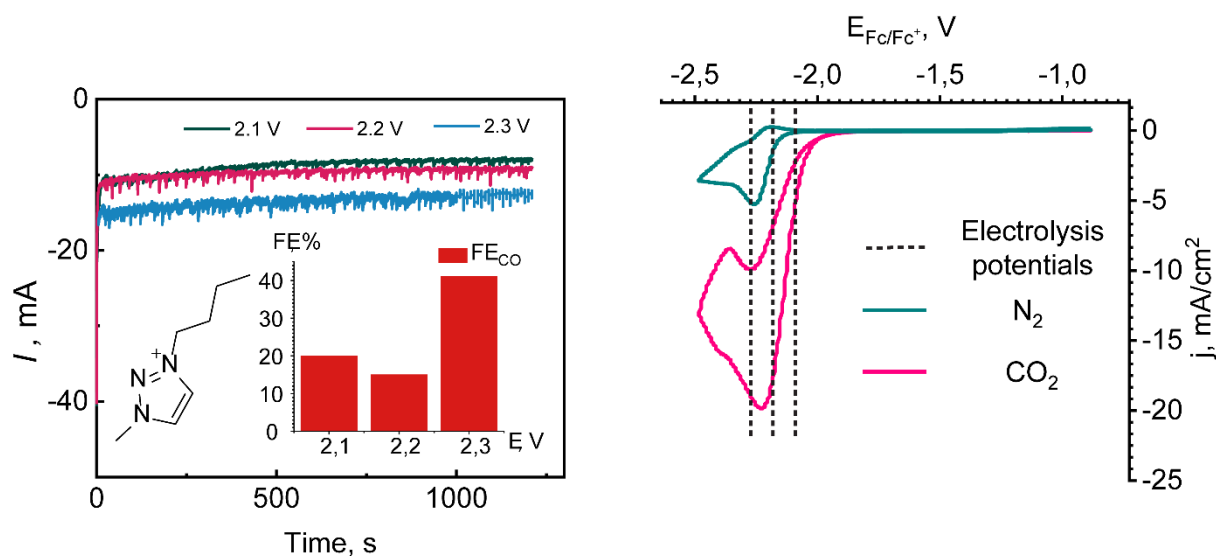


Figure 2.6. Left: Results of potential controlled electrolysis for [MBTz]TFSI - electrolysis traces and FE_{CO}.

Right: CVs of [MBTz]TFSI displayed with the electrolysis potentials.

The FE_{CO} was found to be low at low overpotentials (15-20%) and increase with the higher applied voltage (reaching *ca.* 40%). Traces of H₂ were detected, although no other CO₂-based products were detected. Low Faradaic yields can be explained by competing partial decomposition of the co-catalyst.

2.3 Summary

In conclusion, we have synthesized a new type of ILs for the CO₂RR and assessed their performance. While 1,3,4-substituted Tz ILs do not behave as co-catalysts and are irreversibly decomposed at potentials close to the required for CO₂RR, their 1,3-alkylated analogues can serve as promoters. The FEs for the only CO₂-based product (CO) were found to be low (below 40%) due to decomposition of the co-catalyst. However, the Tz ILs have promising onset potentials for the CO₂RR, which are

close to the theoretical ones for non-aqueous systems. Nonetheless, these results contribute to the understanding of structure/activity relationships for CO₂RR catalysts.

2.4 Experimental

2.4.1 Electrochemical measurements.

Cyclic voltammetry (CV) measurements were carried out using a Bio-Logic SP200 potentiostat and a custom-made glass electrochemical cell. Bu_4NPF_6 (0.1 M, Sigma-Aldrich) in anhydrous acetonitrile (5 mL, 99.9+ %, Extra Dry, Acros) was used as the supporting electrolyte and the concentration of catalysts was 0.02 M for all runs if not stated otherwise. Silver and glassy carbon disk electrodes (5 mm diameter, BioLogic) were used as working electrodes. Before each experiment, the electrodes were polished with Al_2O_3 slurry (1 micron, Electron Microscopy Sciences), washed with water and dried using a stream of air. An Ag/AgCl quasi-reference homemade electrode was employed as the reference. The electrode was prepared by polarization of Ag wire in 2 M HCl (two electrode setup, Ag wire anode (working electrode), Pt cathode (counter electrode + reference), 2V for 180 s). This electrode was operated behind a ceramic diaphragm (6.1240.020, Metrohm) and calibrated to the ferrocene/ferrocenium couple. A Pt wire was used as the counter electrode. All the electrodes were always set at the same positions in the cell prior to every experiment in order to keep ohmic losses constant, and the measurements were corrected for the IR drop. Before conducting each experiment, the solution was flushed with Ar for 15 min under stirring. CV scans were recorded at 100 mV/s. All the ILs were dried at 90°C for 30 min before cyclic voltammetry measurements.

Chronoamperometry experiments followed by gas chromatography(GC) analysis were carried out in a H-type cell employing NBu_4PF_6 (0.1 M) containing the target IL (0.02 M) as catholyte, H_2SO_4 (0.5 M, suprapure, Merck) as anolyte, compartments separated by a polymer membrane Nafion 117, Sigma-Aldrich). As working electrodes, a Ag foil (99.9%, 0.25 mm thickness, Sigma Aldrich) was used. Before measurements, the Ag foil electrode was mechanically polished with alumina paste (1 μm) on polishing cloth, ultrasonicated for about 1 minute, then rinsed with Milli-Q water and dried in Ar stream. A platinized Pt foil and a leakless Ag/AgCl electrode (EDAQ) were used as counter and reference electrodes, respectively. Before each series of experiments, a calibration mixture of H_2 , CO, CO_2 , CH_4 , C_2H_6 and C_3H_8 (Carbagaz) was injected in the GC. HayeSep D 80-100 mesh column was employed for the separation.

Potentiostatic control was provided with a Metrohm Autolab PGSTAT302N instrument. The catholyte was continuously purged with CO_2 gas at the flow rate of 15 mL/min, thereby transporting vol-

atile reaction products from the headspace into the sampling loops of the on-line gas chromatograph (SRI Instruments). The partial current density for a given gaseous product was determined using the following equations:

$$I_i = \frac{c_i \cdot v \cdot F \cdot z}{10^6 \cdot V_m} \quad (1)$$

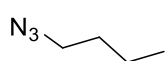
$$FE (\%) = \frac{I_i}{I_{total}} \cdot 100\% \quad (2)$$

I_i is the Partial current for the conversion of CO₂ to product i , c_i represents the volume fraction of the products measured via online GC using an independent calibration standard gas (Carbagas), z is the number of electrons involved in the reaction to form a particular product, F is the Faraday constant (96485 C/mol), v is the flow rate [L/s], V_m represents the molar volume, I_{total} is the total current at the time of measurement. Faradaic efficiency (FE) was obtained by normalizing the partial current density for a given reaction product with respect to the total current density. Gas products were analyzed online during steady-state potentiostatic CO₂ electrolysis at different electrode potentials.

2.4.2 Synthesis and characterization of compounds.

All reagents were obtained commercially and used without further purification unless otherwise stated. CO₂ (99.998 %) and Ar (99.9999 %) were obtained from Carbagas, Switzerland. ¹H, ¹⁹F and proton-decoupled ¹³C-NMR spectra were recorded on a Bruker Avance-400 (400 MHz) spectrometer. All reactions were completed under inert conditions (nitrogen atmosphere).

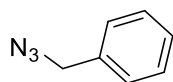
1-azidobutane: To a solution of 1-iodobutane (4.60 mL, 40 mmol) in DMSO (50 mL) was added NaN₃



(3.90 g, 60 mmol), the reaction mixture was left stirring at 90°C for 24 hours. The resulting mixture was cooled down, diluted with water (100 mL) and extracted with

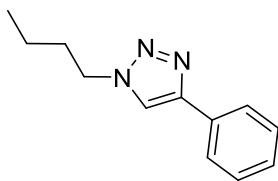
Et₂O (3x100 mL). The combined organic fractions were dried over MgSO₄, then the volume of the solution was reduced under vacuum. The resulting mixture was used without further purification, as BuN₃ is potentially explosive when pure. NMR yield: 78%. ¹H NMR (400 MHz, Chloroform-*d*) δ 3.27 (t, J = 6.9 Hz, 2H), 1.68 – 1.53 (m, 2H), 1.51 – 1.34 (m, 2H), 1.01 – 0.87 (m, 3H).

Benzylazide: To a solution of benzylbromide (3.5 mL, 29 mmol) in a 4:1 mixture of acetone and water (160 and 40 mL respectively) was added NaN₃ (2.85 g, 48 mmol). The reaction



mixture was left stirring at rt for 24 hours. The resulting mixture was extracted with dichloromethane (2x40 mL), the combined organic fractions were washed with brine (50 mL), dried over MgSO_4 and dried under vacuum, affording pale yellow oil (3.97 g, *ca.* 100%). ^1H NMR (400 MHz, Chloroform-*d*) δ 7.59 – 7.28 (m, 5H), 4.37 (s, 2H). ^{13}C NMR (101 MHz, CDCl_3) δ 135.37, 128.83, 128.30, 128.21, 54.82.

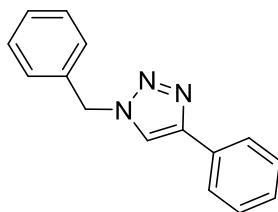
1-butyl-4-phenyl-1,2,3-triazole: To a solution of BuN_3 (1.0 g, 10 mmol) in methanol (50 mL) were



added sodium ascorbate (0.40 g, 2 mmol), copper sulfate pentahydrate (0.38 g, 1.5 mmol) and phenylacetylene (1.11 mL, 10 mmol). The reaction mixture was left for 12 hours at rt, diluted by water (50 mL), extracted by dichloromethane (4x50 mL). The combined organic fractions were washed

with Brine (50 mL), dried over MgSO_4 , filtered through a short silica plug and dried under vacuum, affording pale pink solid (1.63 g, 80%). ^1H NMR (400 MHz, Chloroform-*d*) δ 7.91 – 7.82 (m, 2H), 7.77 (s, 1H), 7.45 (t, J = 7.5 Hz, 2H), 7.41 – 7.31 (m, 1H), 4.43 (t, J = 7.2 Hz, 2H), 1.96 (p, J = 7.3 Hz, 2H), 1.43 (h, J = 7.4 Hz, 2H), 1.00 (t, J = 7.4 Hz, 3H). ^{13}C NMR (101 MHz, CDCl_3) δ 147.73, 130.72, 128.81, 128.06, 125.69, 119.39, 50.15, 32.31, 19.73, 13.46.

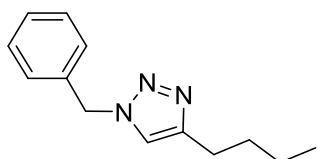
1-benzyl-4-phenyl-1,2,3-triazole: To a solution of copper sulfate pentahydrate (0.04 g, 0.16 mmol),



sodium ascorbate (0.60 g, 0.3 mmol) and benzoic acid (0.17 g, 1.4 mmol) in a 2:1 mixture of H_2O (10 mL) and tert-butanol (5 mL) were added benzylazide (2.00 g, 15 mmol) and phenylacetylene (1.57 mL, 14.3 mmol). The reaction mixture was left for 10 minutes at rt, diluted by dichloromethane

(150 mL), washed by water (100 mL), brine (100 mL), dried over MgSO_4 and filtered through a celite plug. The solvent was removed under vacuum, affording colorless solid (3.4 g, 99%). ^1H NMR (400 MHz, Chloroform-*d*) δ 7.87 – 7.77 (m, 2H), 7.68 (s, 1H), 7.47 – 7.31 (m, 8H), 5.60 (s, 2H). ^{13}C NMR (101 MHz, CDCl_3) δ 148.25, 134.68, 130.53, 129.16, 128.80, 128.17, 128.06, 125.71, 119.47, 54.25.

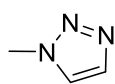
1-benzyl-4-butyl-1,2,3-triazole: Synthesized employing the same protocol, as for 1-benzyl-4-phenyl-



1,2,3-triazole. Starting from 1-hexyne (1.56 mL, 13.6 mmol). Yield 70% (2.1 g). ^1H NMR (400 MHz, Chloroform-*d*) δ 7.43 – 7.36 (m, 2H), 7.31 – 7.25 (m, 3H), 5.52 (s, 2H), 2.77 – 2.67 (m, 2H), 1.65 (t, J = 7.5 Hz, 2H),

1.38 (h, J = 7.4 Hz, 2H), 0.94 (t, J = 7.3 Hz, 3H).

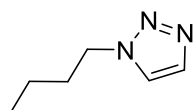
1-methyl-1,2,3-triazole: To an ice-cooled (0°C) suspension of sodium hydride (4.6 g, 0.19 mol) in dry



THF (100 mL) was added dropwise 1H-1,2,3-triazole (10 mL, 0.17 mol), followed by iodomethane (16.6 mL, 0.17 mol). The reaction was left stirring for 2 hours at rt. Water

(100 mL) was added, the mixture was extracted by dichloromethane (3x100 mL), combined organic layers were dried over MgSO₄. Activated charcoal (50 mg) was added, the mixture left stirring for 3 hours at rt, then it was filtered through celite, the solvent was removed under vacuum, yielding colorless liquid (4.7 g, 33%). ¹H NMR (400 MHz, Chloroform-*d*) δ 7.63 (s, 1H), 7.48 (s, 1H), 4.06 (s, 3H).

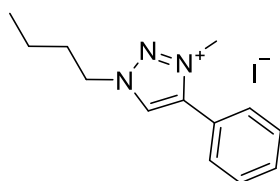
1-methyl-1,2,3-triazole: To a solution of 1H-1,2,3-triazole (10 mL, 0.17 mol) in dry MeCN (70 mL)



were added butyl bromide (20.5 mL, 0.19 mol) and potassium carbonate (36 g, 0.26 mol). The reaction was left stirring for 12 hours at rt. Water (150 mL) was

added, the mixture was extracted by dichloromethane (3x100 mL), combined organic layers were dried over MgSO₄. The solvent was removed under vacuum, yielding colorless liquid (17.51 g). As discussed in the main text, two products were formed: 1-butyl-1H-1,2,3-triazole and 2-butyl-2H-1,2,3-triazole (1:1, 8.8 g and 41% yield each). The mixture was used directly for the alkylation step. ¹H NMR (mixture): ¹H NMR (400 MHz, Chloroform-*d*) δ 7.71 (d, *J* = 1.0 Hz, 1H), 7.59 (s, 1H), 7.55 (d, *J* = 1.0 Hz, 1H), 4.43 (dt, *J* = 20.2, 7.2 Hz, 4H), 2.09 – 1.79 (m, 4H), 1.47 – 1.28 (m, 4H), 1.08 – 0.87 (m, 6H).

1-butyl-3-methyl-4-phenyl-1,2,3-triazolium iodide: To a solution of 1-butyl-4-phenyl-1,2,3-triazole

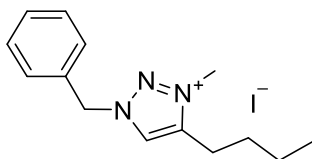


(360 mg, 1.8 mmol) in dry MeCN (10 mL) was added iodomethane (8.8 mL, 17 mmol). The reaction mixture was left for 12 hours at reflux, then dried

under vacuum, adsorbed on silica, washed with MeCN (5 mL) to remove the colored side products, then with water (50 mL). The solvent was re-

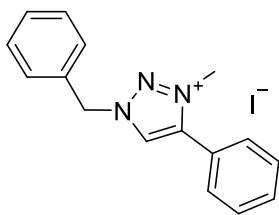
moved under vacuum, yielding yellow viscous oil (0.30 g, 49%). ¹H NMR (400 MHz, Chloroform-*d*) δ 9.53 (s, 1H), 7.84 – 7.74 (m, 2H), 7.69 – 7.50 (m, 3H), 4.83 (t, *J* = 7.4 Hz, 2H), 4.33 (s, 3H), 2.11 (tdd, *J* = 9.2, 6.8, 4.3 Hz, 2H), 1.48 (h, *J* = 7.4 Hz, 2H), 1.00 (t, *J* = 7.4 Hz, 3H).

1-benzyl-3-methyl-4-butyl-1,2,3-triazolium iodide: Synthesized employing the same protocol, as for 1-butyl-3-methyl-4-phenyl-1,2,3-triazolium iodide. Starting from 1-



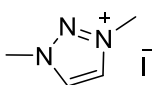
benzyl-4-butyl-1,2,3-triazole (2.1 g, 9.8 mmol). Yield 81% (2.8 g). ^1H NMR (400 MHz, Chloroform- d) δ 9.12 (s, 1H), 7.57 (dd, J = 6.6, 3.0 Hz, 2H), 7.36 (dp, J = 4.8, 1.9 Hz, 3H), 5.90 (s, 2H), 4.19 (s, 3H), 2.88 – 2.70 (m, 2H), 1.79 – 1.61 (m, 2H), 1.39 (h, J = 7.4 Hz, 2H), 0.89 (t, J = 7.3 Hz, 3H).

1-benzyl-3-methyl-4-phenyl-1,2,3-triazolium iodide: To a solution of 1-benzyl-4-phenyl-1,2,3-triazole (3.36 g, 14.3 mmol) in dry MeCN (30 mL) was added iodomethane (7



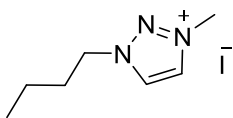
mL, 71 mmol). The reaction mixture was left for 12 hours at reflux, the solvent was removed under vacuum and the residue washed with Et₂O (15 mL). The product was dried under vacuum, yielding yellow crystalline product (4.18 g, 78%). ^1H NMR (400 MHz, Chloroform- d) δ 9.47 (s, 1H), 7.80 – 7.66 (m, 4H), 7.65 – 7.53 (m, 3H), 7.49 – 7.41 (m, 3H), 6.08 (s, 2H), 4.31 (s, 3H).

1,3-dimethyl-1,2,3-triazolium iodide: To a solution of 3-methyl-1,2,3-triazole (0.97 g, 11.7 mmol) in



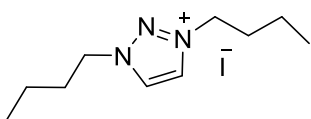
dry MeCN (10 mL) was added iodomethane (1.37 mL, 14 mmol). The reaction mixture was left for 12 hours at reflux, the solvent was removed under vacuum and the product precipitated with Et₂O (15 mL). The precipitate was filtered off and dried under vacuum, yielding colorless crystalline product (1.05 g, 40%). ^1H NMR (400 MHz, DMSO- d_6) δ 8.82 (s, 2H), 4.31 (s, 6H).

1-methyl-3-butyl-1,2,3-triazolium iodide: To the mixture from the synthesis of 1-butyl-1,2,3-tria-



zole (15 g, 120 mmol) was added iodomethane (12 mL, 120 mmol). The reaction mixture was left for 12 hours at room temperature, the solvent was removed under vacuum, water (50 mL) was added and the solution was washed with Et₂O (3x50 mL). The solvent was removed under vacuum, yielding yellow oily product (21.4 g). ^1H NMR (400 MHz, DMSO- d_6) δ 8.91 (d, J = 1.4 Hz, 1H), 8.85 (d, J = 1.4 Hz, 1H), 4.63 (t, J = 7.1 Hz, 2H), 4.31 (s, 3H), 2.04 – 1.72 (m, 2H), 1.40 – 1.12 (m, 2H), 0.92 (t, J = 7.4 Hz, 3H).

1,3-dibutyl-1,2,3-triazolium iodide: To an ice-cooled (0°C) suspension of sodium hydride (1.9 g, 80

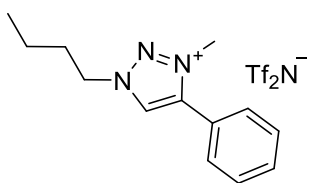


mmol) in dry THF (100 mL) was added dropwise 1H-1,2,3-triazole (4.19 mL, 72 mmol) followed by 1-iodobutane (21 mL, 181 mmol). The reaction was left for 5 days at reflux. Water (100 mL) was added, the mixture was extracted by dichloromethane (3x100 mL), combined organic layers were dried over MgSO₄. The

solvent was removed under vacuum, yielding dark yellow oil (15.4 g, 69%). ^1H NMR (400 MHz, $\text{DMSO}-d_6$) δ 8.98 (s, 2H), 4.65 (t, J = 7.1 Hz, 4H), 2.04 – 1.83 (m, 4H), 1.42 – 1.19 (m, 4H), 0.91 (t, J = 7.4 Hz, 6H). ^{13}C NMR (101 MHz, DMSO) δ 131.26, 53.31, 31.05, 19.20, 13.67.

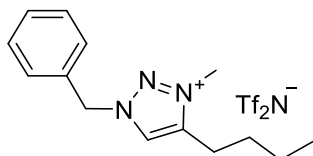
Typical procedure for the anion metathesis: To a solution of triazolium halide salt (1 eq) in a mixture of Milli-Q water and dichloromethane (1:1) was added lithium bis(trifluoromethylsulfonyl)imide (1 eq). The mixture was left stirring for 3-4 hours at rt. The mixture was diluted by Milli-Q water, extracted by DCM (3x equal volumes), the solvent from the combined organic phases was removed under reduced pressure. The residue was washed by Et_2O and dried under vacuum, yielding the target products.

1-butyl-3-methyl-4-phenyl-1,2,3-triazolium bis(trifluoromethylsulfonyl)imide: Yield 97% (503 mg).



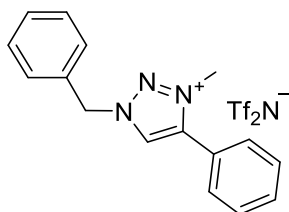
^1H NMR (400 MHz, $\text{DMSO}-d_6$) δ 9.21 (s, 1H), 7.76 (dt, J = 6.9, 2.2 Hz, 2H), 7.69 (dt, J = 5.2, 2.4 Hz, 3H), 4.67 (t, J = 7.1 Hz, 2H), 4.30 (s, 3H), 1.97 (dq, J = 9.3, 7.2 Hz, 2H), 1.39 (ddt, J = 14.6, 9.5, 7.2 Hz, 2H), 0.96 (t, J = 7.4 Hz, 3H). ^{13}C NMR (101 MHz, DMSO) δ 142.76, 131.93, 129.86, 129.77, 129.23, 123.20, 118.35, 53.44, 31.00, 19.22, 13.70. ^{19}F NMR (376 MHz, DMSO) δ -78.72.

1-benzyl-3-methyl-4-butyl-1,2,3-triazolium bis(trifluoromethylsulfonyl)imide: Yield 87% (2.4 g). ^1H



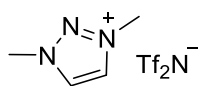
NMR (400 MHz, $\text{Chloroform}-d$) δ 8.08 (s, 1H), 7.46 (s, 5H), 5.68 (s, 2H), 4.20 (s, 3H), 2.79 (ddd, J = 9.0, 6.9, 0.8 Hz, 2H), 1.69 (dddd, J = 9.4, 7.9, 6.9, 5.9 Hz, 2H), 1.44 (dq, J = 14.6, 7.3 Hz, 2H), 0.96 (t, J = 7.3 Hz, 3H). ^{13}C NMR (101 MHz, CDCl_3) δ 145.21, 130.81, 130.14, 129.60, 129.38, 127.47, 57.62, 37.47, 28.68, 23.05, 22.08, 13.32. ^{19}F NMR (376 MHz, CDCl_3) δ -78.87, -78.88.

1-benzyl-3-methyl-4-phenyl-1,2,3-triazolium bis(trifluoromethylsulfonyl)imide: Yield 88% (2.48 g).



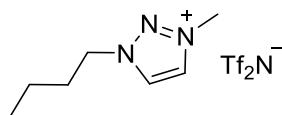
^1H NMR (400 MHz, $\text{DMSO}-d_6$) δ 9.29 (s, 1H), 7.82 – 7.72 (m, 2H), 7.68 (q, J = 4.9, 4.2 Hz, 3H), 7.61 – 7.53 (m, 2H), 7.49 (dd, J = 9.3, 3.9 Hz, 3H), 5.94 (s, 2H), 4.29 (s, 3H). ^{13}C NMR (101 MHz, DMSO) δ 143.11, 133.31, 131.95, 129.84, 129.81, 129.76, 129.55, 129.46, 129.39, 123.09, 121.55, 118.35, 56.75. ^{19}F NMR (376 MHz, DMSO) δ -78.71.

1,3-dimethyl-1,2,3-triazolium bis(trifluoromethylsulfonyl)imide: Yield 75% (630 mg). ^1H NMR (400



MHz, DMSO- d_6) δ 8.80 (s, 2H), 4.30 (s, 6H). ^{13}C NMR (101 MHz, DMSO) δ 132.10, 121.54, 118.34, 40.14. ^{19}F NMR (376 MHz, DMSO) δ -78.73.

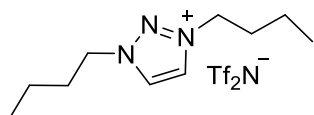
1-methyl-3-butyl-1,2,3-triazolium bis(trifluoromethylsulfonyl)imide: Yield 99% (3.7 g). ^1H NMR



(400 MHz, DMSO- d_6) δ 8.89 (d, J = 1.4 Hz, 1H), 8.83 (d, J = 1.4 Hz, 1H), 4.62 (t, J = 7.1 Hz, 2H), 4.31 (s, 3H), 2.01 – 1.71 (m, 2H), 1.47 – 1.17 (m, 3H), 0.92 (t, J = 7.4 Hz, 3H). ^{13}C NMR (101 MHz, DMSO) δ 132.19, 131.12, 53.20,

31.09, 19.17, 13.61. ^{19}F NMR (376 MHz, DMSO) δ -78.71, -78.71.

1,3-dibutyl-1,2,3-triazolium bis(trifluoromethylsulfonyl)imide: Yield 98% (11.1 g). ^1H NMR (400



MHz, DMSO- d_6) δ 8.93 (s, 1H), 4.63 (t, J = 7.2 Hz, 2H), 2.00 – 1.81 (m, 2H), 1.41 – 1.21 (m, 2H), 0.92 (t, J = 7.4 Hz, 3H). ^{13}C NMR (101 MHz, DMSO) δ 131.23, 53.31, 31.03, 19.19, 13.60. ^{19}F NMR (376 MHz, DMSO) δ -78.71,

-78.72.

2.5 Supporting Information

¹H NMR (400 MHz, Chloroform-*d*) δ 3.27 (t, *J* = 6.9 Hz, 2H), 1.68 – 1.53 (m, 2H), 1.51 – 1.34 (m, 2H), 1.01 – 0.87 (m, 3H).

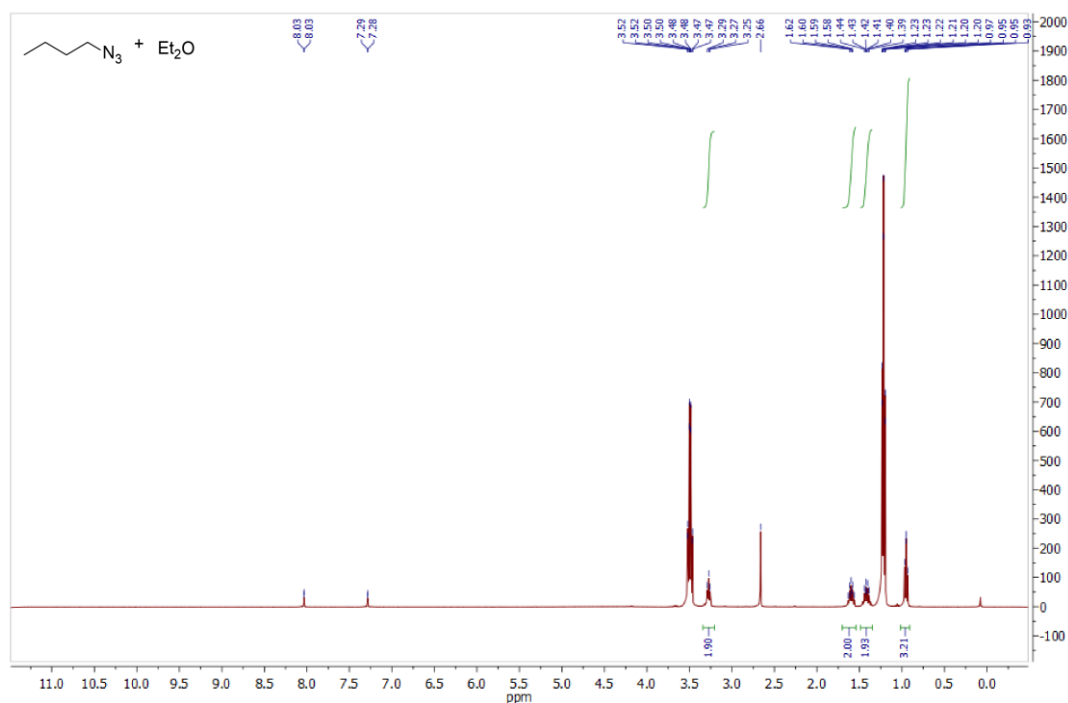


Figure S2.1. NMR ¹H for BuN₃ in Et₂O (400 MHz, CDCl₃).

¹H NMR (400 MHz, Chloroform-*d*) δ 7.59 – 7.28 (m, 5H), 4.37 (s, 2H).

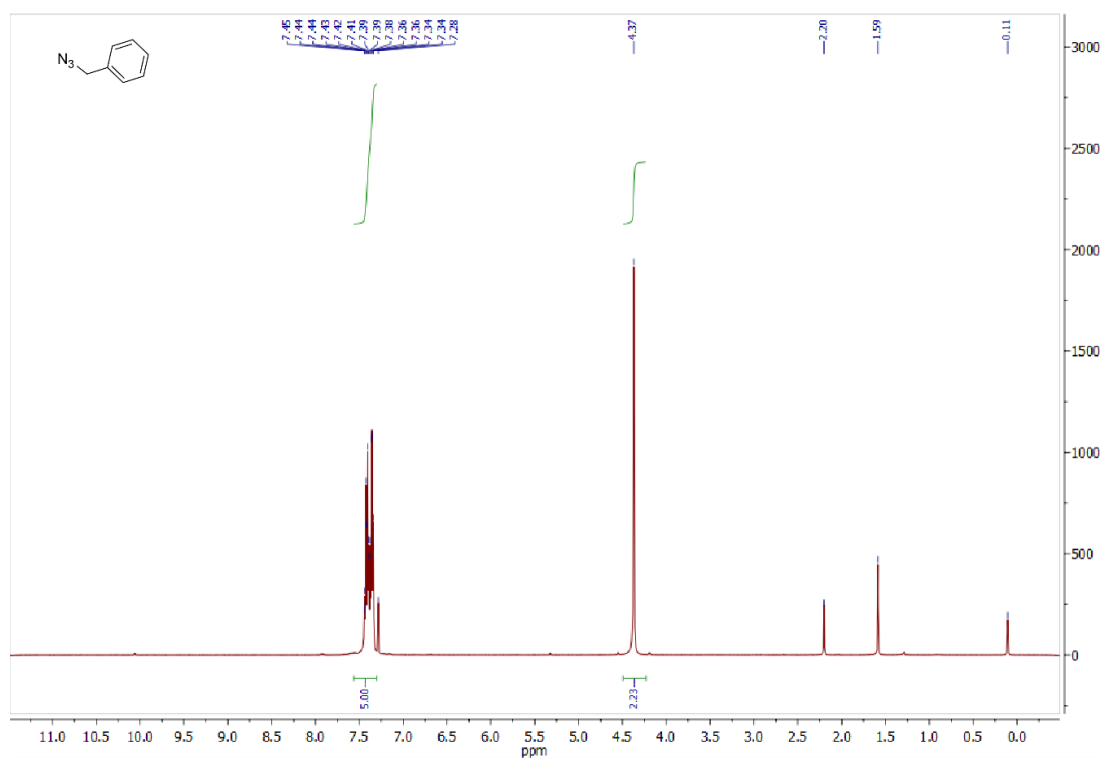
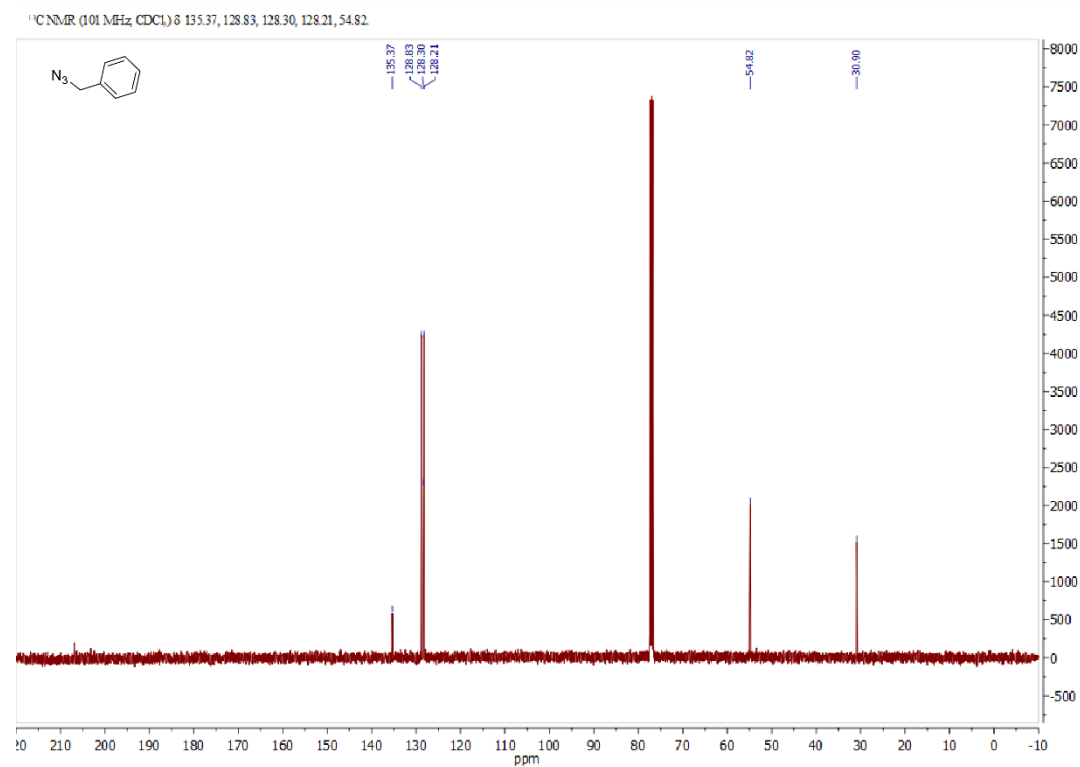
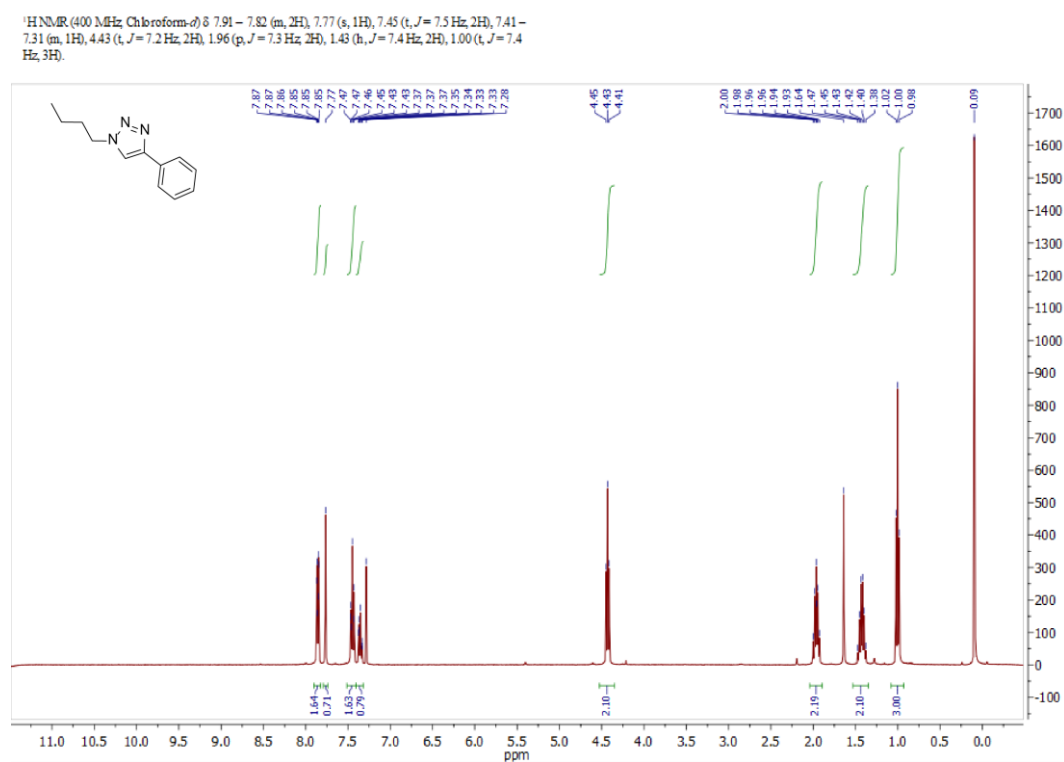
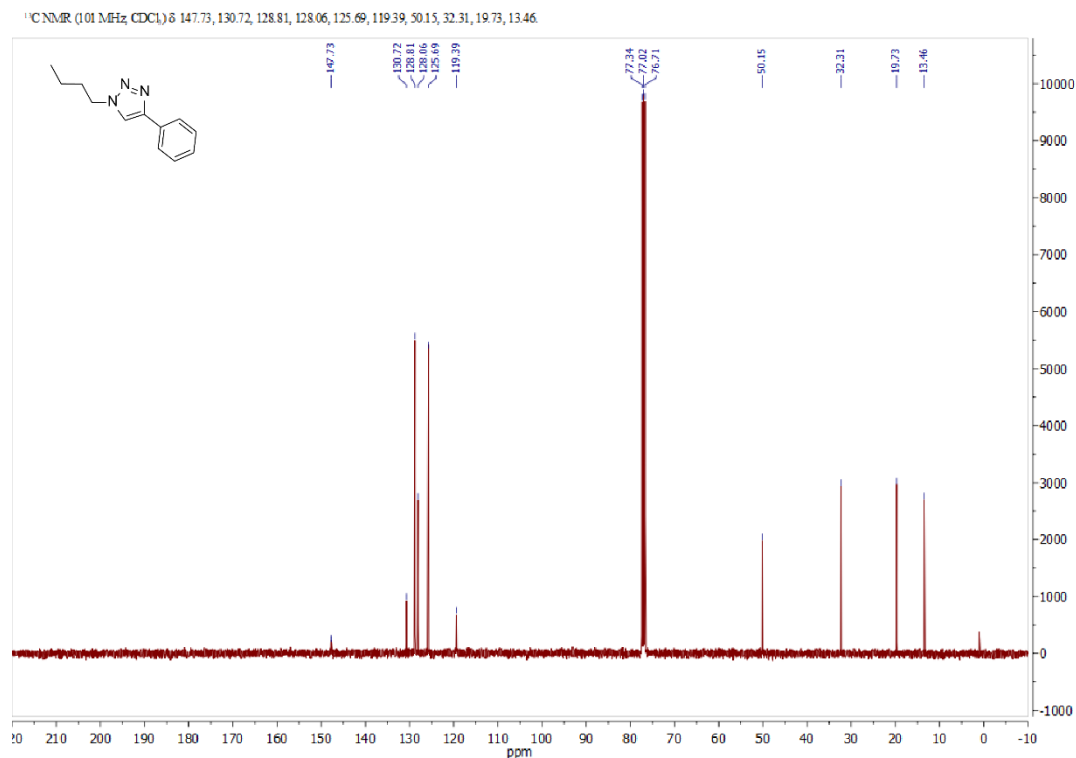
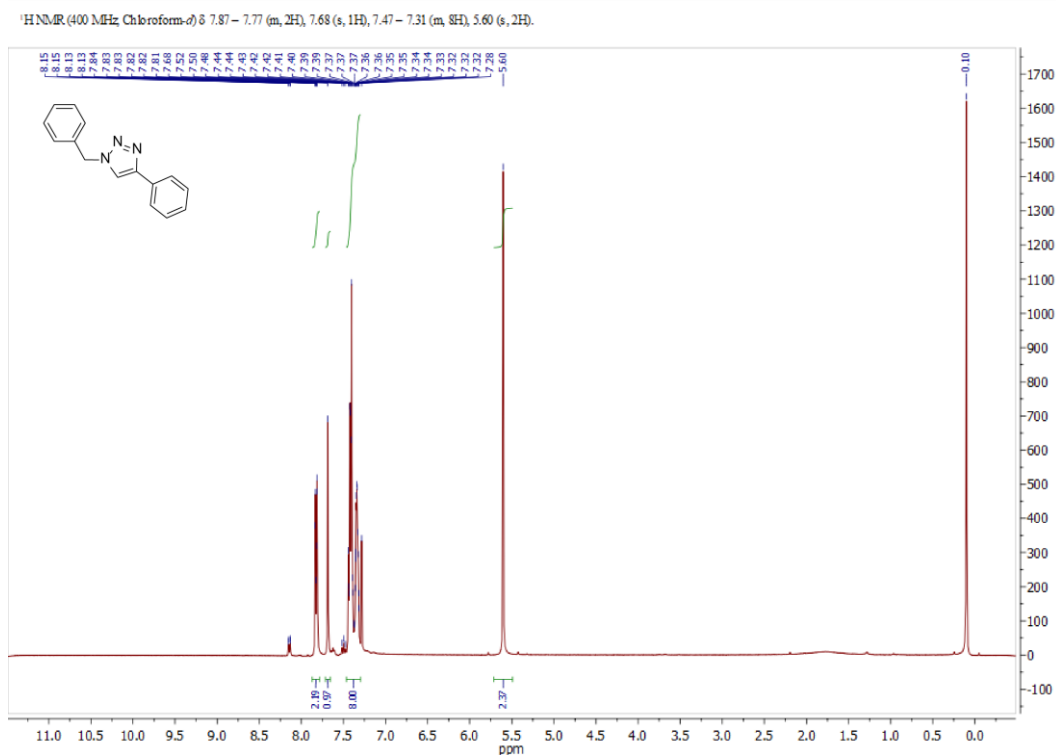
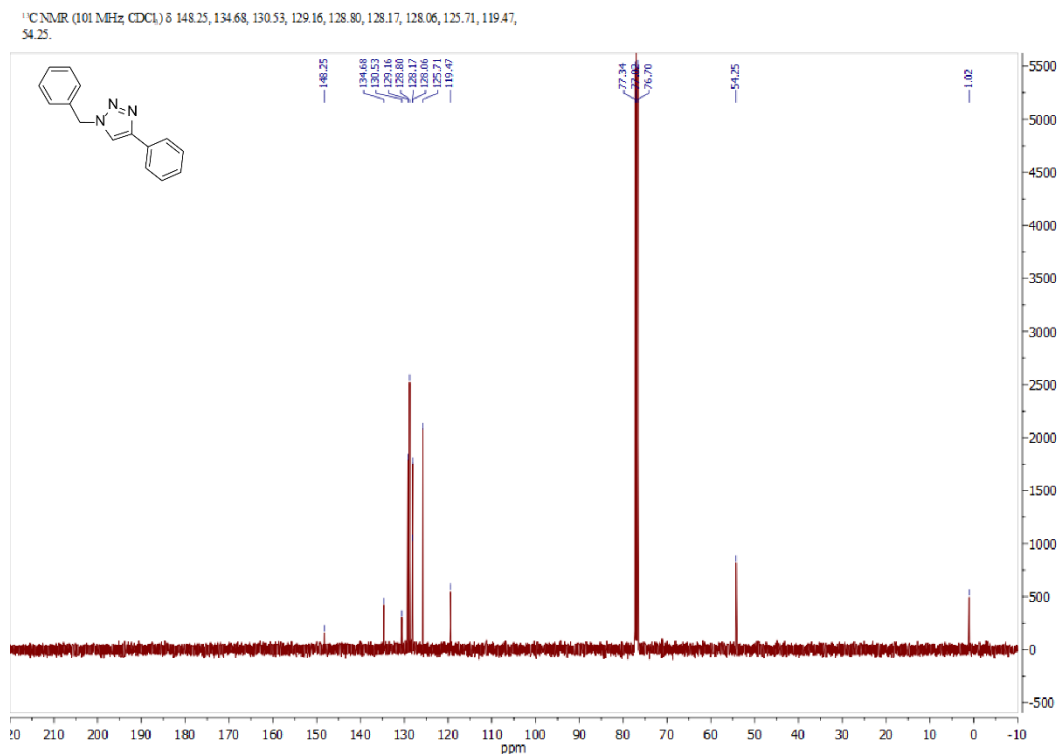
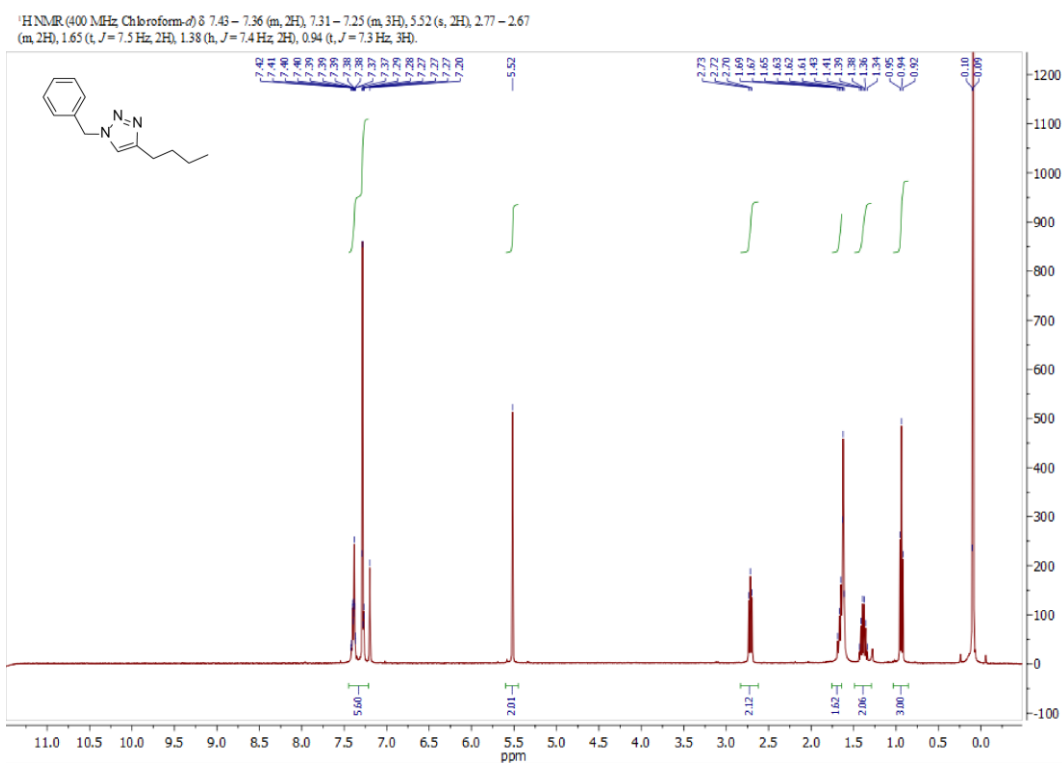
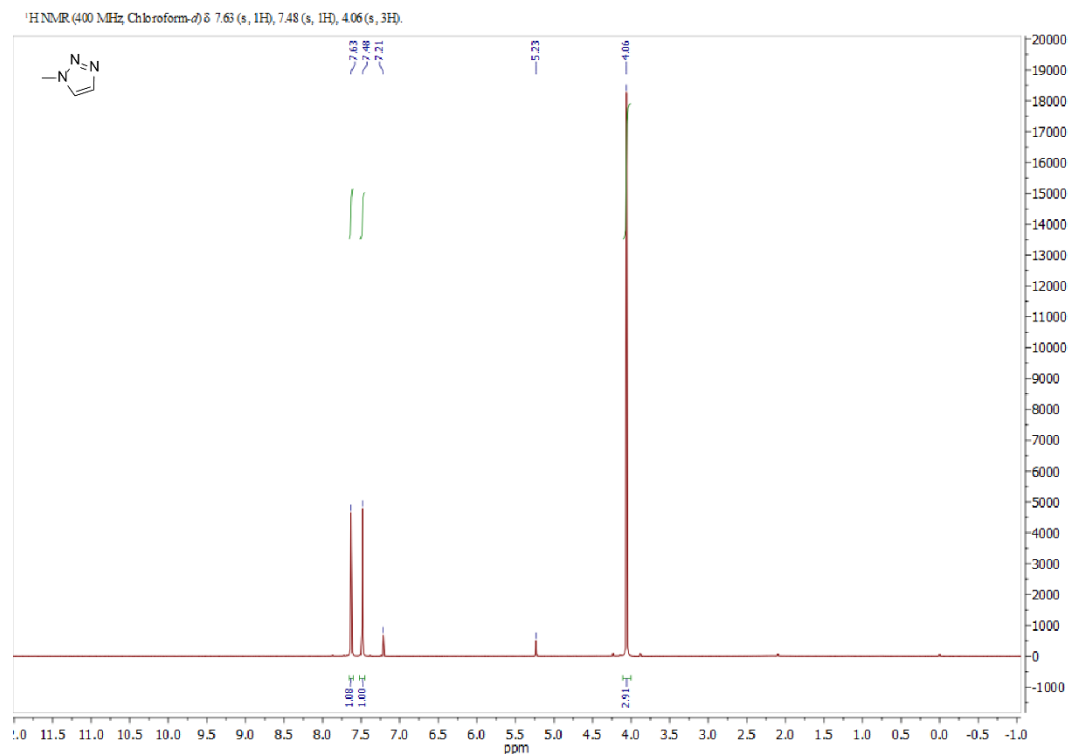
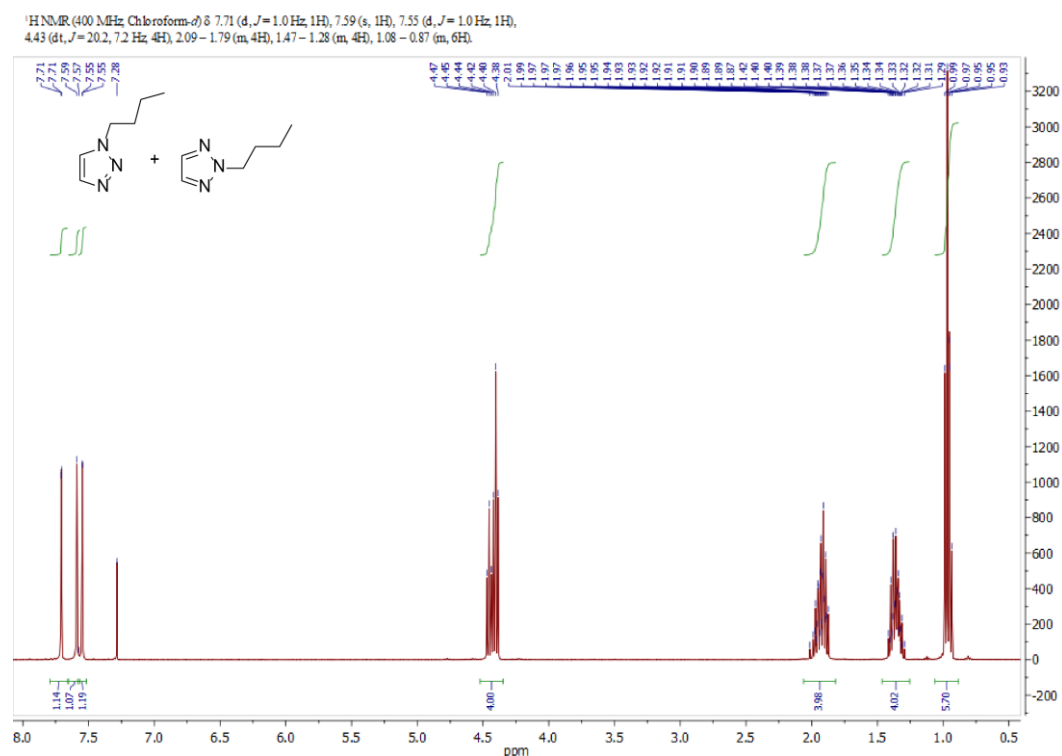


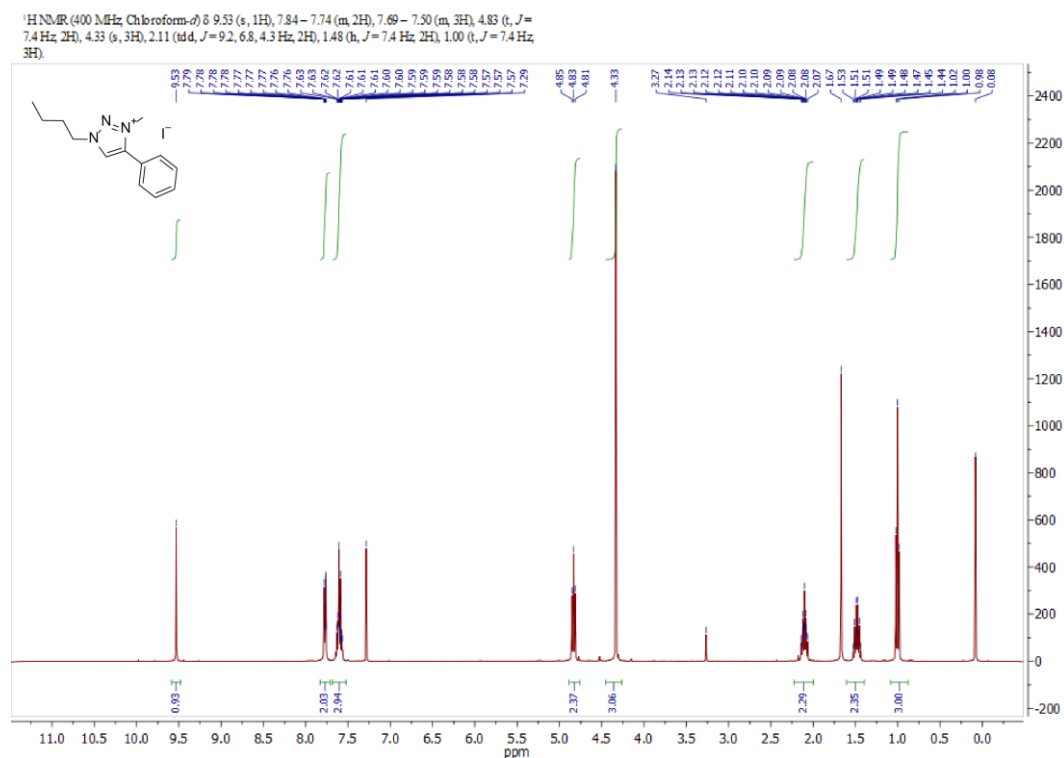
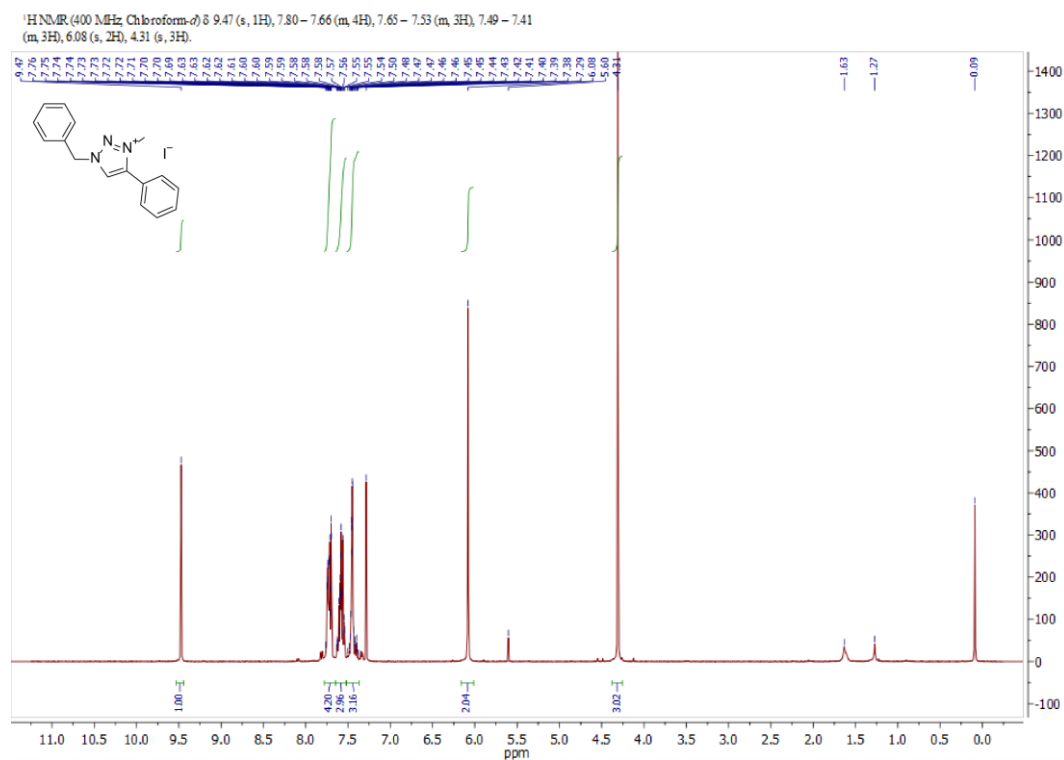
Figure S2.2. ¹H NMR spectrum for BnN₃ (400 MHz, CDCl₃).

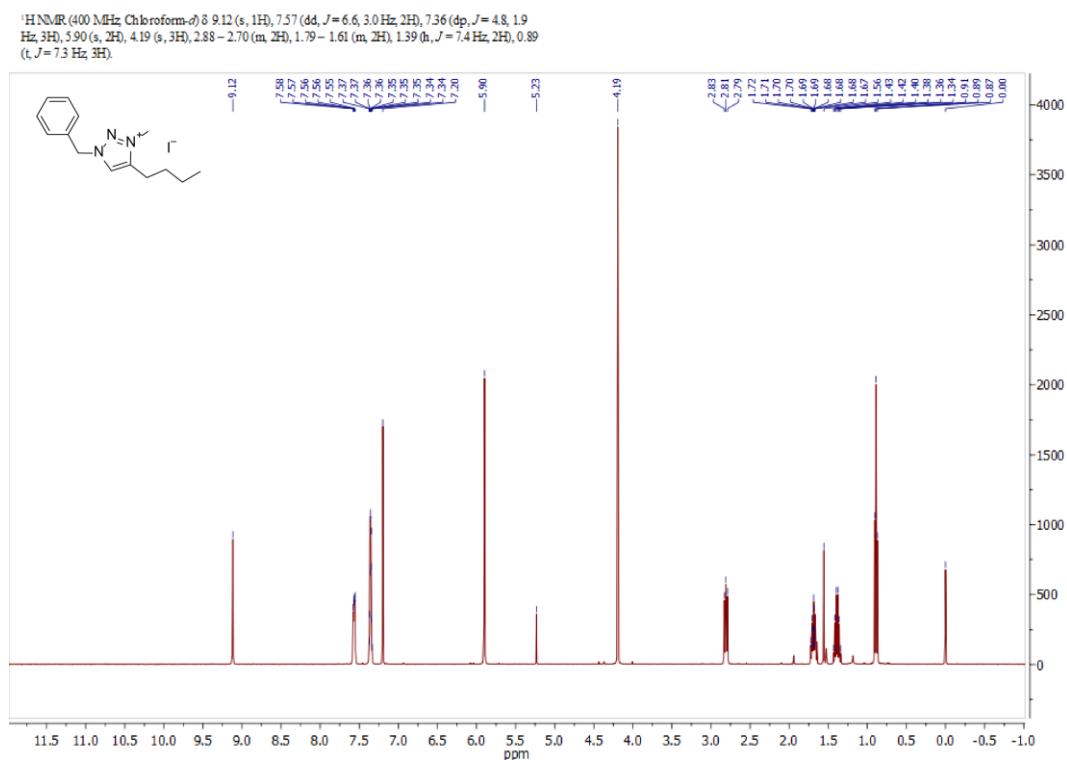
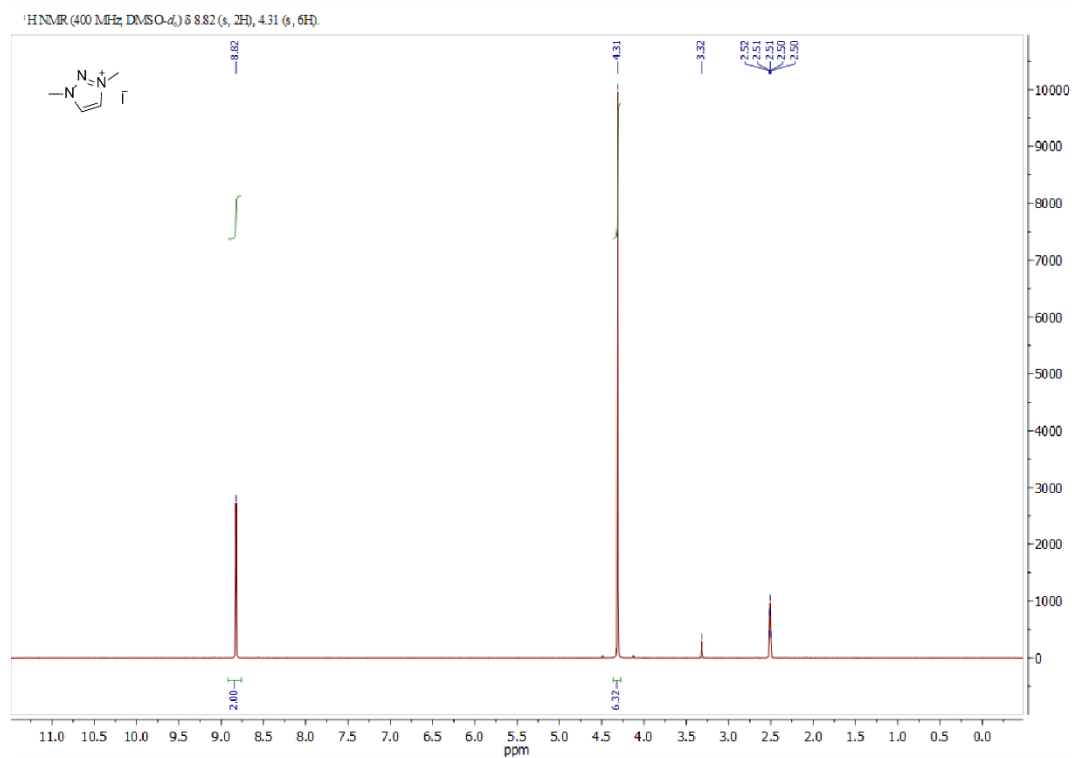
Figure S2.3. ¹³C NMR spectrum for BnN₃ (101 mHz, CDCl₃).Figure S2.4. ¹H NMR spectrum for 1-butyl-4-phenyltriazole (400 mHz, CDCl₃).

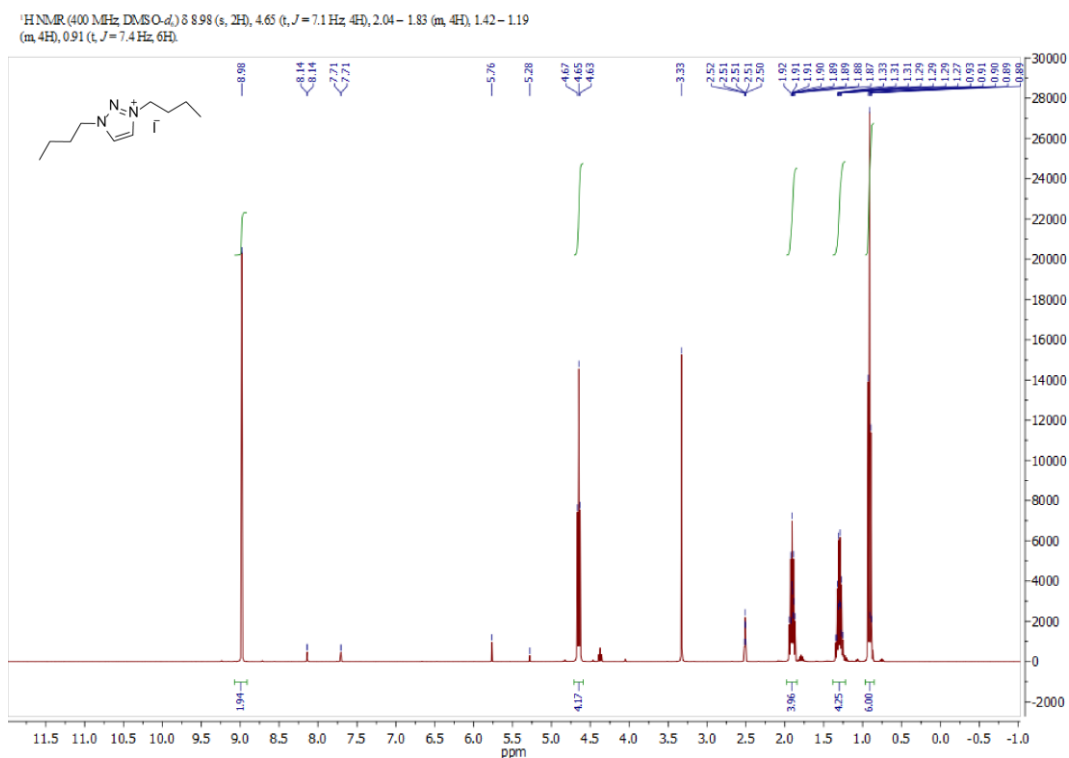
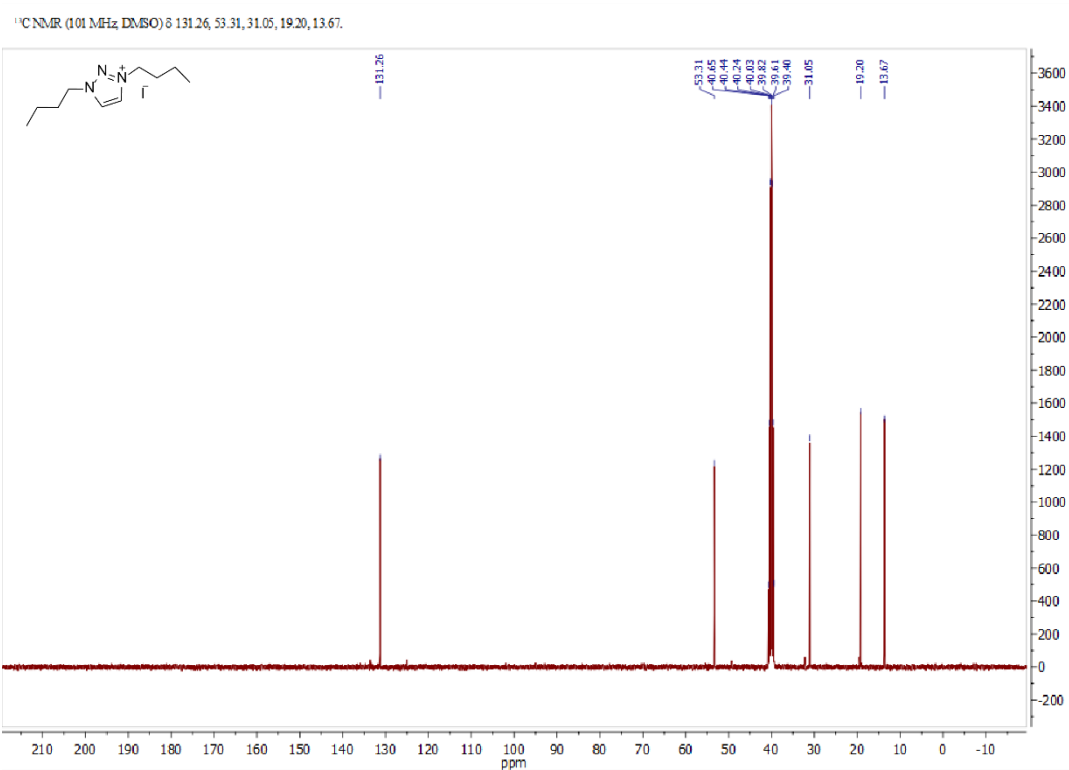
Figure S2.5. ¹³C NMR spectrum for 1-butyl-4-phenyltriazole (101 mHz, CDCl₃).Figure S2.6. ¹H NMR spectrum for 1-benzyl-4-phenyltriazole (400 mHz, CDCl₃).

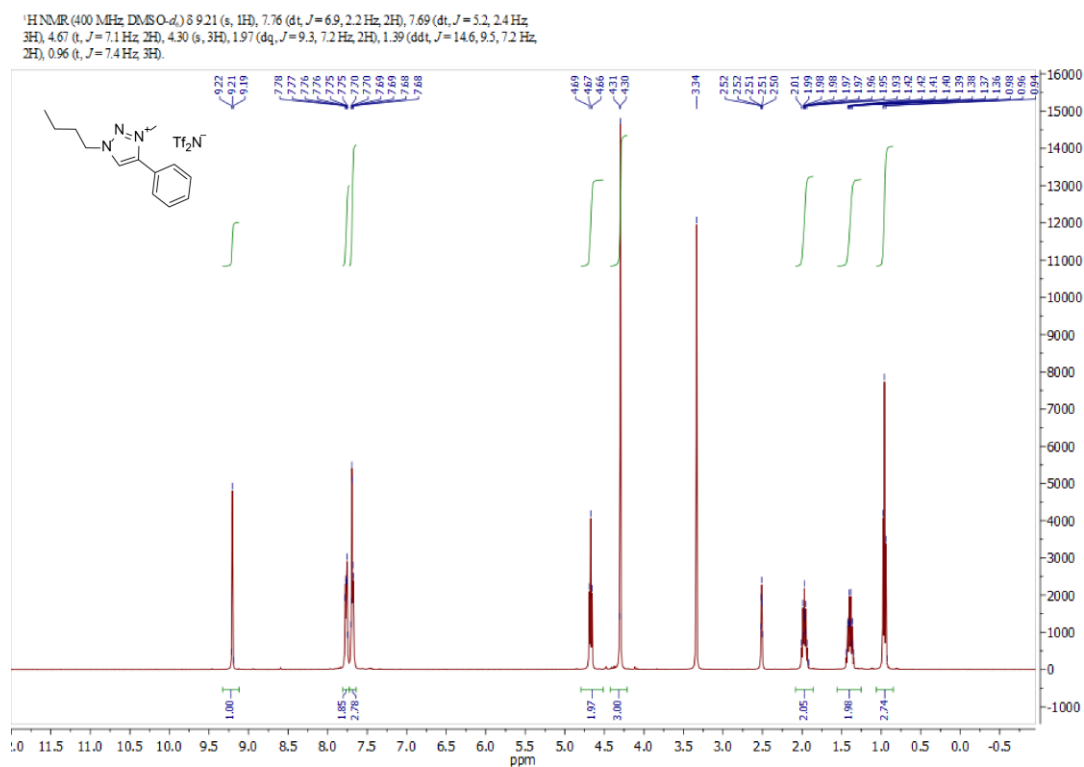
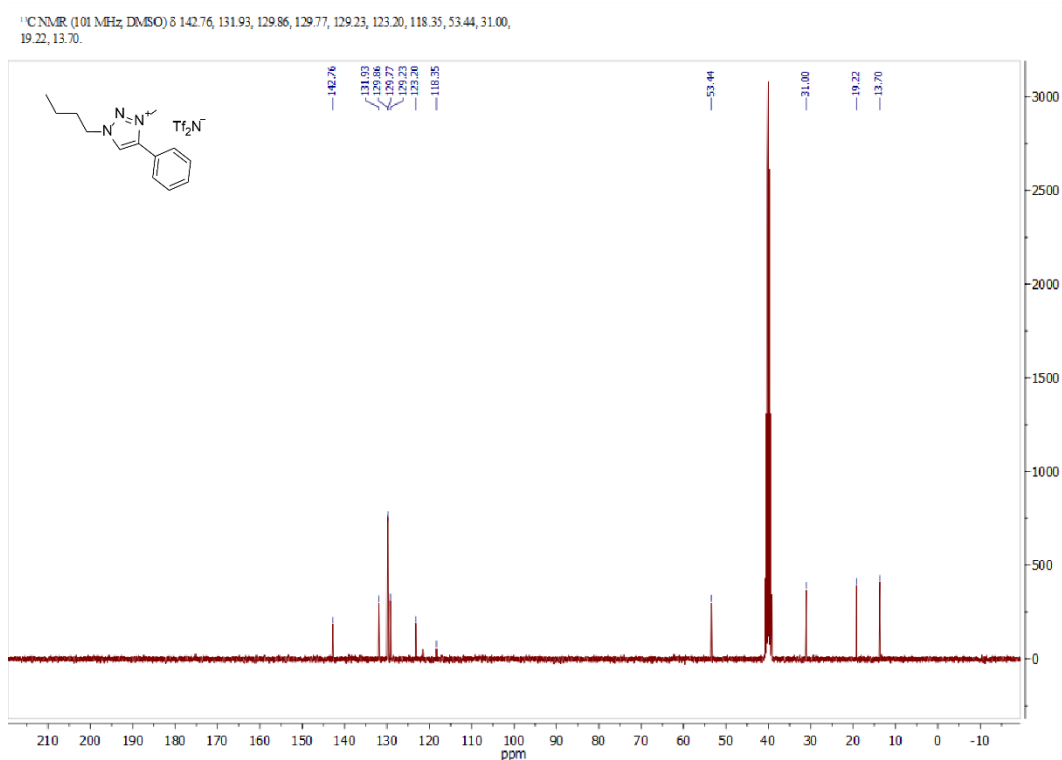
Figure S2.7. ¹³C NMR spectrum for 1-benzyl-4-phenyltriazole (101 MHz, CDCl₃).Figure S2.8. ¹H NMR spectrum for 1-benzyl-4-butyltriazole (400 MHz, CDCl₃).

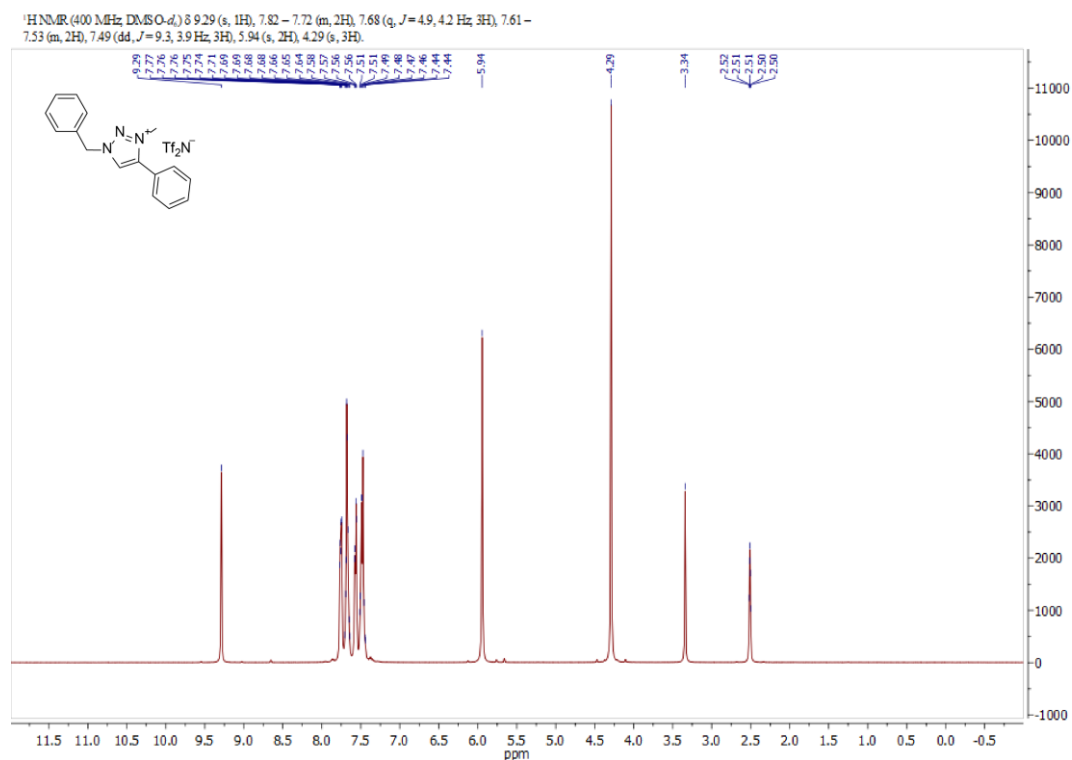
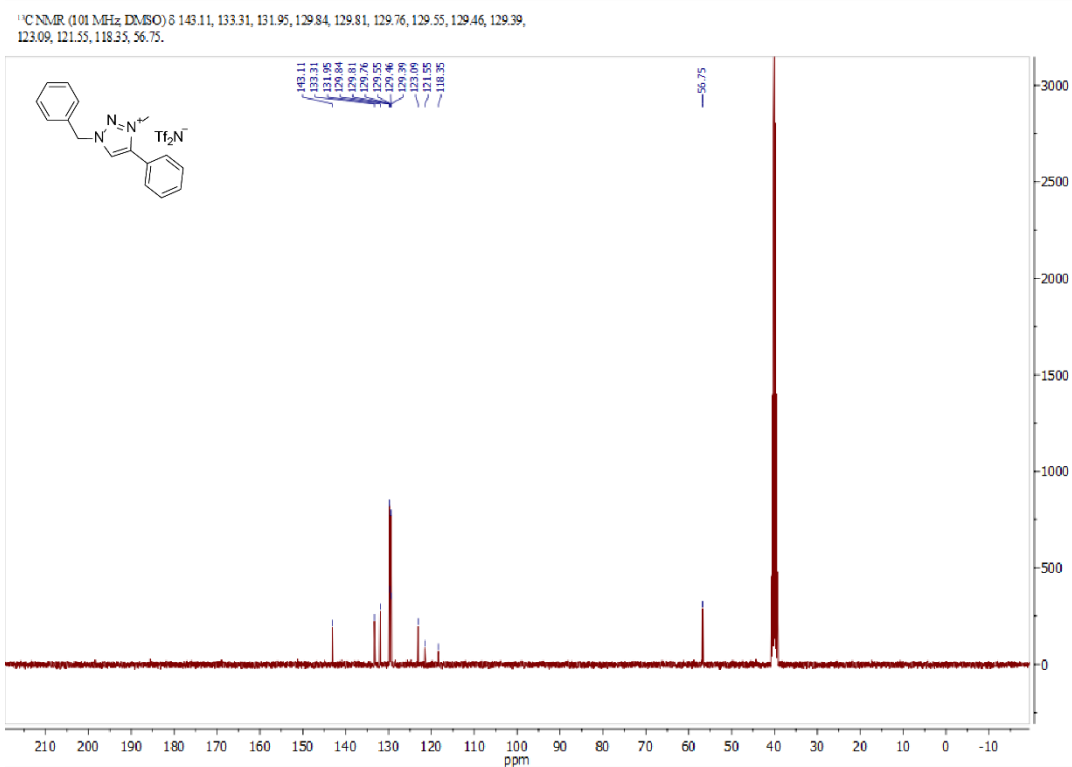
Figure S2.9. ¹H NMR spectrum for 1-methyl-triazole (400 MHz, CDCl₃).Figure S2.10. ¹H NMR spectrum for the mixture of 1-butyls and 2-butyl-triazoles (400 MHz, CDCl₃).

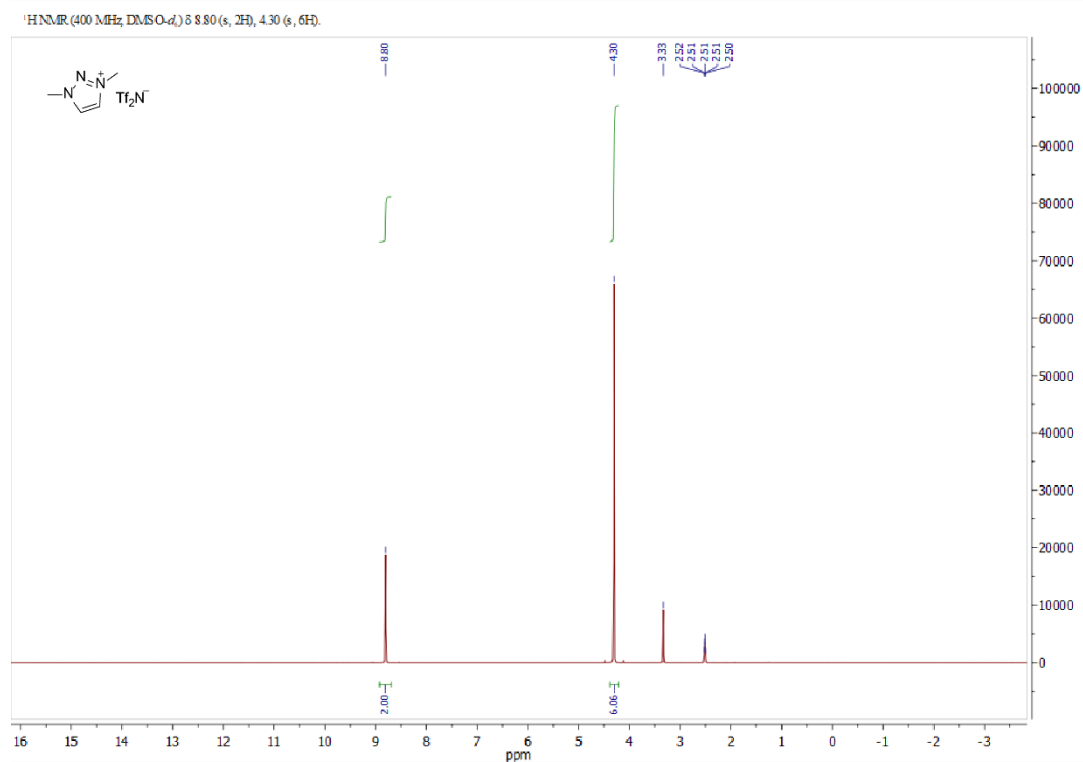
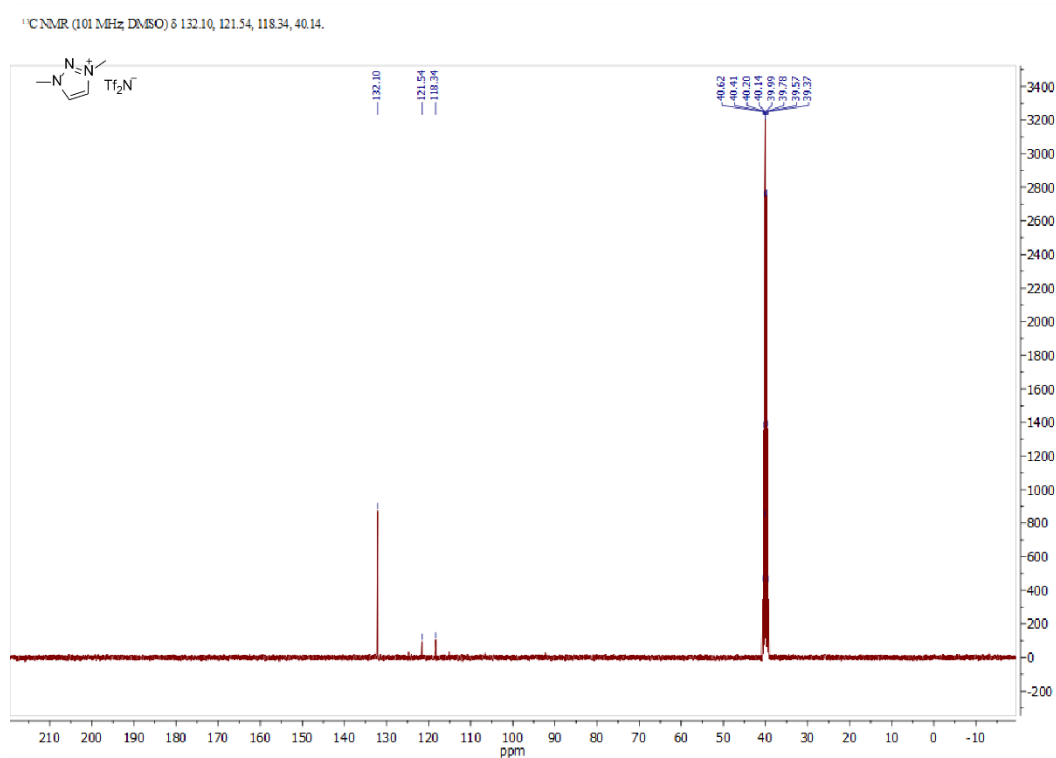
Figure S2.11. ¹H NMR spectrum for 1-butyl-3-methyl-4-phenyltriazolium iodide (400 MHz, CDCl₃).Figure S2.12. ¹H NMR spectrum for 1-benzyl-3-methyl-4-phenyltriazolium iodide (400 MHz, CDCl₃).

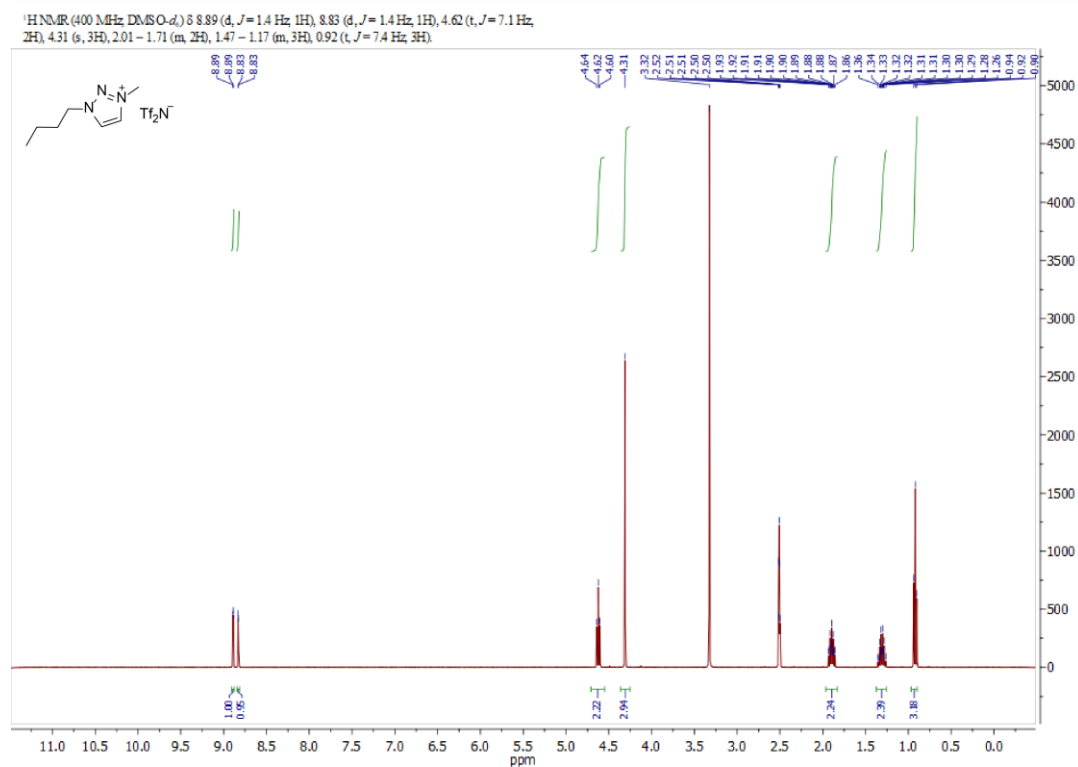
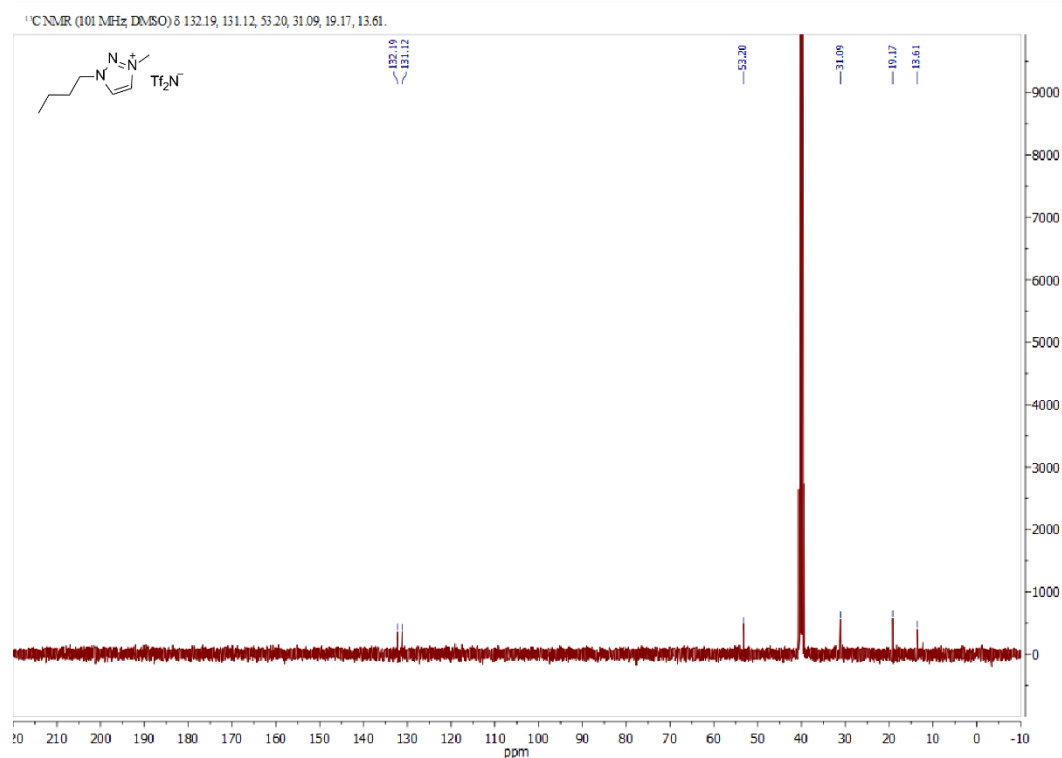
Figure S2.13. ¹H NMR spectrum for 1-benzyl-3-methyl-4-butyltriazolium iodide (400 MHz, CDCl₃).Figure S2.14. ¹H NMR spectrum for 1,3-dimethyltriazolium iodide (400 MHz, DMSO-*d*₆).

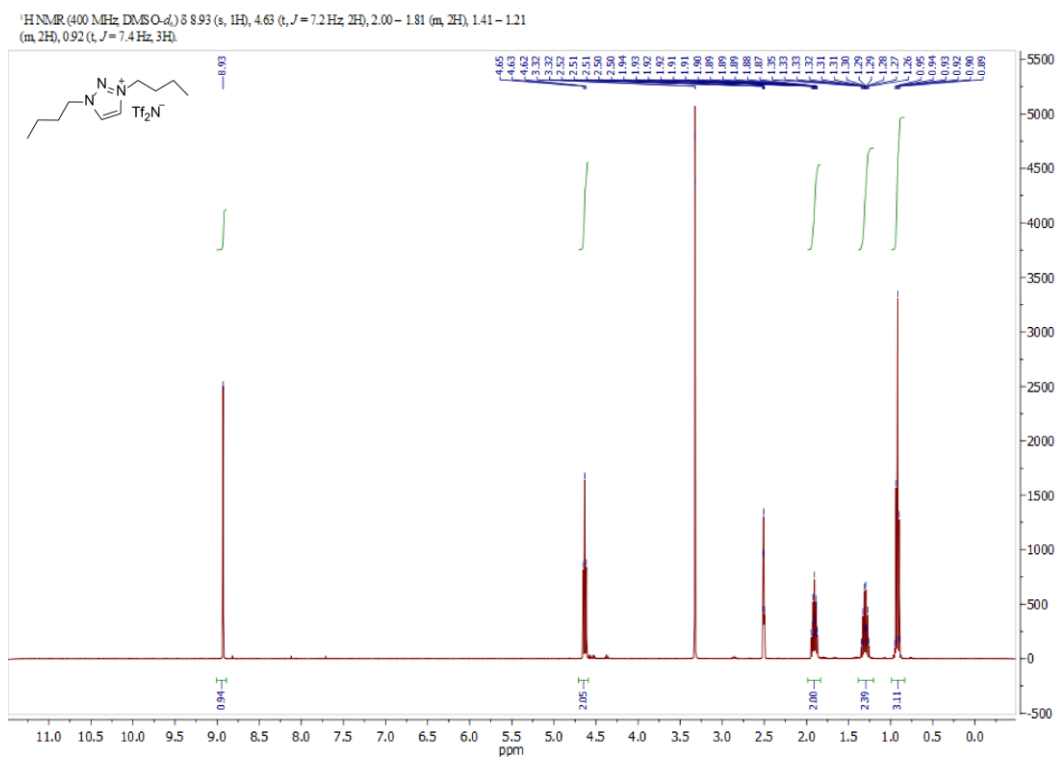
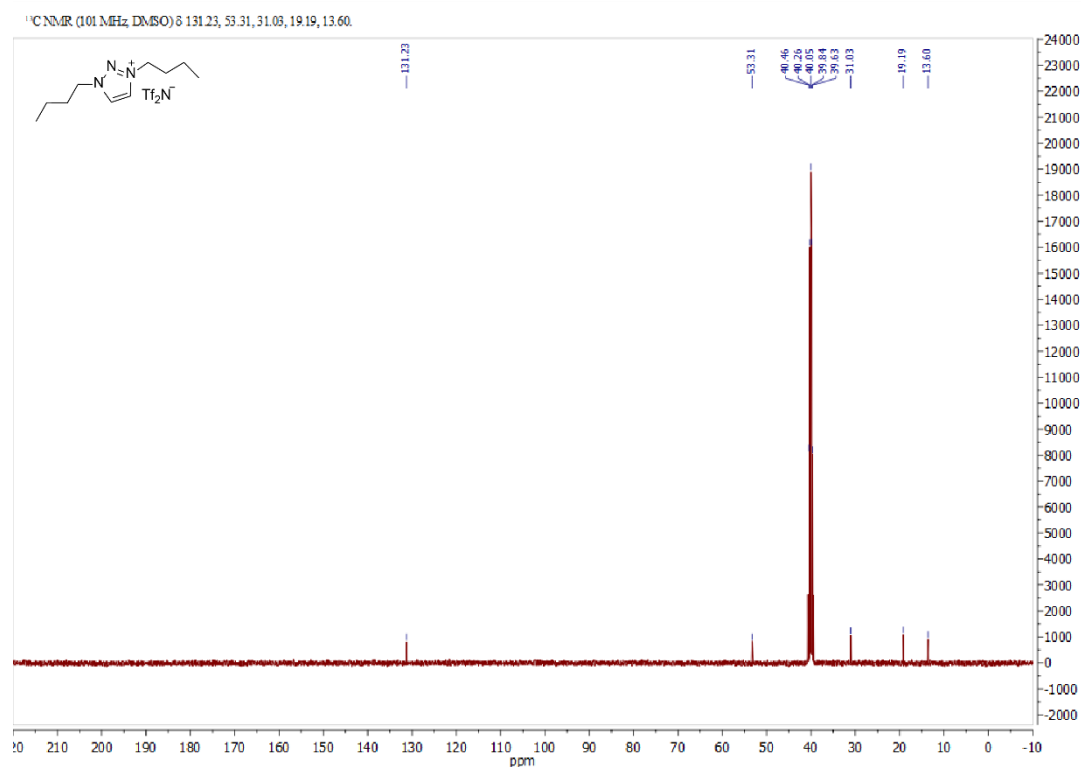
Figure S2.15. ¹H NMR spectrum for 1,3-dibutyltriazolium iodide (400 MHz, DMSO-*d*₆).Figure S2.16. ¹³C NMR spectrum for 1,3-dibutyltriazolium iodide (101 MHz, DMSO-*d*₆).

Figure S2.17. ¹H NMR spectrum for 1-butyl-3-methyl-4-phenyltriazolium TFSI (400 MHz, DMSO-*d*₆).Figure S2.18. ¹³C NMR spectrum for 1-butyl-3-methyl-4-phenyltriazolium TFSI (101 MHz, DMSO-*d*₆).

Figure S2.19. ¹H NMR spectrum for 1-benzyl-3-methyl-4-phenyltriazolium TFSI (400 MHz, DMSO-*d*₆).Figure S2.20. ¹³C NMR spectrum for 1-benzyl-3-methyl-4-phenyltriazolium TFSI (101 MHz, DMSO-*d*₆).

Figure S2.21. ^1H NMR spectrum for 1,3-dimethyltriazolium TFSI (400 MHz, $\text{DMSO-}d_6$).Figure S2.22. ^{13}C NMR spectrum for 1,3-dimethyltriazolium iodide (101 MHz, $\text{DMSO-}d_6$).

Figure S2.23. ¹H NMR spectrum for 1-butyl-3-methyltriazolium TFSI (400 MHz, DMSO-d₆).Figure S2.24. ¹³C NMR spectrum for 1-butyl-3-methyltriazolium TFSI (101 MHz, DMSO-d₆).

Figure S2.25. ¹H NMR spectrum for 1,3-dibutyltriazolium TFSI (400 MHz, DMSO-d₆).Figure S2.26. ¹³C NMR spectrum for 1,3-dibutyltriazolium TFSI (101 MHz, DMSO-d₆).

2.6 References

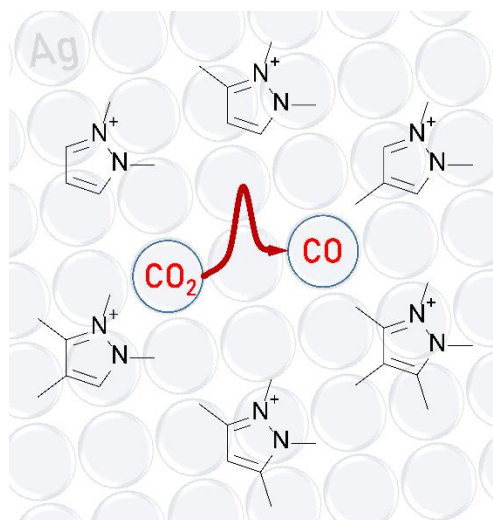
- (1) Lau, G. P. S.; Schreier, M.; Vasilyev, D.; Scopelliti, R.; Grätzel, M.; Dyson, P. J. New Insights into the Role of Im-Based Promoters for the Electroreduction of CO₂ on a Silver Electrode. *J. Am. Chem. Soc.* **2016**, *138*, 7820–7823.
- (2) Arnold, P. L.; Pearson, S. Abnormal N-Heterocyclic Carbenes. *Coord. Chem. Rev.* **2007**, *251*, 596–609.
- (3) Rostovtsev, V. V.; Green, L. G.; Fokin, V. V.; Sharpless, K. B. A Stepwise Huisgen Cycloaddition Process: Copper(I)-Catalyzed Regioselective “Ligation” of Azides and Terminal Alkynes. *Angew. Chemie Int. Ed.* **2002**, *41* (14), 2596–2599.
- (4) Sanghi, S.; Willett, E.; Versek, C.; Tuominen, M.; Coughlin, E. B. Physicochemical Properties of 1,2,3-Triazolium Ionic Liquids. *RSC Adv.* **2012**, *2*, 848–853.
- (5) Lieber, E.; Chao, T. S.; Rao, C. N. R. Improved Method for the Synthesis of Alkyl Azides. *J. Org. Chem.* **1957**, *22*, 238–240.
- (6) Spencer, D. A. XXXVII.—The Action of Bromine on Sodium and Silver Azides. *J. Chem. Soc., Trans.* **1925**, *127* (0), 216–224.
- (7) Bock, H.; Dammel, R. The Pyrolysis of Azides in the Gas Phase. *Angew. Chemie Int. Ed. English* **1987**, *26* (6), 504–526.
- (8) Rosen, B. A.; Salehi-Khojin, A.; Thorson, M. R.; Zhu, W.; Whipple, D. T.; Kenis, P. J. A.; Masel, R. I. Ionic Liquid – Mediated Selective Conversion of CO₂ to CO at Low Overpotentials. *Science* **2011**, *334*, 643–644.
- (9) Du, V.; Behrens, O. K. A Method for Protecting The Imidazole Ring of Histidine During Certain Reactions and Its Application to the Preparation of L-Amino-N-Methylhistidine. **1936**, *117*, 27–36.
- (10) Elgrishi, N. N.; Rountree, K. J.; McCarthy, B. D.; Rountree, E. S.; Eisenhart, T. T.; Dempsey, J. L. A Practical Beginner’s Guide to Cyclic Voltammetry. **2017**.

Chapter 3 Pyrazolium Ionic Liquids

3.1 Introduction

In the previous chapter, we considered application of the Tz ILs for the CO₂RR, which is similar to the usage of the classical Im ILs in the terms of the structure of the co-catalyst. Herein, we report on an even more dramatic change related to the structure of the cation. By switching from Im salts to the pyrazolium (Pz) ILs the reduction of CO₂ to CO proceeds with higher Faradaic efficiencies (FEs) without decomposition while maintaining the same high current densities, therefore making a further step towards a com-

mercial viable electrochemical CO₂ conversion process.^{1,2} To the best of our knowledge, this is the first example describing the use of pyrazolium ILs as co-catalysts in the electroreduction of CO₂. Despite certain similarity of Im and Pz rings, the latter possess different resonance structures, charge distributions and are usually less likely to form carbenes and hydrogen bonds.



3.2 Results

The methyl-substituted Pz ILs used in the electrochemical investigation are shown in Figure 3.1. Methyl groups were systematically introduced onto the ring to investigate the influence of the substitution pattern on the activity. In all cases bis(trifluoromethylsulfonyl)imide (Tf_2N^-) was used as the anion unless stated otherwise.

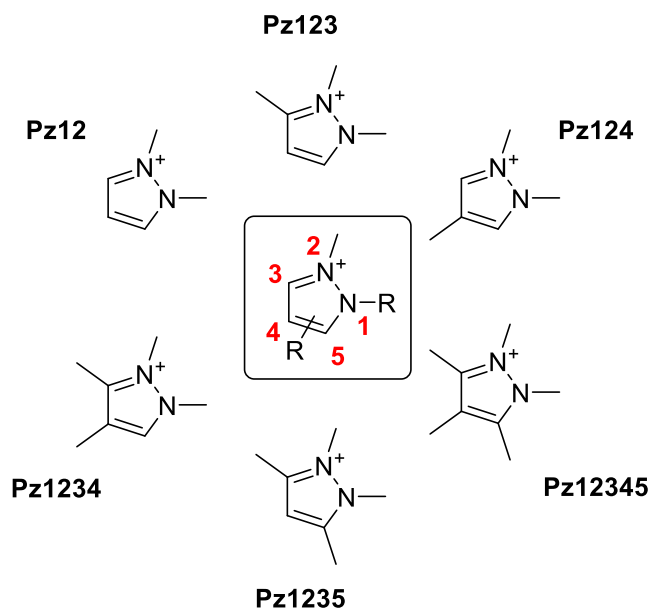


Figure 3.1. Pz cations used in this study.

Electrochemical measurements were performed in dry acetonitrile (MeCN) containing 0.1 M NBu_4PF_6 . This system dissolves significant amounts of CO_2 (eight times higher than water)³ and possesses a potential window exceeding 4 V.⁴ Moreover, conducting the studies in MeCN allows the influence of water on the reaction to be probed separately. A silver commercially available disk electrode was employed as the cathode, since it exhibits high FEs for CO production,⁵ is easy to handle and, moreover, there is a wealth of experimental data accumulated on such electrodes. The Pz ILs were used in the concentration of 0.02 M in order to promote the reduction

The stabilities of the Pz ILs were investigated by cyclic voltammetry (CV) under an argon atmosphere. The decomposition onset potential tends to shift towards more negative values with the introduction of methyl groups on the Pz ring (Figure 3.2), i.e. electron-donating substituents and/or increased steric hindrance of the ring result in higher stabilities. Methyl groups at positions C3 and C5 influence on the stability to a greater extent than methylation of the C4-position, therefore it seems likely that decomposition occurs at C-N or N-N sites.

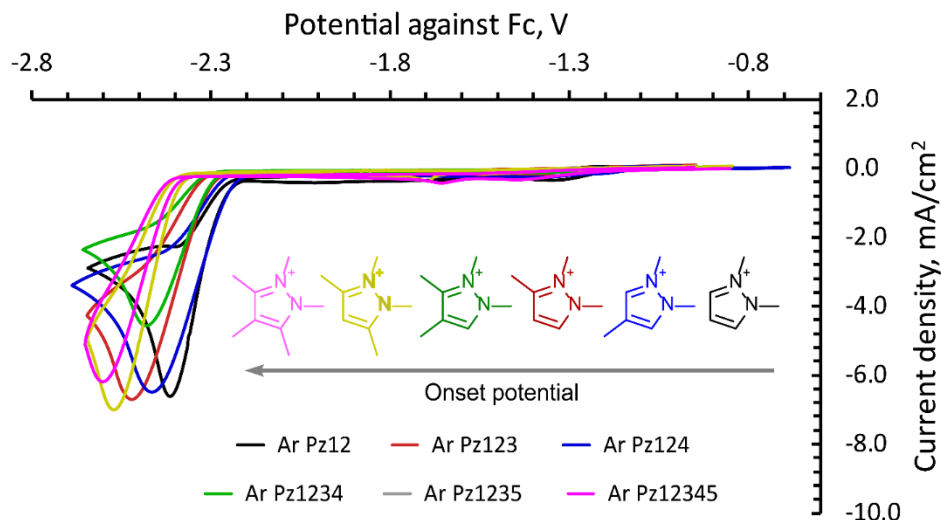


Figure 3.2. CVs for the Pz ILs under Ar, illustrating the differences in stability of diversely substituted Pz cations (Ag polished disk electrode, 0.1 M NBu_4PF_6 in dry acetonitrile, 0.02 M IL additive).

CV experiments were then performed under a CO_2 atmosphere. A significant shift of the onset potential towards more positive values, followed by a steep increase in the current density is observed under these conditions (Figure 3.3).

Different variations of the Pz ILs structures effect the co-catalytic performance in the reduction of CO_2 to CO in the following way: (1) the introduction of methyl groups on the Pz ring leads to a slight increase in the reduction onset potential (SI, Figure S3.1 – S3.5); (2) substitution of the N-methyl group by a butyl group has minor impact on catalytic performance (SI, Figure S3.6); (3) replacement of Tf_2N^- anion by TfO^- does not alter the performance of the co-catalyst, which is expected as the reduction takes place in NBu_4PF_6 solution, and the concentration of PF_6^- is 5 times higher than that of the IL anion (0.1 M vs 0.02 M, respectively, see SI, Figure S3.7). Therefore, neglecting the minor impact in onset potential with substitution, and taking into consideration the increase in their stability, the more substituted Pz ILs are the most attractive co-catalysts.

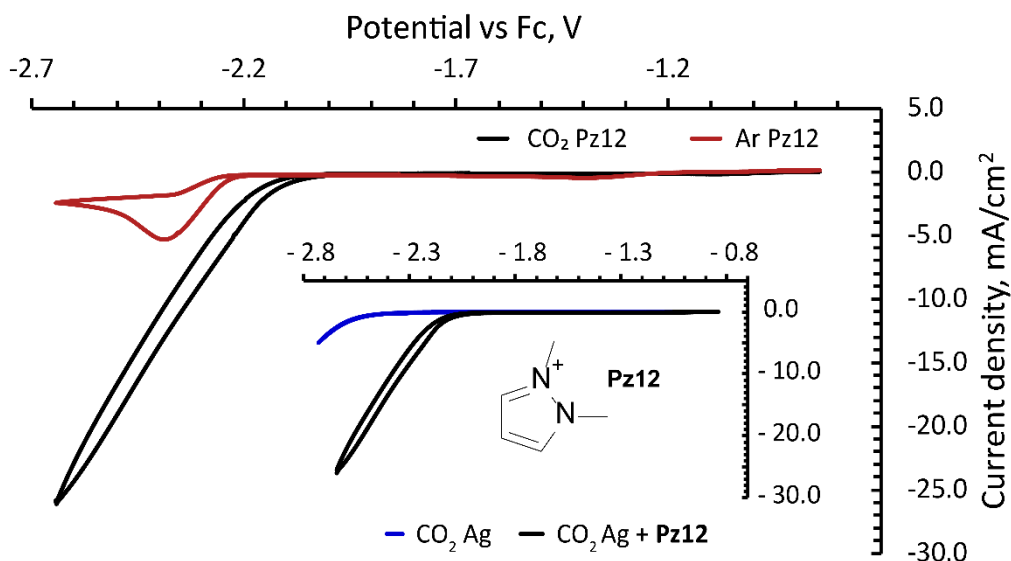


Figure 3.3. Example of the change in the CV after addition of CO₂ using **Pz12** as the co-catalyst (red – argon atmosphere, black – carbon dioxide atmosphere). The performance of the silver electrode towards CO₂ reduction with and without Pz IL additives are compared in the inset. CVs for the other Pz ILs under CO₂ are provided in the SI (Figures S3.1 – S3.5).

The reduction waves for the Pz ILs recorded in the presence of CO₂ do not reach a current limitation peak at the decomposition potential of the co-catalyst (Figure 3.3). This is particularly striking for co-catalyst **Pz1235**, which affords current densities $\approx 30 \text{ mA/cm}^2$ (Figure S3.5).

CVs using a glassy carbon electrode were recorded employing the same conditions both under Ar and under a CO₂ atmosphere. Under Ar, the onset potentials for the CVs do not differ from those recorded on the silver electrode (SI, Figure S3.8). Moreover, the voltammetric response of the glassy carbon remains unchanged when the solution is saturated with CO₂. Combined, this demonstrates that the Ag electrode is the actual catalyst for the reduction, and that the IL behaves as a co-catalyst in the reduction of CO₂ to CO. Notably, the introduction of CO₂ does not result in destabilization of the Pz ILs.

In order to confirm that the changes of the current registered are related to the CO₂ reduction process, rather than catalyst decomposition, chronoamperometric experiments followed by online gas chromatography analysis were performed using a two-compartment H-type cell and IL **Pz1235B** as a compromise between activity and stability of the promoter. An aqueous 0.5 M sulfuric acid solution was used in the compartment with the counter-electrode in order to decrease the impedance of the system and avoid the formation of MeCN decomposition products, which interfere with the separator (a Nafion 117 membrane). As Nafion is able to conduct protons, hydrogen-containing

products or hydrogen itself could be expected if the HER takes place. The results of the measurements are presented in Figure 3.4 and the values are summarized in Table 3.1.

FEs for CO formation are around 100% with current densities up to 30 mA/cm^2 , which suggests that CO is the major product formed. Small amounts of hydrogen (from 1 – 4 %) and formic acid (< 4%) were detected and ^1H NMR spectroscopy, respectively. ^1H NMR spectroscopy revealed no decomposition of the Pz IL over the time of the electrolysis (Figure S3.52). Notably, small amounts of methane (around 0.5 – 1 % FE) were observed as well by GC at low overpotentials (see Table 1). The formation of methane has been detected as well by GC during CO_2 reduction at a Ag foil electrode in aqueous solution,⁶ but to the best of our knowledge not in acetonitrile solution. The maximum amount of methane was obtained at the potential when active decomposition of the catalyst (according to the CVs recorded under Ar, Figure 3.2) does not take place. Thus, the methane must be derived from carbon dioxide.

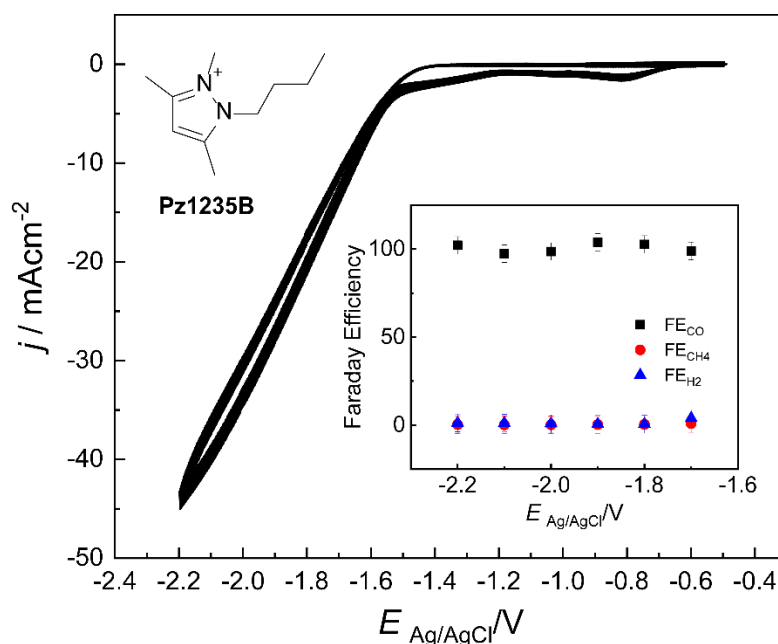


Figure 3.4. Dependency of the Faradaic efficiency in the formation of the detected products on voltage employing **Pz1235B**. Conditions: cathode – Ag foil; anode – Pt foil; catholyte – 0.1 M NBu_4PF_6 in MeCN, 0.02 M IL, saturated with CO_2 ; anolyte – 0.5 M H_2SO_4 (aq); separator – Nafion 117.

Table 3.1. Faradaic efficiencies for different products as a function of the reduction potential for CO₂ electrolysis employing **Pz1235B**.

Potential (vs Fc ⁺ /Fc), V	FE _{CO} , % ^a	FE _{H₂} , % ^a	FE _{CH₄} , % ^a
-2.11	99	4	0.9
-2.21	103	<1	0.4
-2.31	104	<1	0.3
-2.41	99	<1	0.2
-2.51	97	1	0.1
-2.61	102	1	0.3

^a – Estimated error is ±5% from the value obtained

Table 3.2. Faradaic efficiencies for different products as a function of the reduction potential for CO₂ electrolysis employing [BMIm][BF₄].

Potential (vs Fc ⁺ /Fc), V	FE _{CO} , % ^a	FE _{H₂} , % ^a	FE _{CH₄} , % ^a
-2.11	92	<1	-
-2.21	92	<1	-
-2.31	87	1	-

^a – Estimated error is ±5% from the value obtained

Water may impact on the electroreduction process depending upon the nature of the catalyst.^{7,8} For Pz ILs, water significantly shifts the CO₂ reduction onset potential towards more positive values. As an example, the influence of water on co-catalysis **Pz1235** is shown in Figure 3.5. As the water content increases the onset potential for the reduction of CO₂ gradually decreases, until a concentration of 0.3-0.6 mM reached (the value depends on the Pz IL employed).

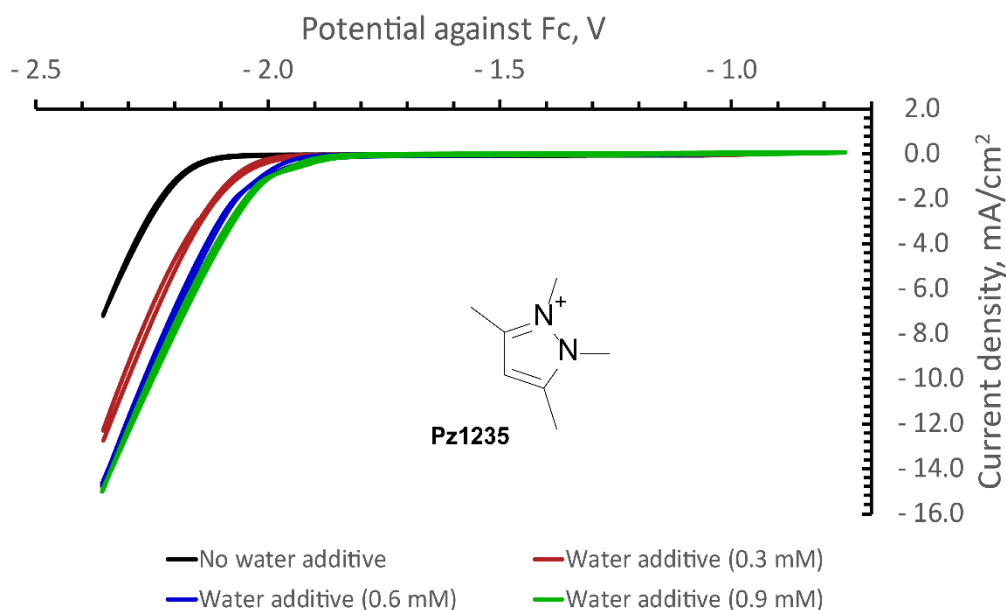


Figure 3.5. Decrease of the electrochemical reduction onset potential for the conversion of CO₂ to CO using co-catalyst **Pz1235** in the presence of water.

The activity of the Pz ILs was compared to [BMIm][BF₄] (where BMIm = the 1-butyl-3-methyl-Im cation, Figure S3.9) using Pz IL **Pz1235B** as a representative example. [BMIm][BF₄] is structurally similar to [EMIm][BF₄] (where EMIm = the 1-ethyl-3-methyl-Im cation), which is considered as the benchmark IL co-catalyst for this reaction.⁵ Under equivalent conditions **Pz1235B** exhibits a comparable onset potential and current density to [BMIm][BF₄], displaying a slightly steeper slope for the reduction wave.

In order to demonstrate consistency of the working procedures, chronoamperometric experiments followed by GC analysis were performed for the [BMIm][BF₄] and Pz IL systems under the same conditions and employing the same equipment (SI, Figure S3.9). The [BMIm][BF₄] co-catalyst results in good FE for CO (ca. 90% for low overpotentials, ca. 80-90% at higher voltages, see the SI), which is consistent with the literature.⁵ However, in case of [BMIm][BF₄] the only reduction products observed are CO and negligible amounts of H₂. No traces of methane or other products were detected by ¹H and ¹³C NMR spectroscopy or GC.

The protons in Pz-based ILs should not be readily reduced to form carbenes from the Pz, which excludes the likelihood of the formation of covalent adducts with CO₂, e.g. carboxylates, as is the case of Im ILs.⁹ Moreover, the fully substituted Pz IL **Pz12345** displays high catalytic performance, excluding the possibility of covalent interactions between the Pz IL and CO₂. As mentioned above, catalysis

occurs when a silver electrode is used as the cathode and not with a glassy carbon electrode. Therefore, the initial step of the reduction most probably corresponds to the formation of a CO_2 -based radical-anion on the surface of the silver electrode (Figure 3.6). The effect of the co-catalyst should then result from stabilization of this intermediate by ion pair, dipole-ion interactions or change of the local microenvironment. According to previous reports, IL cations are able to arrange on the silver surface in a coplanar fashion to form a double layer.^{10,11} The nitrogen-containing domain of the Pz cation is the most positively charged region and substitution at C3 and C5 positions changes the activity of the system more significantly than at the C4 position. Therefore, it is reasonable to assume that the CO_2^- intermediate interacts with the positively charged region of the Pz ring (Figure 3.6), which helps to stabilize the intermediate and lower the overpotential of the reaction.

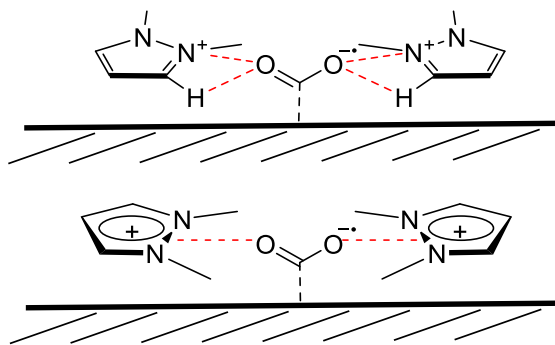


Figure 3.6. Possible intermediate structures between the Pz cations and the $\text{CO}_2^{\bullet-}$ radical anion leading to a lowering of the overpotential in the reduction of CO_2 to CO.

3.3 Summary

In conclusion, a series of substituted Pz ILs was synthesized and shown to be efficient co-catalysts for electrochemical reduction of CO_2 to CO, superior to the benchmark Im ILs in terms of FE for CO formation (100% vs. 80-90%). High current densities (30 mA/cm^2 during electrolysis) were achieved. The influence of the substitution pattern on the Pz ring on stability and activity was investigated, with substituents generally stabilizing the co-catalyst, but slightly decreasing performance. Water significantly decreases the reduction onset potential for most Pz co-catalysts. Additionally, during chronoamperometric experiments the unexpected formation of small quantities of methane and formic acid was observed, which is highly encouraging and warrants further investigation of Pz ILs with other electrode materials.

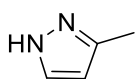
3.4 Experimental

3.4.1 Materials and methods.

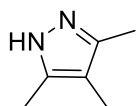
All reagents were obtained commercially and used without further purification unless otherwise stated. CO₂ (99.998 %) and Ar (99.9999 %) were obtained from Carbagas, Switzerland. ¹H, ¹⁹F and proton-decoupled ¹³C-NMR spectra were recorded on a Bruker Avance-400 (400 MHz) spectrometer. All reactions were completed under inert conditions (nitrogen atmosphere). For the graphical representation of NMR spectra please see the Supporting Information. Electrochemical measurements were made in according with the protocols from Chapter 2.

3.4.2 Synthesis and characterization of the compounds.

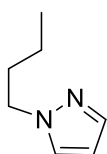
3-methyl-1H-pyrazole: To a cooled (ice water bath) solution of 4,4-dimethoxybutan-2-one (5.00 g, 38 mmol) in methanol (20 mL) a solution of N₂H₄·HCl (3.12 g, 45.6 mmol) in deionized water (10 mL) was added dropwise and stirred for 15 min. The mixture was heated to reflux for 24 h. After cooling, the solvent was removed under reduced pressure, the residue was dissolved in water (20 mL), the pH was adjusted to 8-9 with sodium hydroxide aqueous solution (1 M) and the mixture was extracted by ethyl acetate (3 times equal volume). The combined organic phase was washed with brine (equal volume), organic solvent was removed and the residue was dried under vacuum affording a pale yellow liquid (2.82 g, 93%). ¹H NMR (400 MHz, DMSO-d₆, δ): 7.44 (s, 1H, Pz H), 6.00 (d, 1H, Pz H), 2.21 (s, 3H, CH₃); ¹³C NMR (100 MHz, DMSO-d₆, δ): 104.06, 12.08.



3,4,5-trimethylpyrazole: Prepared employing the same procedure as for 3-methyl-1H-pyrazole, starting with 3-methylpentane-2,4-dione. Colorless solid. Yield 82% (0.78 g). ¹H NMR (400 MHz, DMSO-d₆, δ): 2.06 (s, 6H, CH₃), 1.83 (s, 3H, CH₃); ¹³C NMR (100 MHz, DMSO-d₆, δ): 109.48, 10.87, 7.78.

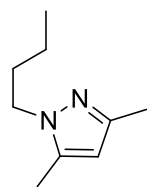


N-butylpyrazole: A mixture of corresponding pyrazole (2.92 g, 43 mmol), potassium carbonate (8.90 g, 64 mmol), bromobutane (11.80 g, 86 mmol) and dry acetonitrile (25 mL) was stirred under reflux for 24 h. Potassium tert-butoxide (1 mg, 9 mmol) was added to the solution and the mixture was heated under reflux for a further 24 h. Then the solvent was evaporated under reduced pressure, diluted with water (ca. 50 mL), and the product extracted with diethyl ether (3 times ca. 50 mL) and washed with brine (ca. 150 mL). Removal of the solvent under vacuum affords the required product. Yield 61% (3.28 g). ¹H NMR (400 MHz, DMSO-d₆, δ): 7.68 (d,



1H, Pz H), 7.41 (d, 1H, Pz H), 6.20 (t, 1H, Pz H), 4.09 (t, 2H, CH₂), 1.74 (m, 2H, CH₂), 1.22 (m, 2H, CH₂), 0.88 (t, 3H, CH₃); ¹³C NMR (100 MHz, DMSO-d₆, δ): 138.68, 129.86, 105.14, 51.19, 32.48, 19.63, 13.81.

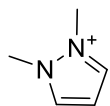
1-butyl-3,5-dimethylpyrazole: Synthesized employing the same protocol as for N-butylpyrazole, starting with 3,5-dimethylpyrazole (5.00 g, 69.4 mmol). Product was purified by vacuum distillation. Yield: 4.28 g, 40.5%. ¹H NMR (400 MHz, DMSO-d₆, δ): 5.74 (s, 1H, Pz H), 3.88 (t, 2H, CH₂), 2.18 (s, 3H, CH₃), 2.07 (s, 3H, CH₃), 1.65 (m, 2H, CH₂), 1.26 (m, 2H, CH₂), 0.89 (t, 3H, CH₃); ¹³C NMR (100 MHz, DMSO-d₆, δ): 145.75, 138.38, 104.66, 47.89, 32.38, 19.76, 13.95, 13.73, 10.93.



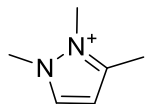
General procedure for pyrazolium iodides:

To a solution of corresponding pyrazole (1 eq) in dry acetonitrile (0.75 mL per mmol of butylpyrazole), iodomethane (2-4 eq) was added and the reaction mixture was stirred at 60°C for 24 h in the dark. After cooling, the solvent was removed under reduced pressure and the solid residue was recrystallized from acetonitrile (1-5 mL/mL) sometimes precipitated with ethyl acetate (ca. 5-10 mL). The product was separated by filtration, washed with ethyl acetate (5-10 mL) and dried under vacuum.

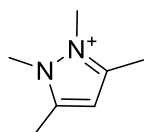
1,2-dimethylpyrazolium iodide: Starting with pyrazole (1.00 g, 14.7 mmol). Yield 22% (0.74 g). ¹H NMR (400 MHz, DMSO-d₆, δ): 8.47 (d, 2H, Pz H), 6.82 (t, 1H, Pz H), 4.12 (s, 6H, CH₃); ¹³C NMR (100 MHz, DMSO-d₆, δ): 137.92, 107.27, 37.00.



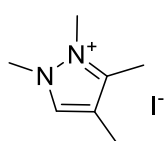
1,2,3-trimethylpyrazolium iodide: Starting with 3-methylpyrazole (0.70 g, 8.5 mmol). Yield 45% (0.91 g). ¹H NMR (400 MHz, DMSO-d₆, δ): 8.34 (d, 1H, Pz H), 6.69 (d, 1H, Pz H), 4.07 (s, 3H, CH₃), 3.94 (s, 3H, CH₃), 2.45 (s, 3H, CH₃); ¹³C NMR (100 MHz, DMSO-d₆, δ): 146.77, 136.85, 107.25, 37.32, 33.97, 12.14.



1,2,3,5-tetramethylpyrazolium iodide: Starting with 3,5-dimethylpyrazole (1.00 g, 10.4 mmol). Colorless crystals. Yield 68% (1.78 g). ¹H NMR (400 MHz, DMSO-d₆, δ): 6.56 (s, 1H, Pz H), 3.93 (s, 6H, CH₃), 2.42 (s, 6H, CH₃); ¹³C NMR (100 MHz, DMSO-d₆, δ): 145.63, 107.44, 34.36, 12.01.

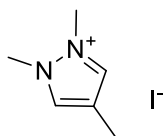


1,2,3,4-tetramethylpyrazolium iodide: Starting with 3,4-dimethylpyrazole (0.50 g, 5.2 mmol). Yield



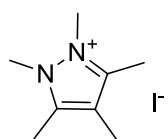
59% (0.78 g). ^1H NMR (400 MHz, DMSO- d_6 , δ): 8.21 (s, 1H, Pz H), 4.04 (s, 3H, CH_3), 3.93 (s, 3H, CH_3), 2.37 (s, 3H, CH_3), 2.05 (s, 3H, CH_3); ^{13}C NMR (100 MHz, DMSO- d_6 , δ): 144.84, 135.65, 115.28, 36.96, 34.06, 10.16, 8.31.

1,2,4-trimethylpyrazolium iodide: Starting with 4-methylpyrazole (0.52 g, 6.3 mmol). Yield 47%



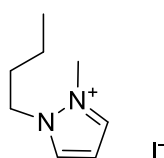
(0.60 g). ^1H NMR (400 MHz, DMSO- d_6 , δ): 8.27 (s, 2H, Pz H), 4.06 (s, 3H, CH_3), 2.10 (s, 3H, CH_3); ^{13}C NMR (100 MHz, DMSO- d_6 , δ): 136.80, 116.87, 36.81, 8.78.

1,2,3,4,5-pentamethylpyrazolium iodide: Starting from 3,4,5-trimethylpyrazole (0.12 g, 1.1 mmol).



Yield 30% (0.08 g). ^1H NMR (400 MHz, DMSO- d_6 , δ): 3.91 (s, 6H, CH_3), 2.35 (s, 6H, CH_3), 2.00 (s, 3H, CH_3); ^{13}C NMR (100 MHz, DMSO- d_6 , δ): 143.62, 133.80, 34.01, 10.16, 7.75.

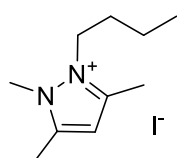
1-butyl-2-methylpyrazolium iodide: To a solution of 1-butylpyrazole (1.00 g, 8.0 mmol) in dry ace-



tonitrile (5 mL) iodomethane (2.30 g, 16.1 mmol) was added and the reaction mixture was stirred at 60°C for 24 h in the dark. After cooling, the solvent was removed under reduced pressure, the solid residue was dissolved in acetonitrile (ca. 5 mL) and the product was precipitated by ethyl acetate (ca. 10 mL). The precipitate was separated

by filtration, washed with ethyl acetate (10 mL) and dried under vacuum. Pale yellowish solid, yield 71% (1.52 g). ^1H NMR (400 MHz, DMSO- d_6 , δ): 8.58 (d, 1H, Pz H), 8.53 (d, 1H, Pz H), 6.88 (t, 1H, Pz H), 4.51 (t, 2H, CH_2), 4.17 (s, 3H, CH_3), 1.82 (m, 2H, CH_2), 1.33 (m, 2H, CH_2), 0.92 (t, 3H, CH_3); ^{13}C NMR (100 MHz, DMSO- d_6 , δ): 138.48, 137.33, 107.52, 49.67, 37.41, 30.39, 19.31, 13.77.

1-butyl-2,3,5-trimethylpyrazolium iodide: was synthesized employing the same protocol as for 1-

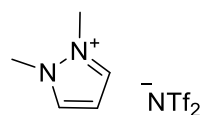


butyl-2-methylpyrazolium iodide. Starting with 1-butyl-3,5-dimethylpyrazole (1.00 g, 6.6 mmol). Yield 97% (1.715 g). ^1H NMR (400 MHz, DMSO- d_6 , δ): 6.58 (s, 1H; Pz H), 4.40 (t, 2H, CH_2), 3.95 (s, 3H, CH_3), 2.45 (s, 3H, CH_3), 2.42 (s, 3H, CH_3), 1.66 (m, 2H, CH_2), 1.33 (m, 2H, CH_2), 0.92 (t, 3H, CH_3); ^{13}C NMR (100 MHz, DMSO- d_6 , δ): 146.63, 145.81, 107.89, 46.63, 34.38, 30.67, 19.44, 13.86, 12.10, 11.90.

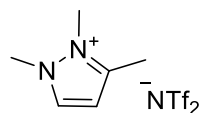
General procedure for pyrazolium bis(trifluoromethylsulfonyl)imide (TFSI) ILs:

Solutions of butylpyrazolium iodide (1 eq) and LiTFSI (1.1 eq) in minimum amounts of water were mixed stirred at room temperature for 12 h. A biphasic mixture formed. Aqueous phase was removed and the IL phase was washed 3 times with deionized water (2-5 mL) and dried under vacuum.

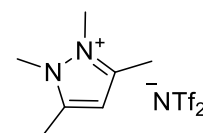
1,2-dimethylpyrazolium TFSI (Pz12): Starting with 1,2-dimethylpyrazolium iodide (0.40 g, 1.8 mmol). Yield 53% (0.36 g). ^1H NMR (400 MHz, DMSO- d_6 , δ): 8.45 (s, 2H, Pz H), 6.85 (s, 1H, Pz H), 4.10 (s, 6H, CH_3); ^{13}C NMR (100 MHz, DMSO- d_6 , δ): 137.93, 121.56, 118.36, 107.25, 36.86; ^{19}F NMR (376 MHz, DMSO- d_6 , δ): -78.71. HR-MS (ESI) m/z : [cation] $^+$ calcd for $\text{C}_5\text{H}_9\text{N}_2^+$: 97.0780; found: 97.0766; [anion] $^-$ calcd for $\text{C}_2\text{F}_6\text{NO}_4\text{S}_2^-$: 279.9178; found: 279.9173.



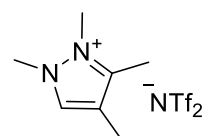
1,2,3-trimethylpyrazolium TFSI (Pz123): Starting with 1,2,3-trimethylpyrazolium iodide (0.30 g, 1.3 mmol). Yield 71% (0.37 g). ^1H NMR (400 MHz, DMSO- d_6 , δ): 8.34 (d, 1H, Pz H), 6.68 (d, 1H, Pz H), 4.06 (s, 3H, CH_3), 3.93 (s, 3H, CH_3), 2.45 (s, 3H, CH_3); ^{13}C NMR (100 MHz, DMSO- d_6 , δ): 146.79, 136.86, 124.76, 121.56, 118.36, 115.16, 107.23, 37.14, 33.72, 11.89; ^{19}F NMR (376 MHz, DMSO- d_6 , δ): -78.71. HR-MS (ESI) m/z : [cation] $^+$ calcd for $\text{C}_6\text{H}_{11}\text{N}_2^+$, 111.0917; found, 111.0922; [anion] $^-$ calcd for $\text{C}_2\text{F}_6\text{NO}_4\text{S}_2^-$, 279.9178; found, 279.9182.



1,2,3,5-tetramethylpyrazolium TFSI (Pz1235): Starting with 1,2,3,5-tetramethylpyrazolium iodide (0.30 g, 1.2 mmol). Yield 79% (0.39 g). ^1H NMR (400 MHz, DMSO- d_6 , δ): 6.53 (s, 1H, Pz H), 3.90 (s, 6H, CH_3), 2.40 (s, 6H, CH_3); ^{13}C NMR (100 MHz, DMSO- d_6 , δ): 145.69, 121.54, 118.34, 107.38, 33.94, 11.74; ^{19}F NMR (376 MHz, DMSO- d_6 , δ): -78.73. HR-MS (ESI) m/z : [cation] $^+$ calcd for $\text{C}_7\text{H}_{13}\text{N}_2^+$: 125.1073; found: 125.1079; [anion] $^-$ calcd for $\text{C}_2\text{F}_6\text{NO}_4\text{S}_2^-$: 279.9178; found: 279.9173.



1,2,3,4-tetramethylpyrazolium TFSI (Pz12345): Starting with 1,2,3,4-tetramethylpyrazolium iodide (0.50 g, 2.0 mmol). Yield 91% (0.74 g). ^1H NMR (400 MHz, DMSO- d_6 , δ): 8.17 (s, 1H, Pz H), 4.02 (s, 3H, CH_3), 3.92 (s, 3H, CH_3), 2.36 (s, 3H, CH_3), 2.05 (s, 3H, CH_3); ^{13}C NMR (100 MHz, DMSO- d_6 , δ): 144.85, 135.64, 124.77, 121.57, 118.37, 115.33, 115.37, 36.78, 33.84, 9.97, 8.15; ^{19}F NMR (376 MHz, DMSO- d_6 , δ): -78.77. HR-MS (ESI) m/z : [cation] $^+$ calcd for $\text{C}_7\text{H}_{13}\text{N}_2^+$: 125.1073; found: 125.1079; [anion] $^-$ calcd for $\text{C}_2\text{F}_6\text{NO}_4\text{S}_2^-$: 279.9178; found: 279.9173.



1,2,4-trimethylpyrazolium TFSI (Pz124): Starting with 1,2,4-trimethylpyrazolium iodide (0.40 g, 1.7 mmol). Yield 64% (0.42 g) of the product. ^1H NMR (400 MHz, DMSO- d_6 , δ): 8.25 (s, 2H, Pz H), 4.05 (s, 6H, CH_3), 2.10 (s, 3H, CH_3); ^{13}C NMR (100 MHz, DMSO- d_6 , δ): 136.80, 121.56, 116.90, 36.71, 8.74; ^{19}F NMR (376 MHz, DMSO- d_6 , δ): -78.71. HR-MS (ESI) m/z : [cation] $^+$ calcd for $\text{C}_6\text{H}_{11}\text{N}_2^+$: 111.0917; found: 111.09177; [anion] $^-$ calcd for $\text{C}_2\text{F}_6\text{NO}_4\text{S}_2^-$: 279.9178; found: 279.9177.

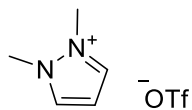
1,2,3,4,5-pentamethylpyrazolium TFSI (Pz12345): Starting with 1,2,3,4,5-pentamethylpyrazolium iodide (0.074 g, 0.28 mmol). Yield 78% (0.092 g). ^1H NMR (400 MHz, DMSO- d_6 , δ): 3.90 (s, 6H, CH_3), 2.35 (s, 6H, CH_3), 2.00 (s, 3H, CH_3); ^{13}C NMR (100 MHz, DMSO- d_6 , δ): 143.63, 113.81, 33.92, 10.10, 7.70; ^{19}F NMR (376 MHz, DMSO- d_6 , δ): -78.71. HR-MS (ESI) m/z : [cation] $^+$ calcd for $\text{C}_8\text{H}_{15}\text{N}_2^+$: 139.1230; found: 139.1235; [anion] $^-$ calcd for $\text{C}_2\text{F}_6\text{NO}_4\text{S}_2^-$: 279.9178; found: 279.9173.

1-butyl-2-methylpyrazolium TFSI (Pz12B): Starting with 1-butyl-2-methylpyrazolium iodide (0.50 g, 1.9 mmol). Yield 84% (0.67 g). ^1H NMR (400 MHz, DMSO- d_6 , δ): 8.52 (d, 1H, Pz H), 8.48 (d, 1H, Pz H), 6.86 (t, 1H, Pz H), 4.45 (t, 2H, CH_2), 4.14 (s, 3H, CH_3), 1.82 (m, 2H, CH_2), 1.34 (m, 2H, CH_2), 0.94 (t, 3H, CH_3); ^{13}C NMR (100 MHz, DMSO- d_6 , δ): 138.52, 137.32, 124.77, 121.57, 118.37, 115.17, 107.48, 49.56, 37.08, 30.36, 19.29, 13.64; ^{19}F NMR (376 MHz, DMSO- d_6 , δ): -78.75. HR-MS (ESI) m/z : [cation] $^+$ calcd for $\text{C}_8\text{H}_{15}\text{N}_2^+$: 139.1230; found: 139.1235; [anion] $^-$ calcd for $\text{C}_2\text{F}_6\text{NO}_4\text{S}_2^-$: 279.9178; found: 279.9173.

1-butyl-2,3,5-trimethylpyrazolium TFSI (Pz1235B): Starting with 1-butyl-2,3,5-trimethylpyrazolium iodide (0.50 g, 1.7 mmol). Yield 91% (0.695 g). ^1H NMR (400 MHz, DMSO- d_6 , δ): 6.55 (s, 1H, Pz H), 4.38 (t, 2H, CH_2), 3.93 (s, 3H, CH_3), 2.44 (s, 3H, CH_3), 2.41 (s, 3H, CH_3), 1.67 (m, 2H, CH_2), 1.34 (m, 2H, CH_2), 0.93 (t, 3H, CH_3); ^{13}C NMR (100 MHz, DMSO- d_6 , δ): 146.58, 145.77, 124.74, 121.54, 118.34, 115.14, 107.81, 46.49, 34.07, 30.63, 19.42, 13.80, 11.90, 11.70; ^{19}F NMR (376 MHz, DMSO- d_6 , δ): -78.71. HR-MS (ESI) m/z : [cation] $^+$ calcd for $\text{C}_{10}\text{H}_{19}\text{N}_2^+$, 167.1543; found, 167.1548; [anion] $^-$ calcd for $\text{C}_2\text{F}_6\text{NO}_4\text{S}_2^-$, 279.9178; found, 279.9173.

1,2-dimethylpyrazolium triflate: Pyrazole (0.5 g, 7.34 mmol), potassium carbonate (0.6 g, 7.35 mmol) and dry acetonitrile (8 mL) were mixed in a Schlenk flask. After 30 min of stirring, the reaction mixture was cooled in an ice water bath and methyl triflate (3.6 g, 0.22 mmol) was added dropwise.

The reaction mixture was then stirred at the room temperature for 12 h. The mixture was filtered and the solvent was removed under vacuum. The solid residue was redissolved in dichloromethane (5 mL), filtered, and the filtrate concentrated under vacuum. The product was precipitated with diethyl ether (5 mL) from methanol (1 mL), the precipitate was removed by filtration, washed with cold ethanol (1 mL) and dried under vacuum, to afford a white solid (250 mg, yield 14%). ¹H NMR (400 MHz, DMSO-d₆, δ): 8.44 (d, 2H, Pz H), 6.81 (t, 1H, Pz H), 4.10 (s, 6H, CH₃); ¹³C NMR (100 MHz, DMSO-d₆, δ): 137.91, 122.76, 119.56, 107.26, 36.85; ¹⁹F NMR (376 MHz, DMSO-d₆, δ): -78.77. HR-MS (ESI) m/z: [cation]⁺ calcd for C₅H₉N₂⁺: 97.0760; found: 97.0766; [anion]⁻ calcd for CF₃O₃S⁻: 148.9526; found: 148.9520.



3.5 Supporting Information

3.5.1 CV data

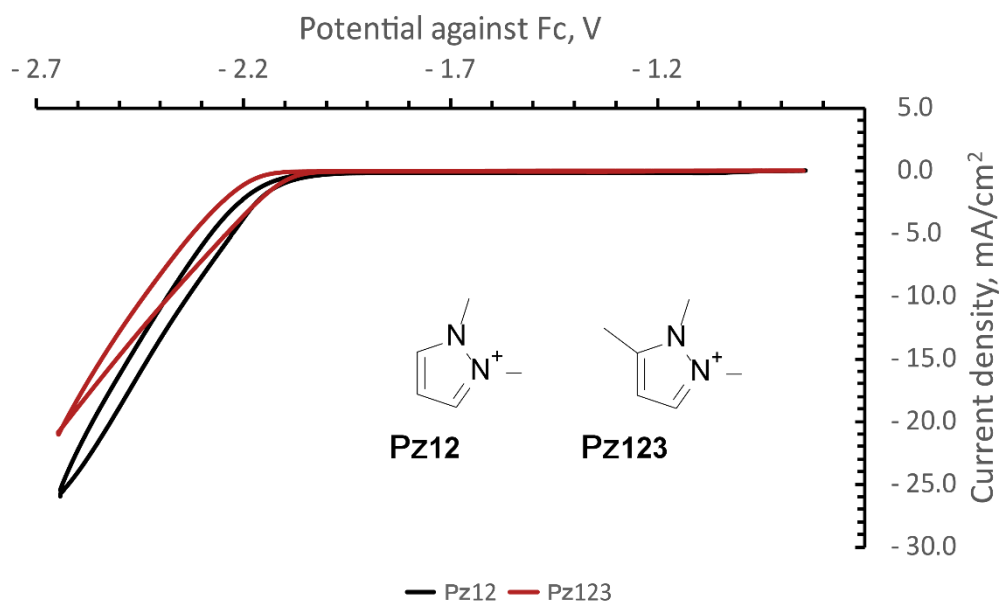


Figure S3.1. Comparison of cyclic voltammograms for **Pz12** and **Pz123** (Ag electrode, CO_2).

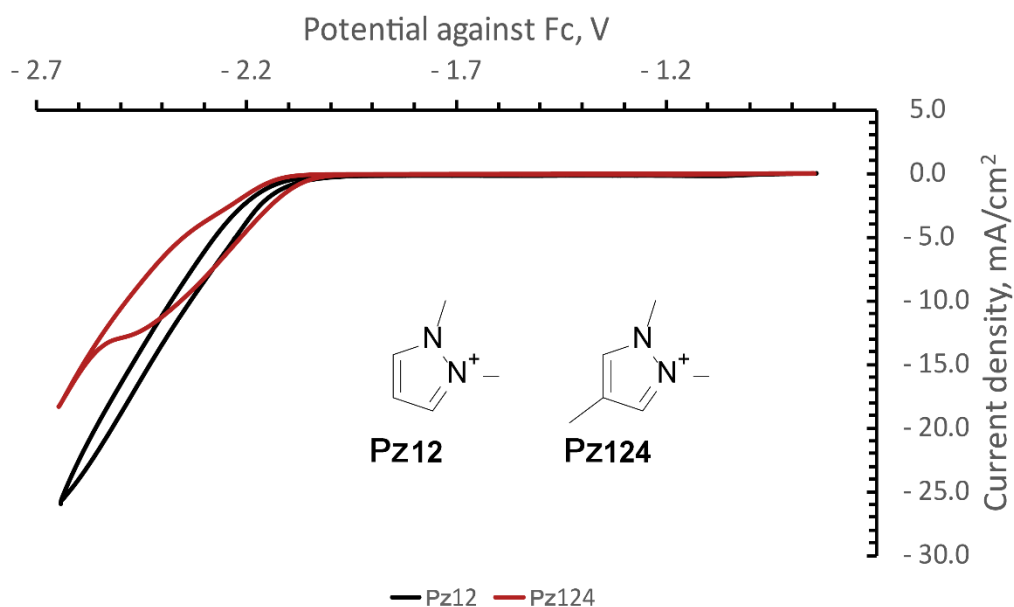
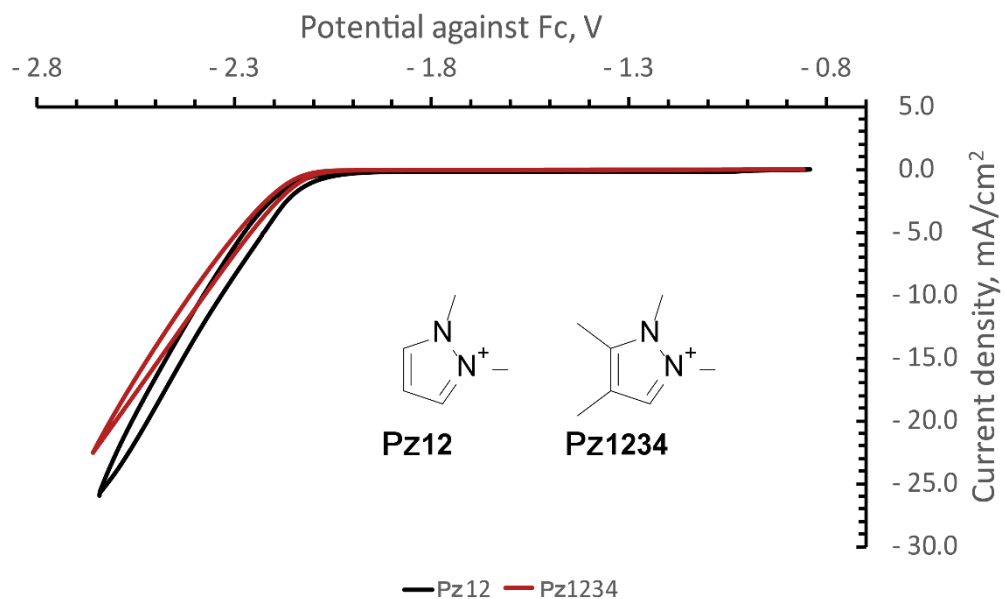
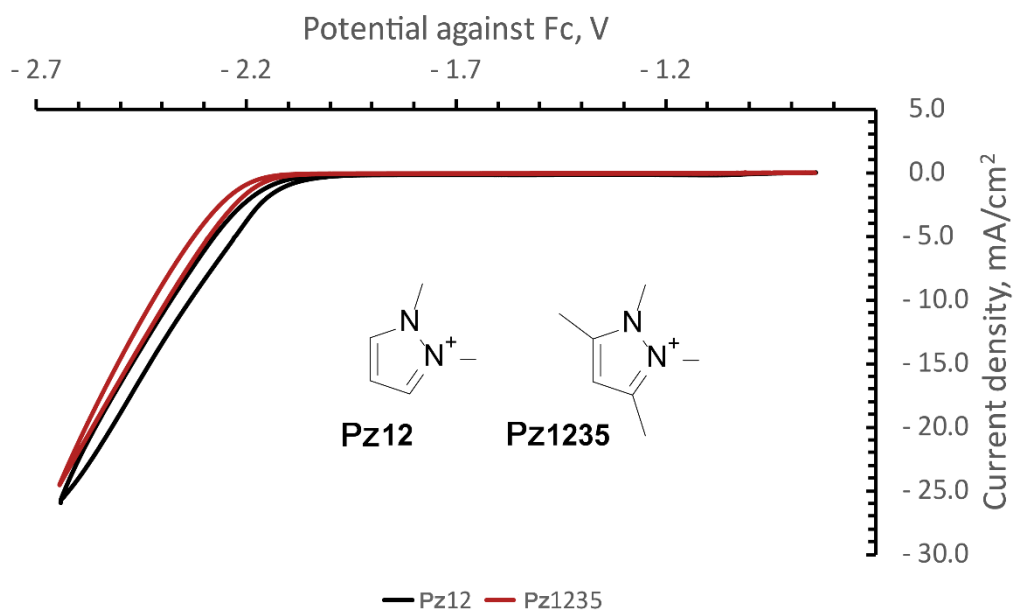


Figure S3.2. Comparison of cyclic voltammograms for **Pz12** and **Pz124** (Ag electrode, CO_2).

Figure S3.3. Comparison of cyclic voltammograms for **Pz12** and **Pz1234** (Ag electrode, CO_2).Figure S3.4. Comparison of cyclic voltammograms for **Pz12** and **Pz1235** (Ag electrode, CO_2).

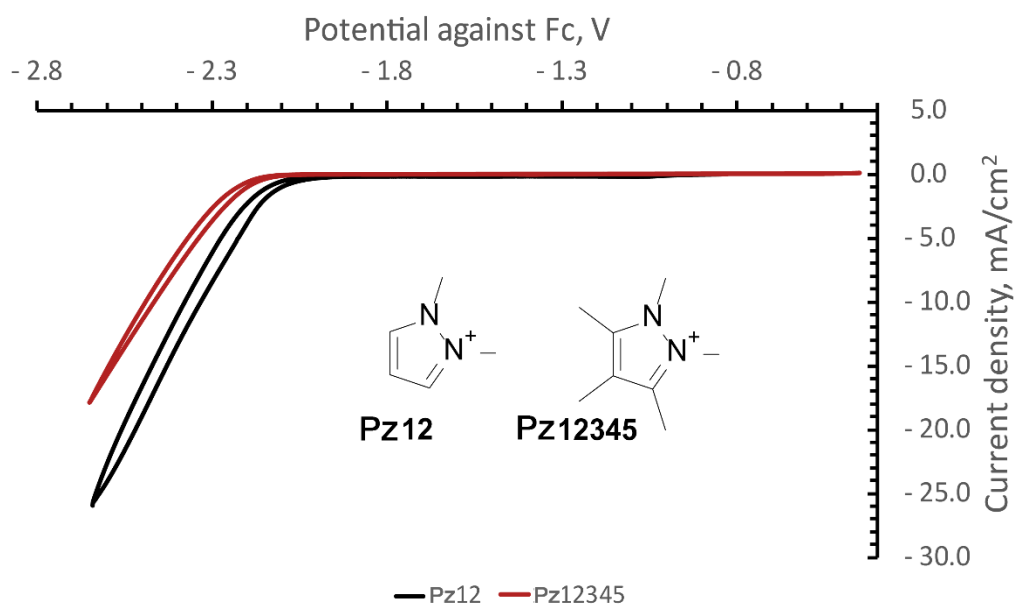


Figure S3.5. Comparison of cyclic voltammograms for **Pz12** and **Pz12345** (Ag electrode, CO₂).

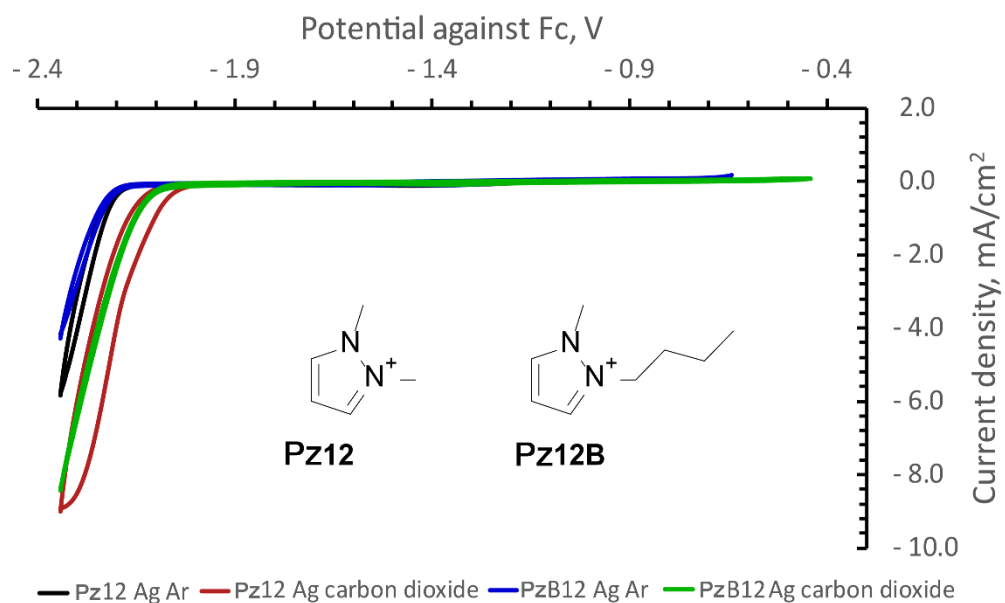


Figure S3.6. Comparison of CV data for methylated and butylated Pz ILs **Pz12** and **Pz12B**.

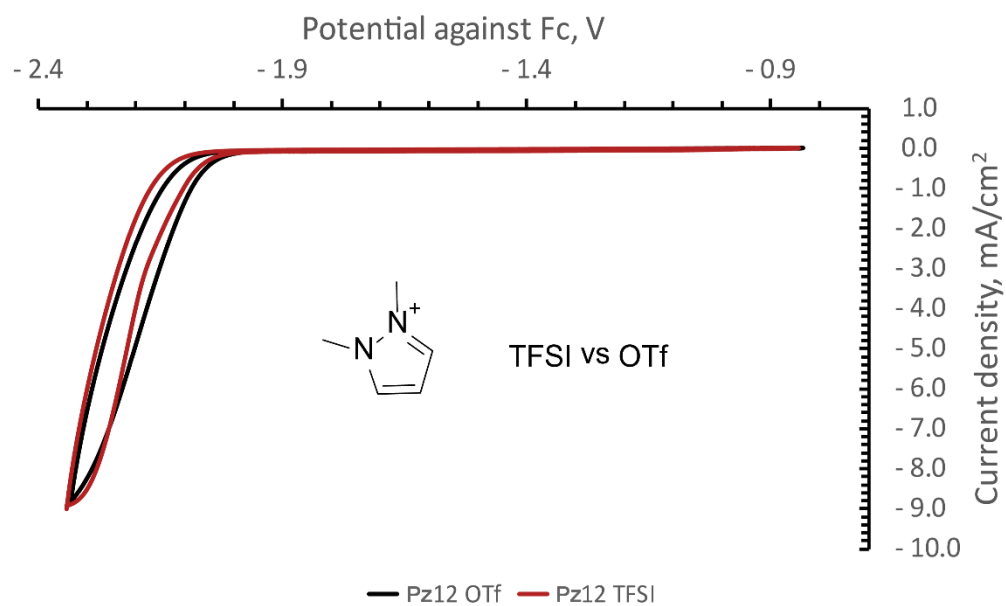


Figure S3.7. Comparison of CV data for **Pz12** with different anions: Tf_2N^- and TfO^- (Ag electrode, CO_2).

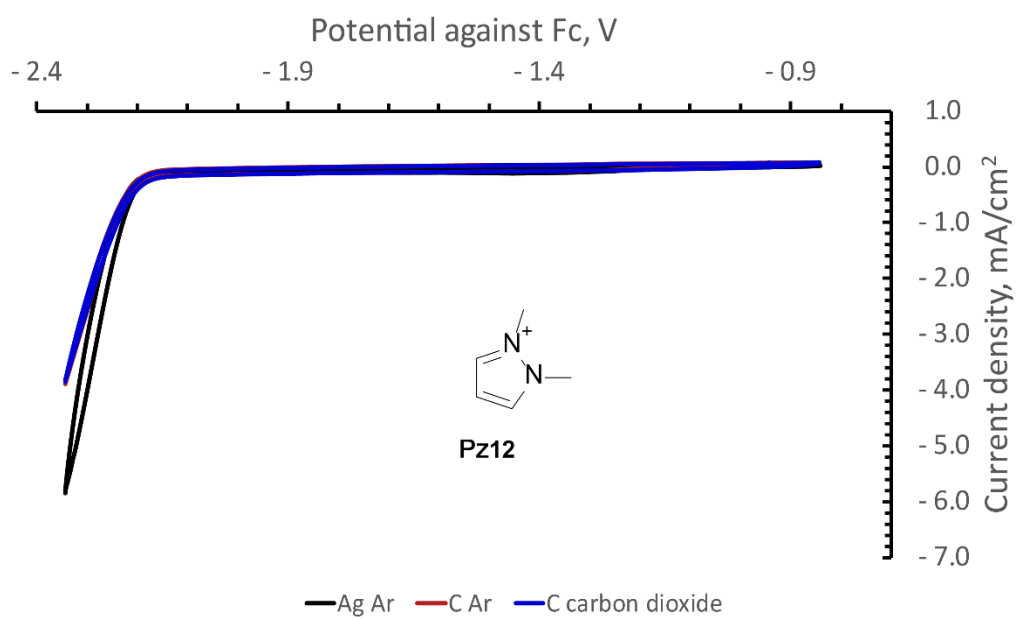


Figure S3.8. Comparison of cyclic voltammetry data recorded on Ag and C electrodes.

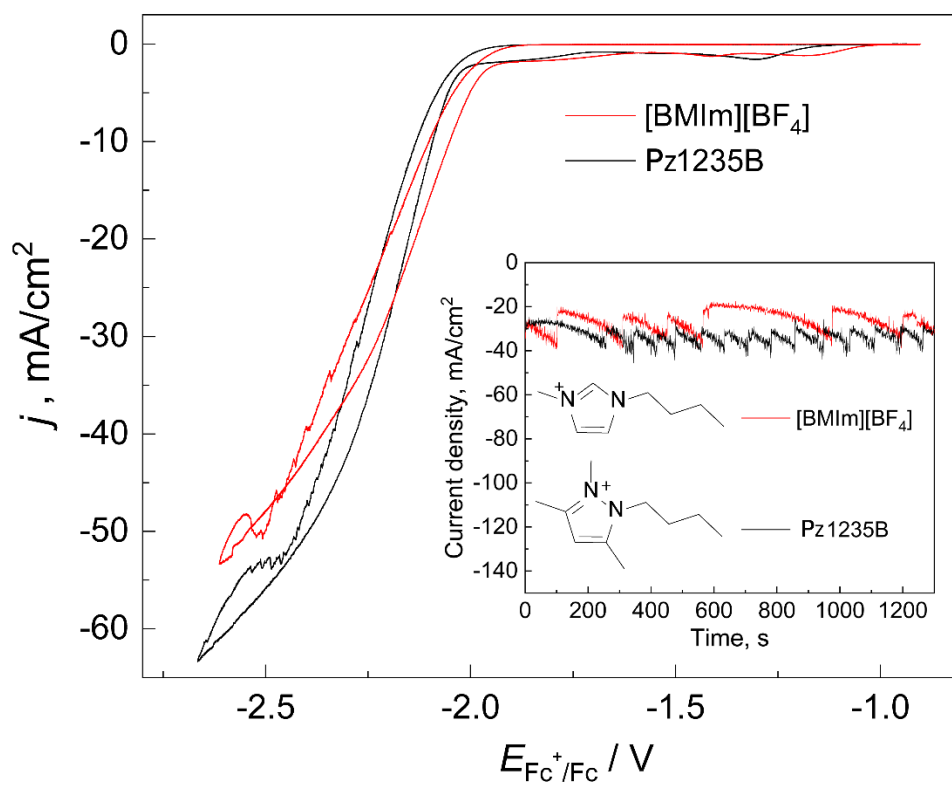
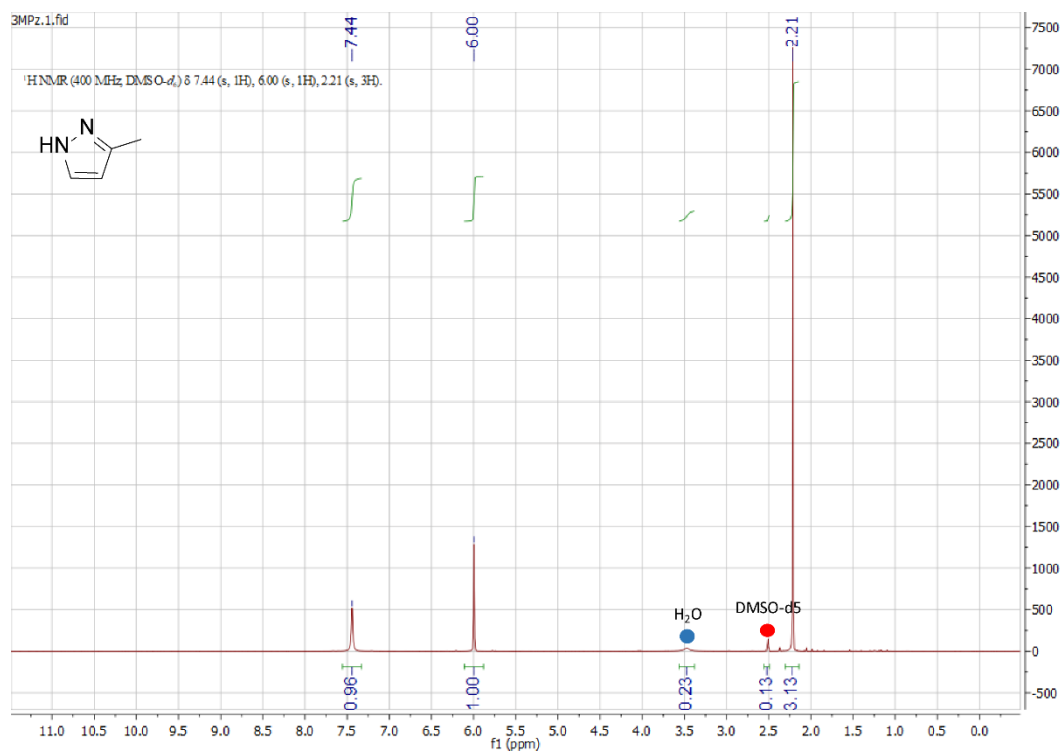
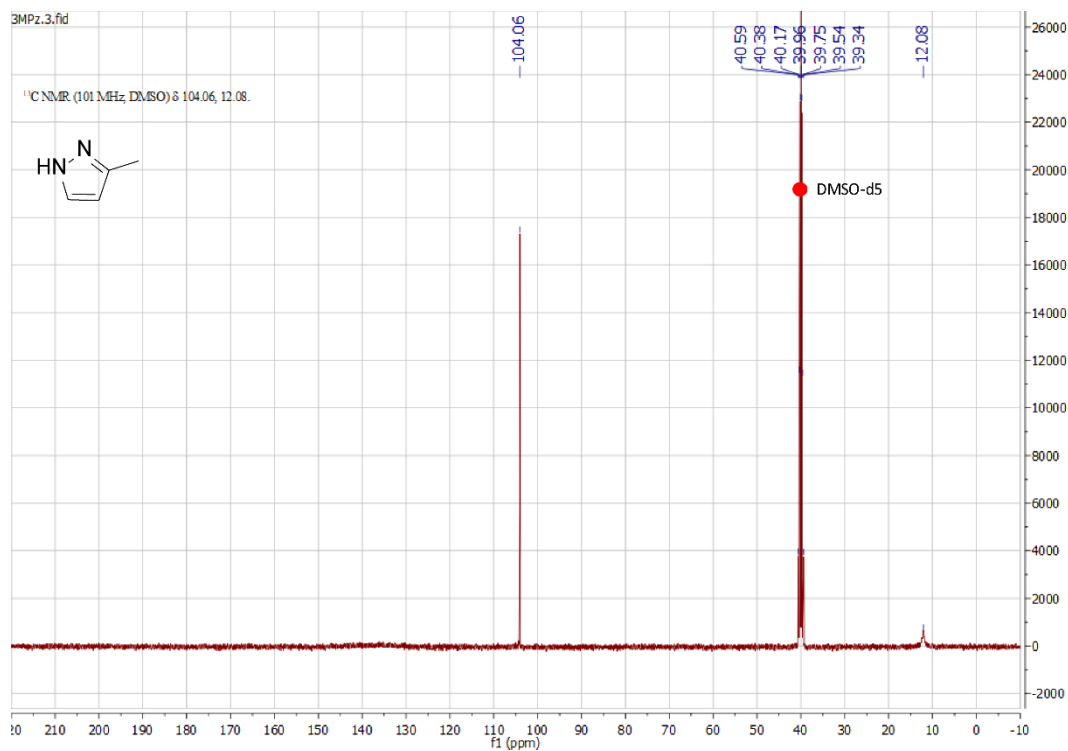
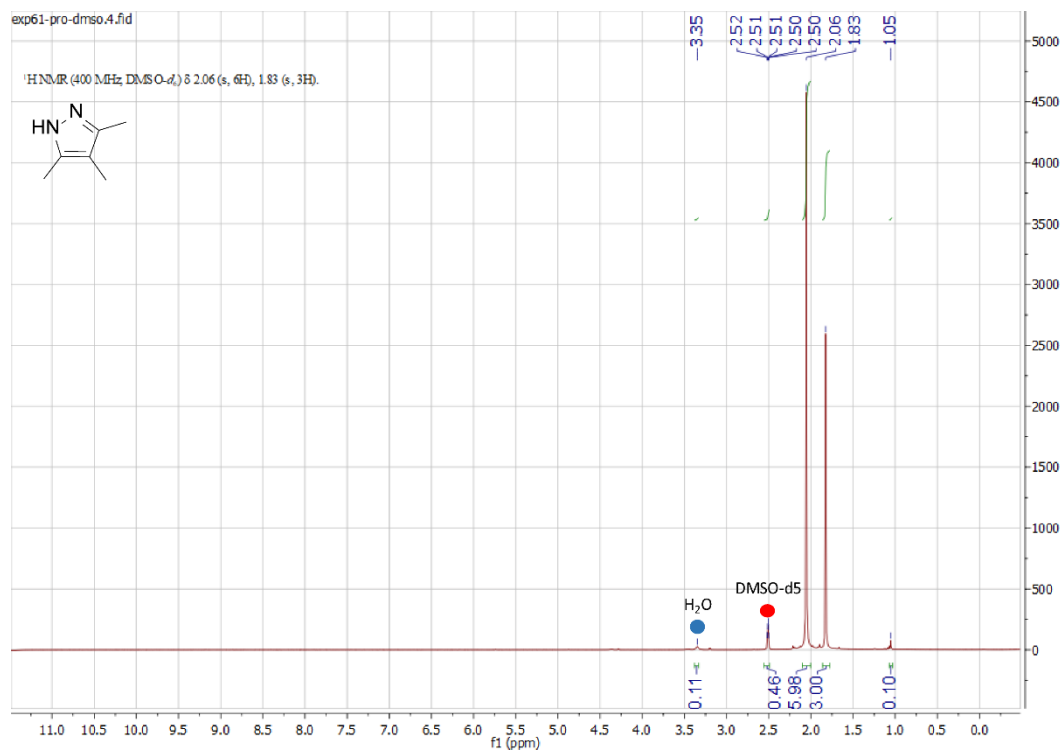
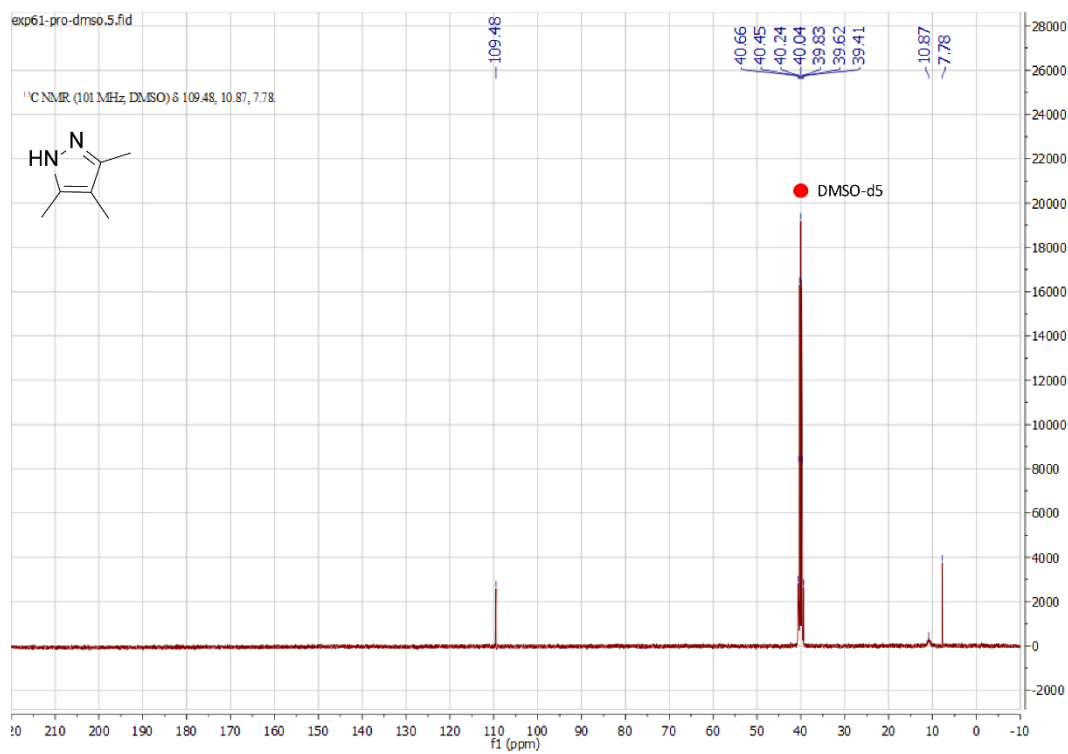
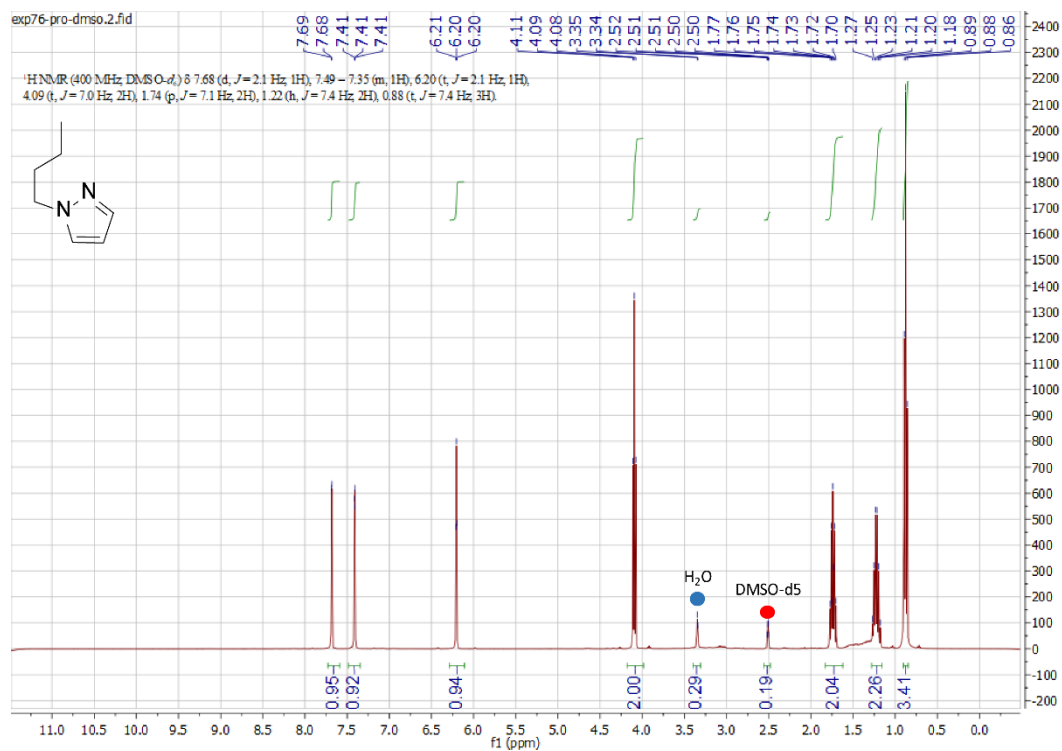
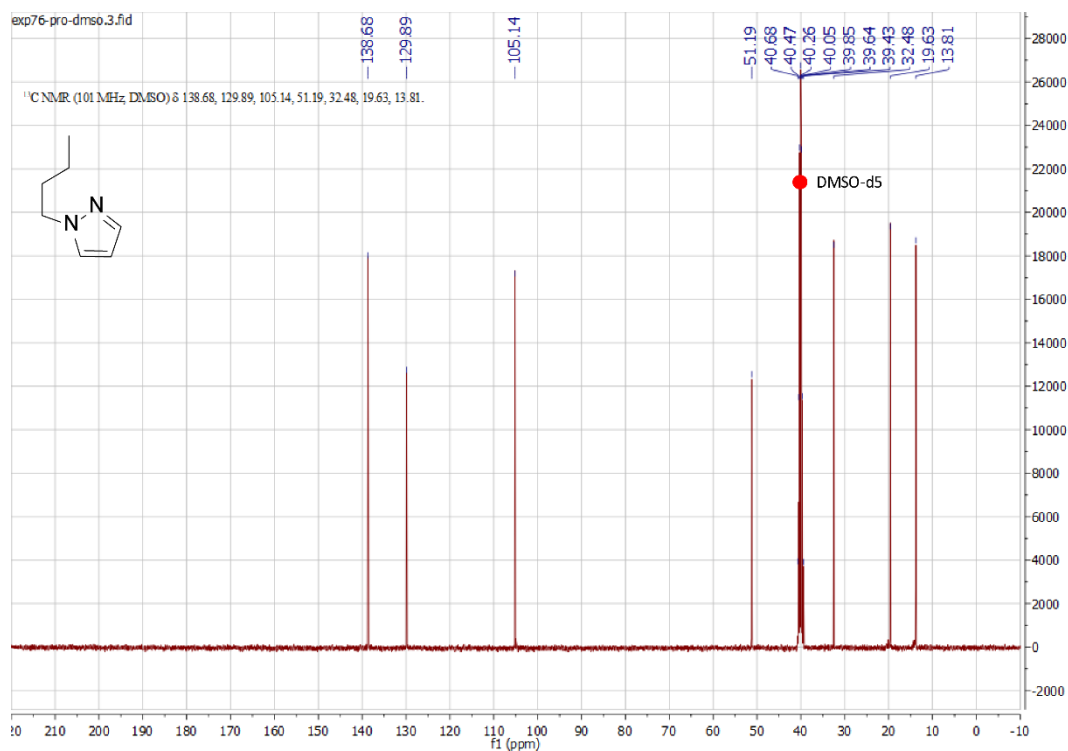


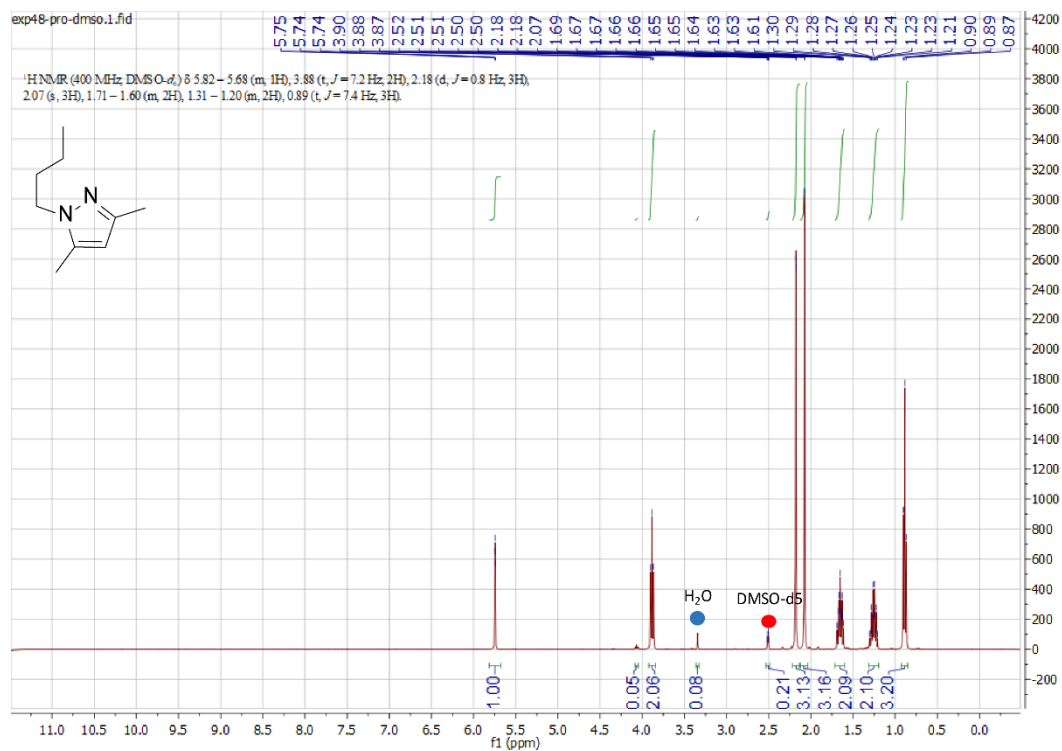
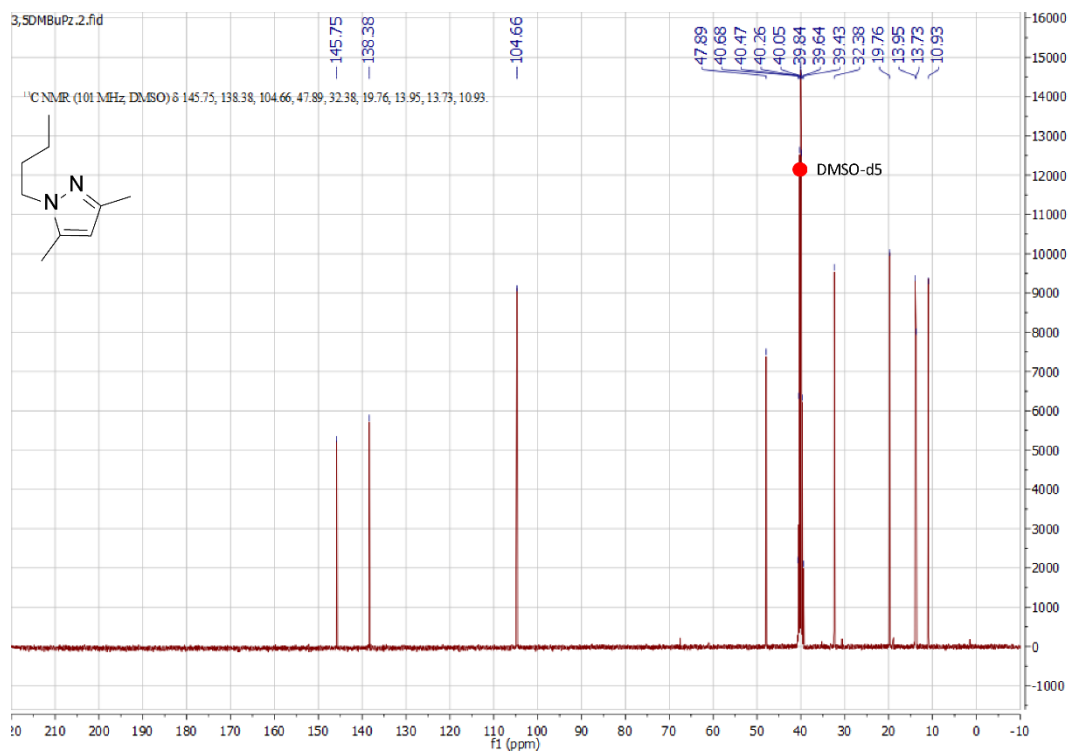
Figure S3.9. CV data plotted together for **Pz1235B** and [BMIm][BF₄]. Examples of transients (-2.21 V vs Fc) are compared in the insert.

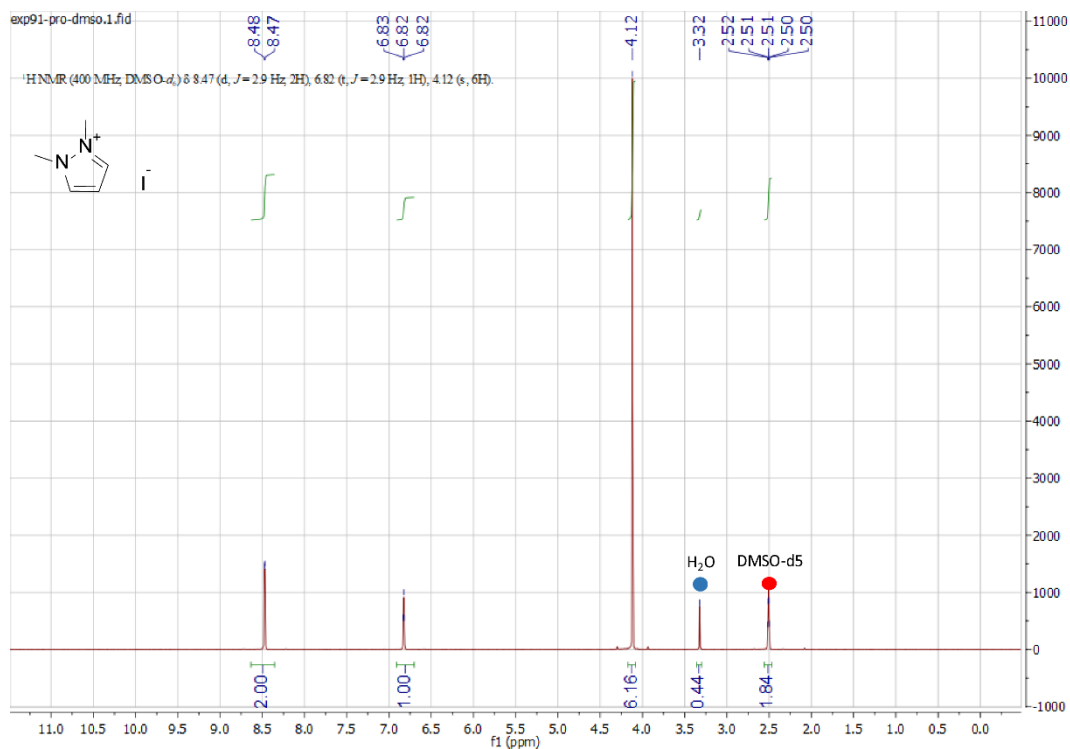
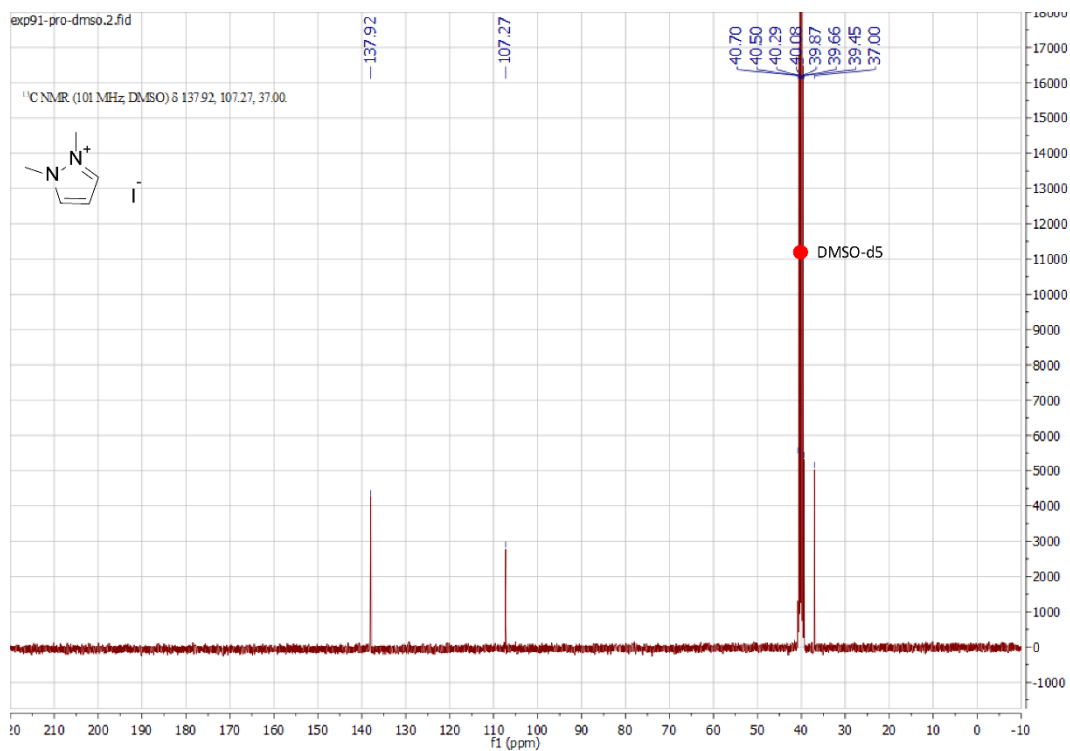
3.5.2 NMR spectra

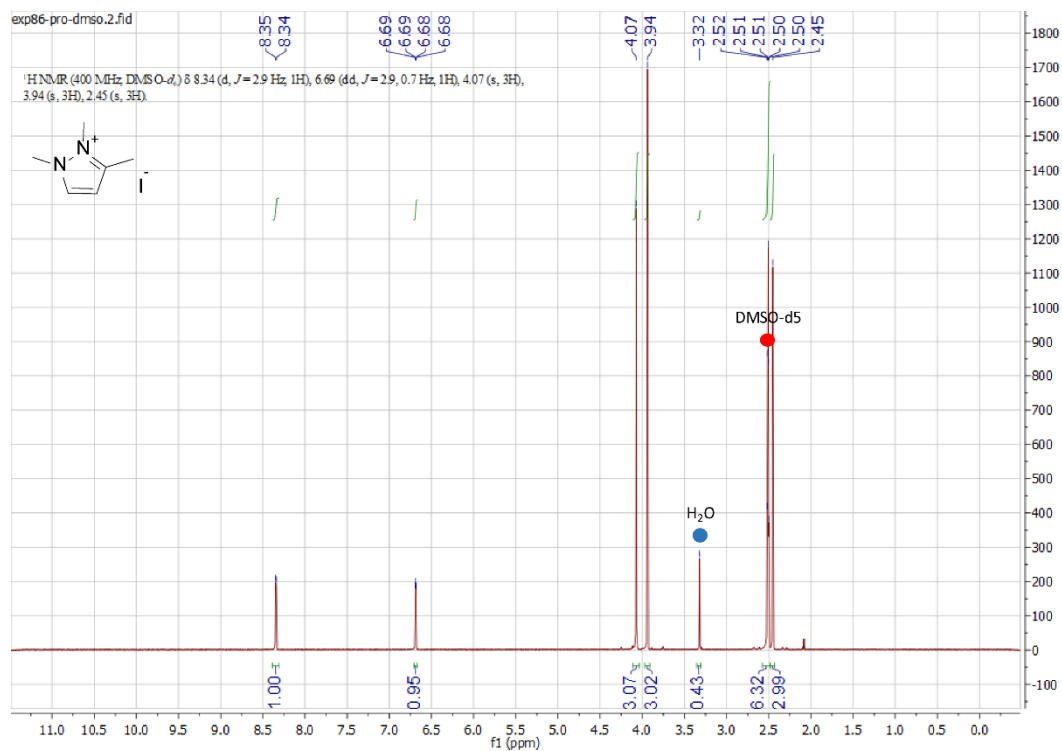
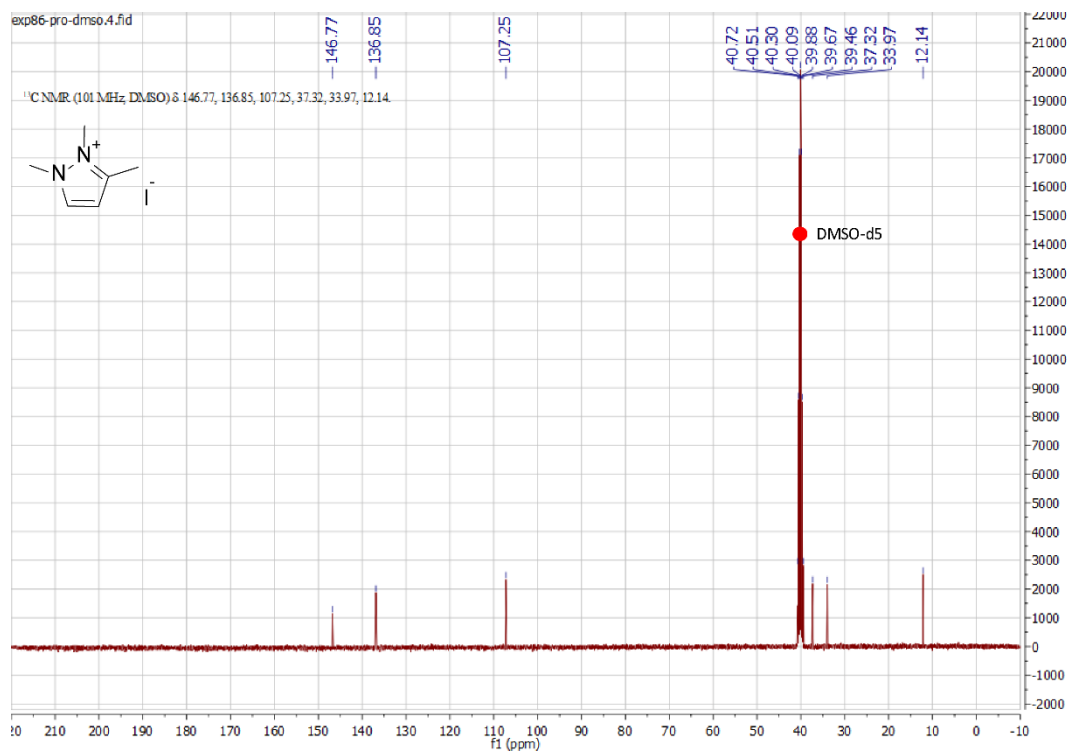
Figure S3.10. ¹H NMR spectrum of 3-methylpyrazole (DMSO-*d*₆).Figure S3.11. ¹³C NMR spectrum of 3-methylpyrazole (DMSO-*d*₆).

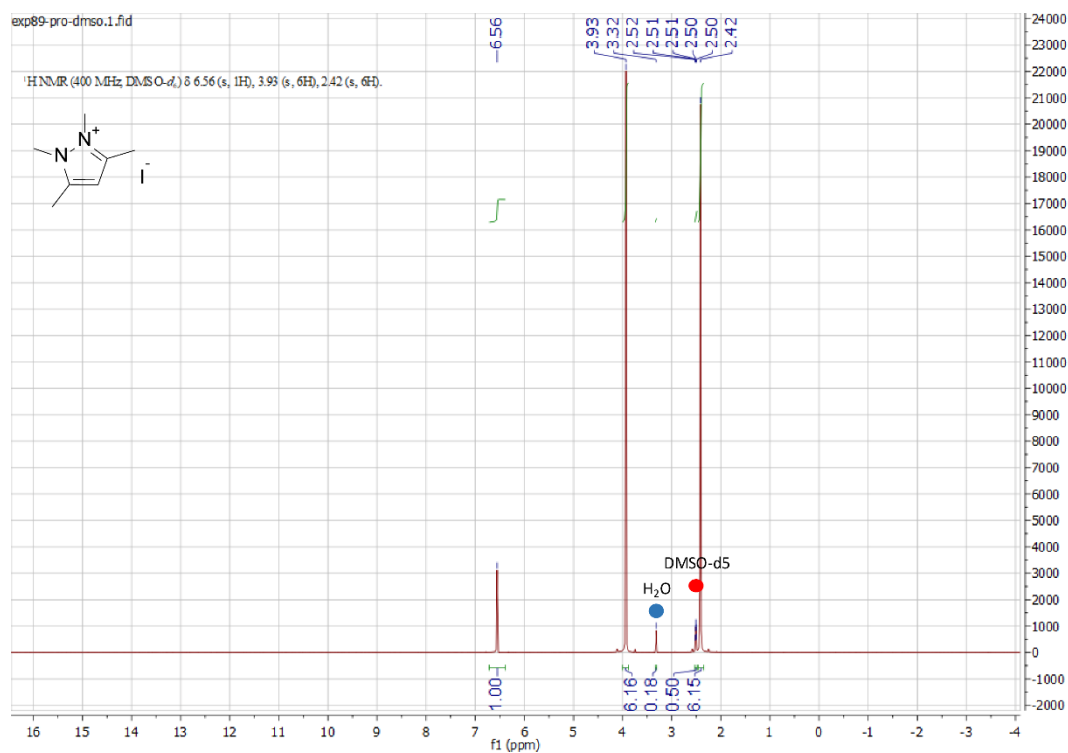
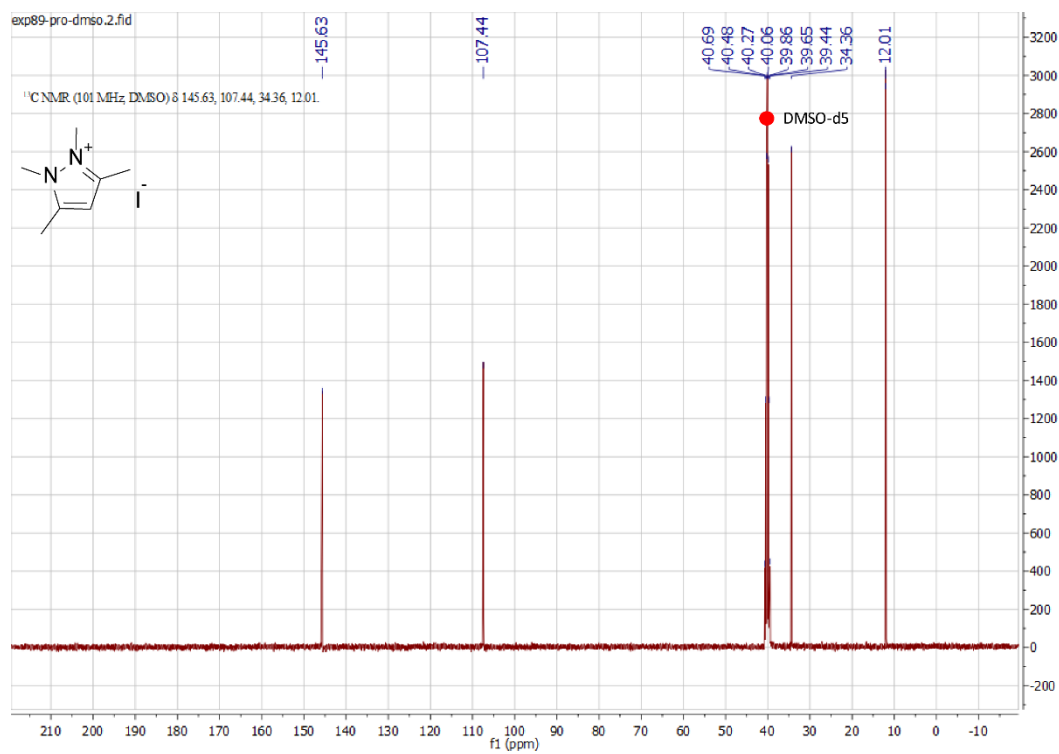
Figure S3.12. ¹H NMR spectrum of 3,4,5-trimethylpyrazole (DMSO-d₆).Figure S3.13. ¹³C NMR spectrum of 3,4,5-trimethylpyrazole (DMSO-d₆).

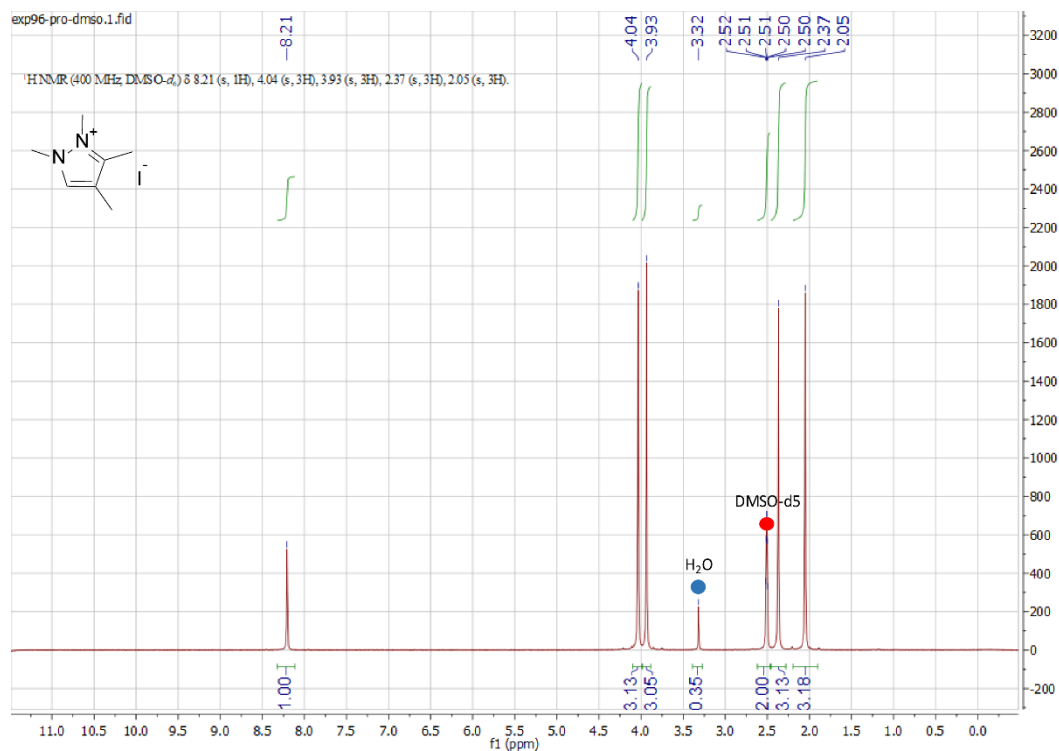
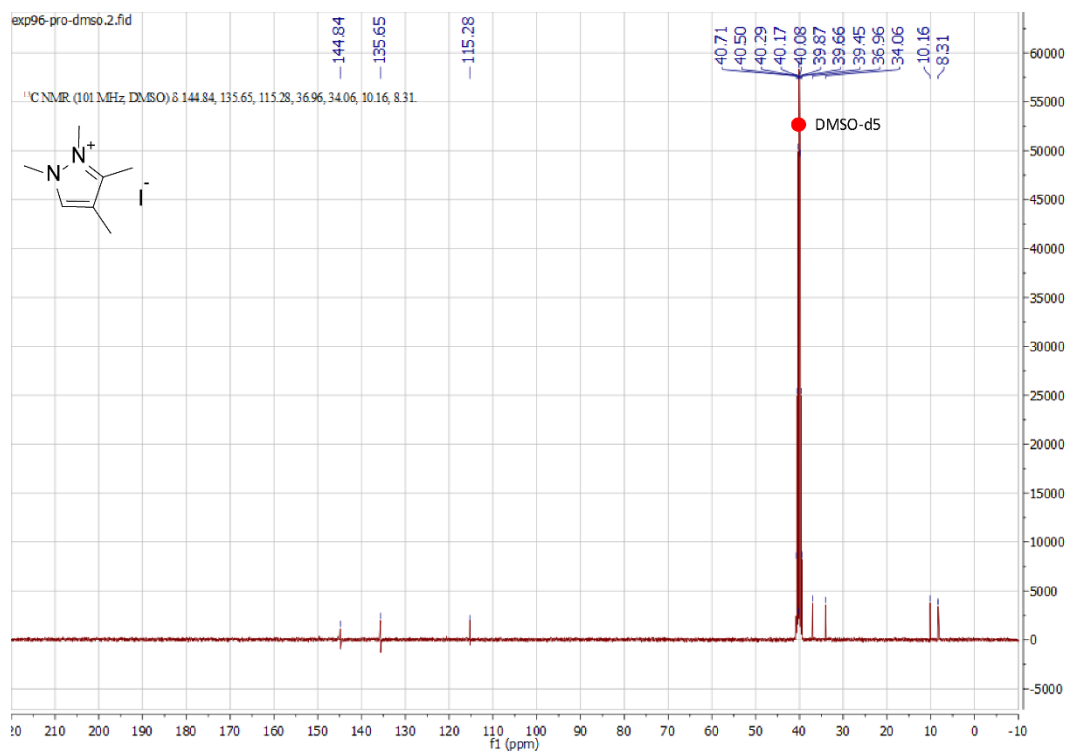
Figure S3.14. ¹H NMR spectrum of 1-butylpyrazole (DMSO-d₆).Figure S3.15. ¹³C NMR spectrum of 1-butylpyrazole (DMSO-d₆).

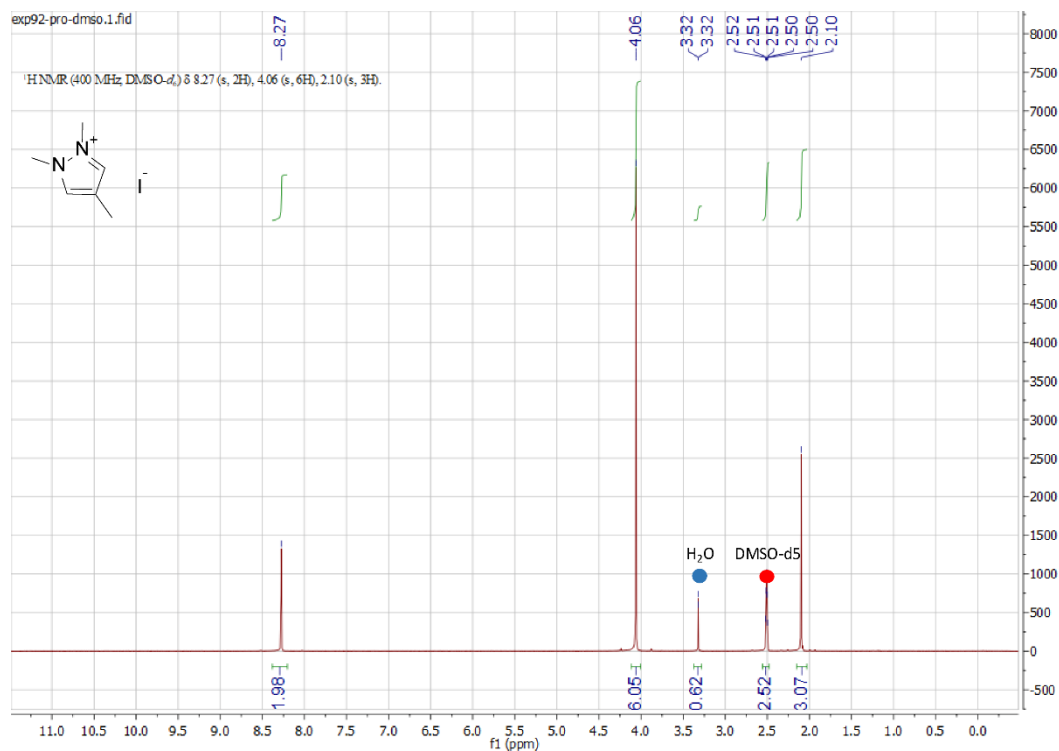
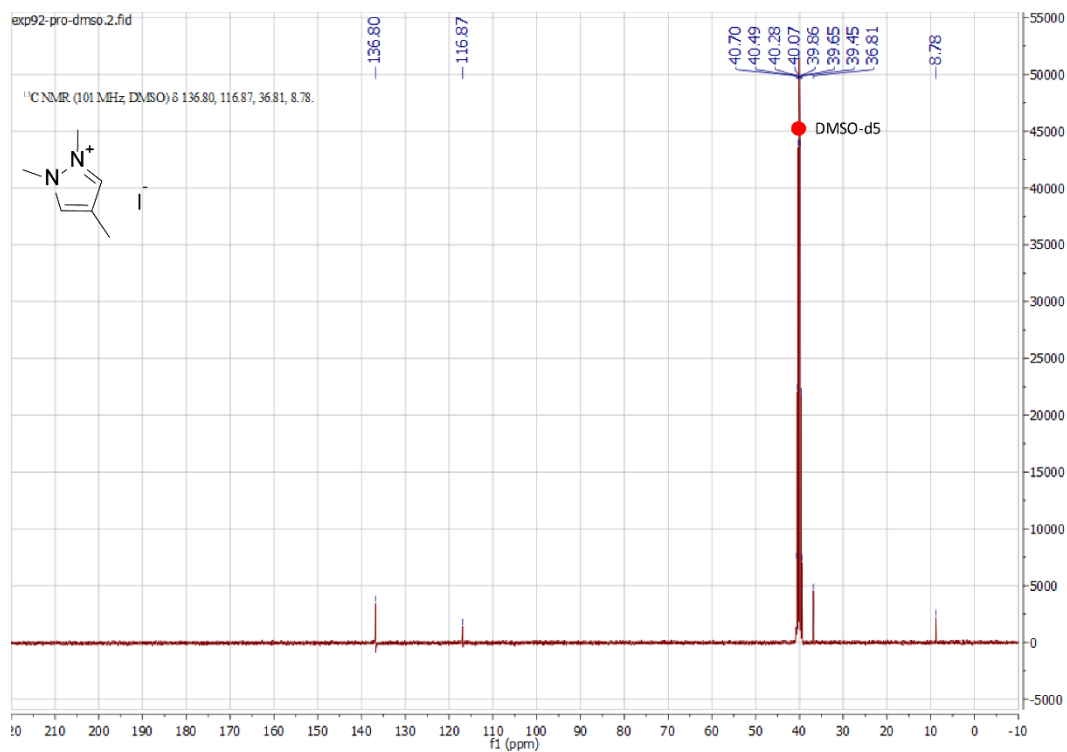
Figure S3.16. ¹H NMR spectrum of 1-butyl-3,5-dimethylpyrazole (DMSO-d₆).Figure S3.17. ¹³C NMR spectrum of 1-butyl-3,5-dimethylpyrazole (DMSO-d₆).

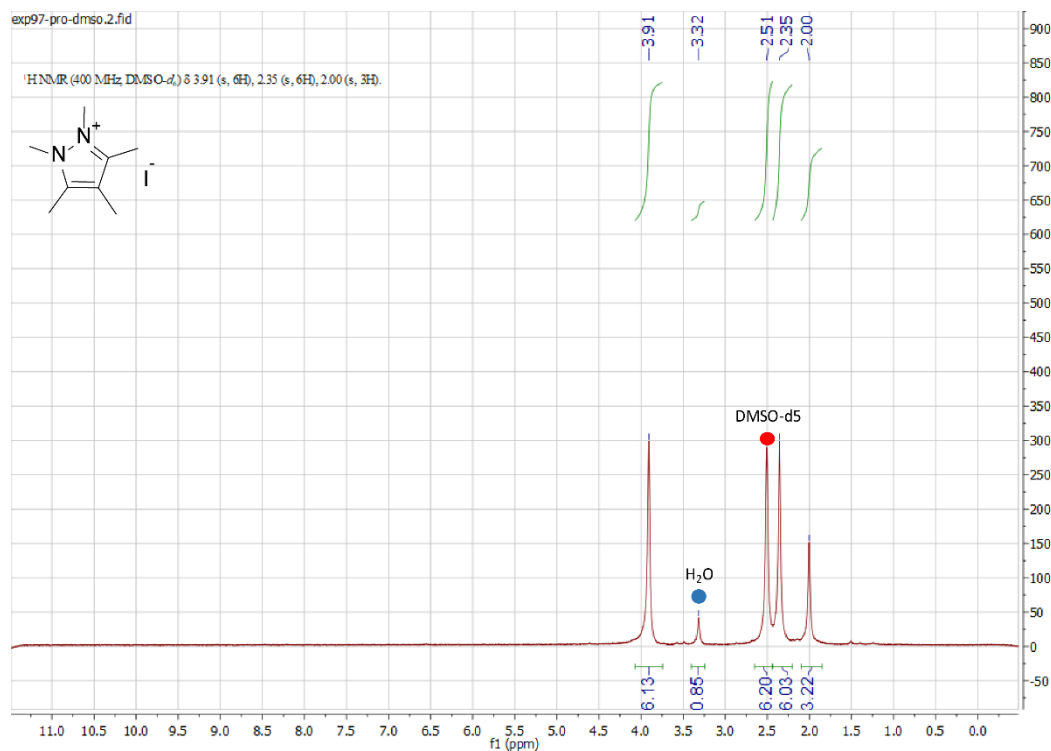
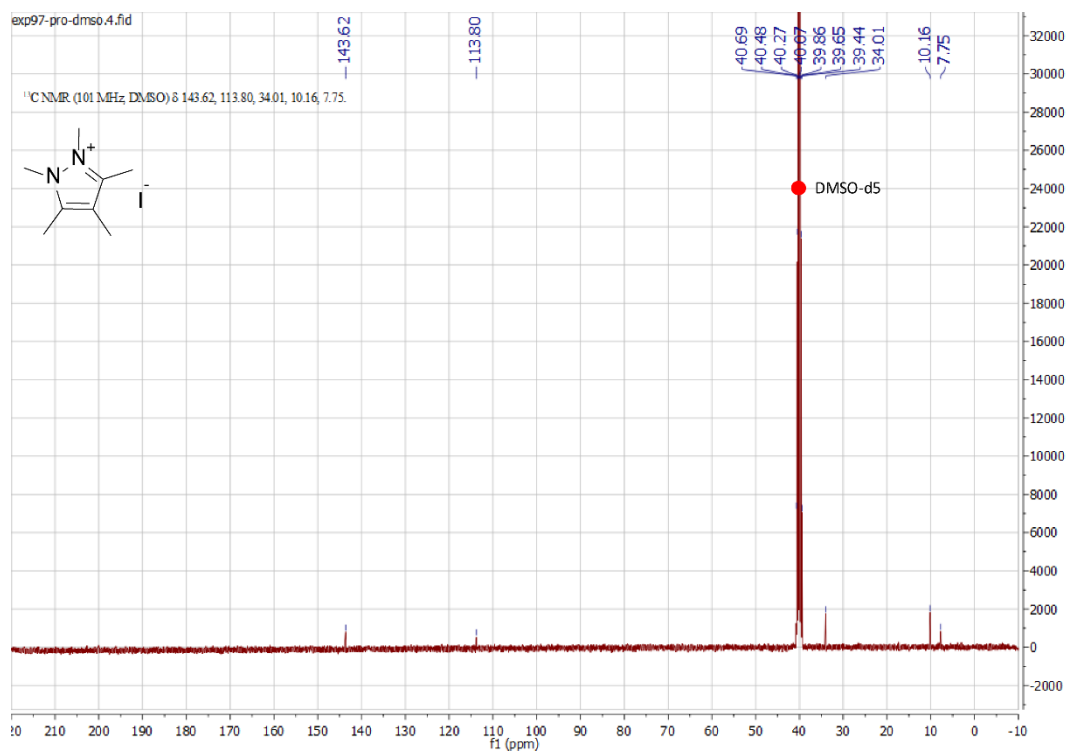
Figure S3.18. ¹H NMR spectrum of 1,2-dimethylpyrazolium iodide (DMSO-d₆).Figure S3.19. ¹³C NMR spectrum of 1,2-dimethylpyrazolium iodide (DMSO-d₆).

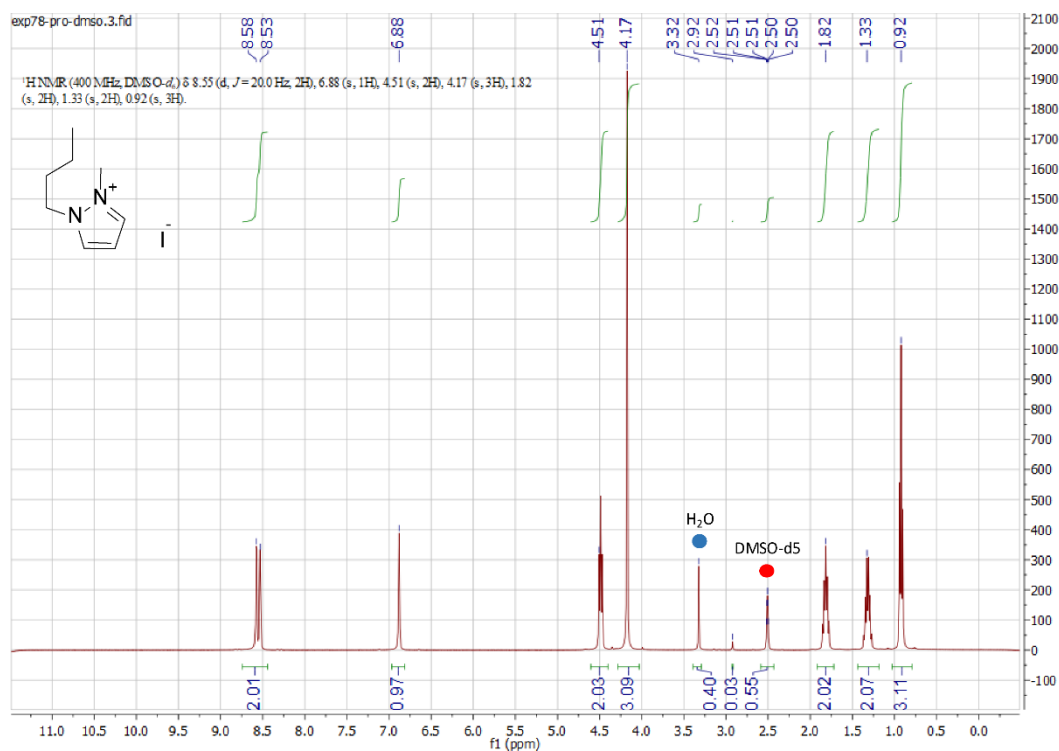
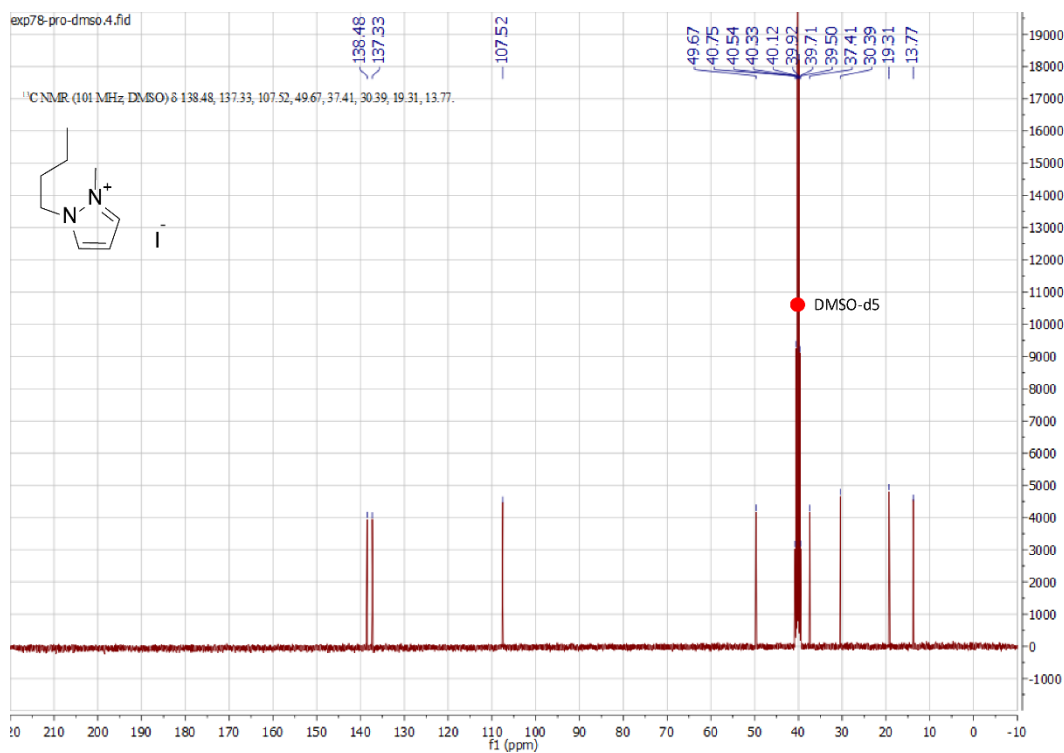
Figure S3.20. ¹H NMR spectrum of 1,2,3-trimethylpyrazolium iodide (DMSO-d₆).Figure S3.21. ¹³C NMR spectrum of 1,2,3-trimethylpyrazolium iodide (DMSO-d₆).

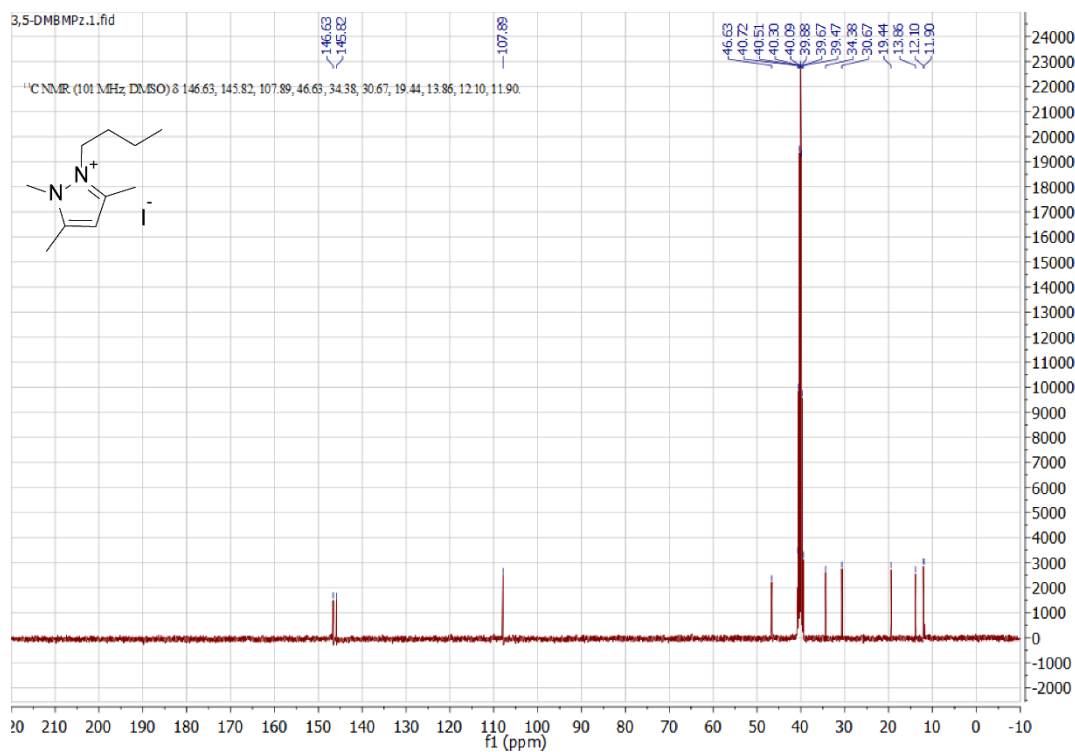
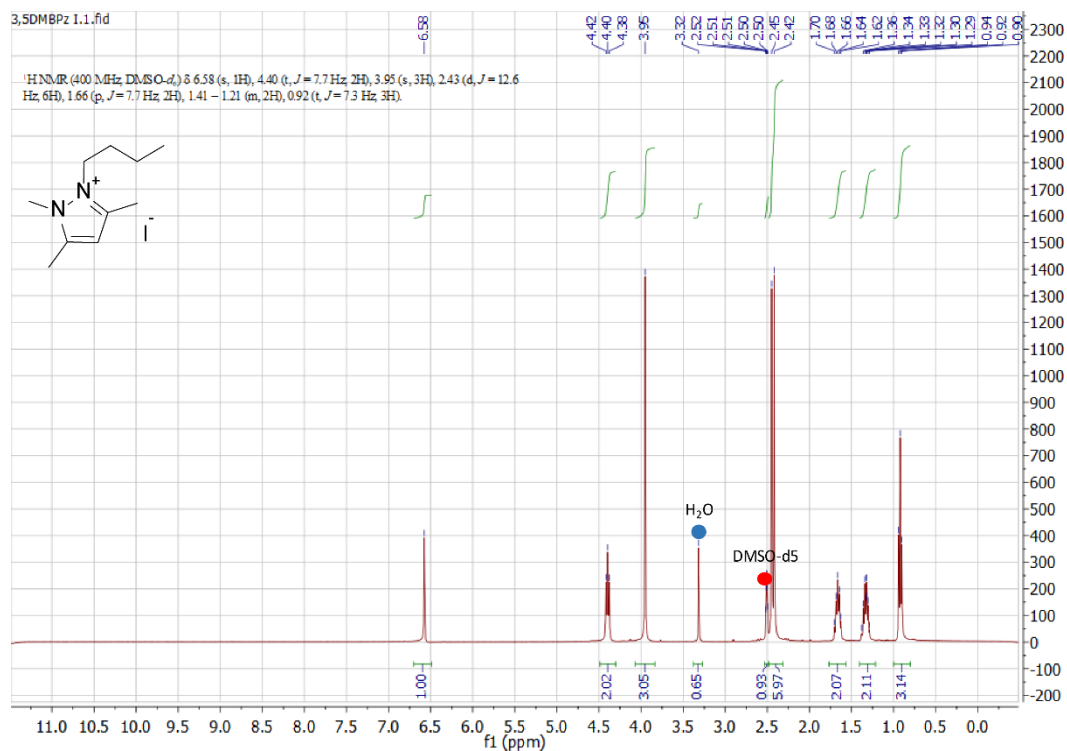
Figure S3.22. ¹H NMR spectrum of 1,2,3,5-tetramethylpyrazolium iodide (DMSO-d₆).Figure S3.23. ¹³C NMR spectrum of 1,2,3,5-tetramethylpyrazolium iodide (DMSO-d₆).

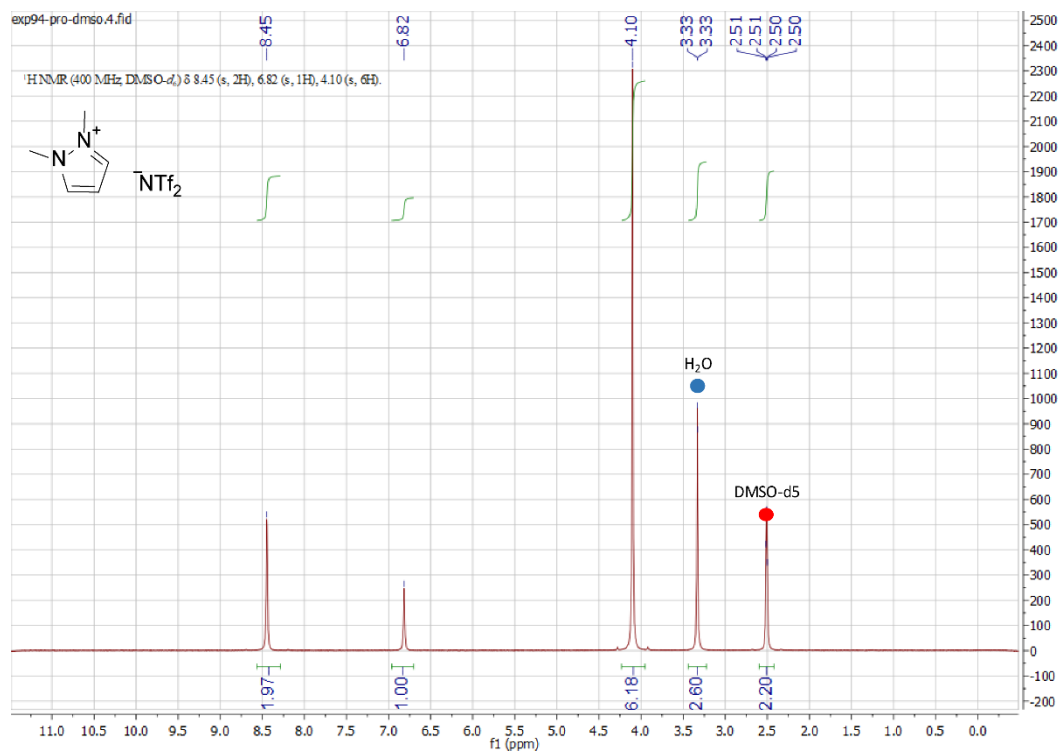
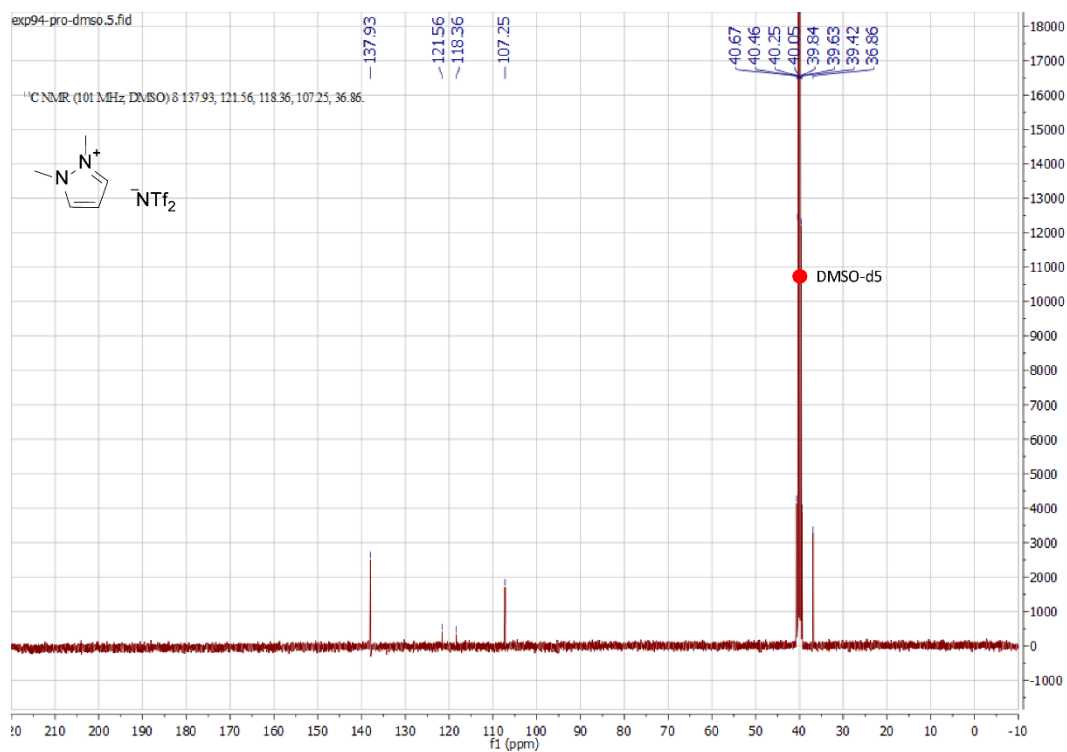
Figure S 3.24. ¹H NMR spectrum of 1,2,3,4-tetramethylpyrazolium iodide (DMSO-d₆).Figure S3.25. ¹³C NMR spectrum of 1,2,3,4-tetramethylpyrazolium iodide (DMSO-d₆).

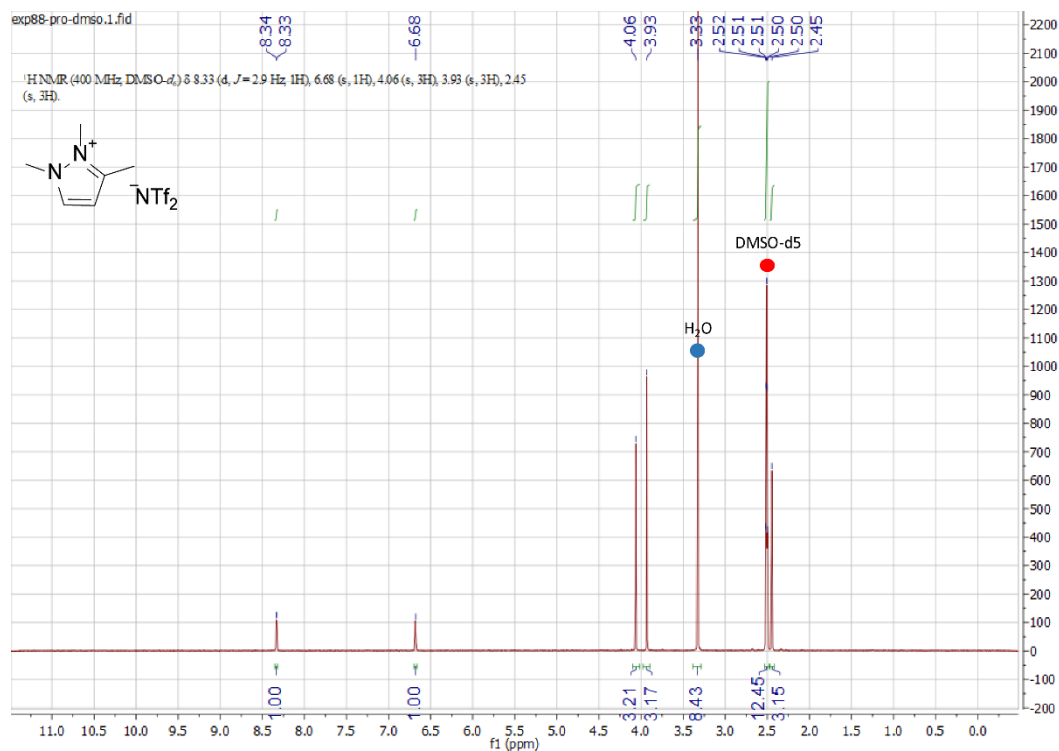
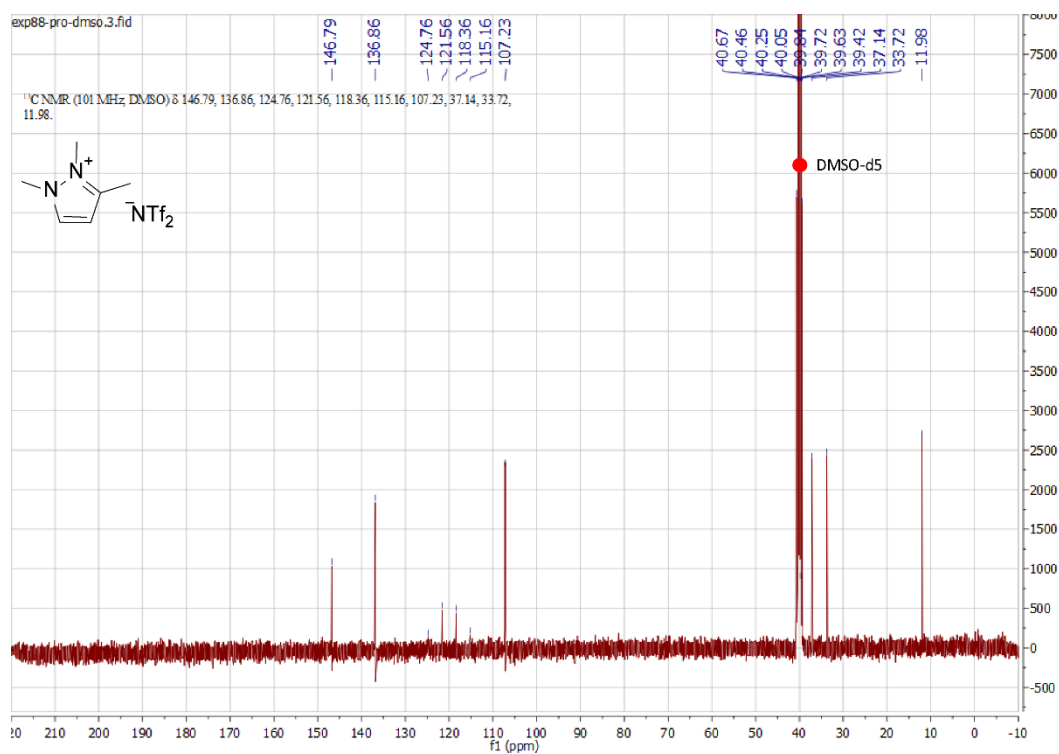
Figure S3.26. ¹H NMR spectrum of 1,2,4-trimethylpyrazolium iodide (DMSO-d₆).Figure S 3.27. ¹³C NMR spectrum of 1,2,4-trimethylpyrazolium iodide (DMSO-d₆).

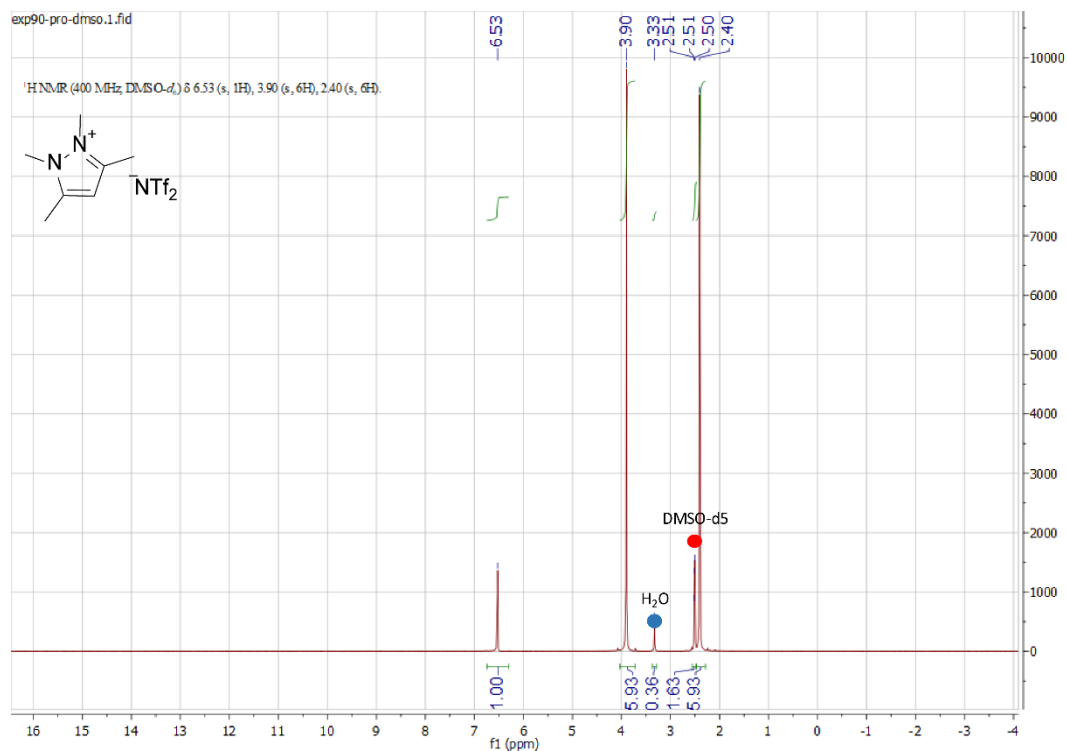
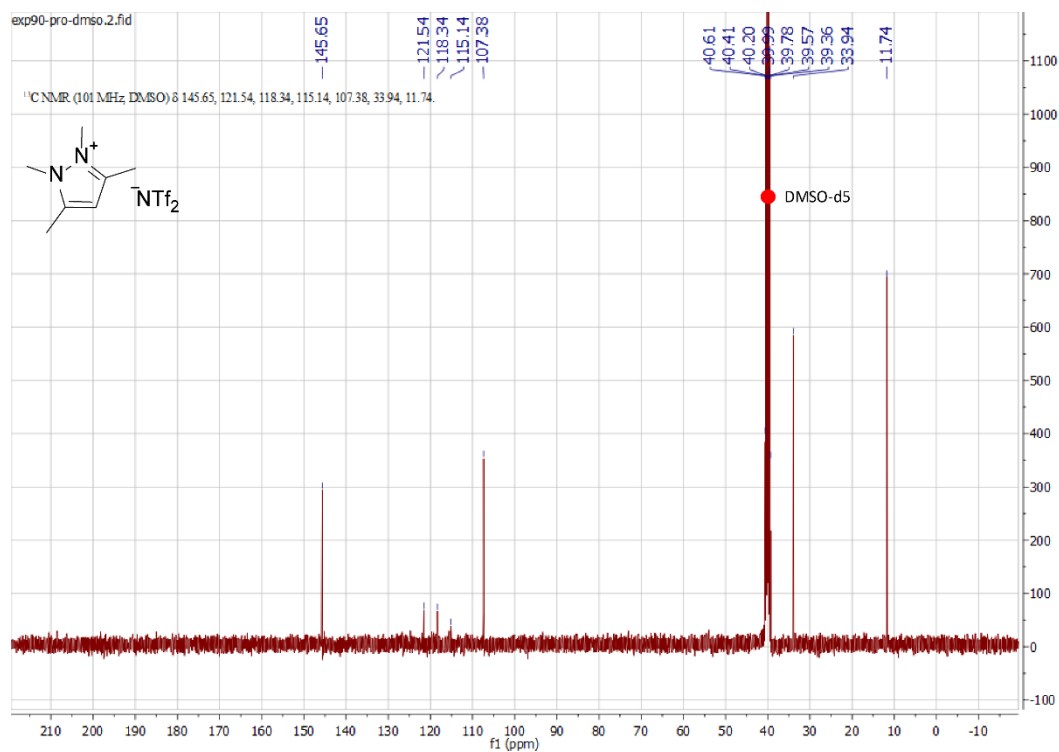
Figure S3.28. ¹H NMR spectrum of 1,2,3,4,5-pentamethylpyrazolium iodide (DMSO-d₆).Figure S3.29. ¹³C NMR spectrum of 1,2,3,4,5-pentamethylpyrazolium iodide (DMSO-d₆).

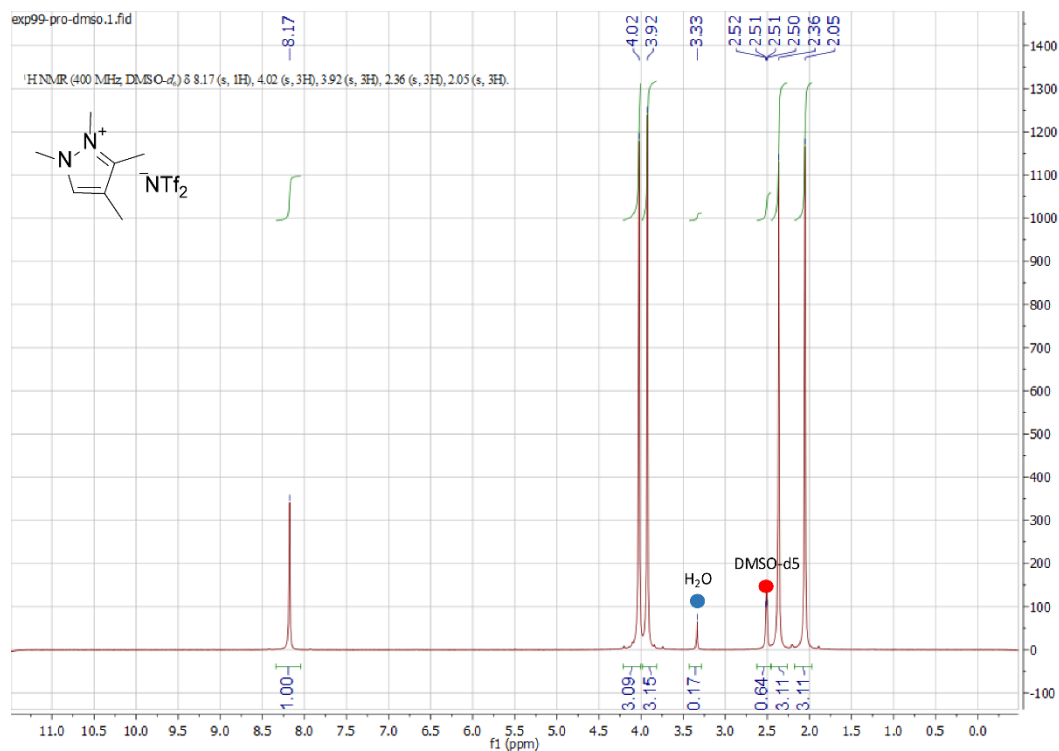
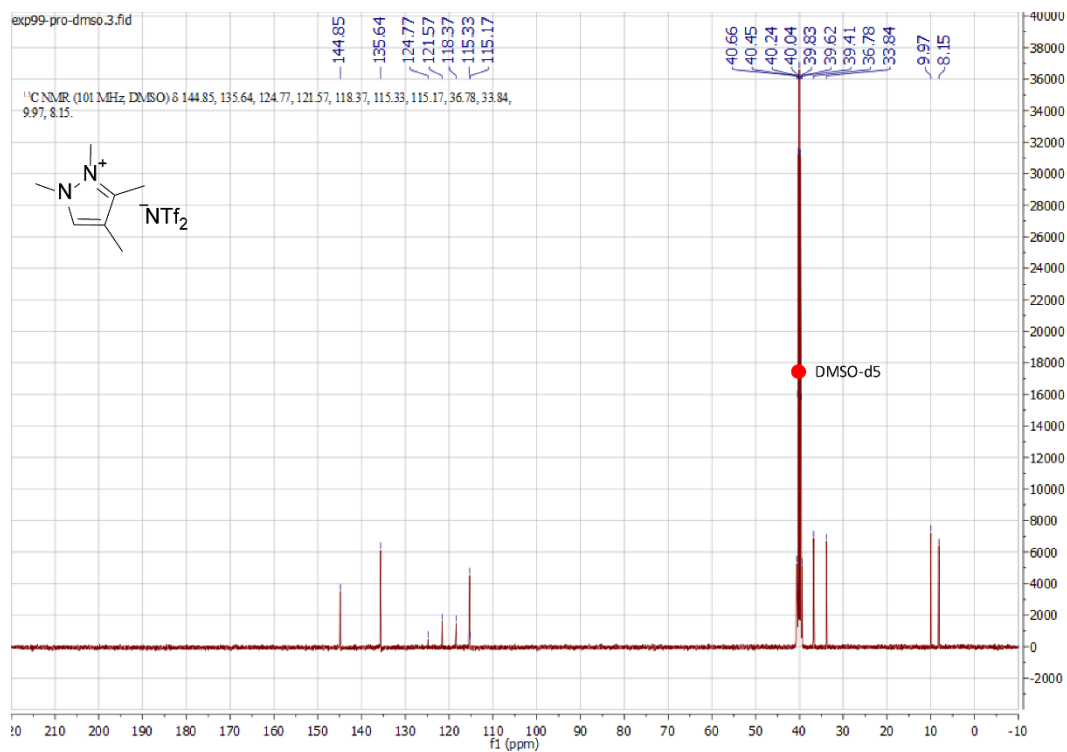
Figure S3.30 ¹H NMR spectrum of 1-butyl-2-methylpyrazolium iodide (DMSO-d₆).Figure S3.31. ¹³C NMR spectrum of 1-butyl-2-methylpyrazolium iodide (DMSO-d₆).

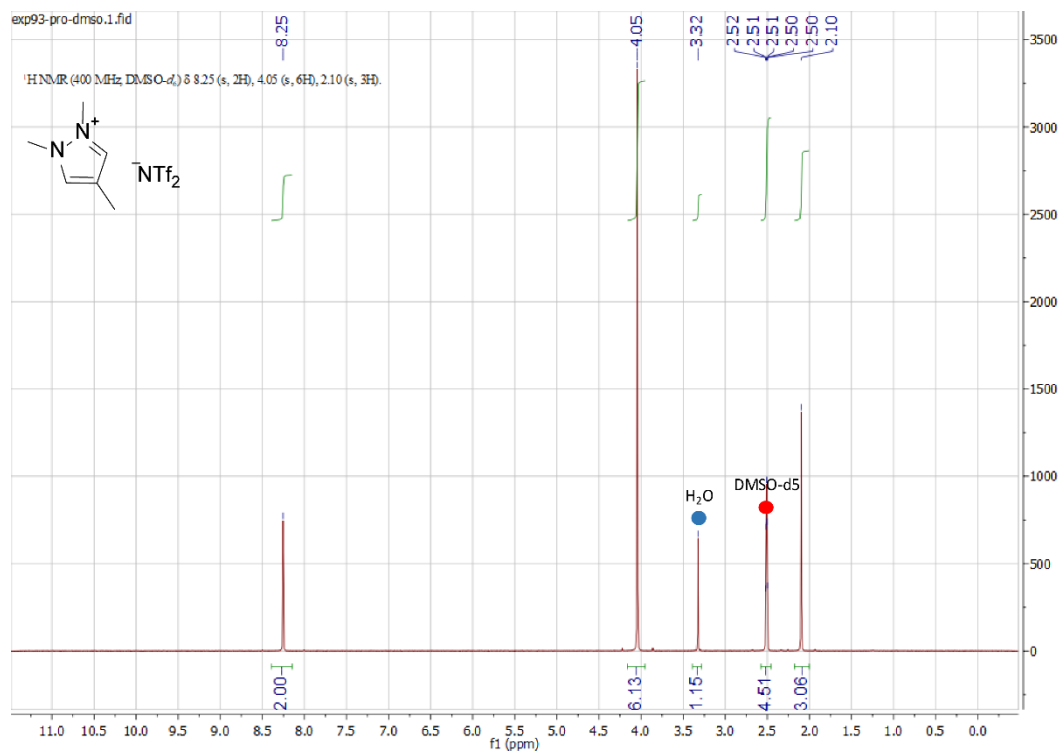
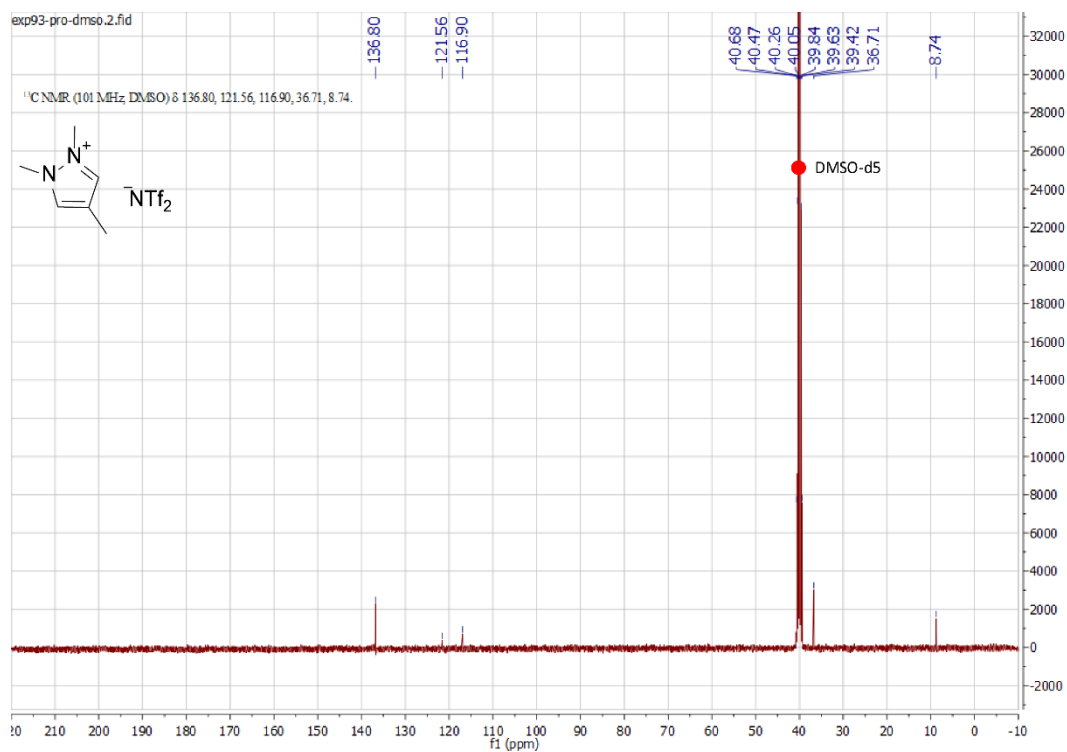


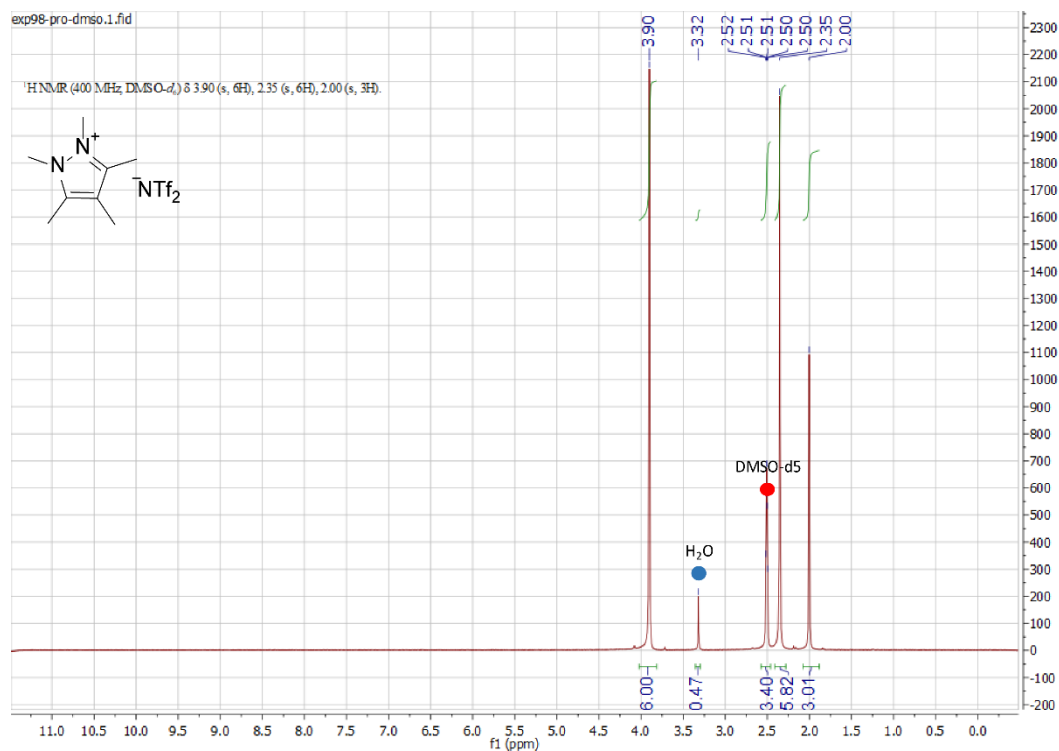
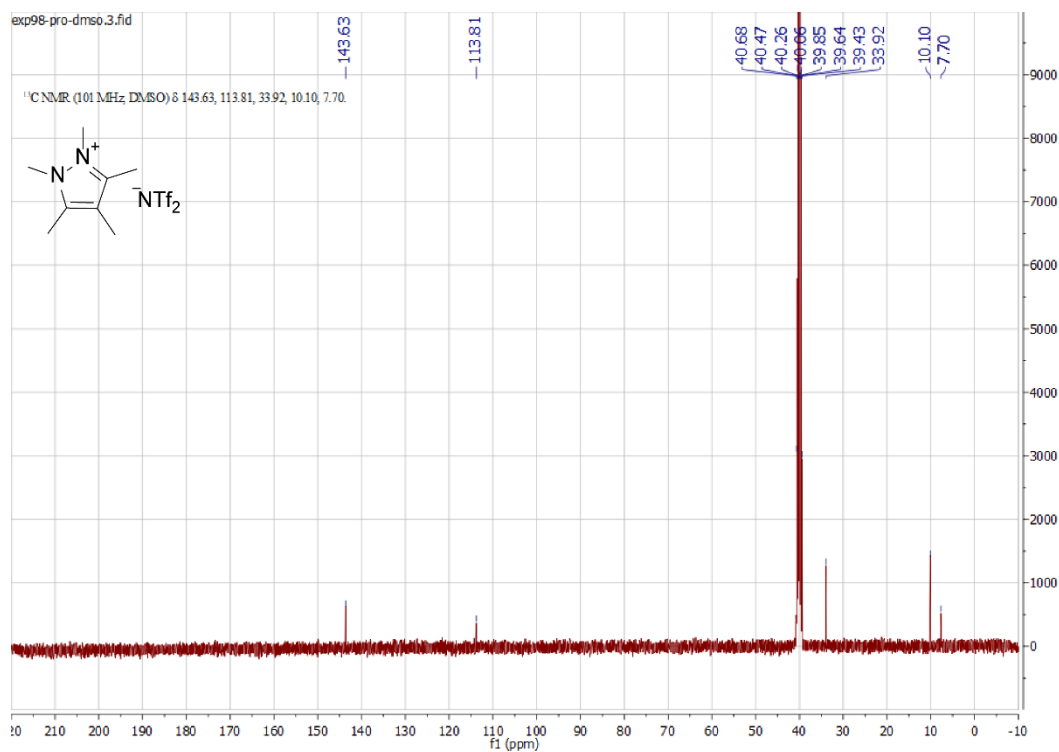
Figure S3.34. ¹H NMR spectrum of 1,2-dimethylpyrazolium TFSI **Pz12** (DMSO-d₆).Figure S3.35. ¹³C NMR spectrum of 1,2-dimethylpyrazolium TFSI **Pz12** (DMSO-d₆).

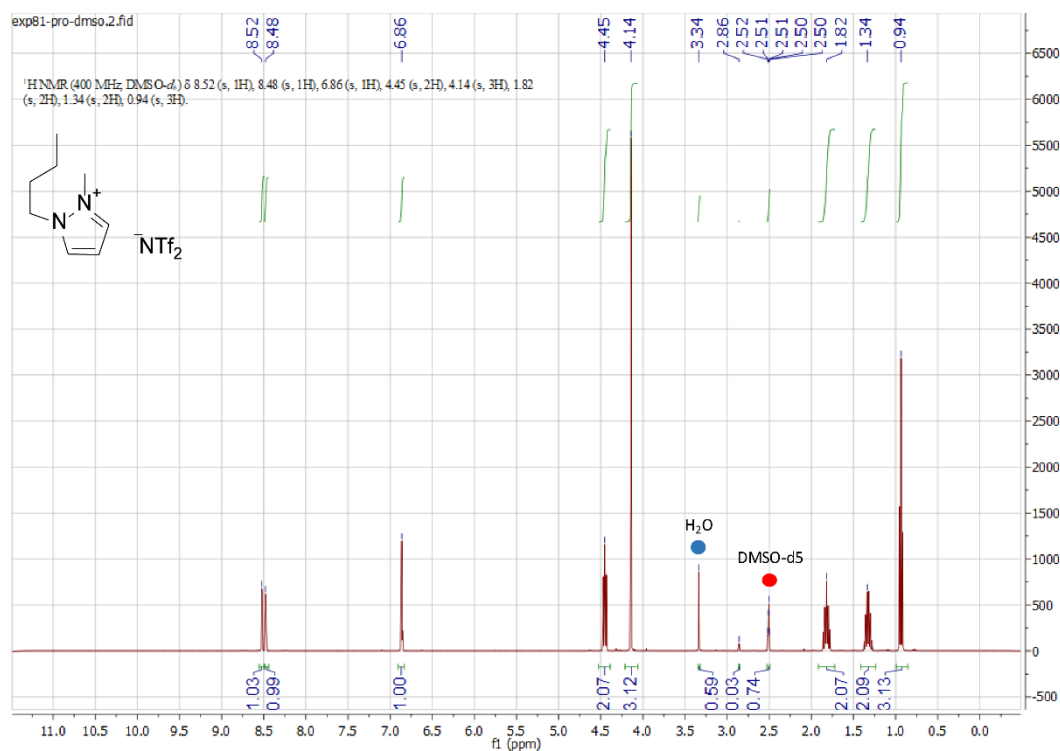
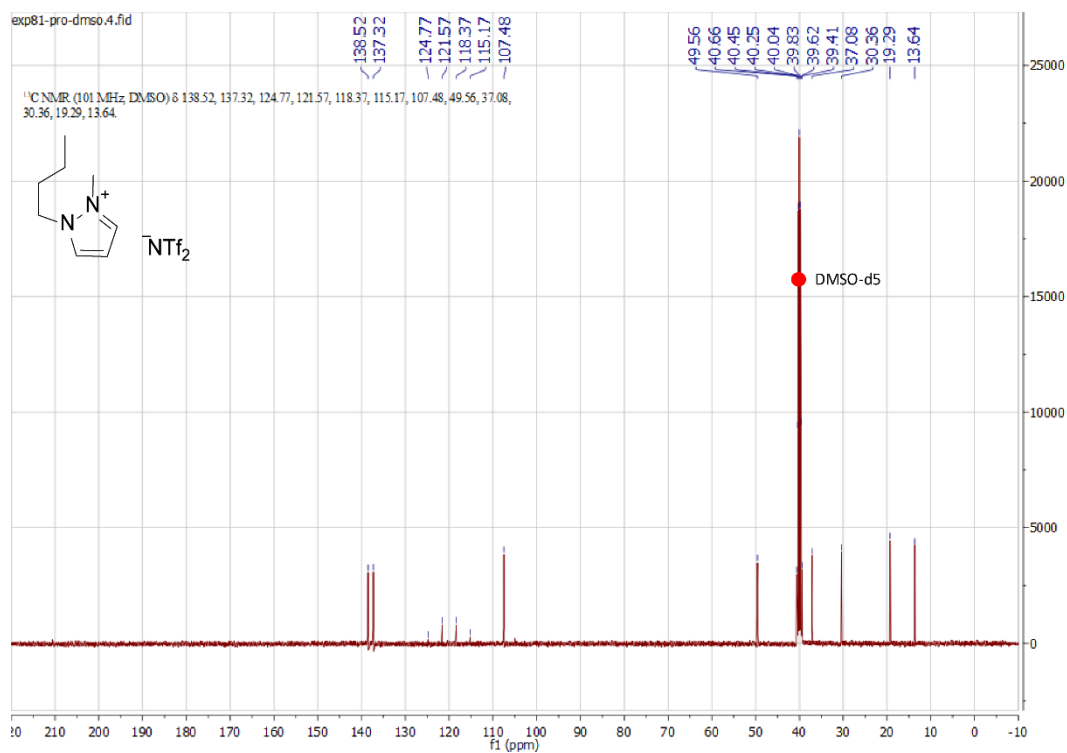
Figure S3.36. ¹H NMR spectrum of 1,2,3-trimethylpyrazolium TFSI **Pz123** (DMSO-d₆).Figure S3.37. ¹³C NMR spectrum of 1,2,3-trimethylpyrazolium TFSI **Pz123** (DMSO-d₆).

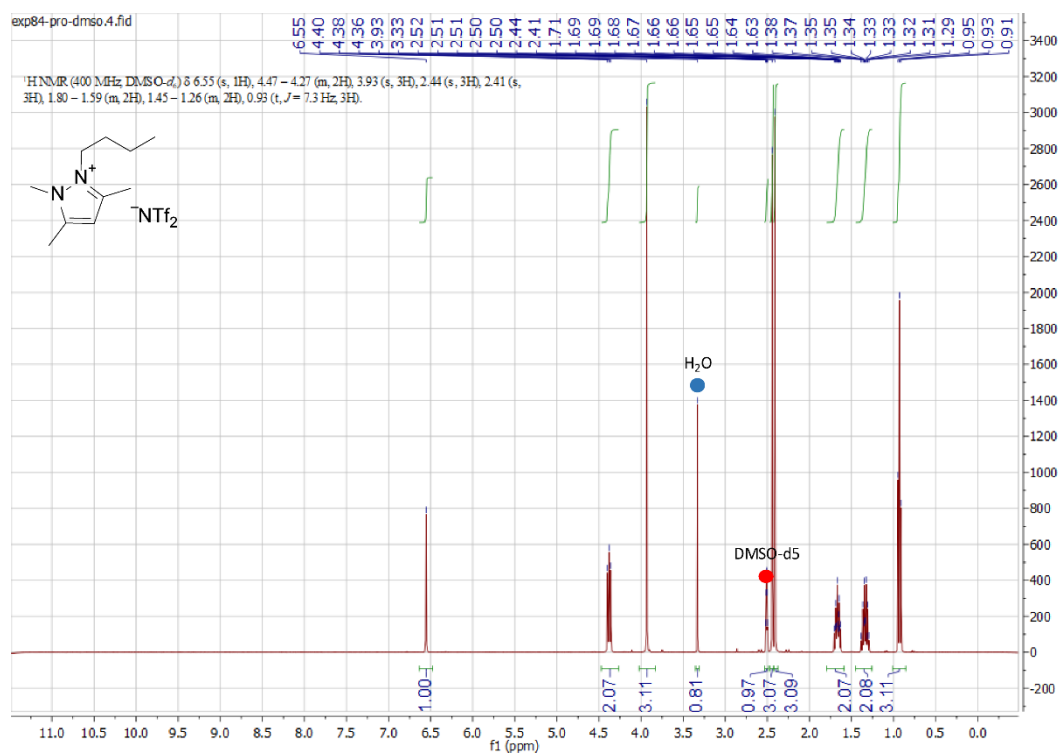
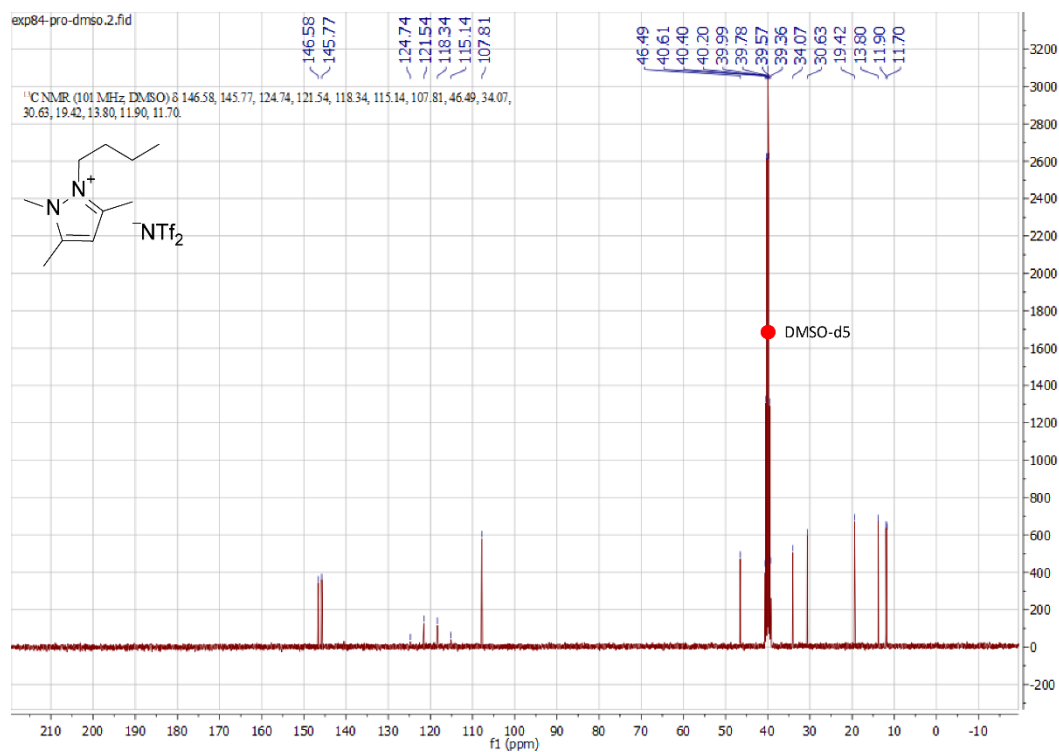
Figure S3.38. ¹H NMR spectrum of 1,2,3,5-tetramethylpyrazolium TFSI **Pz1235** (DMSO-d₆).Figure S3.39. ¹³C NMR spectrum of 1,2,3,5-tetramethylpyrazolium TFSI **Pz1235** (DMSO-d₆).

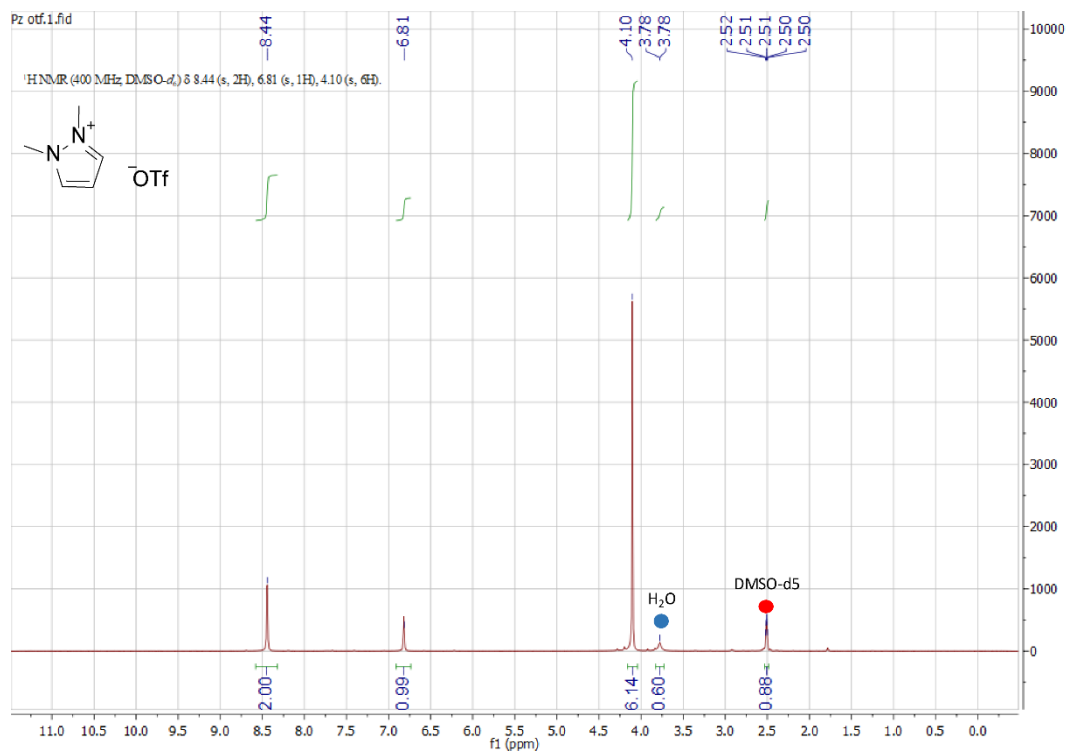
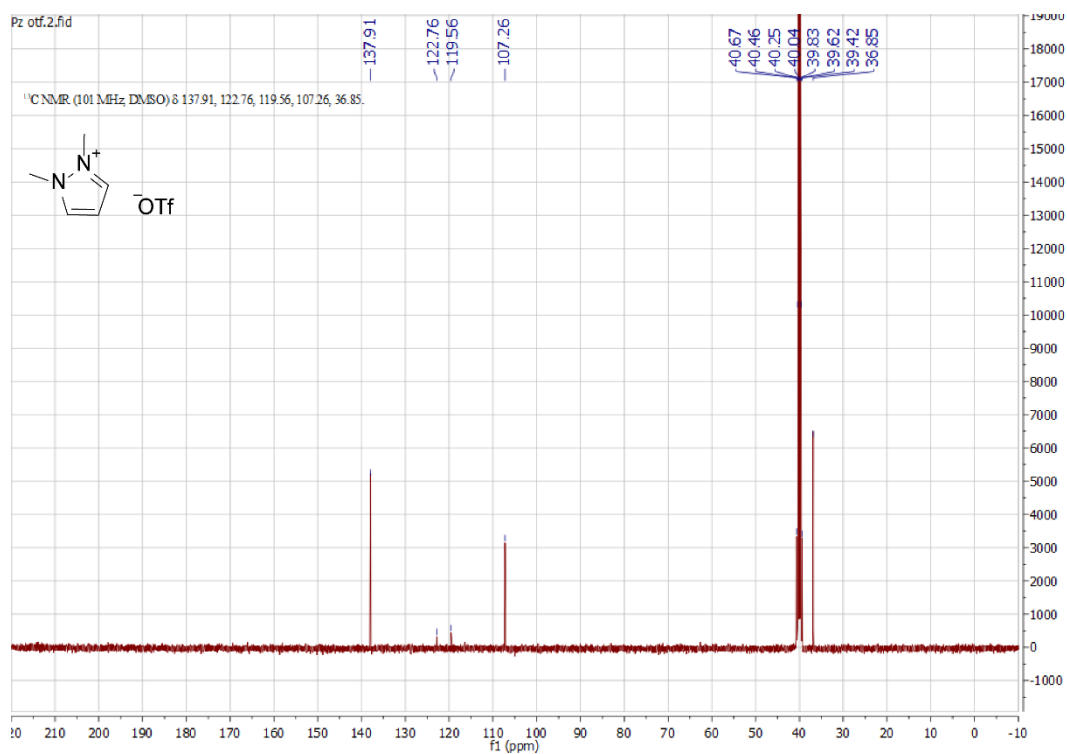
Figure S3.40. ¹H NMR spectrum of 1,2,3,4-tetramethylpyrazolium TFSI **Pz1234** (DMSO-d₆).Figure S3.41. ¹³C NMR spectrum of 1,2,3,4-tetramethylpyrazolium TFSI **Pz1234** (DMSO-d₆).

Figure S3.42. ¹H NMR spectrum of 1,2,4-trimethylpyrazolium TFSI **Pz124** (DMSO-d₆).Figure S3.43. ¹³C NMR spectrum of 1,2,4-trimethylpyrazolium TFSI **Pz124** (DMSO-d₆).

Figure S3.44. ¹H NMR spectrum of 1,2,3,4,5-pentamethylpyrazolium TFSI **Pz12345** (DMSO-d₆).Figure S3.45. ¹³C NMR spectrum of 1,2,3,4,5-pentamethylpyrazolium TFSI **Pz12345** (DMSO-d₆).

Figure S3.46. ¹H NMR spectrum of 1-butyl-2-methylpyrazolium TFSI **Pz12B** (DMSO-d₆).Figure S3.47. ¹³C NMR spectrum of 1-butyl-2-methylpyrazolium TFSI **Pz12B** (DMSO-d₆).

Figure S3.48. ¹H NMR spectrum of 1-butyl-2,3,5-trimethylpyrazolium TFSI **Pz1235B** (DMSO-*d*₆).Figure S3.49. ¹³C NMR spectrum of 1-butyl-2,3,5-trimethylpyrazolium TFSI **Pz1235B** (DMSO-*d*₆).

Figure S3.50. ¹H NMR spectrum of 1,2-dimethylpyrazolium triflate (DMSO-d₆).Figure S3.51. ¹³C NMR spectrum of 1,2-dimethylpyrazolium triflate (DMSO-d₆).

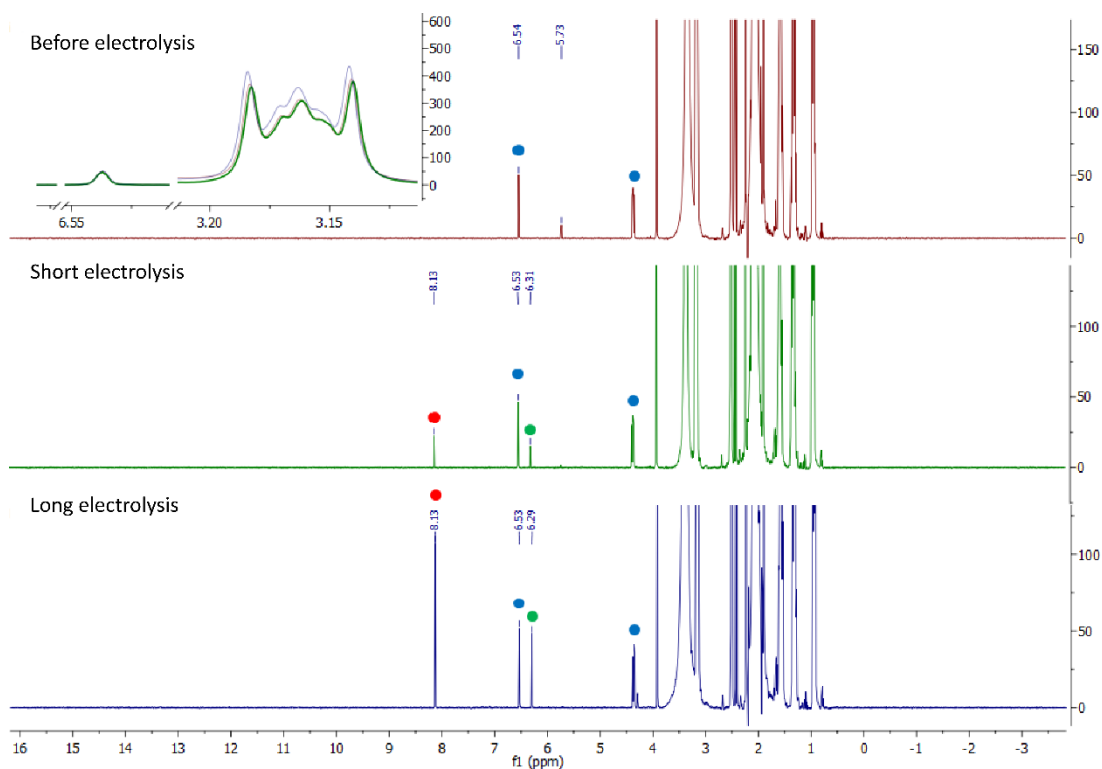


Figure S3.52. Stacked ^1H NMR spectra for the system before, during and after electrolysis (red, green and blue plots respectively; DMSO- d_6). Red dot marks formic acid, blue – **Pz1235B**, green – MeCN decomposition product. Inset: amplified regions of the same overlapped and normalized ^1H NMR spectra for the system before, during and after electrolysis (low field – selected signal of the Pz IL, high field – selected signal of NBu_4PF_6). The inset demonstrates constant relation between intensities of Pz and Bu_4N^+ NMR signals, and, therefore, stability of the catalytic system.

3.6 References

- (1) Taheri Najafabadi, A. CO₂ Chemical Conversion to Useful Products: An Engineering Insight to the Latest Advances toward Sustainability. *Int. J. Energy Res.* **2013**, *37*, 485–499.
- (2) Durst, J.; Rudnev, A.; Dutta, A.; Fu, Y.; Herranz, J.; Kaliginedi, V.; Kuzume, A.; Permyakova, A. A.; Paratcha, Y.; Broekmann, P.; et al. Electrochemical CO₂ Reduction – A Critical View on Fundamentals, Materials and Applications. *Chimia* **2015**, *69*, 769–776.
- (3) Tomita, Y.; Teruya, S.; Koga, O.; Hori, Y. Electrochemical Reduction of Carbon Dioxide at a Platinum Electrode in Acetonitrile-Water Mixtures. *J. Electrochem. Soc.* **2000**, *147*, 4164–4167.
- (4) Buzzeo, M. C.; Hardacre, C.; Compton, R. G. Extended Electrochemical Windows Made Accessible by Room Temperature Ionic Liquid/Organic Solvent Electrolyte Systems. *ChemPhysChem* **2006**, *7*, 176–180.
- (5) Rosen, B. A.; Salehi-Khojin, A.; Thorson, M. R.; Zhu, W.; Whipple, D. T.; Kenis, P. J. A.; Masel, R. I. Ionic Liquid – Mediated Selective Conversion of CO₂ to CO at Low Overpotentials. *Science* **2011**, *334*, 643–644.
- (6) Kuhl, K. P.; Hatsukade, T.; Cave, E. R.; Abram, D. N.; Kibsgaard, J.; Jaramillo, T. F. Electrocatalytic Conversion of Carbon Dioxide to Methane and Methanol on Transition Metal Surfaces. *J. Am. Chem. Soc.* **2014**, *136*, 14107–14113.
- (7) Singh, M. R.; Kwon, Y.; Lum, Y.; Ager, J. W.; Bell, A. T. Hydrolysis of Electrolyte Cations Enhances the Electrochemical Reduction of CO₂ over Ag and Cu. *J. Am. Chem. Soc.* **2016**, *138*, 13006–13012.
- (8) Zhao, S.-F.; Horne, M.; Bond, A. M.; Zhang, J. Is the Imidazolium Cation a Unique Promoter for Electrocatalytic Reduction of Carbon Dioxide? *J. Phys. Chem. C* **2016**, *120*, 23989–24001.
- (9) Sun, L.; Ramesha, G. K.; Kamat, P. V.; Brennecke, J. F. Switching the Reaction Course of Electrochemical CO₂ Reduction with Ionic Liquids. *Langmuir* **2014**, *30*, 6302–6308.
- (10) Rosen, B. A.; Haan, J. L.; Mukherjee, P.; Braunschweig, B.; Zhu, W.; Salehi-Khojin, A.; Dlott, D. D.; Masel, R. I. In Situ Spectroscopic Examination of a Low Overpotential Pathway for Carbon Dioxide Conversion to Carbon Monoxide. *J. Phys. Chem. C* **2012**, *116*, 15307–15312.
- (11) García Rey, N.; Dlott, D. D. Structural Transition in an Ionic Liquid Controls CO₂ Electrochemical Reduction. *J. Phys. Chem. C* **2015**, *119*, 20892–20899.

Chapter 4 Guanidinium Ionic Liquids

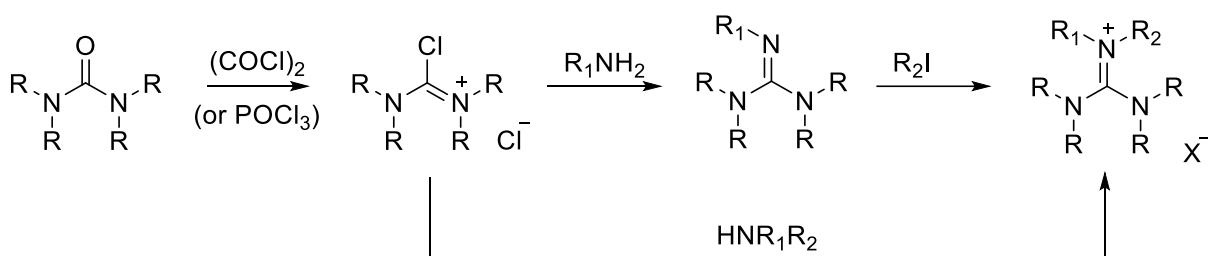
4.1 Introduction

In the previous chapters it was demonstrated that the scope of the ionic compounds able to promote the CO₂RR is not limited to Im-based ILs. Pz and some tetraalkyl ammonium (e.g. pyrrolidinium) salts also display co-catalytic activity. However, the number of room-temperature ILs (RTILs) that are applicable for the CO₂RR remains small, and the structures of these compounds tend to be similar. Therefore, the development of ILs with fundamentally different structures, which can assist the CO₂RR, is of high relevance. In case of activity, such systems provide valuable data on the possible active sites, binding modes and electronic factors that are important for the efficient promotion of the target reaction. Such data facilitates the development of descriptors for a rational design of superior co-catalysts for the CO₂RR.

In this chapter, we show that guanidinium (Gua)-based ILs are promoters for the CO₂RR and can be used to investigate the reduction mechanism. Gua ILs were described as stable¹ and readily available² compounds, which were predicted to dissolve reasonable amounts of CO₂³ and were applied as electrolytes in Li-ion batteries,^{4,5} in dye-sensitized solar cells⁶ and as reaction media for a range of organic reactions.^{7,8} The properties of these ILs can be tuned by variation of six substituents attached to the N-atoms. Due to the conjugation in the guanidinium core, the positive charge is stabilized and distributed over three sites. Therefore, gradual changes in the substitution pattern could be used to elucidate structure/activity dependencies.

4.2 Results

The synthesis of the Gua ILs was performed using a previously reported approach,⁵ employing chloroamidinium chlorides as the precursors (Scheme 4.1). These chlorides were obtained by the treatment of urea derivatives either with oxalyl chloride, or with phosphoryl chloride, although oxalyl chloride is preferable due to the easier purification of the product. The guanidine core is formed on the next step – reaction of the chloroamidinium salt with a primary or secondary amine. Application of secondary amines reduces the number of synthetic steps and affords guanidinium salts directly. In the case of cyclic ureas the synthesis of Gua ILs is more complicated, probably due to the slower double bond rearrangement in the strained systems compared to the acyclic systems.



Scheme 4.1. Synthesis of Gua ILs.

The Gua cations prepared are presented in Figure 4.1. As mentioned above, Gua ILs have three symmetrically placed charged N-sites and the stepwise changes of the substitution patterns, and hence charge accessibility, should influence the activity of the salt. The substituents were selected in a way to gradually increase the steric hindrance of the nitrogen sites by introduction of cyclic groups. Furthermore, the accessibility of the nitrogen center can be tuned by changing the N-C-N angle of the guanidinium core. For this purpose, cyclic ureas were employed as precursors for the Gua ILs in order to introduce intramolecular links between the nitrogen atoms.

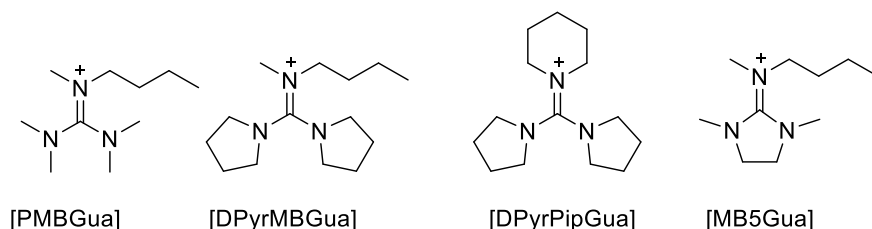


Figure 4.1. Cations of the synthesized Gua ILs.

As in the previous chapters, non-aqueous electrolytes were selected in order to minimize the possibility of the HER. The non-aqueous environment permits the use of PF_6^- and Tf_2N^- as suitable anions

for the ILs, as they provide good solubilities in organic solvents. Gua hexafluorophosphates are easy to synthesize, purify and work with due to the high crystallinity of the compounds, while Tf_2N^- ILs with asymmetric cation are liquid at room-temperature and can be probed as media for the CO_2RR . Notably, some of the chloroamidinium precursors for the ILs are also commercially available in the PF_6^- form, which significantly simplifies synthesis of the co-catalysts.

As in the previous studies, a silver polished polycrystalline electrode was selected as the actual catalyst for the reduction. A glassy carbon electrode was used to probe the stability of the catalysts in the presence and absence of CO_2 , as this electrode is inert and no CO_2RR is expected. Tetrabutylammonium hexafluorophosphate was employed as a part of the supporting electrolyte to ensure high conductivities.

The stabilities and activities of the ILs were first tested by the CV experiments. Scans were performed under a N_2 atmosphere (for the silver electrode) and under both N_2 and CO_2 (for the glassy carbon electrode), and reveal excellent stability of the Gua ILs as no current indicating decomposition of the ILs was observed within the electrochemical window of the solvent, i.e. acetonitrile (Figure 4.2).

When CO_2 is flushed through the system and the silver electrode is employed, steep reduction waves appear on the CV, which may be attributed to the CO_2RR (Figures 4.3, 4.6). The onset potential for the reduction shifts towards more positive voltages compared to the reference system, not containing the IL co-catalyst, as demonstrated by the representative example of $[\text{MB5Gua}]\text{PF}_6$ (Figure 4.3). Meanwhile, no currents are observed when the C electrode is employed, supporting the co-catalytic behavior of the Ag electrode.

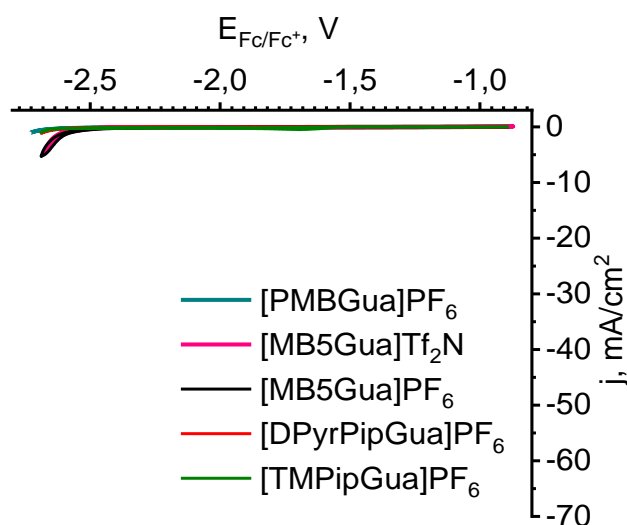


Figure 4.2. Cyclic voltamograms for the Gua ILs under N_2 , illustrating stability of diversely substituted Gua cations (Ag polished disk electrode, NBu_4PF_6 (0.1 M) in acetonitrile, IL additive (0.02 M), system flushed with N_2).

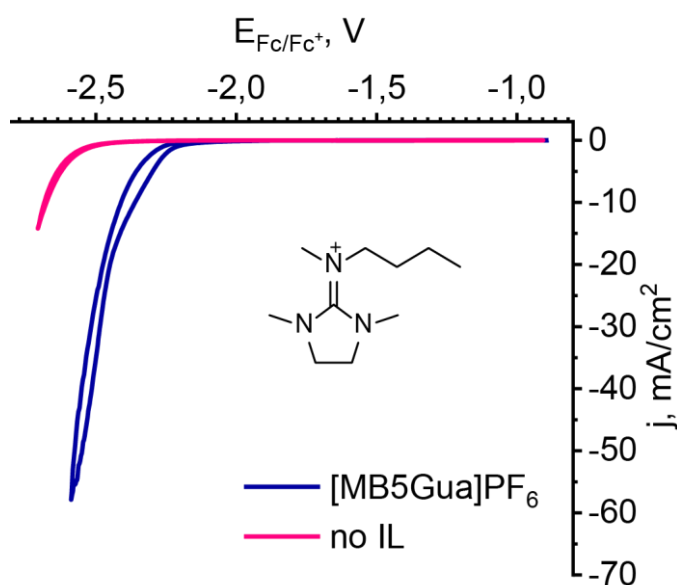


Figure 4.3. Comparison of CV data, recorded in the presence and in the absence of the co-catalysts on the example of $[MB5Gua]PF_6$ (Ag polished disk electrode, NBu_4PF_6 (0.1 M) in acetonitrile, IL additive (0.02 M), system flushed with CO_2).

In order to confirm that the observed currents are attributed to the CO_2RR rather than to decomposition of the co-catalyst or other side reactions, potentiostatic electrolysis followed by online GC

analysis was performed for [MB5Gua]Tf₂N, as the representative co-catalyst (Figure 4.4). CO was found to be the predominant product of the reduction.

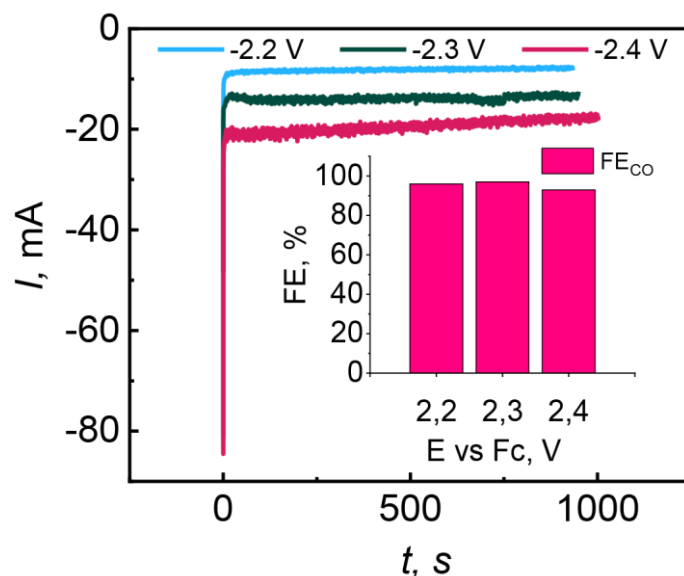


Figure 4.4. Performance of [MB5Gua]Tf₂N for the CO₂RR. Potentiostatic electrolysis followed by online GC measurements, Ag working electrode, IL additive (0.02 M) and NBu₄PF₆ (0.1 M) in acetonitrile. Inset: Faradaic efficiencies for CO.

From a comparison of the activities of the Gua co-catalysts several trends can be deduced. With the introduction of the cyclic substituents to the nitrogen atoms the onset potentials for the reduction remain essentially unchanged. However, the current densities are significantly decreased. This observation supports the hypothesis, that promotion of the CO₂RR by the Gua ILs occurs through the interactions, co-axial with the Gua C-N bond, of the positively charged N-site with the negatively charged O-atom from the CO₂-based intermediate (Figure 4.5). Blocking of the active sites by the substitution reduces the number of active sites, and, therefore, the overall speed of the reaction, which leads to a decrease in the current. Moreover, the strength of the interaction between the rest of the charged sides and CO₂^{•-} remains the same, which results in no changes in the reduction onset potential for the CO₂RR.

Another feature is apparent from a comparison of the acyclic Gua ILs and cyclic [MB5Gua]PF₆ (Figure 4.6). The latter co-catalyst has a noticeably lower reduction onset potential compared to the other catalysts in the series. This difference might be due to two factors, i.e. a lower electron donating effect of the methylenide group compared to the methyl and the strain in the cyclic molecule. The strained group in the structure of [MB5Gua] cation increases the C-N-C angles in the Gua cation,

thus increasing the availability of the positively charged nitrogen for the interaction with the CO₂-derived intermediate.

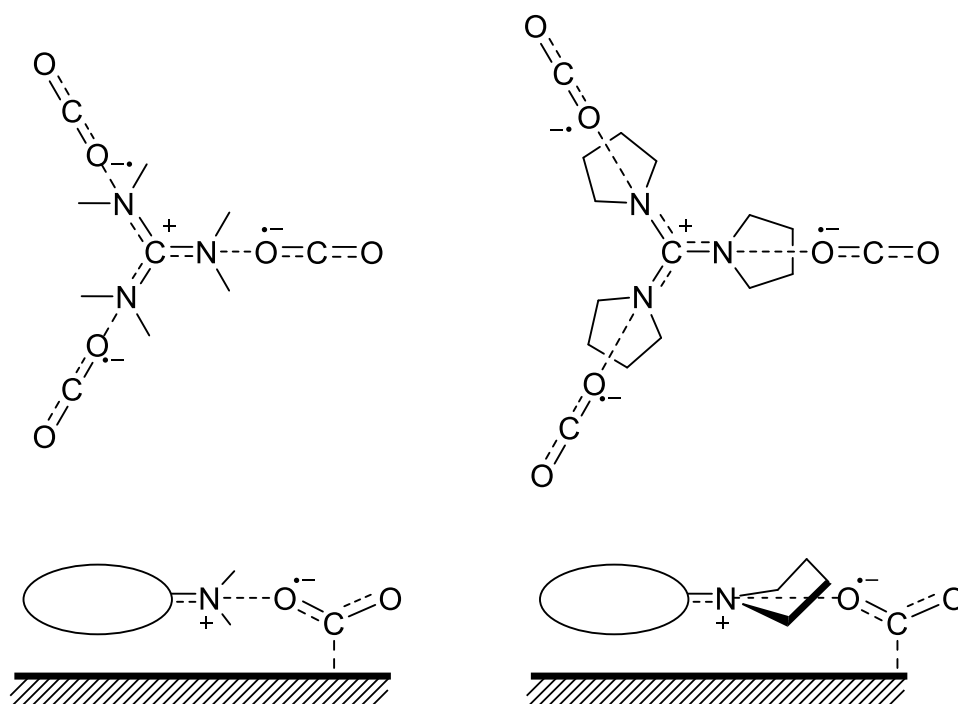


Figure 4.5 Suggested bonding modes for Gua ILs and CO₂-based intermediates, two projections. Left: interaction of CO₂ intermediate with unhindered Gua ILs. Right: blocking of the stabilizing interaction by introduction of cyclic substituents.

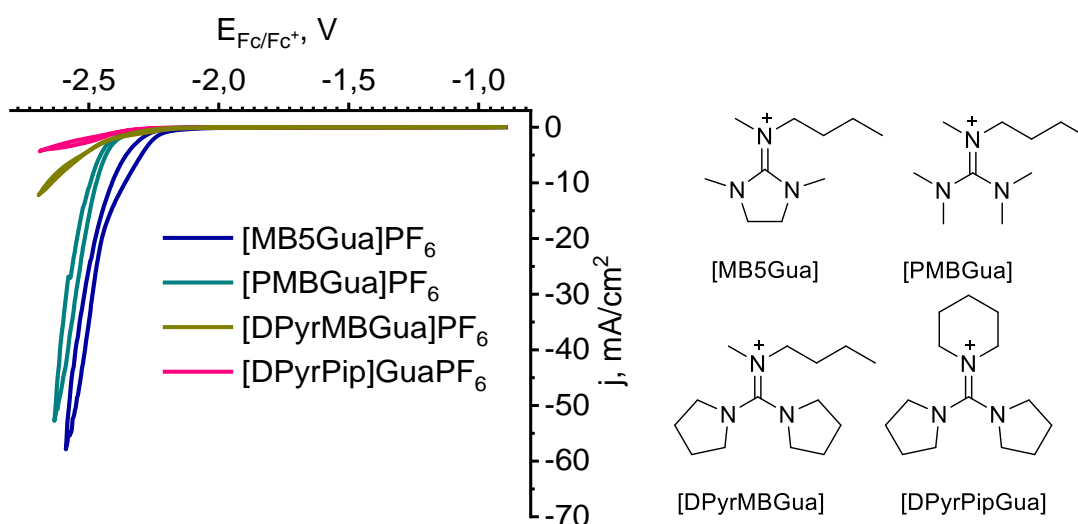


Figure 4.6. Comparison of the activities of diversely substituted Gua ILs. Left: CV data for the representative Gua ILs (Ag electrode, IL additive (0.02 M) and NBu₄PF₆ (0.1 M) in acetonitrile). Right: structures of the corresponding Gua ILs.

Indeed, the concept of charge availability can be used to describe activities of other classes of ILs. Im ILs, for example, have around 150 mV more positive onset potentials compared to the Gua ILs. The C-N-C angle for Im ILs is same as for the Gua ILs (around 120°), while the positive charge is distributed between two nitrogen centers, while for less active Gua ILs the effective charge is lower, as it is distributed between three nitrogen centers. However, fully substituted Im ILs lose their co-catalytic activity,⁹ as the availability of the charged centers for the species in the same plane significantly drops. Although pyrrolidinium (Pyrd) ILs¹⁰ have a positive charge localized on one N-center, the nitrogen atom of the Pyrd ILs has sp^3 -hybridization, which 1) limits availability of the co-catalyst for the interaction with counter-ions; 2) makes the nitrogen less electronegative compared to the sp^2 -hybridized nitrogens of Im ILs. Pyrd ILs are usually more active co-catalysts than tetraalkylammonium salts,¹⁰ which can probably be explained by the strain in the Pyrd cycle, which broadens the angles between the alkyl groups and makes the interaction with the CO_2 -based species more plausible. Therefore, we support the statement, that CO_2RR is governed by the local electrical field environment.

4.3 Summary

We describe Gua ILs as co-catalysts for the CO_2RR , which are efficient co-catalysts although somewhat less effective than Im ILs and provide valuable information on the structure/activity correlation. Based on the series of Gua ILs studied, the activity appears to be related to the accessibility of the positively charged nitrogen sites and on the ring. This hypothesis also fits the general activity trend for various classes of cations with Im ILs > Gua ILs, Pyrd ILs > tetraalkylammonium salts, Pz ILs \approx Im ILs in the terms of activity. Furthermore, based on this hypothesis, the rational design of efficient co-catalysts for the CO_2RR should be possible.

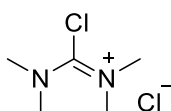
4.4 Experimental

4.4.1 Materials and methods.

All reagents were obtained commercially and used without further purification unless otherwise stated. CO₂ (99.998 %) and Ar (99.9999 %) were obtained from Carbagas, Switzerland. ¹H, ¹⁹F and proton-decoupled ¹³C-NMR spectra were recorded on a Bruker Avance-400 (400 MHz) spectrometer. All reactions were completed under inert conditions (nitrogen atmosphere). For the graphical representation of NMR spectra please see the Supporting Information. Electrochemical measurements were made in according with the protocols from Chapter 2.

4.4.2 Synthesis and characterization of the compounds

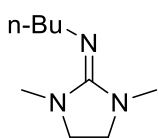
N,N,N',N'-tetramethylchloroformamidinium chloride: Solution of freshly distilled tetramethylurea



(20 mL, 0.167 mmol, 1 eq) in dry dichloromethane (20 mL) was added dropwise to oxalyl chloride (15.7 mL, 183 mmol, 1.1 eq). Intense gas evolution was observed.

The solution was left stirring for 24 hours at room temperature, the solvent was removed under vacuum. The solid residue was washed with diethyl ether and dried under vacuum, yielding the product (24 g, 85%) as colorless powder. ¹H NMR (400 MHz, DMSO-*d*₆) δ 2.69 (s, 12H). ¹³C NMR (101 MHz, DMSO) δ 164.73, 38.71.

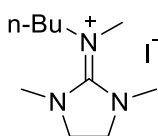
N-butyl-1,3-dimethylimidazolidin-2-imine. To a solution of 2-chloro-1,3-dimethyl-4,5-dihydro-1H-



imidazol-3-ium chloride (2.00 g, 11.83 mmol, 1 eq) in dry acetonitrile (30 mL) n-butylamine (2.34 mL, 23.66 mmol, 2 eq.) was added dropwise at 0°C. The reaction mixture was refluxed for 16 h, then cooled to rt, diluted with 1M NaOH (100 mL) and

extracted with DCM (3×50 mL). The combined organic layers were dried over Na₂SO₄ and then concentrated under reduced pressure to afford pale yellow oil (2.01 g, 96%). ¹H NMR (400 MHz, Chloroform-*d*) δ 3.36 – 3.26 (m, 2H), 3.11 (d, *J* = 4.9 Hz, 5H), 2.94 – 2.81 (m, 3H), 2.65 (s, 3H), 1.57 – 1.44 (m, 2H), 1.44 – 1.26 (m, 2H), 0.89 (t, *J* = 7.3 Hz, 3H). ¹³C NMR (101 MHz, CDCl₃) δ 157.03, 50.92, 48.16, 48.14, 47.40, 38.48, 35.76, 34.64, 20.48, 14.13.

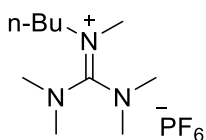
N-butyl-1,3-dimethylimidazolidin-2-iminium iodide. To a solution of N-butyl-1,3-dimethylimidazol-



idin-2-imine (2.1 g, 12.4 mmol, 1 eq) in dry acetonitrile (10 mL) iodomethane (1.34 mL, 13.6 mmol, 1.1 eq.) was added dropwise. The reaction mixture was left stirring at room temperature for 24 hours, then concentrated under reduced pressure and dried under vacuum to afford dark yellow oil (3.03 g, 78%). ¹H NMR (400 MHz, DMSO-*d*₆)

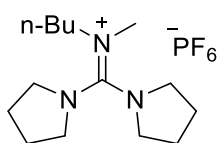
δ 3.68 (s, 4H), 3.31 – 3.23 (m, 2H), 2.97 (d, J = 1.0 Hz, 9H), 1.72 – 1.42 (m, 2H), 1.28 (h, J = 7.4 Hz, 2H), 0.91 (t, J = 7.4 Hz, 3H). ^{13}C NMR (101 MHz, DMSO) δ 164.07, 52.14, 49.76, 37.73, 36.65, 29.47, 19.56, 14.08.

N-(bis(dimethylamino)methylene)-N-methylbutan-1-aminium hexafluorophosphate. To a solu-



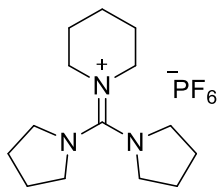
tion of 2.00 g (11.69 mmol) of N-(chloro(dimethylamino)methylene)-N-methylmethanaminium chloride in 20 mL of dry acetonitrile a solution of 1.385 mL (11.69 mmol, 1 eq.) of N-methylbutylamine and 1.625 mL (11.69 mmol, 1 eq.) of triethylamine in 10 mL of dry diethyl ether was added dropwise at 0°C. The reaction mixture was allowed to warm up to rt and stirred for 16 h, then diluted with 100 mL of water. Colored contaminants were extracted with DCM (3x50 mL). Half of the aqueous layer was separated and directly used for the anion exchange. To the solution of butyl-pentamethylguanidinium chloride (1.3 g, 5.8 mmol, 1 eq) in Milli-Q water (ca.10 mL) solution of potassium hexafluorophosphate (1.2 g, 1.1 eq) in Milli-Q water (ca. 100 mL) was added. Colorless precipitate was formed immediately. The mixture was left stirring at rt for 3 hours, the product was separated by filtration, washed with Et₂O (3x50 mL) and dried under vacuum, affording the product as colorless powder (1.4 g, 72%). ^1H NMR (400 MHz, DMSO-*d*₆) δ 3.15 (q, J = 8.0 Hz, 2H), 2.87 (2s, 15H), 1.64 – 1.41 (m, 2H), 1.26 (dq, J = 15.2, 7.5 Hz, 2H), 0.91 (t, J = 7.3 Hz, 3H). ^{13}C NMR (101 MHz, DMSO) δ 163.03, 51.78, 37.66, 29.31, 19.85, 14.03. ^{31}P NMR (162 MHz, DMSO-*d*₆) δ -118.50 – -172.13 (m). ^{19}F NMR (376 MHz, DMSO) δ -70.20 (d, 711 Hz).

N-(di(pyrrolidin-1-yl)methylene)-N-methylbutan-1-aminium hexafluorophosphate. To a solution



of 2.00 g (6.01 mmol) of 1-(chloro(pyrrolidin-1-yl)methylene)pyrrolidin-1-ium hexafluorophosphate in 20 mL of dry acetonitrile a solution of 0.7122 mL (6.01 mmol, 1 eq.) of N-methylbutylamine and 0.836 mL (6.01 mmol, 1 eq.) of triethylamine in 10 mL of dry diethyl ether was added dropwise at 0°C. The reaction mixture was allowed to warm up to rt and stirred for 16 h, then diluted with 100 mL of water and extracted with DCM (3x50 mL). The combined organic layers were dried over Na₂SO₄ and concentrated under reduced pressure to afford pale yellow solid (2.20 g, 95%). ^1H NMR (400 MHz, DMSO-*d*₆) δ 3.37 (td, J = 6.7, 5.4, 2.9 Hz, 8H), 3.15 – 3.04 (m, 2H), 2.82 (s, 3H), 1.97 – 1.82 (m, 8H), 1.60 – 1.44 (m, 2H), 1.27 (dq, J = 14.6, 7.4 Hz, 2H), 0.90 (t, J = 7.4 Hz, 3H). ^{13}C NMR (101 MHz, DMSO) δ 154.78, 49.97, 47.44, 35.49, 27.45, 23.16, 17.63, 11.96, -0.50. ^{31}P NMR (162 MHz, DMSO-*d*₆) δ -144.21 (sept, J = 711.1 Hz). ^{19}F NMR (376 MHz, DMSO) δ -70.27 (d, 711 Hz).

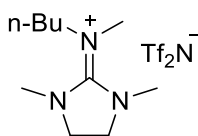
1-(di(pyrrolidin-1-yl)methylene)piperidin-1-ium hexafluorophosphate. To a solution of 2.00 g



(6.01 mmol) of 1-(chloro(pyrrolidin-1-yl)methylene)pyrrolidin-1-ium hexafluorophosphate in 20 mL of dry acetonitrile a solution of 0.59 mL (6.012 mmol, 1 eq.) of piperidine and 0.84 mL (6.012 mmol, 1 eq.) of triethylamine in 10 mL of dry diethyl ether was added dropwise at 0°C. The reaction mixture was al-

lowed to warm up to rt and stirred for 16 h, then diluted with 100 mL of water and extracted with DCM (3x50 mL). The combined organic layers were dried over Na₂SO₄ and concentrated under reduced pressure to afford white solid (2.23 g, 97%). ¹H NMR (400 MHz, DMSO-*d*₆) δ 3.37 (d, *J* = 6.6 Hz, 8H), 3.18 (t, *J* = 4.6 Hz, 4H), 1.96 – 1.84 (m, 8H), 1.67 – 1.52 (m, 6H). ¹³C NMR (101 MHz, DMSO) δ 156.29, 49.75, 49.57, 25.49, 25.32, 23.81. ¹⁹F NMR (376 MHz, DMSO) δ -70.28 (d, *J* = 707 Hz). ³¹P NMR (162 MHz, DMSO-*d*₆) δ -144.2 (septet, *J* = 711 Hz).

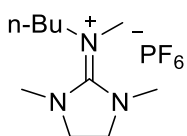
N-butyl-1,3-dimethylimidazolidin-2-iminium bis(trifluoromethylsulfonyl)imide. To a solution of N-



butyl-1,3-dimethylimidazolidin-2-iminium iodide (2.0 g, 6.4 mmol, 1 eq) in water (10 mL) was added LiTf₂N (1.94 g, 6.7 mmol, 1.05 eq.) and dichloromethane (10 mL). The reaction mixture was left stirring at room temperature for 24 hours,

then the organic phase was separated, washed by water (3x50 mL), concentrated under reduced pressure and dried under vacuum to afford pale yellow oil (2.93 g, 98%). ¹H NMR (400 MHz, DMSO-*d*₆) δ 3.67 (s, 4H), 3.29 – 3.22 (m, 2H), 2.96 (d, *J* = 1.0 Hz, 9H), 1.66 – 1.48 (m, 2H), 1.35 – 1.18 (m, 6H), 0.93 – 0.82 (m, 3H). ¹³C NMR (101 MHz, DMSO) δ 164.08, 121.55, 118.35, 52.39, 49.72, 37.61, 36.54, 31.29, 27.35, 25.90, 22.45, 14.30. ¹⁹F NMR (376 MHz, DMSO) δ -78.75.

N-butyl-1,3-dimethylimidazolidin-2-iminium hexafluorophosphate. To a solution of N-butyl-1,3-di-



methylimidazolidin-2-iminium iodide (0.5 g, 1.6 mmol, 1 eq) in Milli-Q water (5 mL) was added KPF₆ (0.33 g, 1.8 mmol, 1.1 eq.). The reaction mixture was left stirring at room temperature for 12 hours, dichloromethane (10 mL) was added. The aque-

ous phase was washed with Milli-Q water (2x10 mL), then dried under vacuum to afford pale yellow oil (0.53 g, 100%). ¹H NMR (400 MHz, DMSO-*d*₆) δ 3.67 (s, 4H), 3.30 – 3.23 (m, 2H), 2.96 (s, 9H), 1.63 – 1.49 (m, 2H), 1.28 (h, *J* = 7.3 Hz, 2H), 0.91 (t, *J* = 7.4 Hz, 3H). ¹³C NMR (101 MHz, DMSO) δ 164.08, 52.12, 49.73, 37.65, 36.57, 29.45, 19.55, 14.05. ¹⁹F NMR (376 MHz, DMSO) δ -70.21 (d, *J* = 711 Hz). ³¹P NMR (162 MHz, DMSO-*d*₆) δ -144.2 (septet, *J* = 711 Hz).

4.1 Supporting Information

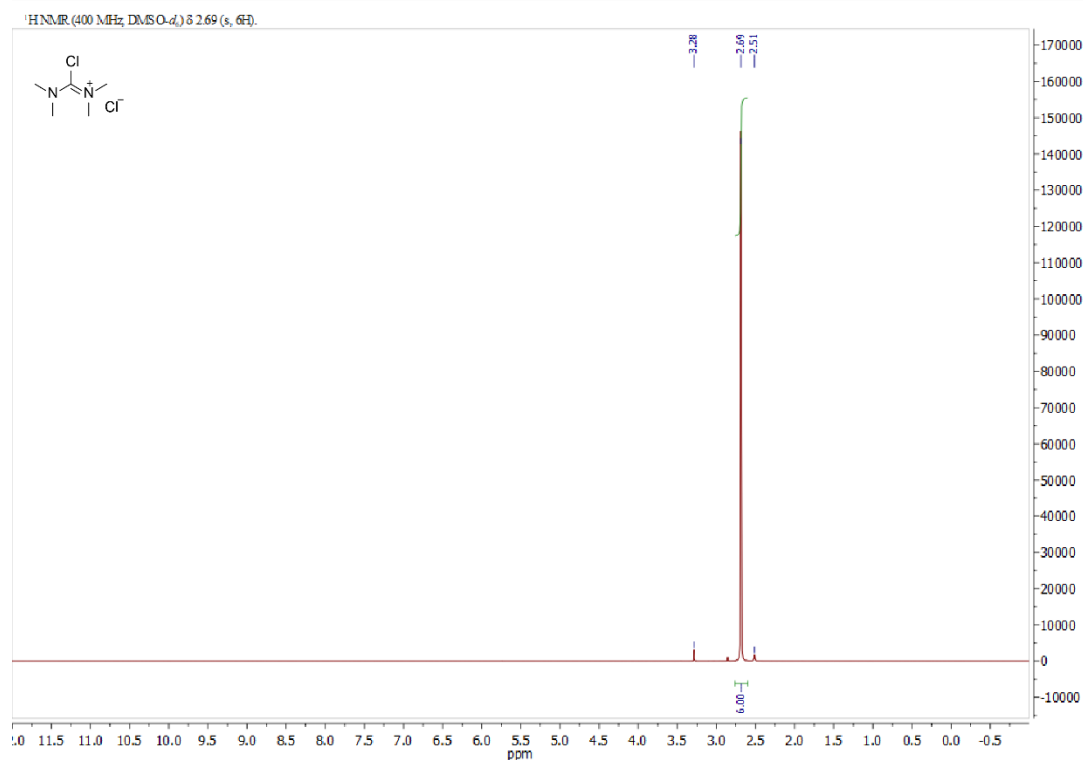


Figure S4.1. ¹H NMR spectrum of N,N,N',N'-tetramethylchloroformamidinium chloride (400 MHz, DMSO-*d*₆).

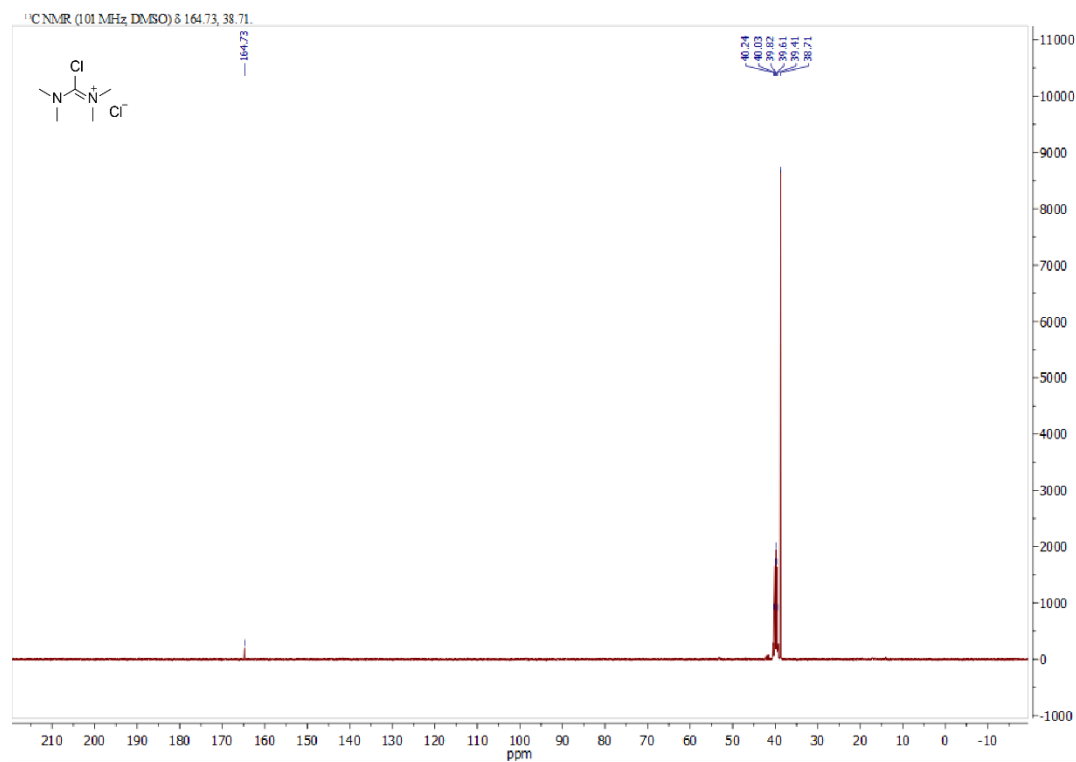
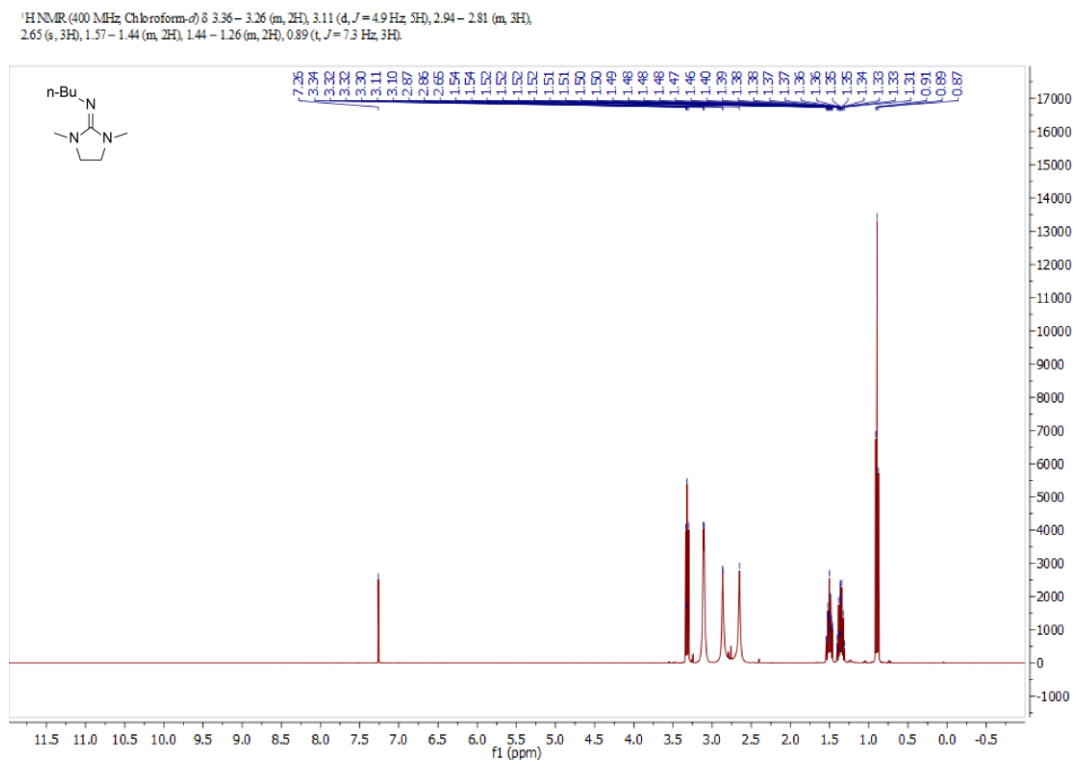
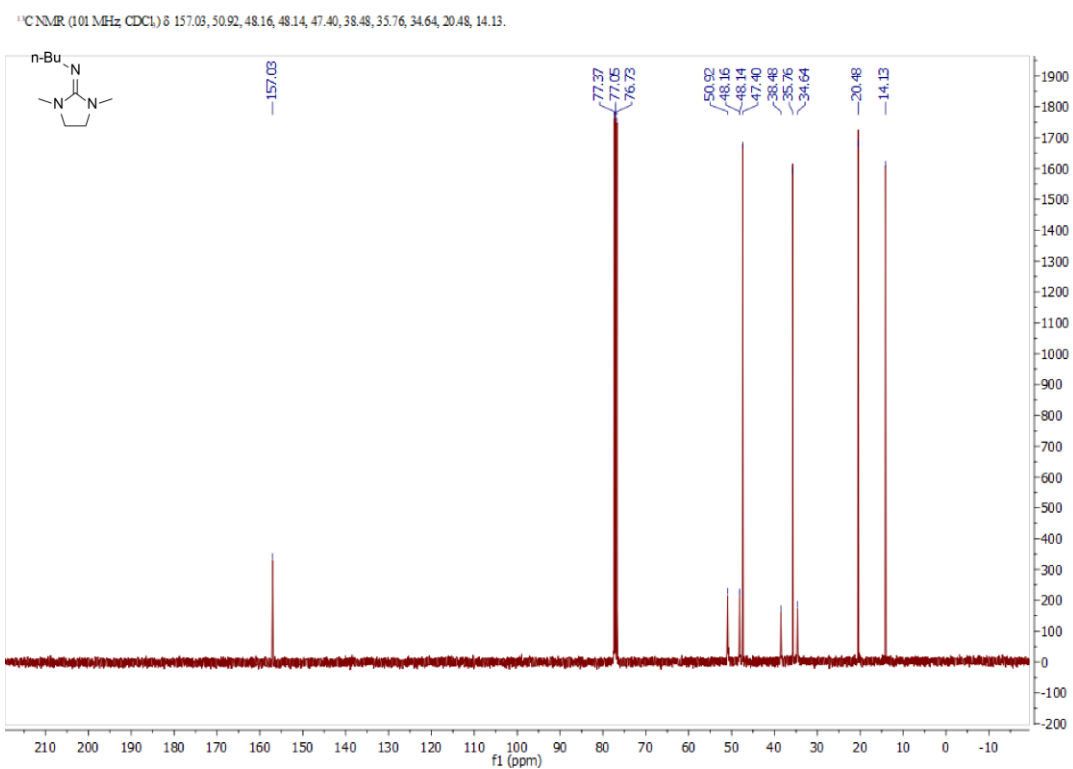
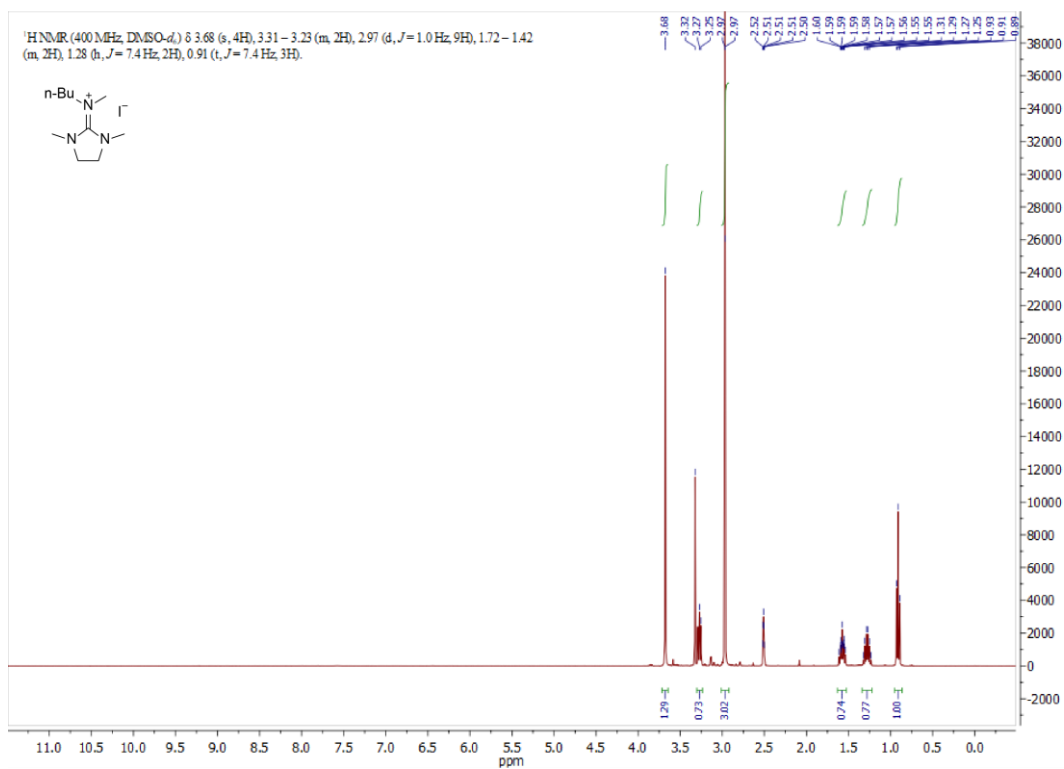
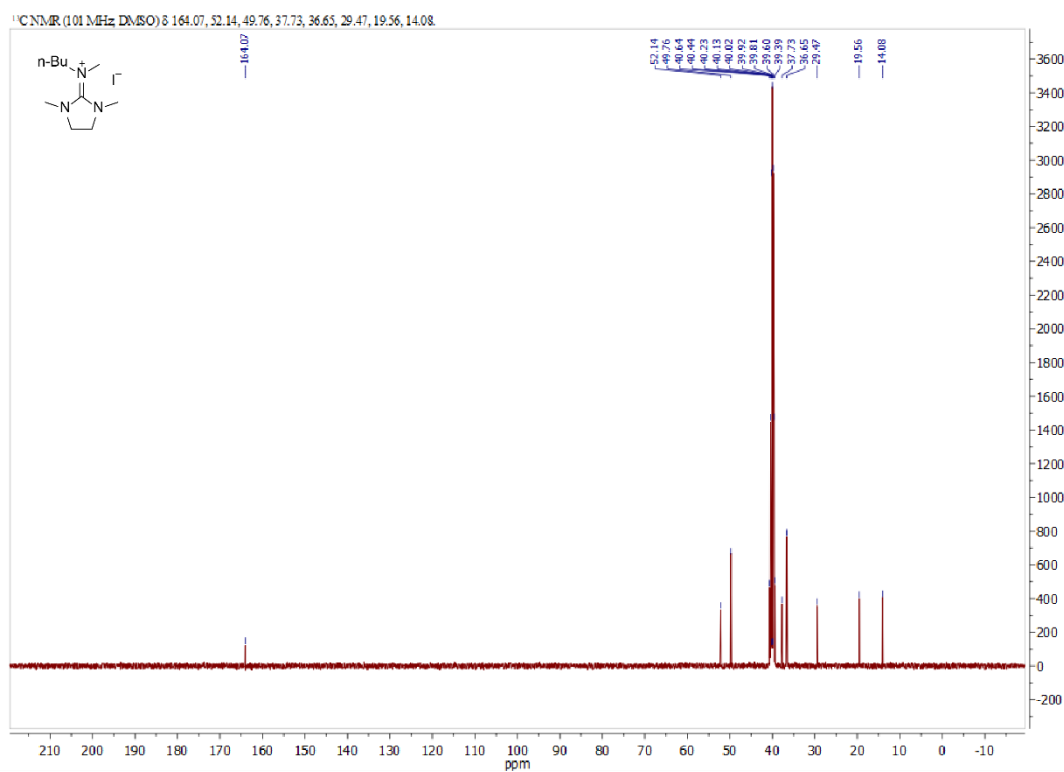


Figure S4.2. ¹³C NMR spectrum of N,N,N',N'-tetramethylchloroformamidinium chloride (101 MHz, DMSO-*d*₆).

Figure S4.3. ¹H NMR spectrum of N-butyl-1,3-dimethylimidazolidin-2-imine (400 MHz, DMSO-*d*₆).Figure S4.4. ¹³C NMR spectrum of N-butyl-1,3-dimethylimidazolidin-2-imine (101 MHz, DMSO-*d*₆).

Figure S4.5. ¹H NMR spectrum of [MB5Gua]I (400 MHz, DMSO-d₆).Figure S 4.6. ¹³C NMR spectrum of [MB5Gua]I (101 MHz, DMSO-d₆).

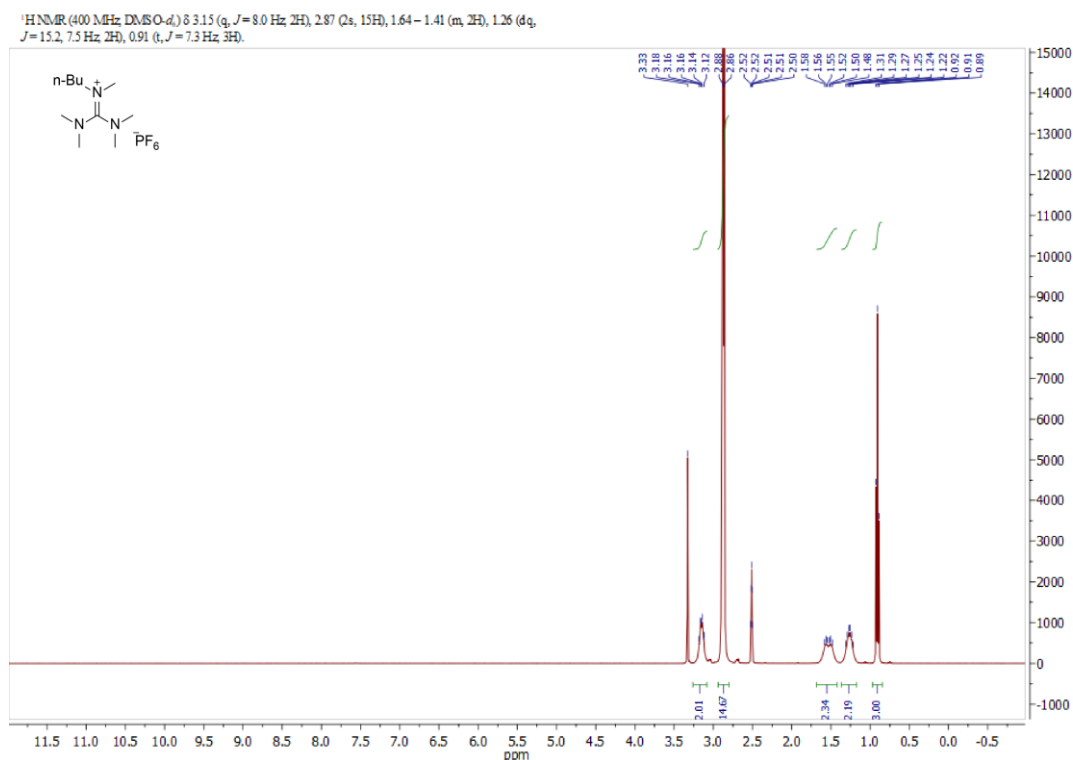


Figure S4.7. ^1H NMR spectrum of [PMBGua] PF_6 (400 MHz, DMSO-d_6).

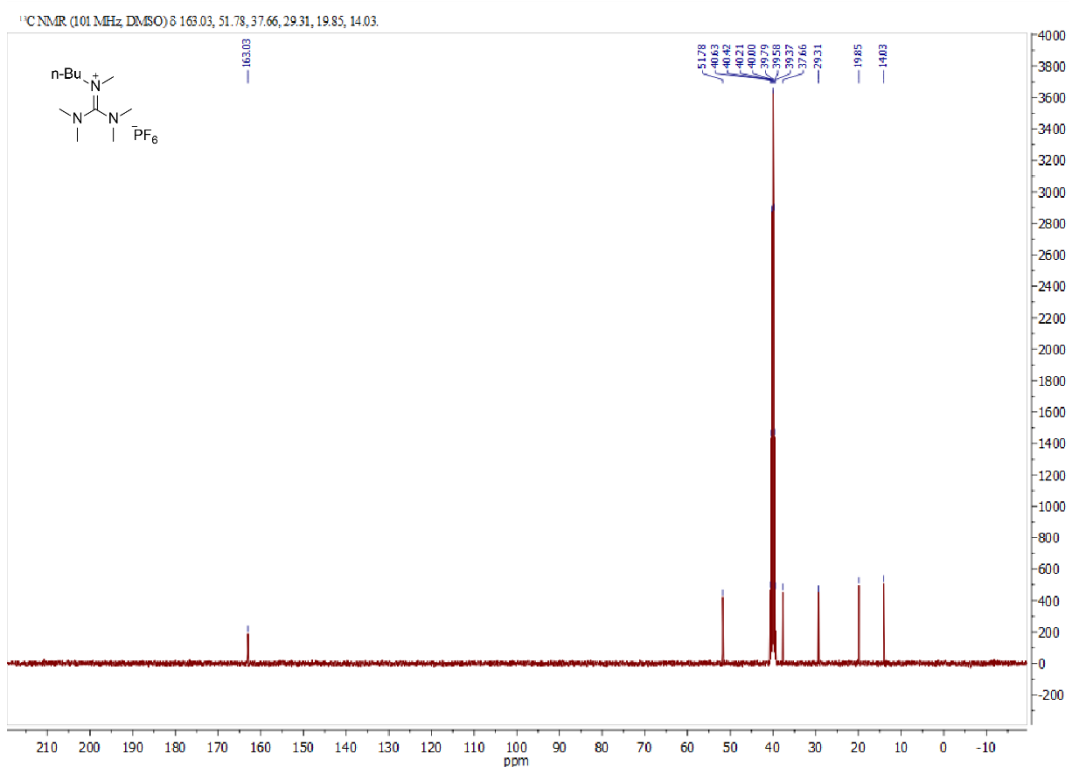
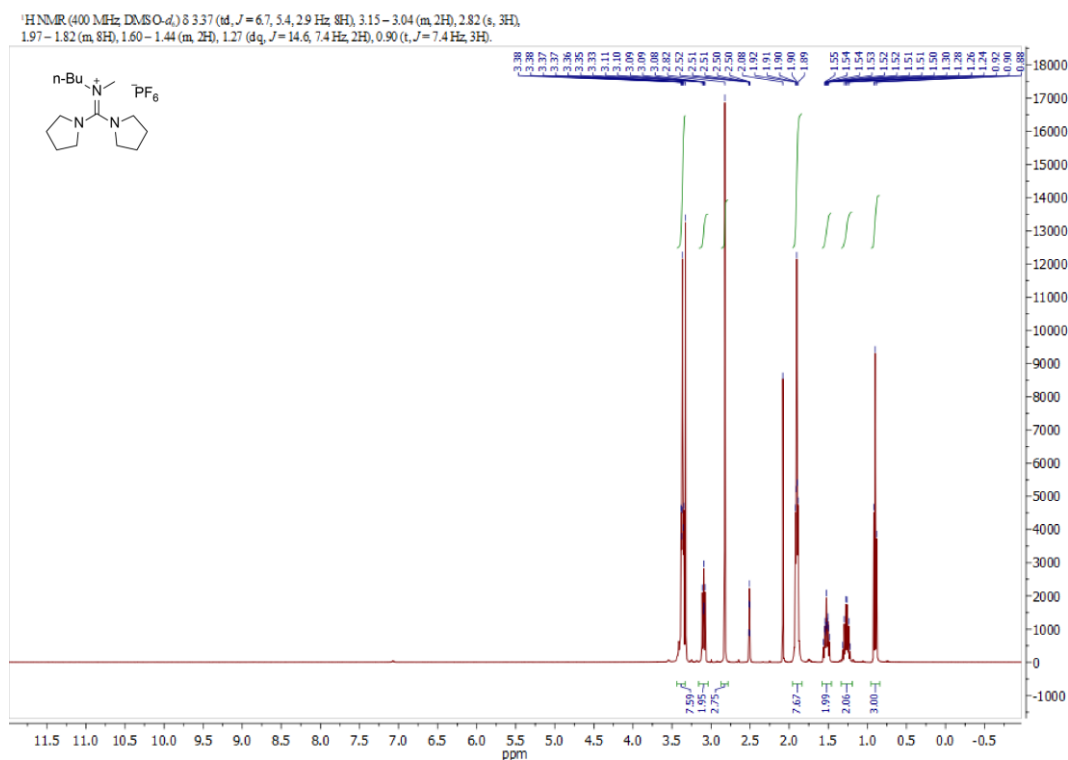
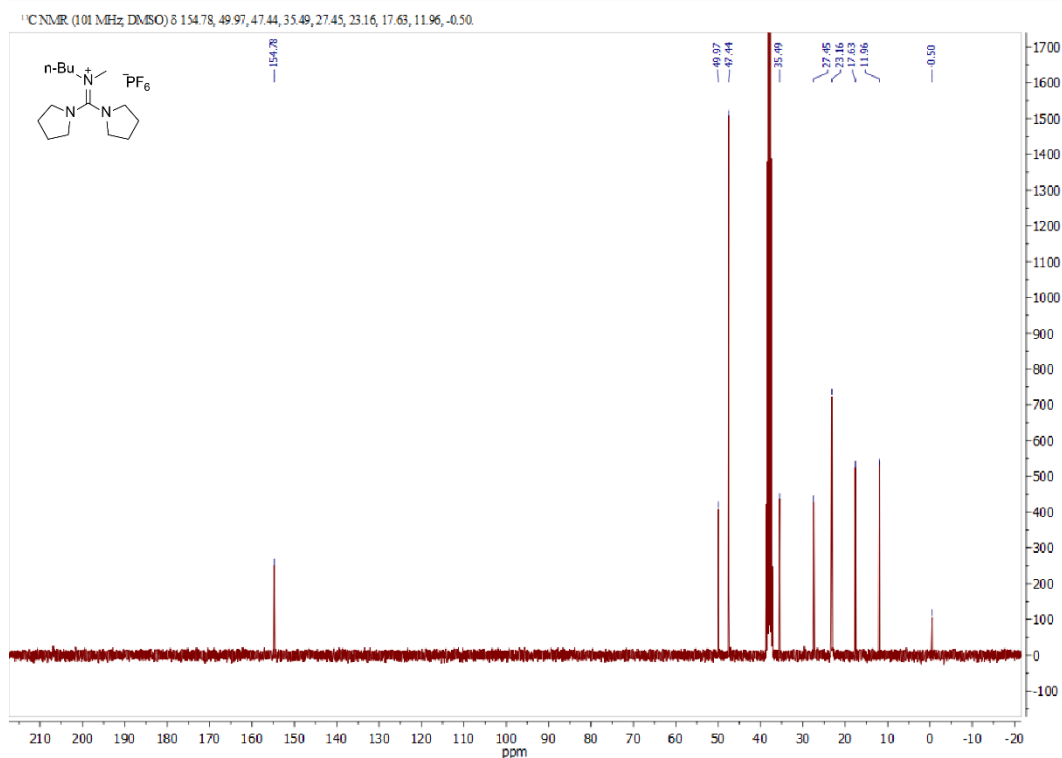
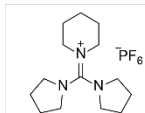
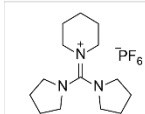
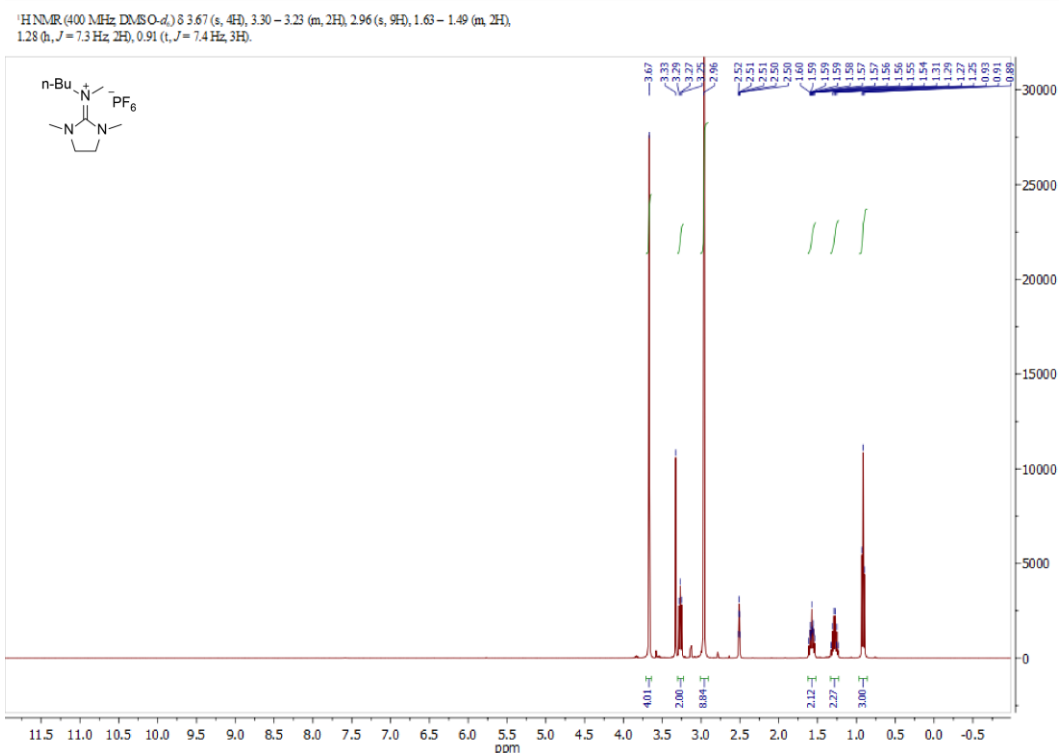
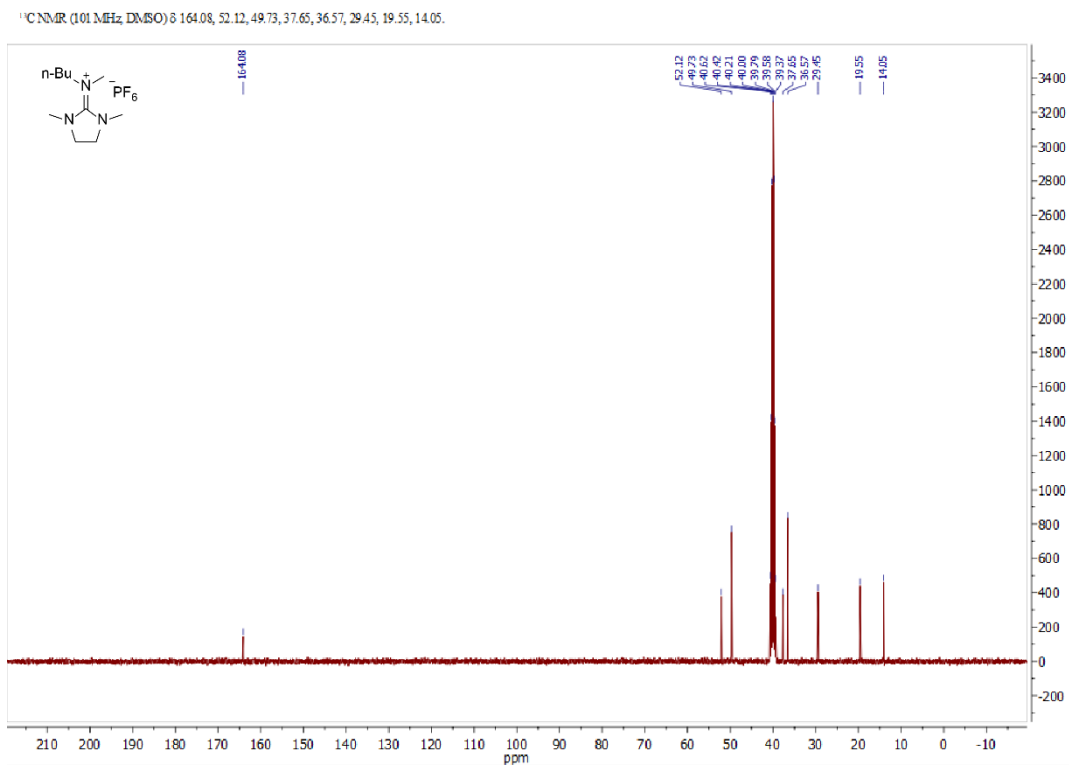
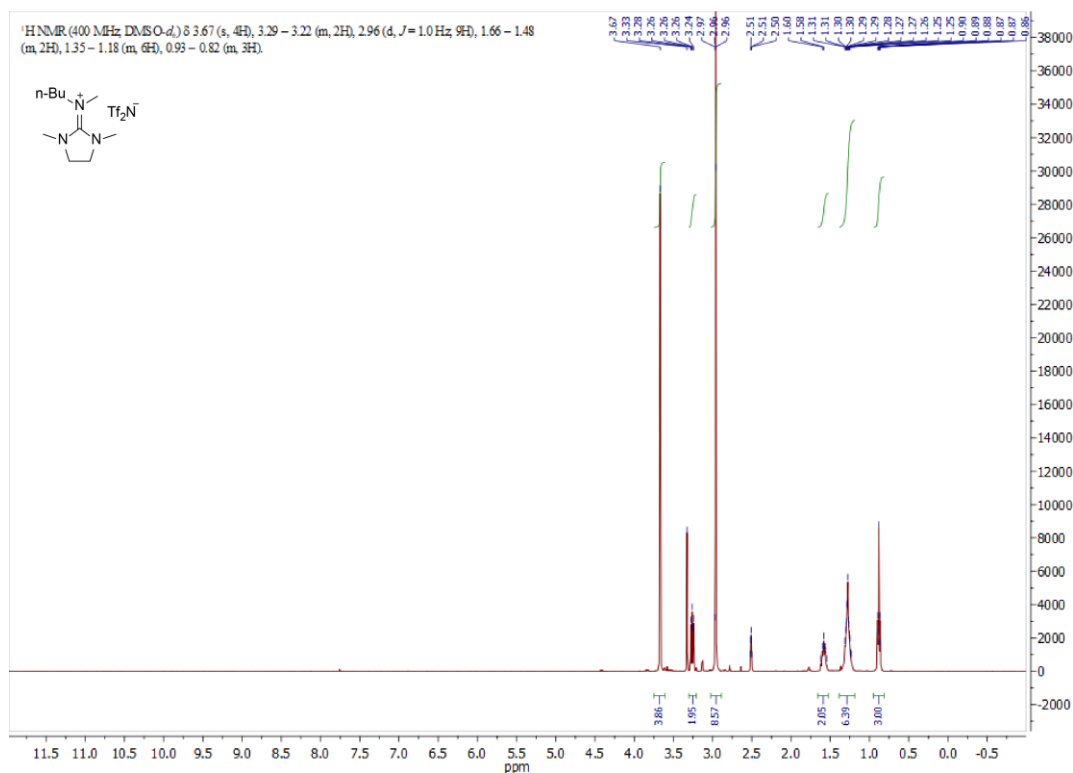
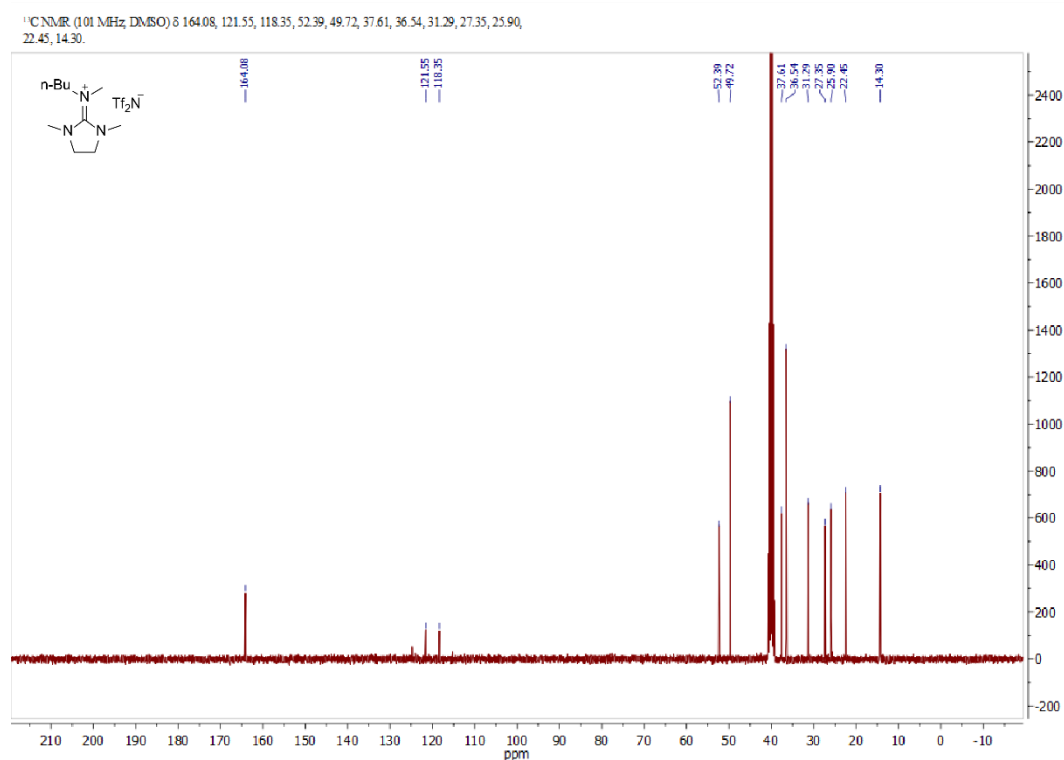


Figure S4.8. ^{13}C NMR spectrum of [PMBGua]PF₆ (101 MHz, DMSO-d₆).

Figure S4.9. ¹H NMR spectrum of [DPyrMBGua]PF₆ (400 MHz, DMSO-d₆).Figure S4.10. ¹³C NMR spectrum of [DPyrMBGua]PF₆ (101 MHz, DMSO-d₆).



Figure S4.13. ¹H NMR spectrum of [MB5Gua]PF₆ (400 MHz, DMSO-d₆).Figure S4.14. ¹³C NMR spectrum of [MB5Gua]PF₆ (101 MHz, DMSO-d₆).

Figure S4.15. ¹H NMR spectrum of [MB5Gua]Tf₂N (400 MHz, DMSO-*d*₆).Figure S4.16. ¹³C NMR spectrum of [MB5Gua]Tf₂N (101 MHz, DMSO-*d*₆).

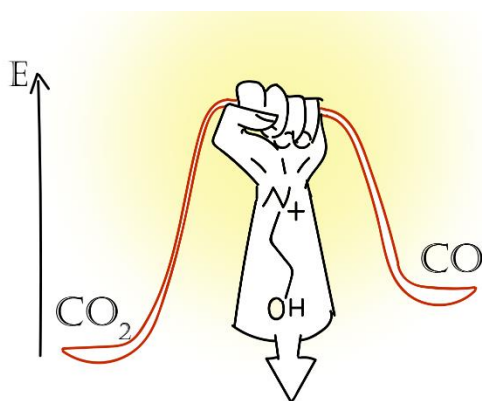
4.2 References

- (1) Mateus, N. M. M.; Branco, L. C.; Lourenço, N. M. T.; Afonso, C. A. M. Synthesis and Properties of Tetra-Alkyl-Dimethylguanidinium Salts as a Potential New Generation of Ionic Liquids. *Green Chem.* **2003**, 5 (3), 347–352.
- (2) Kunkel, H.; Maas, G. Hexaalkylguanidinium Trifluoromethanesulfonates - A General Synthesis from Tetraalkylureas and Triflic Anhydride, and Properties as Ionic Liquids. *European J. Org. Chem.* **2007**, No. 22, 3746–3757.
- (3) Zhang, X.; Liu, X.; Yao, X.; Zhang, S. Microscopic Structure, Interaction, and Properties of a Guanidinium-Based Ionic Liquid and Its Mixture with CO₂. *Ind. Eng. Chem. Res* **2011**, 50, 8323–8332.
- (4) Hess, S.; Arkhipova, M.; Wohlfahrt-Mehrens, M.; Maas, G.; Wachtler, M. Synthesis and Characterization of Guanidinium-Based Ionic Liquids as Possible Electrolytes in Lithium-Ion Batteries. *J. Electrochem. Soc.* **2014**, 161 (5), A753–A761.
- (5) Bucher, N.; Hartung, S.; Arkhipova, M.; Yu, D.; Kratzer, P.; Maas, G.; Srinivasan, M.; Hoster, H. E. A Novel Ionic Liquid for Li Ion Batteries – Uniting the Advantages of Guanidinium and Piperidinium Cations. *RSC Adv.* **2014**, 4 (4), 1996–2003.
- (6) Wang, P.; Zakeeruddin, S. M.; Gratzel, M.; Kantlehner, W.; Mezger, J.; Stoyanov, E. V.; Scherr, O. Novel Room Temperature Ionic Liquids of Hexaalkyl Substituted Guanidinium Salts for Dye-Sensitized Solar Cells. *Appl. Phys. A Mater. Sci. Process.* **2004**, 79 (1), 73–77.
- (7) Xin, X.; Guo, X.; Duan, H.; Lin, Y.; Sun, H. Efficient Knoevenagel Condensation Catalyzed by Cyclic Guanidinium Lactate Ionic Liquid as Medium. *Catal. Commun.* **2007**, 8 (2), 115–117.
- (8) Li, S.; Lin, Y.; Xie, H.; Zhang, S.; Xu, J. Brønsted Guanidine Acid–Base Ionic Liquids: Novel Reaction Media for the Palladium-Catalyzed Heck Reaction. *Org. Lett.* **2006**, 8, 391–394.
- (9) Lau, G. P. S.; Schreier, M. R.; Vasilyev, D.; Scopelliti, R.; Grätzel, M.; Dyson, P. J. New Insights Into the Role of Imidazolium-Based Promoters for the Electroreduction of CO₂ on a Silver Electrode. *J. Am. Chem. Soc.* **2016**, 138, 7820–7823.
- (10) Zhao, S.-F.; Horne, M.; Bond, A. M.; Zhang, J. Is the Imidazolium Cation a Unique Promoter

for Electrocatalytic Reduction of Carbon Dioxide? *J. Phys. Chem. C* **2016**, *120*, 23989–24001.

Chapter 5 Deep Eutectic Solvents

5.1 Introduction



Altering the composition of the electrolyte is one of the main approaches aimed at decreasing the overpotential and increasing the selectivity of the CO₂RR reaction.^{1–3} The most investigated solvents for the CO₂RR are water,⁴ acetonitrile,⁵ dimethylsulfoxide,⁶ dimethyl formamide,⁷ and propylene carbonate.⁸ Aqueous electrolytes, probably the most investigated and environmen-

tally benign, allow the synthesis of hydrogenated products, such as formic acid, methanol, methane, etc. However, disadvantages of aqueous systems include the low solubility of CO₂⁹ and, in many cases, the necessity to suppress the parasitic hydrogen evolution reaction (HER).⁹ Non-aqueous systems may dissolve higher concentrations of CO₂ and the HER does not take place due to absence of accessible protons in the system. Furthermore, reduction of CO₂ to CO, inherent for non-aqueous systems, appears to be one of the most attractive types of CO₂RR.¹⁰

The addition of ionic liquids (ILs) to electrolytes significantly decreases the onset potential for the CO₂RR and helps to suppress HER.¹¹ ILs based on Im,^{11,12} Pyrd¹³ and Pz¹⁴ cations were found to be efficient co-catalysts. However, the high cost of ILs and their high viscosities hamper their direct application in the CO₂RR.

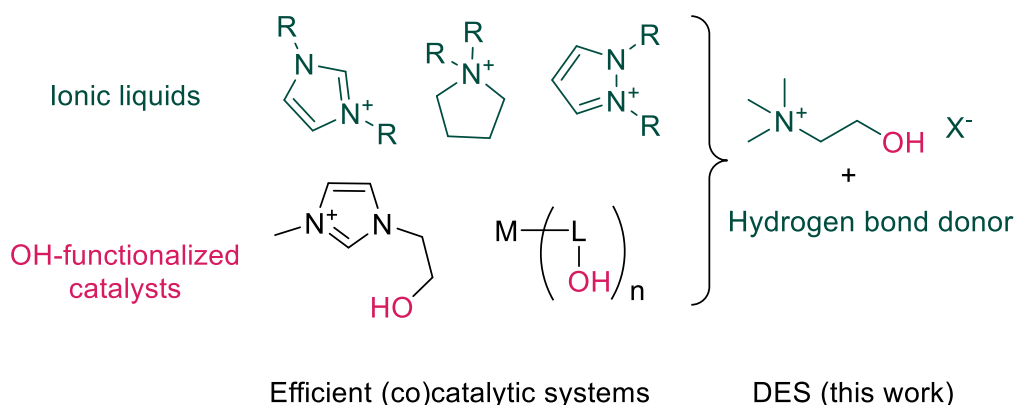


Figure 5.1 Left: Ionic liquids (green) and OH-functionalized compounds (magenta) that promote the CO₂RR.
Right: choline DES.

The presence of the hydroxyl group in the structure of the IL cation^{3,15,16} or in close proximity to a catalytic metal center in an appropriate complex¹⁷ further enhances the CO₂RR. A positive influence was also observed for the hydrolysis of cations in the proximity of the electrode¹⁸ or for the presence of water in the electrolyte.^{13,19} Consequently, choline chloride ([Ch]Cl), a hydroxyl-bearing ammonium salt, was investigated as an additive in an aqueous electrolyte for the CO₂RR on a Pt electrode.¹⁶ Notably, [Ch]Cl is one of the components of deep eutectic solvents (DESs).²⁰ DESs are usually binary mixtures possessing melting points substantially below that of the individual compounds.²¹ Many of the properties of DESs (e.g. large potential windows, high solubility of CO₂, low vapor pressure, high conductivity) are similar to those of ILs, and DESs were investigated in similar applications including CO₂ capture, metal deposition, electropolishing, etc.^{20,22} Simple DESs are much less expensive than simple ILs and, since [Ch]Cl is derived from choline, a nutrient, are in general less toxic.²³ Surprisingly, despite DES appear to be promising alternatives to ILs, their application in the CO₂RR has not been systematically explored (the only example we found in the literature is the work of Verma et al.,³ where DES solution in water was screened among other electrolytes). Here, we demonstrate the utility of pure DESs and DES-additives to non-aqueous solvents in the CO₂RR (Figure 5.1) and describe a simple and general approach combining IL chlorides with EG to generate DESs for application in the CO₂RR.

5.2 Results

Silver was selected as the working electrode in these studies as it is known to catalyze the reduction of CO₂ to CO with high Faradaic efficiencies and low overpotentials,²⁴ which eliminates alternative reaction pathways. Initially, the performance of the neat [Ch]Cl-urea (1:2) system, one

of the most widely investigated DESs, was probed by cyclic voltammetry (CV). Addition of CO_2 to the electrolytic system results in the appearance of a reduction wave in the low potential region, where decomposition of the [Ch]Cl-urea DES is not observed (Figure S5.1). It should be noted that the CO_2RR occurs at the silver cathode, which is the catalyst, and the DES serves as a promoter (or co-catalyst) and medium for the reduction. The CO_2RR does not take place when a glassy carbon working electrode is employed in place of the silver electrode (Figure S5.2).

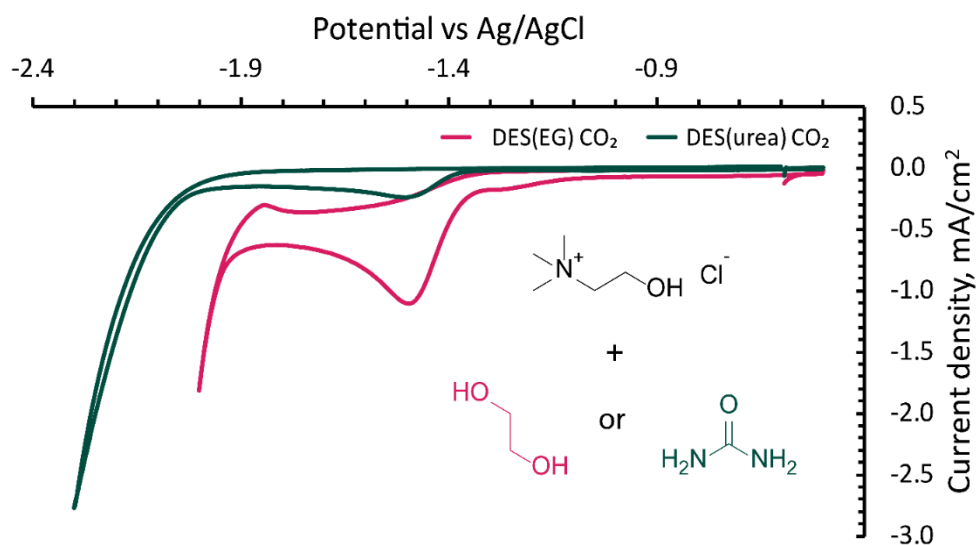


Figure 5.2. Cyclic voltammograms (CVs) of the urea and EG-based DESs employed for the ERC: Ag working electrode, CO_2 atmosphere, undivided cell.

Despite the promising data obtained from the CV experiments, chronoamperometric measurements with online product analysis indicate low applicability of the neat [Ch]Cl-urea DES as an electrolyte for the CO_2RR . The current densities are less than 0.1 mA/cm^2 and the Faradaic efficiency for CO_2 to CO conversion is rather low (Table 5.1). These results are attributed to the high viscosity of the [Ch]Cl-urea DES (Table S5.1, 830 cP at 25°C^{25}), which leads to the rapid depletion of CO_2 at the surface of the electrode and the development of the competing HER and other side reaction (e.g. electrolyte reduction).

Water (1 to 15 % vol) was added to reduce the viscosity of the [Ch]Cl-urea DES (viscosity drops from 1244 cP to $\sim 30 \text{ cP}$ at 15% of water at 21°C^{25}). Current densities of the order of 0.6 mA/cm^2 and Faradaic efficiencies for CO (FE_{CO}) of *ca.* 70% were obtained (Table 5.1, Figure S5.1). Since addition of water increases the FE_{CO} it is apparent that the high viscosity is the main obstacle in the CO_2RR when using the neat [Ch]Cl-urea DES. Therefore, we switched to [Ch]Cl-ethylene glycol (EG) DES

(1:2), as it has the lowest viscosity (36 cP²², 40 cP according to our data, Table S5.1) of the widespread room temperature DESs. As expected, the [Ch]Cl-EG DES exhibited better performance compared to urea-based DES with respect to both CV and chronoamperometric experiments. Under N₂, a steep reduction wave for H₂ evolution arises on the I-V curve (Figure S5.3). However, introduction of CO₂ in the cell results in the appearance of a new reduction wave at low potentials. According to the chronoamperometric measurements followed by GC analysis, the new wave appears due to the CO₂RR. During electrolysis a current density of magnitude *ca.* 0.4 mA/cm² was reached with FE_{CO} remaining around 78% (Table 5.1). Addition of water (7 % by vol.) leads to an increase of current density, but with a decrease in the selectivity, i.e. FE_{CO} = 40%. From the abovementioned results, it appears that the application of pure DESs in the CO₂RR is possible, but is challenging due to slow mass transport. Possible solutions to overcome the problem of slow diffusion of CO₂ is to use gas diffusion electrodes or to vary the cell configuration (e.g. the distance between electrodes, electrode surface, etc.). An alternative approach is to employ the DES as an additive in a low viscous solvent. The choice of the diluted solvent should be defined by miscibility with the DES, high solubility of CO₂ and, ideally, low volatility, low toxicity and low price.

As mentioned above, the application of [Ch]Cl additives in an aqueous electrolyte was demonstrated before.^[9,19] However, employing 1M [Ch]Cl in water as the electrolyte was rather discouraging, i.e. hydrogen was the main product of the reduction with only traces of CO formed (Table 1). Addition of EG (2 eq. vs [Ch]Cl) improves the FE_{CO} to the level of only *ca.* 23% (Table 5.1, Figure 5.3a). Possibly, the difference in pH between our system and the one explored by Verma et al. (we used 0.5 M H₂SO₄, and they – KHCO₃ solution as anolyte)³ leads to the different outcomes of the [Ch]Cl-urea DES in water as Nafion, used as separator, is permeable for protons.

Acetonitrile (MeCN) is an aprotic polar solvent widely explored in the CO₂RR; CO₂ is *ca.* 8 times more soluble in it compared to water.⁹ Consequently, the electrochemical behavior of [Ch]Cl (0.02 M) in MeCN solution (containing NBu₄PF₆, 0.1 M) in the presence and absence of CO₂ was studied. Under a nitrogen atmosphere a wave at *ca.* -1.9 V vs Ag/AgCl for the reduction of the [Ch] cation is observed. Addition of CO₂ to the system results in a sharp growth of a new wave on the I-V curve, indicating the development of the CO₂RR (Figure S5.4). The fact that the co-catalytic activity can be attributed to the presence of [Ch]Cl in the system was demonstrated by comparing CV curves registered in the presence and in the absence of [Ch]Cl: the onset potential for the latter was *ca.* 600 mV more negative (Figure S5.5). Potentiostatic electrolysis combined with online GC detection reveal

CO to be the dominant product, with a Faradaic efficiency approaching 100% at *ca.* -2.0 V vs Ag/AgCl (Figure S5.4).

However, [Ch]Cl is poorly soluble in MeCN, with only low concentrations achieved after prolonged sonication. To overcome the solubility limitation, the chloride anion in [Ch]Cl was exchanged with bis(trifluoromethylsulfonyl)imide (Tf_2N^-), to afford IL which is miscible with MeCN. CV and potentiostatic electrolysis reveal the effect of [Ch][Tf_2N] being comparable to that of [Ch]Cl at the same concentration (Figure S5.5).

In an alternative approach, a DES was obtained by mixing [Ch]Cl and EG (1:2) allowing a concentration of [Ch]Cl of 1 M to be achieved in MeCN. According to the CV curves and chronoamperometric data (Figure 5.3b, Table 5.1), the addition of EG to the [Ch]Cl solution resulted in a highly active system with both excellent FE_{CO} (99%) and j_{CO} (*ca.* 7 mA/cm²). Moreover, additives of EG do not significantly change the reduction onset potential (Figure S5.6). In order to distinguish the effect of the [Ch] cation from that of EG, additional experiments excluding [Ch] derivatives from the electrolyte were performed, which indicate that EG does not have a considerable impact on the CO_2RR (Figure S5.7).

In order to broaden the applicability of our strategy for the employment of DESs in organic solvents, propylene carbonate (PC) and 2-(2-ethoxyethoxy)ethanol (3EOH) were also studied. Both are industrially important solvents with high boiling points. [Ch]Cl is insoluble in 3EOH, but with the addition of 2 equivalents of EG a concentration of 1 M [Ch]Cl was reached. The resulting solution was examined in the CO_2RR with current densities being 2-3 times higher than those achieved in neat DES (Figure 5.3c). Moreover, FE_{CO} values exceeding 90% (Table 1) with current densities around 4 mA/cm² (Table S5.1) were obtained.

[Ch]Cl is poorly soluble in PC as well, whereas a combination of [Ch]Cl and EG (1:2) readily provided 1 M solutions. Reduction of CO_2 in this media proceeds with around 100% FE_{CO} (Figure 5.3d, Table 5.1) at relatively high (*ca.* 8 mA/cm², Table S5.1) current densities. Interestingly, water, which is a by-product during the CO_2RR ($\text{CO}_2 + 2\text{H}^+ \rightarrow \text{CO} + \text{H}_2\text{O}$), forms a second phase above the electrolyte.

Table 5.1. Reduction onset potentials for the CO₂RR and product distribution at optimal potentials for chronoamperometric experiments employing DESs or DES-like systems (neat or as an additive in various solvents).^[a]

Catholyte	FE _{CO} , % ^[b]	FE _{H₂} , % ^[c] b]	E _{Ag/AgCl} , V
[Ch]Cl-Urea (1:2)	15.8	17.0	-1.40
[Ch]Cl-Urea (1:2) + H ₂ O (15% vol)	59.0	26.3	-1.38
[Ch]Cl-EG (1:2)	78.0	9.9	-1.43
[BMIm]Cl-EG (1:2)	95.8	6.8	-1.44
1M [Ch]Cl + 2M EG in H ₂ O	23.3	75.6	N/A ^[c]
1M [Ch]Cl + 2M EG in MeCN	98.8	4.7	-1.52
1M [Ch]Cl + 2M EG in 3EOH	92.3	8.4	-1.4
1M [Ch]Cl + 2M EG in PC	101.5	0.5	-1.5
1M [Ch]Cl in EG	71.1	28.2	-1.42
1M [Ch]Cl in PEG-200	83.2	7.9	-1.40
1M [BMIm]Cl in PEG-200	85.9	3.7	-1.41
1M [EMImOH]Cl + 2M EG in PC	101.8	1.6	-1.45

[a] Experimental conditions: U-type divided cell, Ag polished disc cathode, Pt wire anode, Ag/AgCl reference, anolyte – H₂SO₄ (aq, 0.5 M), catholyte – given in the Table, Nafion 117 membrane separator. [b] Estimated error is ±5%. [c] Cannot be determined due to concomitant HER.

In an extension to the use of EG as HBD, polyethylene glycol (PEG), a cheap and stable non-toxic class of polymers, was also evaluated. [Ch]Cl dissolves in PEG-200, and 1M [Ch]Cl in PEG-200 represents a stable system with low onset potential of the CO₂RR and good FE_{CO} (Table 5.1, Figure S5.8).

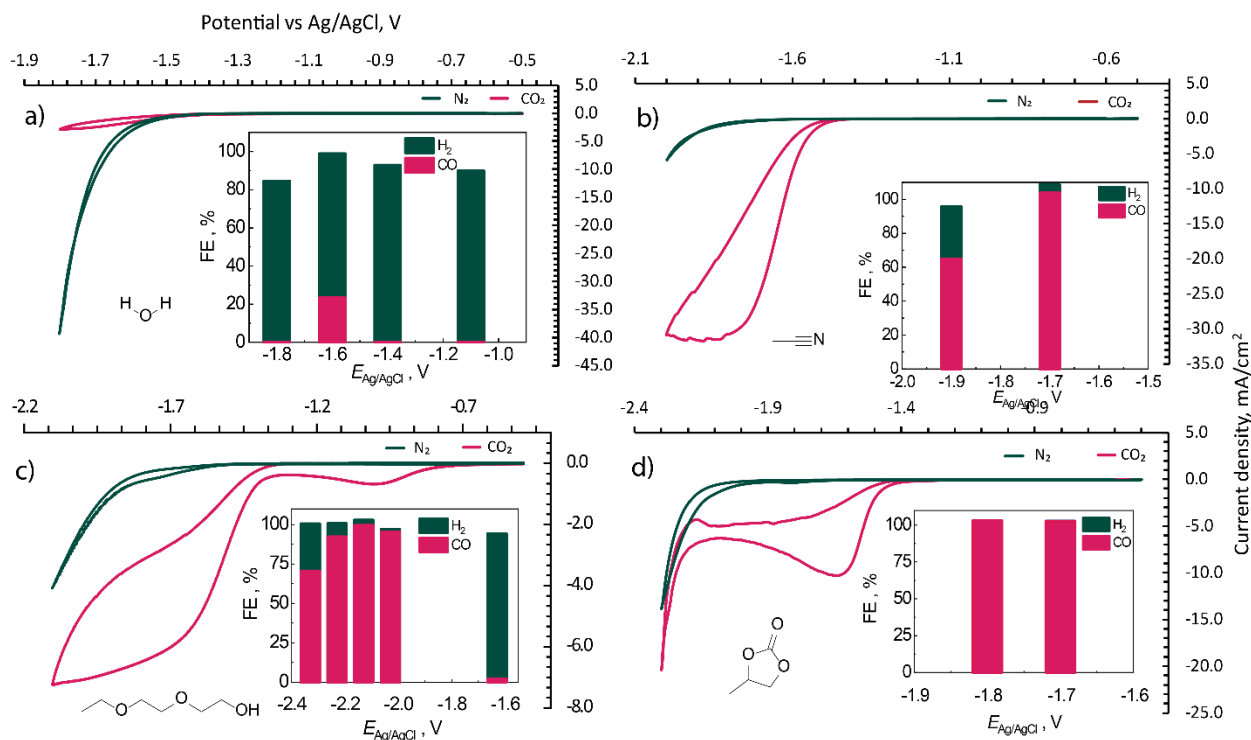


Figure 5.3. Cyclic voltammograms of [Ch]Cl/EG (1/2) DES solutions in a) water; b) MeCN; c) 3EOH; d) PC under N₂ (green) and under CO₂ (magenta). Insets: FEs obtained during potentiostatic electrolysis in presence of CO₂. All curves were recorded using Ag electrodes. Estimated error for the determination of the FE is $\pm 5\%$.

The idea to employ the concept of DES in order to solubilize [Ch]Cl in organic media can be expanded to other IL co-catalysts. [BMIm]Cl ([BMIm] = the 1-butyl-3-methylimidazolium cation), a “classical” co-catalyst for CO₂RR, is a crystalline low-melting solid compound (mp = 65°C).²⁶ When mixed with EG (1:2 respectively), it forms a liquid with viscosity similar to that for [Ch]Cl-EG DES (36.9 cP and 40.1 cP respectively at 21°C, Table S5.1). The resulting solution was used for the CO₂RR, exhibiting a similar performance to the pure IL [BMIm][BF₄] (Tables 5.1, S5.1, Figure S5.9).²⁷

The hydroxyl-functionalized IL, 1-(3-hydroxypropyl)-3-methylimidazolium tetrafluoroborate [PMImOH][BF₄], was found to be a promising promoter for CO₂RR.¹⁵ Inspired by this work, we decided to broaden our IL scope by 1-(2-hydroxyethyl)-3-methylimidazolium chloride. Although the direct use of this salt is limited by its low solubility in organic solvents and by the fact that it is not a room-temperature IL, the addition of 2 equivalents of EG affords a homogeneous system which dissolves well in solvents like MeCN and PC (Figure 5.4). The resulting electrolytes (1 M) showed excellent activity for the CO₂RR in terms of FE_{CO} (both up to ~100%) and onset potentials (both *ca.* -1.45 vs Ag/AgCl) for the reduction (Tables 5.1, S5.1, Figures S5.10, S5.11).



Figure 5.4. Mixtures of MeCN with a) [EMImOH]Cl (1M, left); b) [EMImOH]Cl + EG (1M and 2M respectively, right).

From the viscosities of the investigated electrolytes there is an inverse correlation with the current densities, which is as expected as the higher the viscosity the slower the diffusion of CO_2 (Table S5.1). Consequently, since the potentials for the CO_2RR are similar for all systems, mass transport limitations appear to be the main factor leading to the differences in the current densities.

5.3 Summary

In conclusion, we show that [Ch]-based DESs facilitate the CO_2RR , exhibiting similar characteristics to IL-based systems. However, unlike ILs they are abundant, non-toxic, inexpensive and facile to prepare and handle. Like ILs, DESs have high viscosities and therefore must be applied in organic solvents, providing excellent co-catalytic systems. Following the same strategy of combining chlorides with EG, liquid electrolytes based on non-room temperature ILs can be prepared. Such systems exhibit improved solubility of the catalyst in organic solvents avoiding the additional synthetic step of anion exchange, which increases the purity and reduces the cost of the co-catalyst. We believe that this approach can be expanded to other [organic cation]Cl salts, which would vastly increase the number of co-catalysts/electrolytes that can be employed for the CO_2RR , and might lead to the discovery of even more efficient systems for this and other important reactions.

5.4 Experimental

5.4.1 Materials and methods

All the reagents except 1-(2-hydroxyethyl)-3-methylimidazolium chloride were purchased from commercial sources and used without further purification. The following reagents were employed: acetonitrile ($\geq 99.9\%$, HPLC gradient grade, Fisher Chemical), 1-butyl-3-methylimidazolium chloride (98.0%, Sigma), choline chloride (98+%, AlfaAesar), 2-(2-ethoxyethoxy)ethanol (98+%, Acros Organics), ethylene glycol (99.5%, for analysis, Acros Organics), polyethylene glycol (BioUltra, 200, Sigma), propylene carbonate (99.7%, anhydrous, Sigma), urea (molecular biology grade, Lubio Science). 1-(2-hydroxyethyl)-3-methylimidazolium chloride was synthesized according to a published protocol.²⁸ CO₂ (99.998 %) and Ar (99.9999 %) were obtained from Carbagas, Switzerland. Electrochemical measurements were made in according with the protocols from Chapter 2.

5.4.2 Viscosities of electrolytes and the current densities for the electrolysis

Table S1. Current densities for electrolysis at optimal potentials and viscosities of DESs and DES-like systems.

Catholyte	j_{co} , mA/cm ²	η_l , mPa s ^[a]
[Ch]Cl-Urea (1:2)	-0.01	1244 ^[b]
[Ch]Cl-Urea (1:2) + H ₂ O (15% vol)	-0.35	30 ^[b]
[Ch]Cl-EG (1:2)	-0.41	40.1
[BMIm]Cl-EG (1:2)	-0.88	36.9
1M [Ch]Cl + 2M EG in H ₂ O	-2.34	1.5
1M [Ch]Cl + 2M EG in MeCN	-6.94	0.8
1M [Ch]Cl + 2M EG in 3EOH	-4.24	9.3
1M [Ch]Cl + 2M EG in PC	-7.68	5.0
1M [Ch]Cl in EG	-0.94	19.3
1M [Ch]Cl in PEG-200	-0.76	87.8
1M [BMIm]Cl in PEG-200	-0.64	77.9
1M [EMImOH]Cl + 2M EG in PC	-4.68	5.2

[a] Viscosities were measured at 21°C.

[b] Data points from Yadav A. and Pandey S, measured at 21°C.²⁵

5.4.3 Cyclic voltammetry data

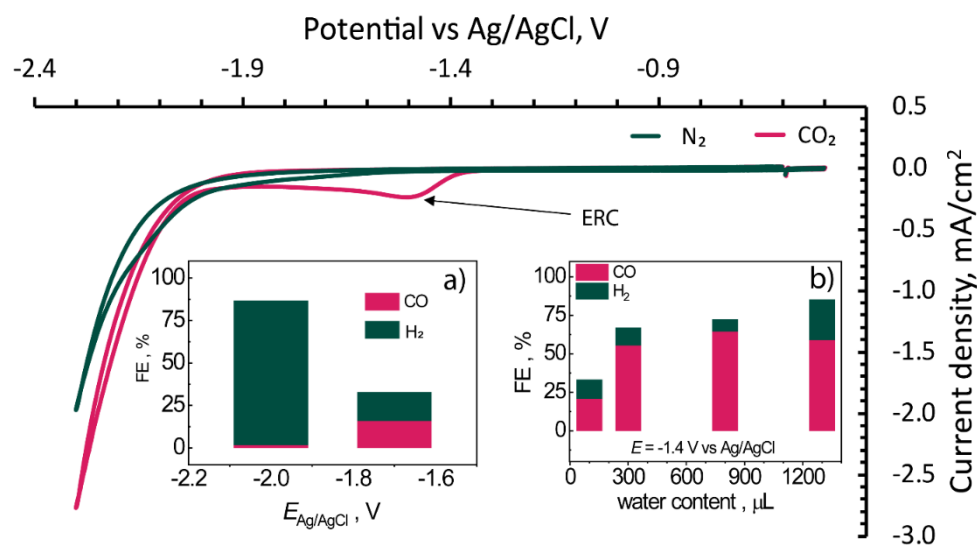


Figure S5.1. Cyclic voltammograms for the [Ch]Cl-urea (1:2) mixture, recorded under N_2 (green) and under CO_2 (magenta). Insets: a) FE_{H_2} and FE_{CO} during electrolysis for this system (Ag electrode, CO_2 atmosphere); b) system evolution with water addition.

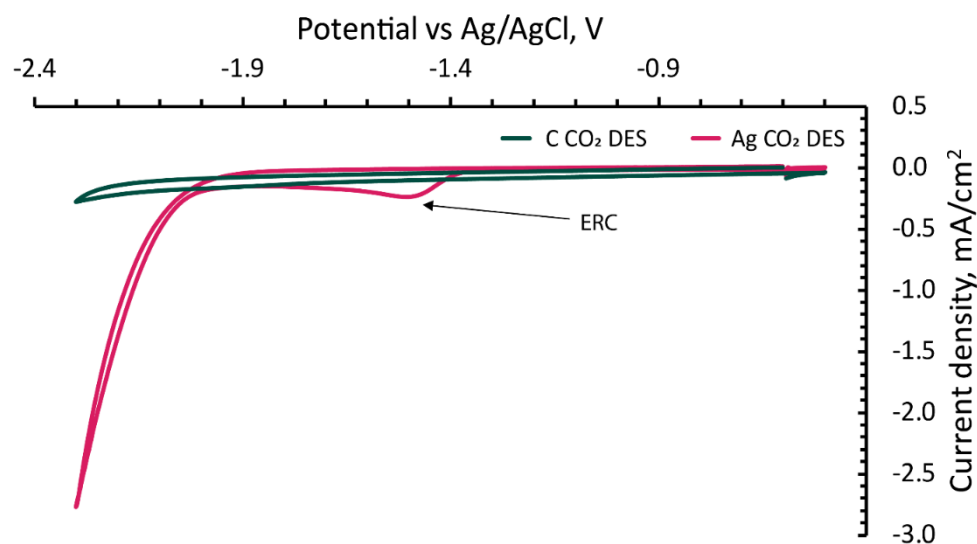


Figure S5.2. Cyclic voltammograms for the [Ch]Cl-urea (1:2) mixture under CO_2 atmosphere, recorded employing glassy carbon (green) and silver (magenta) electrodes.

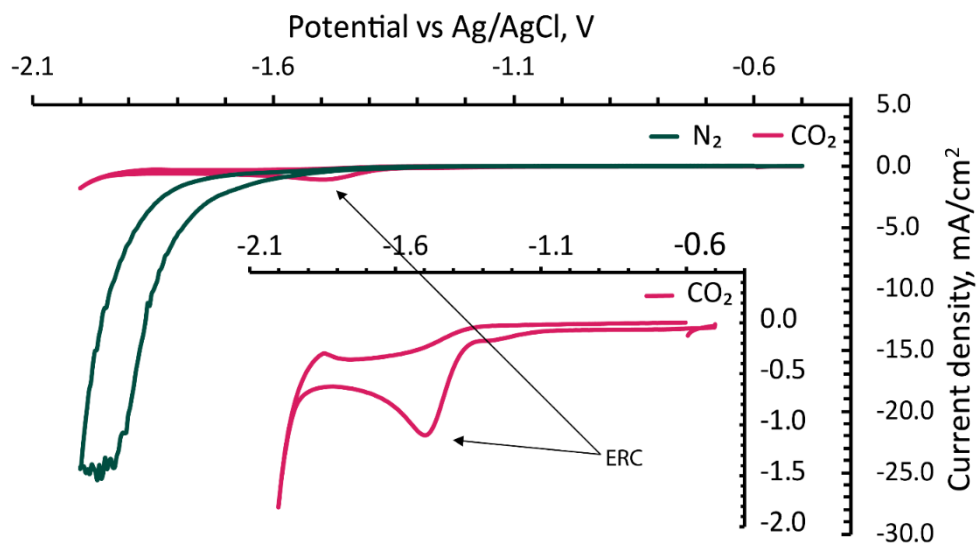


Figure S5.3. Cyclic voltammograms for the [Ch]Cl-EG (1:2) mixture, recorded under N₂ (green) and under CO₂ (magenta). Inset: amplified cyclic voltammogram for the reduction under CO₂.

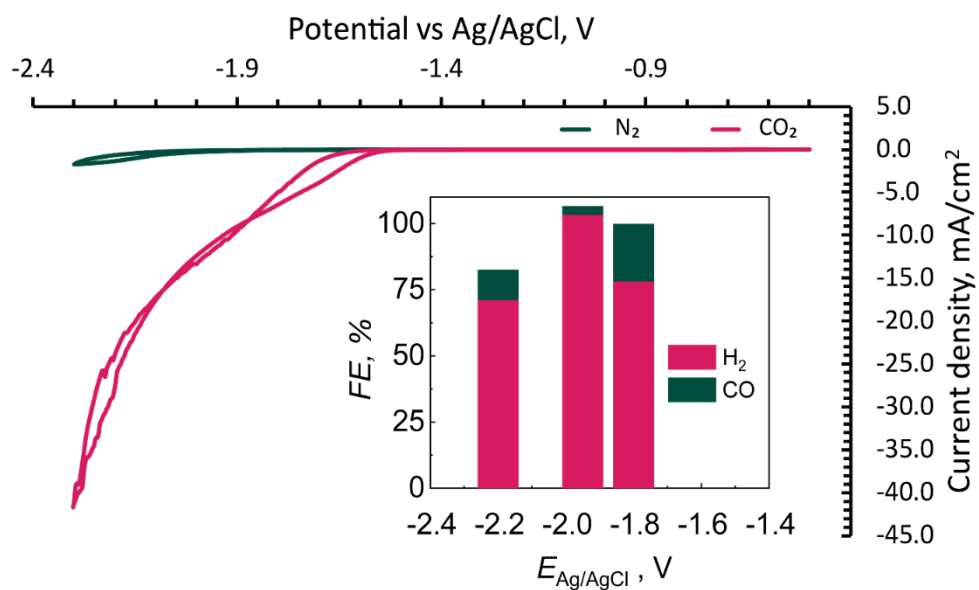


Figure S5.4. Cyclic voltammograms for the system, consisting of [Ch]Cl (0.02 M), NBu₄PF₆ (0.1 M) and MeCN, recorded under N₂ (green) and under CO₂ (magenta). Inset: FE_{H₂} and FE_{CO} during electrolysis for this system (Ag electrode).

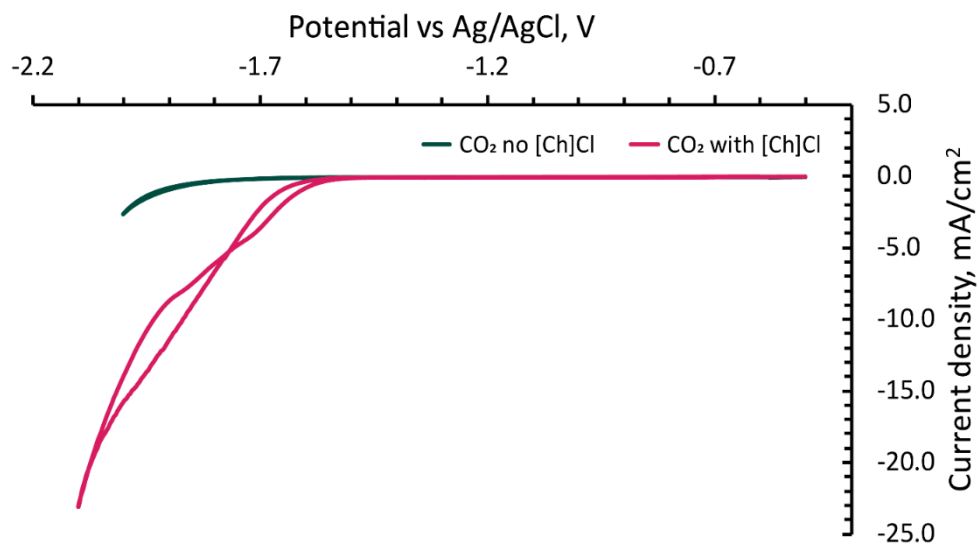


Figure S5.5. Cyclic voltammograms for CO₂-saturated electrolytes (0.1 M NBu₄PF₆ in MeCN) with (magenta) and without (green) [Ch]Cl (0.02 M).

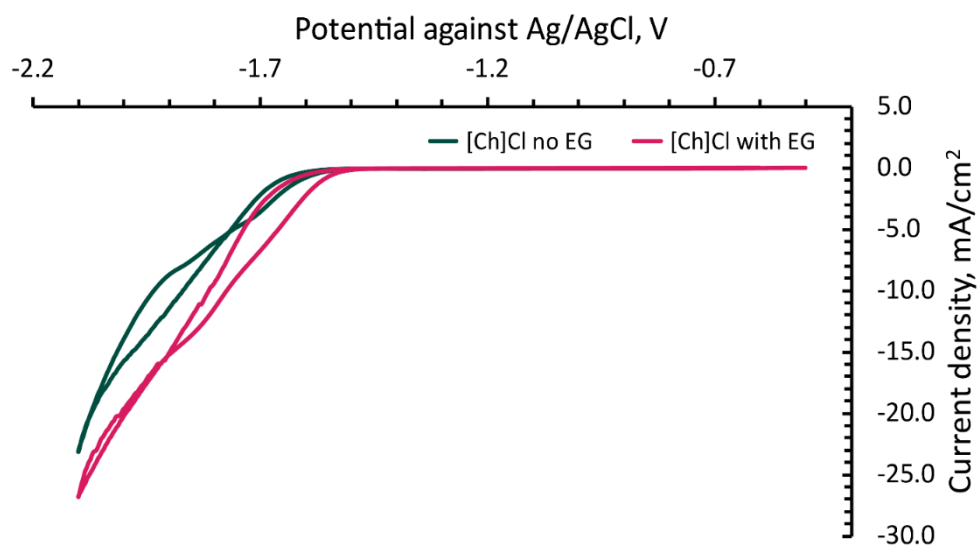


Figure S5.6. Cyclic voltammograms for CO₂-saturated electrolytes (0.02 M [Ch]Cl + 0.1 M NBu₄PF₆ in MeCN) with (magenta) and without (green) EG.

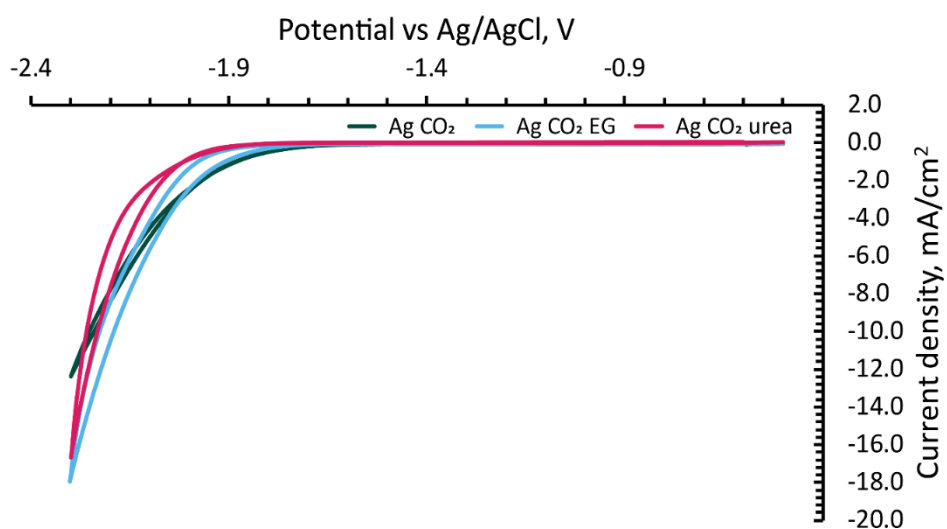


Figure S5.7. Cyclic voltammograms for CO_2 -saturated electrolytes (0.1 M NBu_4PF_6 in MeCN) without any additives (green), with 0.02 M urea (magenta) and with 0.02 M EG (blue).

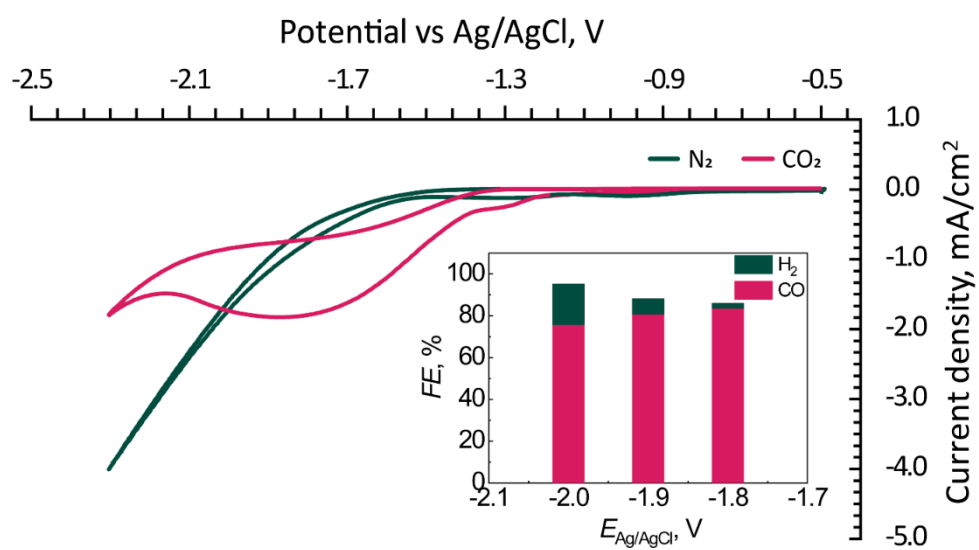


Figure S5.8. Cyclic voltammograms for solution of $[\text{Ch}]\text{Cl}$ (1M) in PEG-200 under N_2 (green) and CO_2 (magenta) atmosphere. Inset: FE_{H_2} and FE_{CO} during electrolysis for this system (Ag electrode).

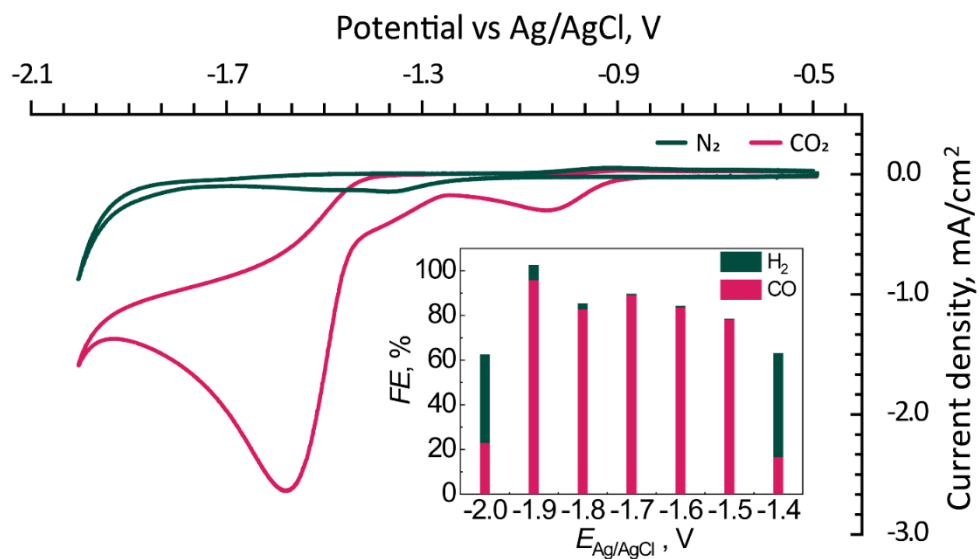


Figure S5.9. Cyclic voltammograms for the mixture of [BMIm]Cl and EG (1:2) under N_2 (green) and CO_2 (magenta) atmosphere. Inset: FE_{H_2} and FE_{CO} during electrolysis for this system (Ag electrode).

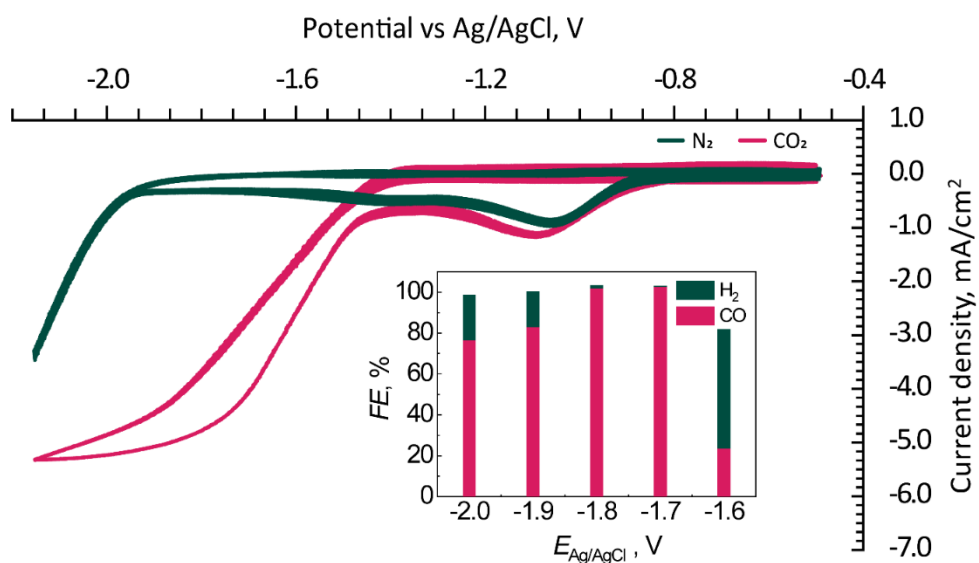


Figure S5.10. Cyclic voltammograms for the solution of [EMImOH]Cl (1 M) and EG (2 M) in propylene carbonate under N_2 (green) and CO_2 (magenta) atmosphere. Inset: FE_{H_2} and FE_{CO} during electrolysis for this system (Ag electrode).

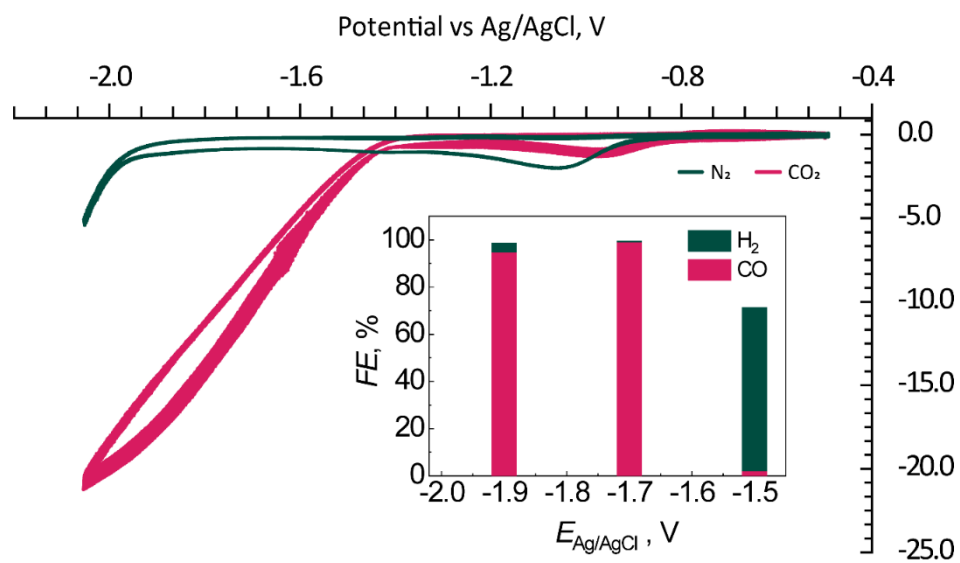


Figure S5.11. Cyclic voltammograms for the solution of [EMImOH]Cl (1 M) and EG (2 M) in MeCN under N₂ (green) and CO₂ (magenta) atmosphere. Inset: FE_{H₂} and FE_{CO} during electrolysis for this system (Ag electrode).

5.1 References

- (1) Thorson, M. R.; Siil, K. I.; Kenis, P. J. a. Effect of Cations on the Electrochemical Conversion of CO₂ to CO. *J. Electrochem. Soc.* **2013**, *160* (1), F69–F74.
- (2) Resasco, J.; Chen, L. D.; Clark, E.; Tsai, C.; Hahn, C.; Jaramillo, T. F.; Chan, K.; Bell, A. T. Promoter Effects of Alkali Metal Cations on the Electrochemical Reduction of Carbon Dioxide. *J. Am. Chem. Soc.* **2017**, *139*, 11277–11287.
- (3) Verma, S.; Lu, X.; Ma, S.; Masel, R. I.; Kenis, P. J. A. The Effect of Electrolyte Composition on the Electroreduction of CO₂ to CO on Ag Based Gas Diffusion Electrodes. *Phys. Chem. Chem. Phys.* **2016**, *18*, 7075–7084.
- (4) Gattrell, M.; Gupta, N.; Co, A. A Review of the Aqueous Electrochemical Reduction of CO₂ to Hydrocarbons at Copper. *J. Electroanal. Chem.* **2006**, *594* (1), 1–19.
- (5) Desilvestro, J.; Pons, S. The Cathodic Reduction of Carbon Dioxide in Acetonitrile: An Electrochemical and Infrared Spectroelectrochemical Study. *J. Electroanal. Chem. Interfacial Electrochem.* **1989**, *267* (1–2), 207–220.
- (6) Haynes, L. V.; Sawyer, D. T. Electrochemistry of Carbon Dioxide in Dimethyl Sulfoxide at Gold and Mercury Electrodes. *Anal. Chem.* **1967**, *39* (3), 332–338.
- (7) Amatore, C.; Savéant, J.-M. Amatore and Savéant 5022. *J. Am. Chem. Soc.* **1981**, *103* (17), 5021–5023.
- (8) Shi, J.; Shen, F.; Shi, F.; Song, N.; Jia, Y.-J.; Hu, Y.-Q.; Li, Q.-Y.; Liu, J.; Chen, T.-Y.; Dai, Y.-N. Electrochemical Reduction of CO₂ into CO in Tetrabutylammonium Perchlorate/Propylene Carbonate: Water Effects and Mechanism. *Electrochim. Acta* **2017**, *240*, 114–121.
- (9) Tomita, Y.; Teruya, S.; Koga, O.; Hori, Y. Electrochemical Reduction of Carbon Dioxide at a Platinum Electrode in Acetonitrile-Water Mixtures. *J. Electrochem. Soc.* **2000**, *147*, 4164–4167.
- (10) Durst, J.; Rudnev, A.; Dutta, A.; Fu, Y.; Herranz, J.; Kaliginedi, V.; Kuzume, A.; Permyakova, A. A.; Paratcha, Y.; Broekmann, P.; et al. Electrochemical CO₂ Reduction – A Critical View on

Fundamentals, Materials and Applications. *Chimia* **2015**, *69*, 769–776.

- (11) Rosen, B. A.; Salehi-Khojin, A.; Thorson, M. R.; Zhu, W.; Whipple, D. T.; Kenis, P. J. A.; Masel, R. I. Ionic Liquid – Mediated Selective Conversion of CO₂ to CO at Low Overpotentials. *Science* **2011**, *334*, 643–644.
- (12) Lau, G. P. S.; Schreier, M.; Vasilyev, D.; Scopelliti, R.; Grätzel, M.; Dyson, P. J. New Insights into the Role of Imidazolium-Based Promoters for the Electroreduction of CO₂ on a Silver Electrode. *J. Am. Chem. Soc.* **2016**, *138*, 7820–7823.
- (13) Zhao, S.-F.; Horne, M.; Bond, A. M.; Zhang, J. Is the Imidazolium Cation a Unique Promoter for Electrocatalytic Reduction of Carbon Dioxide? *J. Phys. Chem. C* **2016**, *120*, 23989–24001.
- (14) Vasilyev, D.; Shirzadi, E.; Rudnev, A. V.; Broekmann, P.; Dyson, P. J. Pyrazolium Ionic Liquid Co-Catalysts for the Electroreduction of CO₂. *ACS Appl. Energy Mater.* **2018**, *1*, 5124–5128.
- (15) Zhang, L.; Wu, N.; Zhang, J.; Hu, Y.; Wang, Z.; Zhuang, L.; Jin, X. Imidazolium Ions with an Alcohol Substituent for Enhanced Electrocatalytic Reduction of CO₂. *ChemSusChem* **2017**, *10* (24), 4824–4828.
- (16) Zhu, W.; Rosen, B. A.; Salehi-Khojin, A.; Masel, R. I. Monolayers of Choline Chloride Can Enhance Desired Electrochemical Reactions and Inhibit Undesirable Ones. *Electrochim. Acta* **2013**, *96*, 18–22.
- (17) Francke, R.; Schille, B.; Roemelt, M. Homogeneously Catalyzed Electroreduction of Carbon Dioxide - Methods, Mechanisms, and Catalysts. *Chem. Rev.* **2018**, *118*, 4631–4701.
- (18) Singh, M. R.; Kwon, Y.; Lum, Y.; Ager, J. W.; Bell, A. T. Hydrolysis of Electrolyte Cations Enhances the Electrochemical Reduction of CO₂ over Ag and Cu. *J. Am. Chem. Soc.* **2016**, *138*, 13006–13012.
- (19) Rudnev, A. V.; Zhumaev, U. E.; Kuzume, A.; Veszteg, S.; Furrer, J.; Broekmann, P.; Wandlowski, T. The Promoting Effect of Water on the Electroreduction of CO₂ in Acetonitrile. *Electrochim. Acta* **2016**, *189*, 38–44.
- (20) Smith, E. L.; Abbott, A. P.; Ryder, K. S. Deep Eutectic Solvents (DESs) and Their Applications. *Chem. Rev.* **2014**, *114* (21), 11060–11082.

- (21) Garcia, G.; Aparicio, S.; Ullah, R.; Atilhan, M. Deep Eutectic Solvents: Physicochemical Properties and Gas Separation Applications. *Energy Fuels* **2015**, *29*, 2616–2644.
- (22) Zhang, Q.; De Oliveira Vigier, K.; Sebastien, R. F.; Jerome, F. Deep Eutectic Solvents : Syntheses, Properties and Applications. *Chem Soc Rev* **2012**, *41*, 7108–7146.
- (23) Kudłak, B.; Owczarek, K.; Namieśnik, J. Selected Issues Related to the Toxicity of Ionic Liquids and Deep Eutectic Solvents-a Review. *Environ. Sci. Pollut. Res.* **2015**, *22*, 11975–11992.
- (24) Hori, Y.; Wakebe, H.; Tsukamoto, T.; Koga, O. Electrocatalytic Process of CO Selectivity in Electrochemical Reduction of CO₂ at Metal Electrodes in Aqueous Media. *Electrochim. Acta* **1994**, *39*, 1833–1839.
- (25) Yadav, A.; Pandey, S. Densities and Viscosities of (Choline Chloride + Urea) Deep Eutectic Solvent and Its Aqueous Mixtures in the Temperature Range 293.15 K to 363.15 K. *J. Chem. Eng. Data* **2014**, *59*, 2221–2229.
- (26) Nishikawa, K.; Wang, S.; Katayanagi, H.; Hayashi, S.; Hamaguchi, H.-O.; Koga, Y.; Tozaki, K.-I. Melting and Freezing Behaviors of Prototype Ionic Liquids, 1-Butyl-3-Methylimidazolium Bromide and Its Chloride, Studied by Using a Nano-Watt Differential Scanning Calorimeter. *J. Phys. Chem. B* **2007**, *111*, 4894–4900.
- (27) Rudnev, A. V.; Fu, Y.-C.; Gjuroski, I.; Stricker, F.; Furrer, J.; Kovács, N.; Vesztergom, S.; Broekmann, P. Transport Matters: Boosting CO₂ Electroreduction in Mixtures of [BMIm][BF₄]/Water by Enhanced Diffusion. *ChemPhysChem* **2017**, *18* (22), 3153–3162.
- (28) Yang, H.; Liu, Y.; Ning, H.; Lei, J.; Hu, G. Synthesis, Structure and Properties of Imidazolium-Based Energetic Ionic Liquids. *RSC Adv.* **2017**, *7* (53), 33231–33240.

Chapter 6 Conclusions

Three new classes of ILs – Tz, Pz and Gua – were assessed as co-catalysts in the CO₂RR in non-aqueous electrolytes. The activity of the Tz ILs was highly dependent on the substitution pattern. While 1,3-alkylated Tz ILs show some co-catalytic activity at low overpotentials, their higher substituted 1,3,4-analogues display no co-catalytic activity (which resembles the behavior of the known Im ILs) and are reduced instead of CO₂. Despite the low substituted Tz ILs having promising onset potentials for the CO₂RR, close to the theoretical limit for non-aqueous systems, their instability makes them less attractive for the application compared to the conventional Im ILs. However, information on the influence of substitution patterns and onset potentials described above is an important contribution to the understanding of structure/activity relationships for CO₂RR catalysts.

The synthesized Pz ILs were shown to be efficient co-catalysts for the CO₂RR, superior to the benchmark Im ILs in terms of FE_{CO} (100% vs. 80-90% at the same potentials). Introduction of substituents in the Pz ring results in an increase of the stability of the co-catalysts along with a decrease in their activities. However, unlike the fully substituted Im and Tz ILs, peralkylated Pz ILs show good activities for the CO₂RR. Notably, the presence of water in the electrolyte significantly decreases the reduction onset potential for most Pz co-catalysts. Another interesting feature of the Pz ILs is the generation of small amounts of formic acid and methane during the electrolysis, which is not typical of polycrystalline Ag electrodes in the presence of Im ILs. The change product selectivity encourages application of the Pz IL with other electrodes and electrolytes.

Gua ILs have also shown co-catalytic activity for the CO₂RR, although lower than that compared to the Im ILs. The peculiarities of the Gua structure allow gradual substitution and introduction of bulky substituents, which makes Gua ILs versatile synthetic tools for the research on the IL structure/activity correlations. Decreasing the availability of the N-atoms of the Gua core suppresses the interactions with the CO₂-based intermediates, resulting in a decrease in the rate of the reduction, whereas introduction of a strain between the nitrogen results in the decrease of the reduction onset potential for the CO₂RR.

Additionally to broadening the scope of room-temperature ILs capable of promoting the CO₂RR, we hypothesize that the main descriptors for the IL catalysts with high activity is the accessibility and

charge of the active cationic center, which appears to be crucial in forming interaction with CO₂. The importance of the accessibility is demonstrated for the Gua ILs, where the reaction rates gradually decrease with the introduction of blocking substituents on the nitrogen atoms. This mechanism also explains why peralkylated Im and Tz ILs have negligible activity compared to their non-substituted analogues. Furthermore, we suspect that the higher activity of cyclic Gua IL compared to the acyclic analogue (see Chapter 4) is due to the strain in the cyclic compound, which widens the C-N-C angle between the methyl group and the Gua core and makes the charged centers more accessible for interactions with CO₂. The influence of the charge can be demonstrated by comparing the activity of Gua with Im or Pz ILs. The former have higher reduction overpotentials as the charge is more delocalized, whereas Tz ILs exhibit even lower overpotentials compared to Im ILs due to the electronegative N2 atom in the structure. Finally, the relative weight of the charge distribution/charge accessibility can be appreciated from a comparison of Im and Pyrd ILs. The former have slightly higher co-catalytic activity than the latter, possessing more distributed charge but higher accessibility of the charged sites. We believe that based on this hypothesis, the rational design of efficient co-catalysts for the CO₂RR should be possible.

We also developed a new type of non-aqueous electrolytes based on DESs for the CO₂RR. The presence of the OH-group in the structure of the cations was found to significantly facilitate the reduction. The resulting systems possess similar properties to ILs, but unlike ILs, they are abundant, non-toxic, inexpensive and facile to prepare and handle. The solubility of conventional DESs in organic solvents allows viscosity issues to be overcome, thus providing excellent co-catalytic systems. We believe that this strategy may allow the anion exchange stage for the synthesis of IL to be avoided, employing DESs based on the IL chlorides. This strategy significantly simplifies preparation of ionic electrolytes, broadening the scope of catalytic media and making a further step towards green and efficient electrolytes.

Curriculum Vitae : Dmitry V. Vasilyev



mitya.vasilyev@gmail.com



22.10.1992



+41 78 901 41 48



Russian



Chemin de la Dôle, 17
1024, Ecublens, Switzerland



0000-0001-
7956-0307



EDUCATION

- 2015 – present** **PhD:** École polytechnique fédérale de Lausanne (EPFL), Institute of Chemical Sciences and Engineering (ISIC). Topic: Development of organic electrolytes promoting electrochemical reduction of carbon dioxide. *Scientific advisor: Prof. P. J. Dyson*
- 2010 – 2015** **Bachelor & master:** Lomonosov Moscow State University, Department of Chemistry (*with honors, GPA = 5.0 / 5.0*).

OTHER RESEARCH EXPERIENCE

- 2013 – 2015** **Master thesis:** A. N. Nesmeyanov Institute of Organoelement Compounds RAS (Russia). Project: Cyclization of 1,11-dien-6-yne by cobalt (I) catalysis (*supervisor: Dr D. S. Perekalin*).
- July-August 2013** **Short term scholar visitor:** University of Missouri – St. Louis (USA). Project: Investigation of the mechanism of the rearrangement of 1-acetoxy- α -saccharides promoted by CAN (*supervisor: Prof. A. V. Demchenko*)

PRACTICAL SKILLS

Research techniques

- Synthesis under inert conditions (Schlenk, glovebox)
- Preparative chromatography (manual/automatic)
- Chronoamperometry
- Chronopotentiometry
- Cyclic voltammetry
- Impedance spectroscopy (basics)
- Analytical and spectroscopic methods (GC; MS; UV-vis; IR; NMR: 1D, COSY, HSQC, HMBC, DOSY)

Computer literacy

- MS Office
- ChemDraw
- MestReNova
- IgorPro
- Visual Basic (Excel VBA)
- Origin
- Adobe Illustrator
- Adobe Photoshop
- Gaussian (basics)
- Mendeley

LANGUAGES

Russian (native); English (fluent); French (upper intermediate)

PUBLICATIONS

- 1) M. Hulla, D. Ortiz, S. Katsyuba, D. Vasilyev, P. J. Dyson. Delineation of the Critical Parameters of Salts Catalysts in the N-Formylation of Amines with CO₂. *Chem. Eur. J.* **2019** *Doi: [10.1002/chem.201901686](https://doi.org/10.1002/chem.201901686)*
- 2) D. V. Vasilyev, A. V. Rudnev, P. Broekmann, P. J. Dyson. A General and Facile Approach for the Electrochemical Reduction of Carbon Dioxide Inspired by Deep Eutectic Solvents. *ChemSusChem* **2019**, *12*, 1635-1639
- 3) D. Vasilyev, E. Shirzadi, A. V. Rudnev, P. Broekmann, P. J. Dyson. Pyrazolium Ionic Liquid Co-catalysts for the Electroreduction of CO₂. *ACS Appl. Energy Mater.* **2018**, *1*, 5124-5128
- 4) F. D. Bobbink, D. Vasilyev, M. Hulla, S. Chamam, F. Menoud, G. Laurenczy, S. Katsyuba, P. J. Dyson. Intricacies of Cation–Anion Combinations in Imidazolium Salt-Catalyzed Cycloaddition of CO₂ Into Epoxides. *ACS Catal.* **2018**, *8*, 2589-2594
- 5) A. A. Suleymanov, D. V. Vasilyev, V. V. Novikov, Y. V. Nelyubina, D. S. Perekalin. Unpredictable cycloisomerization of 1,11-dien-6-yne by a common cobalt catalyst. *Beilstein J. Org. Chem.* **2017**, *13*, 639-643
- 6) G. P. S. Lau, M. Schreier, D. Vasilyev, R. Scopelliti, M. Grätzel, P. J. Dyson. New Insights Into the Role of Imidazolium-Based Promoters for the Electroreduction of CO₂ on a Silver Electrode. *J. Am. Chem. Soc.* **2016**, *138*, 25, 7820-7823
- 7) D.S. Volkov, M.A. Proskurnin, I.V. Mikheev, D.V. Vasil'ev, M.V. Korobov, D.A. Nedosekin, V.P. Zharov. Application of photothermal and photoacoustic spectroscopy for the monitoring of aqueous dispersions of carbon nanomaterials. *Advanced Laser Technologies*, **1**, **2012**. DOI: 10.12684/alt.1.94

CONFERENCES & SCHOOLS

2018	International Summer School “Power to X: Fundamentals and Applications of Modern Electrosynthesis” (<i>poster</i>)
2017 – 2019	Swiss Snow Symposia (<i>organizing committee</i>)
2016	International Summer School on CO ₂ Conversion: From Fundamentals Towards Applications
2016 – 2018	SCCER Annual Conferences (<i>talks</i>)
2015 – 2018	Swiss Chemical Society Fall Meetings (<i>posters</i>)
2010	Intel International Science and Engineering Fair (ISEF) (<i>poster</i>)

AWARDS

2017	Best teaching award (PhD students, Chemistry and Chemical Engineering Section)
------	--

INTERESTS & ACTIVITIES

Sports (judo, aikido, climbing, hiking, skiing); guitar

2018 – 2019	President of Swiss Young Chemists' Association
2017 – 2018	Vice-President of Swiss Young Chemists' Association
2016 – 2017	Treasurer of Swiss Young Chemists' Association